

**Mixed Ionic/Electronic Conducting Ceramic Membranes
for Oxygen-Assisted CO₂ Reforming**

by

David A. Slade

Submitted to the graduate degree program in Chemical and Petroleum Engineering
and the Graduate Faculty of the University of Kansas School of Engineering
in partial fulfillment of the requirements for the degree of
Doctor of Philosophy.

Chairperson: _____
Susan Stagg-Williams

Committee members: _____
Trung Nguyen

Karen Nordheden

Bala Subramaniam

Judy Wu

Date Defended: _____

The Dissertation Committee for David A. Slade certifies
that this is the approved version of the following dissertation:

**Mixed Ionic/Electronic Conducting Ceramic Membranes
for Oxygen-Assisted CO₂ Reforming**

Chairperson: _____
Susan Stagg-Williams

Committee members: _____
Trung Nguyen

Karen Nordheden

Bala Subramaniam

Judy Wu

Date Approved: _____

Abstract

Synthesis gas is often discussed as a preferred intermediate between underutilized hydrocarbon feedstocks (biomass, stranded natural gas) and ultra-clean fuels (hydrogen, fuel alcohols, synthetic diesel). As the global demand for renewable and clean fuels increases, synthesis gas production could become the limiting step for utilization of these feedstocks. The use of ceramic membranes that conduct both oxygen ions and electrons (O-MIEC membranes) as oxygen supplies for synthesis gas production reactors is one promising strategy to improve synthesis gas production economics and also to obtain other potential benefits of O-MIEC membrane reactors such as improved product selectivity. This dissertation represents the first published application of an O-MIEC membrane reactor for synthesis gas production via CO₂ reforming.

The fact that CO₂ reforming consumes CO₂ has recently led to increased interest in the reaction, but it has not been commercialized significantly because of its strong tendency for catalyst deactivation. This work demonstrates conclusively that incorporating a SrFeCo_{0.5}O_x (SFC) membrane into a CO₂ reforming reactor can more than double the methane conversion activity of a powder Pt/ZrO₂ catalyst and can substantially retard deactivation of both Pt/ZrO₂ and a more active Pt/CeZrO₂ catalyst. The catalyst performance improvement is attributed to a beneficial *in situ* effect on catalyst oxidation state that is observed when the powder catalyst is distributed across the surface of the SFC membrane. The SFC membrane itself exhibits no significant methane conversion activity.

Because of the potential for side reactions in a membrane reactor, the traditional reforming reaction metrics of methane conversion and H₂:CO product ratio are insufficient to determine the comprehensive effect of an O-MIEC membrane on a reforming reaction. This analysis therefore evaluates all reactant conversion and product distribution trends in an unprecedented assessment of the potential molecular-level effects of O-MIEC membranes, conventional powder catalyst oxidation state, and co-fed gas-phase O₂. A novel single parameter (the Oxidation Factor) is proposed and evaluated for assessing CO₂ reforming product selectivity in the presence of oxygen.

Perhaps the most significant result of this work is the claim that hydrogen oxidation on the membrane surface is the primary mode of membrane oxygen release under reforming reaction conditions with the catalyst bed proximate to the membrane. This claim contradicts the long-standing mechanistic assumption in the O-MIEC membrane reactor literature that membrane oxygen participates in reforming reactions as molecular O₂. Correct assignment of the general mechanism of membrane oxygen utilization is critical both for effective membrane reactor design and for productive investigations into the fundamental mechanisms of membrane activity.

Acknowledgments

It is simply not possible to thank my wife, Cathy, enough for indulging my pursuit of a Ph.D. under domestic circumstances that didn't easily conform to such a pursuit. Now that the endeavor is almost finished, I can begin preparing myself for the lifelong process of earning her forgiveness. But as challenging as it is has been, I still believe we will someday, somehow see that it was worth the efforts on both of our parts.

I am also deeply grateful to my advisor, Susan Williams, both for her enthusiastic technical acumen and for her appreciation of my situation in life. The latter may have been the source of her seemingly limitless patience with me as I struggled to balance graduate school with a family. Her tolerance and flexibility allowed this to happen, and I can only hope it was worth the effort for her too.

Table of Contents

| | |
|--|-------------|
| Title Page | i |
| Acceptance Page | ii |
| Abstract | iii |
| Acknowledgments | iv |
| Table of Contents | v |
| List of Tables | xii |
| List of Figures | xiii |
| | |
| Chapter 1: Introduction | 1 |
| 1.1: <u>Overview of the Topic</u> | 1 |
| 1.2: <u>Scope of the Investigation</u> | 3 |
| 1.3: <u>Objectives</u> | 4 |
| 1.4: <u>Structure of the Dissertation</u> | 5 |
| References Cited in Chapter 1 | 6 |
| | |
| Chapter 2: Motivation and State of the Art | 8 |
| 2.1: <u>Syngas from Methane</u> | 8 |
| 2.1.1: Overview of reforming reactions | 9 |
| 2.2: <u>Oxygen Conducting Ceramic Membranes (O-MIEC ceramics)</u> | 11 |
| 2.2.1: O-MIECs for methane conversion | 13 |
| 2.2.2: O-MIEC compositions | 14 |
| 2.3: <u>In situ Membrane Behavior</u> | 15 |
| 2.3.1: Oxygen nonstoichiometry and membrane fracture | 15 |
| 2.3.2: Self-adjusting phase equilibria | 14 |
| 2.3.3: Reforming reactor conditions | 18 |
| 2.4: <u>Membrane Performance Criteria</u> | 18 |
| 2.5: <u>Oxygen Flux in Membrane Reactors</u> | 19 |
| 2.6: <u>CO₂ Reforming with O-MIEC Membranes</u> | 20 |
| 2.6.1: Overview of published work on combined reforming | 21 |
| 2.6.2: Conclusions from published work on combined reforming | 23 |
| 2.6.3: Published work on CO ₂ reforming with O-MIEC membranes | 24 |
| 2.6.4: O-MIEC membrane oxygen-assisted CO ₂ reforming | 25 |
| 2.7: <u>Net Reaction Profiles as a Critical Performance Indicator</u> | 25 |
| References Cited in Chapter 2 | 27 |

| | |
|--|-----------|
| Chapter 3: Experimental Methodology | 32 |
| 3.1: <u>Flux Testing</u> | 32 |
| 3.2: <u>Reaction Testing</u> | 34 |
| 3.2.1: Test reactions and parameters | 34 |
| 3.2.2: Powder catalysts | 35 |
| 3.2.3: Reaction tests in the membrane reactors | 35 |
| 3.2.4: Reaction product analysis | 37 |
| 3.2.5: Plug-flow reactor (PFR) tests | 38 |
| 3.2.6: Post-reaction catalyst analysis | 38 |
| References Cited in Chapter 3 | 39 |
| | |
| Chapter 4: Reactor Design and Assembly | 41 |
| 4.1: <u>Stainless Steel Membrane Reactor (SSMR)</u> | 41 |
| 4.1.1: SSMR construction | 41 |
| 4.1.2: SSMR assembly | 43 |
| 4.1.3: SSMR conclusions | 44 |
| 4.2: <u>Quartz Tube Membrane Reactor (QTMR)</u> | 45 |
| 4.2.1: QTMR construction | 45 |
| 4.2.2: QTMR assembly | 48 |
| 4.2.3: QTMR conclusions | 49 |
| 4.3: <u>Reactor Sealing</u> | 50 |
| 4.3.1: Copper gaskets | 50 |
| 4.3.2: Graphite gaskets | 50 |
| 4.3.3: Gold gaskets | 52 |
| 4.3.4: Reactor sealing conclusions | 52 |
| | |
| Chapter 5: Initial Reaction Studies: The SSMR and Patterned Membranes | 54 |
| 5.1: <u>Initial SSMR Tests</u> | 55 |
| 5.1.1: Methane conversion | 55 |
| 5.1.2: CO ₂ conversion | 56 |
| 5.1.3: H ₂ :CO ratio | 57 |
| 5.1.4: Hydrogen selectivity | 58 |
| 5.2: <u>Methane Conversion Assessment with Patterned Membranes</u> | 60 |

| | |
|--|-----------|
| 5.2.1: Fractional conversion | 60 |
| 5.2.2: Molar conversion rate | 61 |
| 5.2.3: Turnover frequency (TOF) | 62 |
| 5.2.4: Reaction temperature | 64 |
| 5.2.5: Catalyst powder distribution | 64 |
| 5.2.6: Other factors affecting the comparison of patterned membranes and powder catalyst | 65 |
| 5.3: <u>Available Oxygen and Catalyst Activity</u> | 66 |
| 5.3.1: Total oxygen | 66 |
| 5.3.2: Membrane oxygen flux | 68 |
| 5.4: <u>The Effect of Reduction on Membrane Activity</u> | 69 |
| 5.4.1: Methane conversion and oxygen flux | 69 |
| 5.4.2: CO ₂ conversion and membrane reduction | 70 |
| 5.4.3: Motivation for reactant and product ratio analysis | 73 |
| 5.5: <u>Combustion Analysis with the Patterned Membranes</u> | 74 |
| 5.5.1: CO ₂ evaluation | 74 |
| 5.5.2: Methane conversion and molar oxygen supply rate | 75 |
| 5.5.3: Water production | 77 |
| 5.5.4: Hydrogen selectivity | 79 |
| 5.5.5: Hydrogen selectivity with no membrane | 81 |
| 5.5.6: H ₂ :CO ratio evaluation | 82 |
| 5.5.7: The effect of oxygen over time | 83 |
| 5.6: <u>Alternative Approach to Turnover Frequency</u> | 85 |
| 5.7: <u>Revisiting the Earliest Tests</u> | 86 |
| 5.8: <u>Observations and Conclusions from Chapter 5</u> | 90 |
| References Cited in Chapter 5 | 91 |
| Chapter 6: QTMR Reaction Studies: the SFC Membrane Effect | 92 |
| 6.1: <u>Hypotheses and Reaction Pathways</u> | 93 |
| 6.1.1: Proposed hypotheses | 94 |
| 6.1.2: Reaction pathways | 94 |
| 6.2: <u>Initial Baseline QTMR Tests (#1)</u> | 96 |
| 6.2.1: Methane conversion | 96 |
| 6.2.2: Oxygen flux during reaction | 98 |

| | |
|--|------------|
| 6.2.3: Membrane recharge and reaction re-start | 99 |
| 6.2.4: Membrane surface reaction hypothesis evaluation | 101 |
| 6.3: <u>Additional QTMR Test Results</u> | 103 |
| 6.3.1: Improved system baseline tests (#2) | 103 |
| 6.3.2: Membrane oxygen flux overview | 104 |
| 6.3.3: Methane conversion in membrane tests | 105 |
| 6.3.4: H ₂ :CO ratio in membrane tests | 106 |
| 6.4: <u>Reactor and Membrane Testing without Catalyst</u> | 107 |
| 6.4.1: Oxygen and methane conversion without catalyst | 108 |
| 6.4.2: Water production without catalyst | 110 |
| 6.5: <u>Membrane Mechanism Hypothesis</u> | 111 |
| 6.5.1: Possible activity mechanisms for membrane oxygen | 111 |
| 6.5.2: Proposed SFC activity mechanism | 112 |
| 6.5.3: Trace oxygen uptake by SFC | 114 |
| 6.6: <u>Observations and Conclusions from Chapter 6</u> | 116 |
| References Cited in Chapter 6 | 117 |
| | |
| Chapter 7: The Role of Membrane Oxygen | 118 |
| 7.1: <u>Initial QTMR Testing with 1% Co-Fed Oxygen</u> | 118 |
| 7.1.1: Methane conversion | 118 |
| 7.1.2: Catalyst deactivation | 120 |
| 7.1.3: H ₂ :CO ratio | 120 |
| 7.2: <u>Improved System with 1% Co-Fed Oxygen</u> | 122 |
| 7.2.1: Methane conversion | 122 |
| 7.2.2: H ₂ :CO ratio | 124 |
| 7.3: <u>Improved System with Other Co-Fed Oxygen Amounts</u> | 124 |
| 7.3.1: Selection of additional co-fed oxygen amounts | 124 |
| 7.3.2: Additional co-fed oxygen amount testing | 126 |
| 7.4: <u>Product Ratio Analysis for All Co-Fed Oxygen Tests</u> | 127 |
| 7.4.1: H ₂ :CO ratio | 128 |
| 7.4.2: Relative water production | 129 |
| 7.4.3: Relative CO ₂ consumption | 130 |
| 7.4.4: The blank test with no oxygen | 131 |
| 7.4.5: Relative CO production | 132 |

| | |
|---|------------|
| 7.4.6: The SFC membrane test | 133 |
| 7.5: <u>Equilibrium Conversions and Product Ratios</u> | 136 |
| 7.6: <u>Product Ratio Analysis for All SFC Membrane Tests</u> | 137 |
| 7.6.1: Relative CO ₂ conversion | 137 |
| 7.6.2: Relative water production | 138 |
| 7.7: <u>Post-Reaction Carbon Analysis</u> | 140 |
| 7.8: <u>Observations and Conclusions from Chapter 7</u> | 142 |
| References Cited in Chapter 7 | 142 |
| | |
| Chapter 8: The Effect of Catalyst Oxidation State | 143 |
| 8.1: <u>Catalyst Pretreatment Tests in the QTMR</u> | 143 |
| 8.1.1: Catalyst reduction prior to loading | 144 |
| 8.1.2: Pre-reaction catalyst reduction | 145 |
| 8.1.3: Water production and CO ₂ conversion | 147 |
| 8.1.4: H ₂ :CO ratio | 148 |
| 8.1.5: Methane conversion | 150 |
| 8.2: <u>Assessing Reaction Selectivity: the Oxidation Factor</u> | 151 |
| 8.2.1: Defining a selectivity expression | 151 |
| 8.2.2: Oxidation Factor range and values | 153 |
| 8.2.3: Evaluating the Oxidation Factor | 154 |
| 8.3: <u>Pre-Reaction Exposure Testing in a PFR</u> | 159 |
| 8.3.1: Methane conversion in the PFR | 159 |
| 8.3.2: Water production in the PFR | 161 |
| 8.3.3: CO ₂ conversion and H ₂ :CO ratio in the PFR | 162 |
| 8.3.4: Oxidation Factor in the PFR | 164 |
| 8.3.5: Relative rWGS activity in the QTMR and PFR | 165 |
| 8.4: <u>Observations and Conclusions from Chapter 8</u> | 167 |
| | |
| Chapter 9: Catalyst Comparison and Membrane Reactor Evaluation | 168 |
| 9.1: <u>Catalyst Comparison in the PFR</u> | 169 |
| 9.1.1: Methane and CO ₂ conversion | 169 |
| 9.1.2: Other ratios | 170 |
| 9.1.3: Absolute water production | 172 |
| 9.1.4: Reduction and oxidation of the catalyst supports | 173 |

| | |
|--|------------|
| 9.2: <u>Catalyst Comparison in the QTMR</u> | 174 |
| 9.2.1: Conversion and product ratios | 174 |
| 9.2.2: Comparison of the evidence for <i>in situ</i> reduction | 176 |
| 9.2.3: Hydrogen concentration in the reactor | 177 |
| 9.2.4: Delayed membrane effect with the Pt/CeZrO ₂ catalyst | 178 |
| 9.3: <u>Pretreatment Effects on the Pt/CeZrO₂ Catalyst</u> | 180 |
| 9.3.1: Catalyst oxidation (“aging”) and reduction | 180 |
| 9.3.2: Additional evidence for <i>in situ</i> catalyst reduction | 181 |
| 9.3.3: Conversion/product ratios | 182 |
| 9.3.4: The impact of the CeZrO ₂ support on catalyst activity | 184 |
| 9.4: <u>Other Catalyst Performance Comparisons</u> | 185 |
| 9.4.1: Oxidation Factor | 185 |
| 9.4.2: Reverse Water-Gas Shift | 188 |
| 9.4.3: Carbon deposition | 189 |
| 9.5: <u>Observations and Conclusions from Chapter 9</u> | 191 |
| References Cited in Chapter 9 | 192 |
| | |
| Chapter 10: Conclusions and Recommendations | 193 |
| 10.1: <u>Overview of Primary Ideas</u> | 193 |
| 10.1.1: Net reaction profiles | 193 |
| 10.1.2: The influence of reduction on catalyst activity | 194 |
| 10.1.3: <i>In situ</i> oxidation and reduction | 195 |
| 10.1.4: Support-SFC analogy | 196 |
| 10.1.5: Direct catalyst-membrane interactions | 197 |
| 10.1.6: Oxygen-assisted CO ₂ reforming | 199 |
| 10.2: <u>Review of the Proposed Hypotheses</u> | 200 |
| 10.3: <u>Recommendations for Future Work</u> | 202 |
| 10.3.1: Water condensation in the reactor system | 202 |
| 10.3.2: Carbonate collection on the SFC surface | 203 |
| 10.3.3: Isotope tracer studies | 204 |
| 10.3.4: Membrane surface reaction thermodynamics | 206 |
| 10.3.5: QTMR modeling and operational configuration | 207 |
| 10.3.6: Membrane-catalyst proximity effect | 209 |
| 10.3.7: Other membrane materials and catalysts | 210 |

| | |
|--------------------------------|-----|
| 10.3.8: Long-term testing | 211 |
| References Cited in Chapter 10 | 211 |

Appendices

| | |
|---|----|
| Appendix A: <u>Membrane Transport Fundamentals</u> | A1 |
| Appendix B: <u>SFC Overview</u> | B1 |
| Appendix C: <u>Membrane Fabrication</u> | C1 |
| Appendix D: <u>SFC Membrane Phase Decomposition Overview</u> | D1 |
| Appendix E: <u>Flux Test Methodology and Data Analysis</u> | E1 |
| Appendix F: <u>Flux Study Overview</u> | F1 |
| Appendix G: <u>Reaction Test and Data Analysis Methodology</u> | G1 |
| Appendix H: <u>Summary of Membrane Reaction Test Results</u> | H1 |
| Appendix I: <u>Calculation Methodology for Flux during Reaction</u> | I1 |
| Appendix J: <u>Combustion Factor Sensitivity Assessment and Optimization</u> | J1 |
| Appendix K: <u>Extent of Reaction Calculation Basis</u> | K1 |
| Appendix L: <u>Dispersion and Adsorption in the QTMR System</u> | L1 |
| Appendix M: <u>Thermochemical Interactions between SFC and Individual Gaseous Species</u> | M1 |
| Appendix N: <u>Reaction Equilibrium Data and Additional Thermal Effects in the QTMR</u> | N1 |
| Appendix O: <u>QTMR Dimensions and Parts Identification</u> | O1 |

List of Tables

| | <u>Page</u> |
|--|-------------|
| Table 2.1: Summary of relevant reactions | 8 |
| Table 2.2: Oxygen flux results for various membrane materials; temperature of 850 °C and membrane thicknesses of ~1 mm unless noted | 18 |
| Table 2.3: Overview of reactor feed compositions in published combined reforming studies | 21 |
| Table 4.1: Gasket material performance comparison | 51 |
| Table 6.1: Summary of tests with no catalyst; CH ₄ conversions as [mol _{converted} / mol _{fed}] | 104 |

List of Figures

- Figure 3.1:** Example output from an SSMR flux test with a plain SFC membrane (7/14/05)
- Figure 3.2:** Schematic of an O-MIEC membrane under reaction conditions
- Figure 4.1:** Stainless steel membrane reactor (SSMR) internal schematic and photograph
- Figure 4.2:** Stainless steel membrane reactor (SSMR) system
- Figure 4.3:** Quartz Tube Membrane Reactor (QTMR) system
- Figure 4.4:** Quartz Tube Membrane Reactor (QTMR) system
- Figure 5.1:** Fractional CH₄ conversion during CO₂ reforming over a Pt/ZrO₂ catalyst in the original SSMR. Reaction temperature=700 °C, GHSV=75 L/h/gcat, CH₄:CO₂ feed ratio=1:1 with no Ar/O₂ dilution.
- Figure 5.2:** Fractional CO₂ conversion during CO₂ reforming over a Pt/ZrO₂ catalyst in the original SSMR. Reaction temperature=700 °C, GHSV=75 L/h/gcat, CH₄:CO₂ feed ratio=1:1 with no Ar/O₂ dilution.
- Figure 5.3:** H₂:CO ratio during CO₂ reforming over a Pt/ZrO₂ catalyst in the original SSMR. Reaction temperature=700 °C, GHSV=75 L/h/gcat, CH₄:CO₂ feed ratio=1:1 with no Ar/O₂ dilution.
- Figure 5.4:** Molar ratio of H₂ production-to-CH₄ conversion during CO₂ reforming over a Pt/ZrO₂ catalyst in the original SSMR. Reaction temperature=700 °C, GHSV=75 L/h/gcat, CH₄:CO₂ feed ratio=1:1 with no Ar/O₂ dilution.
- Figure 5.5:** Fractional CH₄ conversion during CO₂ reforming over a Pt/ZrO₂ catalyst and Pt-patterned membranes in the original SSMR. Reaction temperature as indicated, CH₄:CO₂ feed ratio=1:1 with no Ar/O₂ dilution, various feed flowrates.
- Figure 5.6:** Molar CH₄ conversion during CO₂ reforming over a Pt/ZrO₂ catalyst and Pt-patterned membranes in the original SSMR. Reaction temperature as indicated, CH₄:CO₂ feed ratio=1:1 with no Ar/O₂ dilution, various feed flowrates.
- Figure 5.7:** CH₄ conversion turnover frequency (TOF) during CO₂ reforming over a Pt/ZrO₂ catalyst and Pt-patterned membranes in the original SSMR. Reaction temperature as indicated, CH₄:CO₂ feed ratio=1:1 with no Ar/O₂ dilution, various feed flowrates.
- Figure 5.8:** Molar CH₄ conversion vs. total available oxygen during CO₂ reforming over a Pt/ZrO₂ catalyst and Pt-patterned membranes in the original SSMR. Reaction temperature as indicated, CH₄:CO₂ feed ratio=1:1 with no Ar/O₂ dilution, various feed flowrates.

- Figure 5.9:** Membrane oxygen production during CO₂ reforming over a Pt/ZrO₂ catalyst and Pt-patterned membranes in the original SSMR. Reaction temperature as indicated, CH₄:CO₂ feed ratio=1:1 with no Ar/O₂ dilution, various feed flowrates.
- Figure 5.10:** Fractional CO₂ conversion during CO₂ reforming over a Pt/ZrO₂ catalyst and Pt-patterned membranes in the original SSMR. Reaction temperature as indicated, CH₄:CO₂ feed ratio=1:1 with no Ar/O₂ dilution, various feed flowrates.
- Figure 5.11:** Fractional CH₄ conversion during CO₂ reforming over a Pt/ZrO₂ catalyst and Pt-patterned membranes in the original SSMR. Reaction temperature as indicated, CH₄:CO₂ feed ratio=1:1 with no Ar/O₂ dilution, various feed flowrates.
- Figure 5.12:** CO production during CO₂ reforming over a Pt/ZrO₂ catalyst and Pt-patterned membranes in the original SSMR. Reaction temperature as indicated, CH₄:CO₂ feed ratio=1:1 with no Ar/O₂ dilution, various feed flowrates.
- Figure 5.13:** Membrane oxygen production during CO₂ reforming over a Pt/ZrO₂ catalyst and Pt-patterned membranes in the original SSMR. Reaction temperature as indicated, CH₄:CO₂ feed ratio=1:1 with no Ar/O₂ dilution, various feed flowrates.
- Figure 5.14:** Molar CO₂:CH₄ conversion ratio during CO₂ reforming over a Pt/ZrO₂ catalyst and Pt-patterned membranes in the original SSMR. Reaction temperature as indicated, CH₄:CO₂ feed ratio=1:1 with no Ar/O₂ dilution, various feed flowrates.
- Figure 5.15:** Molar CH₄ conversion vs. total available oxygen during CO₂ reforming over a Pt/ZrO₂ catalyst and Pt-patterned membranes in the original SSMR. Reaction temperature as indicated, CH₄:CO₂ feed ratio=1:1 with no Ar/O₂ dilution, various feed flowrates.
- Figure 5.16:** Molar H₂O production vs. total available oxygen during CO₂ reforming over a Pt/ZrO₂ catalyst and Pt-patterned membranes in the original SSMR. Reaction temperature as indicated, CH₄:CO₂ feed ratio=1:1 with no Ar/O₂ dilution, various feed flowrates.
- Figure 5.17:** Molar H₂O production vs. molar CH₄ conversion during CO₂ reforming over a Pt/ZrO₂ catalyst and Pt-patterned membranes in the original SSMR. Reaction temperature as indicated, CH₄:CO₂ feed ratio=1:1 with no Ar/O₂ dilution, various feed flowrates.
- Figure 5.18:** Molar ratio of H₂ production-to-CH₄ conversion during CO₂ reforming over a Pt/ZrO₂ catalyst and Pt-patterned membranes in the original SSMR. Reaction temperature as indicated, CH₄:CO₂ feed ratio=1:1 with no Ar/O₂ dilution, various feed flowrates.
- Figure 5.19:** Molar H₂ production vs. molar CH₄ conversion during CO₂ reforming over a Pt/ZrO₂ catalyst and Pt-patterned membranes in the original SSMR. Reaction temperature as indicated, CH₄:CO₂ feed ratio=1:1 with no Ar/O₂ dilution, various feed flowrates.
- Figure 5.20:** H₂:CO ratio vs. fractional CH₄ conversion during CO₂ reforming over a Pt/ZrO₂ catalyst and Pt-patterned membranes in the original SSMR. Reaction temperature as indicated, CH₄:CO₂ feed ratio=1:1 with no Ar/O₂ dilution, various feed flowrates.

- Figure 5.21:** Molar ratio of CH₄ conversion-to-oxygen supply during CO₂ reforming over a Pt/ZrO₂ catalyst and Pt-patterned membranes in the original SSMR. Reaction temperature as indicated, CH₄:CO₂ feed ratio=1:1 with no Ar/O₂ dilution, various feed flowrates.
- Figure 5.22:** CH₄ conversion turnover frequency (TOF) based on total Pt mass during CO₂ reforming over a Pt/ZrO₂ catalyst and Pt-patterned membranes in the original SSMR. Reaction temperature as indicated, CH₄:CO₂ feed ratio=1:1 with no Ar/O₂ dilution, various feed flowrates.
- Figure 5.23:** Molar CO₂:CH₄ conversion ratio during CO₂ reforming over a Pt/ZrO₂ catalyst in the original SSMR. Reaction temperature=700 °C, GHSV=75 L/h/g_{cat}, CH₄:CO₂ feed ratio=1:1 with no Ar/O₂ dilution.
- Figure 5.24:** Molar ratio of CH₄ conversion-to-oxygen supply during CO₂ reforming over a Pt/ZrO₂ catalyst in the original SSMR. Reaction temperature=700 °C, GHSV=75 L/h/g_{cat}, CH₄:CO₂ feed ratio=1:1 with no Ar/O₂ dilution.
- Figure 5.25:** Molar ratio of water production-to-CH₄ conversion during CO₂ reforming over a Pt/ZrO₂ catalyst in the original SSMR. Reaction temperature=700 °C, GHSV=75 L/h/g_{cat}, CH₄:CO₂ feed ratio=1:1 with no Ar/O₂ dilution.
- Figure 6.1:** CH₄ conversion turnover frequency (TOF) during CO₂ reforming over a Pt/ZrO₂ catalyst in the original QTMR. Reaction temperature=800 °C, GHSV=150 L/h/g_{cat}, CH₄:CO₂:Ar feed ratio=4:4:2.
- Figure 6.2:** Reactor effluent composition and membrane oxygen flux (O₂ equivalent) during CO₂ reforming over a Pt/ZrO₂ catalyst in the original QTMR with an SFC membrane. Reaction temperature=800 °C, GHSV=150 L/h/g_{cat}, CH₄:CO₂:Ar feed ratio=4:4:2.
- Figure 6.3:** CH₄ conversion turnover frequency (TOF) during CO₂ reforming over a Pt/ZrO₂ catalyst in the original QTMR. Reaction temperature=800 °C, GHSV=150 L/h/g_{cat}, CH₄:CO₂:Ar feed ratio=4:4:2. With pause and re-start.
- Figure 6.4:** Reactor effluent composition and membrane oxygen flux (O₂ equivalent) during CO₂ reforming over a Pt/ZrO₂ catalyst in the original QTMR with an SFC membrane. Reaction temperature=800 °C, GHSV=150 L/h/g_{cat}, CH₄:CO₂:Ar feed ratio=4:4:2. With pause and re-start.
- Figure 6.5:** Membrane oxygen flux (O₂ equivalent) vs. H₂:CO₂ ratio during CO₂ reforming over a Pt/ZrO₂ catalyst in the original QTMR with an SFC membrane. Reaction temperature=800 °C, GHSV=150 L/h/g_{cat}, CH₄:CO₂:Ar feed ratio=4:4:2.
- Figure 6.6:** CH₄ conversion turnover frequency (TOF) during CO₂ reforming over a Pt/ZrO₂ catalyst in the improved QTMR. Reaction temperature=800 °C, GHSV=150 L/h/g_{cat}, CH₄:CO₂:Ar/O₂ feed ratio=4:4:2.
- Figure 6.7:** Membrane oxygen flux (O₂ equivalent) as mol% of feed during CO₂ reforming over a Pt/ZrO₂ catalyst in both QTMRs with SFC membranes. Reaction temperature=800 °C, GHSV=150 L/h/g_{cat}, CH₄:CO₂:Ar feed ratio=4:4:2.

- Figure 6.8:** CH₄ conversion turnover frequency (TOF) during CO₂ reforming over a Pt/ZrO₂ catalyst in both QTMRs. Reaction temperature=800 °C, GHSV=150 L/h/g_{cat}, CH₄:CO₂:Ar feed ratio=4:4:2.
- Figure 6.9:** H₂:CO ratio during CO₂ reforming over a Pt/ZrO₂ catalyst in both QTMRs. Reaction temperature=800 °C, GHSV=150 L/h/g_{cat}, CH₄:CO₂:Ar feed ratio=4:4:2.
- Figure 6.10:** Average fractional CH₄ conversion vs. air leak estimate during CO₂ reforming with no catalyst in both QTMRs. Reaction temperature=800 °C, GHSV=150 L/h/g_{cat}, CH₄:CO₂:Ar feed ratio=4:4:2.
- Figure 6.11:** Average fractional CH₄ conversion vs. average total oxygen into reactor during CO₂ reforming with no catalyst in both QTMRs. Reaction temperature=800 °C, GHSV=150 L/h/g_{cat}, CH₄:CO₂:Ar feed ratio=4:4:2.
- Figure 6.12:** Average relative water production vs. average fractional CH₄ conversion during CO₂ reforming with no catalyst in both QTMRs. Reaction temperature=800 °C, GHSV=150 L/h/g_{cat}, CH₄:CO₂:Ar feed ratio=4:4:2.
- Figure 6.13:** Membrane oxygen flux (O₂ equivalent) during cool-down following CO₂ reforming over a Pt/ZrO₂ catalyst in the original QTMR with an SFC membrane. Ar sweep gas flowrate=25 ccm.
- Figure 6.14:** Membrane oxygen flux (O₂ equivalent) during heat-up prior to CO₂ reforming over a Pt/ZrO₂ catalyst in the original QTMR with an SFC membrane. Ar sweep gas flowrate=25 ccm.
- Figure 7.1:** CH₄ conversion turnover frequency (TOF) during CO₂ reforming over a Pt/ZrO₂ catalyst in the original QTMR. Reaction temperature=800 °C, GHSV=150 L/h/g_{cat}, CH₄:CO₂:Ar/O₂ feed ratio=4:4:2.
- Figure 7.2:** H₂:CO ratio during CO₂ reforming over a Pt/ZrO₂ catalyst in the original QTMR. Reaction temperature=800 °C, GHSV=150 L/h/g_{cat}, CH₄:CO₂:Ar/O₂ feed ratio=4:4:2.
- Figure 7.3:** H₂:CO ratio during CO₂ reforming over a Pt/ZrO₂ catalyst in the original QTMR. Reaction temperature=800 °C, GHSV=150 L/h/g_{cat}, CH₄:CO₂:Ar/O₂ feed ratio=4:4:2.
- Figure 7.4:** CH₄ conversion turnover frequency (TOF) during CO₂ reforming over a Pt/ZrO₂ catalyst in the original QTMR. Reaction temperature=800 °C, GHSV=150 L/h/g_{cat}, CH₄:CO₂:Ar/O₂ feed ratio=4:4:2.
- Figure 7.5:** H₂:CO ratio during CO₂ reforming over a Pt/ZrO₂ catalyst in the improved QTMR. Reaction temperature=800 °C, GHSV=150 L/h/g_{cat}, CH₄:CO₂:Ar/O₂ feed ratio=4:4:2.
- Figure 7.6:** CH₄ conversion turnover frequency (TOF) during CO₂ reforming over a Pt/ZrO₂ catalyst in the improved QTMR. Reaction temperature=800 °C, GHSV=150 L/h/g_{cat}, CH₄:CO₂:Ar/O₂ feed ratio=4:4:2.

- Figure 7.7:** H₂:CO ratio during CO₂ reforming over a Pt/ZrO₂ catalyst in the improved QTMR. Reaction temperature=800 °C, GHSV=150 L/h/g_{cat}, CH₄:CO₂:Ar/O₂ feed ratio=4:4:2.
- Figure 7.8:** Molar ratio of water production-to-CH₄ conversion during CO₂ reforming over a Pt/ZrO₂ catalyst in the improved QTMR. Reaction temperature=800 °C, GHSV=150 L/h/g_{cat}, CH₄:CO₂:Ar/O₂ feed ratio=4:4:2.
- Figure 7.9:** Molar CO₂:CH₄ conversion ratio during CO₂ reforming over a Pt/ZrO₂ catalyst in the improved QTMR. Reaction temperature=800 °C, GHSV=150 L/h/g_{cat}, CH₄:CO₂:Ar/O₂ feed ratio=4:4:2.
- Figure 7.10:** Molar ratio of CO production-to-CH₄ conversion during CO₂ reforming over a Pt/ZrO₂ catalyst in the improved QTMR. Reaction temperature=800 °C, GHSV=150 L/h/g_{cat}, CH₄:CO₂:Ar/O₂ feed ratio=4:4:2.
- Figure 7.11:** H₂:CO ratio vs. fractional CH₄ conversion during CO₂ reforming over a Pt/ZrO₂ catalyst in the improved QTMR. Reaction temperature=800 °C, GHSV=150 L/h/g_{cat}, CH₄:CO₂:Ar/O₂ feed ratio=4:4:2.
- Figure 7.12:** CH₄ conversion turnover frequency (TOF) during CO₂ reforming over a Pt/ZrO₂ catalyst in both QTMRs. Reaction temperature=800 °C, GHSV=150 L/h/g_{cat}, CH₄:CO₂:Ar/O₂ feed ratio=4:4:2.
- Figure 7.13:** Molar CO₂:CH₄ conversion ratio during CO₂ reforming over a Pt/ZrO₂ catalyst in both QTMRs. Reaction temperature=800 °C, GHSV=150 L/h/g_{cat}, CH₄:CO₂:Ar/O₂ feed ratio=4:4:2.
- Figure 7.14:** Molar ratio of water production-to-CH₄ conversion during CO₂ reforming over a Pt/ZrO₂ catalyst in both QTMRs. Reaction temperature=800 °C, GHSV=150 L/h/g_{cat}, CH₄:CO₂:Ar/O₂ feed ratio=4:4:2.
- Figure 7.15:** Molar ratio of net carbon removed-to-net CH₄ converted from Pt/ZrO₂ catalyst following CO₂ reforming in the improved QTMR. Obtained by oxidation at 800 °C using 500 µl injections of 10% O₂/Ar into Ar at 20 ccm.
- Figure 8.1:** CH₄ conversion turnover frequency (TOF) during CO₂ reforming over a Pt/ZrO₂ catalyst in the improved QTMR. Reaction temperature=800 °C, GHSV=150 L/h/g_{cat}, CH₄:CO₂:Ar/O₂ feed ratio=4:4:2.
- Figure 8.2:** CH₄ conversion turnover frequency (TOF) during CO₂ reforming over a Pt/ZrO₂ catalyst in the improved QTMR. Reaction temperature=800 °C, GHSV=150 L/h/g_{cat}, CH₄:CO₂:Ar/O₂ feed ratio=4:4:2.
- Figure 8.3:** Molar ratio of water production-to-CH₄ conversion during CO₂ reforming over a Pt/ZrO₂ catalyst in the improved QTMR. Reaction temperature=800 °C, GHSV=150 L/h/g_{cat}, CH₄:CO₂:Ar/O₂ feed ratio=4:4:2.

- Figure 8.4:** Molar CO₂:CH₄ conversion ratio during CO₂ reforming over a Pt/ZrO₂ catalyst in the improved QTMR. Reaction temperature=800 °C, GHSV=150 L/h/g_{cat}, CH₄:CO₂:Ar/O₂ feed ratio=4:4:2.
- Figure 8.5:** H₂:CO ratio during CO₂ reforming over a Pt/ZrO₂ catalyst in the improved QTMR. Reaction temperature=800 °C, GHSV=150 L/h/g_{cat}, CH₄:CO₂:Ar/O₂ feed ratio=4:4:2.
- Figure 8.6:** CH₄ conversion turnover frequency (TOF) during CO₂ reforming over a Pt/ZrO₂ catalyst in the original QTMR. Reaction temperature=800 °C, GHSV=150 L/h/g_{cat}, CH₄:CO₂:Ar/O₂ feed ratio=4:4:2.
- Figure 8.7:** Theoretical maximum Oxidation Factor and required O₂ vs. combustion proportion (as % of CH₄ conversion) with and without concurrent rWGS at 65% of CH₄ conversion
- Figure 8.8:** Oxidation Factor during CO₂ reforming over a Pt/ZrO₂ catalyst in the improved QTMR. Reaction temperature=800 °C, GHSV=150 L/h/g_{cat}, CH₄:CO₂:Ar/O₂ feed ratio=4:4:2.
- Figure 8.9:** Oxidation Factor during CO₂ reforming over a Pt/ZrO₂ catalyst in the improved QTMR. Reaction temperature=800 °C, GHSV=150 L/h/g_{cat}, CH₄:CO₂:Ar/O₂ feed ratio=4:4:2.
- Figure 8.10:** Theoretical maximum Oxidation Factor vs. required O₂ with and without concurrent rWGS at 65% of CH₄ conversion; and actual Oxidation Factor for 2% co-fed O₂ test vs. actual available O₂
- Figure 8.11:** CH₄ consuming reaction distribution (as % of total CH₄ conversion) and net CH₄ TOF during CO₂ reforming with 2% co-fed O₂ over a Pt/ZrO₂ catalyst in the original QTMR. Reaction temperature=800 °C, GHSV=150 L/h/g_{cat}, CH₄:CO₂:Ar/O₂ feed ratio=4:4:2.
- Figure 8.12:** CH₄ conversion turnover frequency (TOF) during CO₂ reforming over a Pt/ZrO₂ catalyst in the PFR. Reaction temperature=800 °C, GHSV=150 L/h/g_{cat}, CH₄:CO₂:Ar/O₂ feed ratio=4:4:2.
- Figure 8.13:** Molar ratio of water production-to-CH₄ conversion during CO₂ reforming over a Pt/ZrO₂ catalyst in the PFR. Reaction temperature=800 °C, GHSV=150 L/h/g_{cat}, CH₄:CO₂:Ar/O₂ feed ratio=4:4:2.
- Figure 8.14:** H₂:CO ratio during CO₂ reforming over a Pt/ZrO₂ catalyst in the PFR. Reaction temperature=800 °C, GHSV=150 L/h/g_{cat}, CH₄:CO₂:Ar/O₂ feed ratio=4:4:2.
- Figure 8.15:** Molar CO₂:CH₄ conversion ratio during CO₂ reforming over a Pt/ZrO₂ catalyst in the PFR. Reaction temperature=800 °C, GHSV=150 L/h/g_{cat}, CH₄:CO₂:Ar/O₂ feed ratio=4:4:2.
- Figure 8.16:** Oxidation Factor during CO₂ reforming over a Pt/ZrO₂ catalyst in the PFR. Reaction temperature=800 °C, GHSV=150 L/h/g_{cat}, CH₄:CO₂:Ar/O₂ feed ratio=4:4:2.

- Figure 8.17:** RWGS extent during CO₂ reforming over a Pt/ZrO₂ catalyst in both reactor types. Reaction temperature=800 °C, GHSV=150 L/h/g_{cat}, CH₄:CO₂:Ar/O₂ feed ratio=4:4:2.
- Figure 9.1:** CH₄ conversion turnover frequency (TOF) during CO₂ reforming over a Pt/ZrO₂ and a Pt/CeZrO₂ catalyst in the PFR. Reaction temperature=800 °C, GHSV=150 L/h/g_{cat}, CH₄:CO₂:Ar/O₂ feed ratio=4:4:2.
- Figure 9.2:** Molar CO₂:CH₄ conversion ratio during CO₂ reforming over a Pt/ZrO₂ and a Pt/CeZrO₂ catalyst in the PFR. Reaction temperature=800 °C, GHSV=150 L/h/g_{cat}, CH₄:CO₂:Ar/O₂ feed ratio=4:4:2.
- Figure 9.3:** H₂:CO ratio during CO₂ reforming over a Pt/ZrO₂ and a Pt/CeZrO₂ catalyst in the PFR. Reaction temperature=800 °C, GHSV=150 L/h/g_{cat}, CH₄:CO₂:Ar/O₂ feed ratio=4:4:2.
- Figure 9.4:** Molar ratio of water production-to-CH₄ conversion during CO₂ reforming over a Pt/ZrO₂ and a Pt/CeZrO₂ catalyst in the PFR. Reaction temperature=800 °C, GHSV=150 L/h/g_{cat}, CH₄:CO₂:Ar/O₂ feed ratio=4:4:2.
- Figure 9.5:** Water production during CO₂ reforming over a Pt/ZrO₂ and a Pt/CeZrO₂ catalyst in the PFR. Reaction temperature=800 °C, GHSV=150 L/h/g_{cat}, CH₄:CO₂:Ar/O₂ feed ratio=4:4:2.
- Figure 9.6:** CH₄ conversion turnover frequency (TOF) during CO₂ reforming over a Pt/CeZrO₂ catalyst in both reactor types. Reaction temperature=800 °C, GHSV=150 L/h/g_{cat}, CH₄:CO₂:Ar/O₂ feed ratio=4:4:2.
- Figure 9.7:** H₂:CO ratio during CO₂ reforming over a Pt/CeZrO₂ catalyst in both reactor types. Reaction temperature=800 °C, GHSV=150 L/h/g_{cat}, CH₄:CO₂:Ar/O₂ feed ratio=4:4:2.
- Figure 9.8:** Average H₂ concentration in the reactor during CO₂ reforming over a Pt/CeZrO₂ catalyst in both reactor types. Reaction temperature=800 °C, GHSV=150 L/h/g_{cat}, CH₄:CO₂:Ar/O₂ feed ratio=4:4:2.
- Figure 9.9:** Membrane oxygen flux (O₂ equivalent) as mol% of feed during CO₂ reforming over a Pt/CeZrO₂ catalyst in the QTMR with an SFC membrane. Reaction temperature=800 °C, GHSV=150 L/h/g_{cat}, CH₄:CO₂:Ar/O₂ feed ratio=4:4:2.
- Figure 9.10:** CH₄ conversion turnover frequency (TOF) during CO₂ reforming over aged and fresh Pt/CeZrO₂ catalyst in both reactor types with no co-fed O₂. Reaction temperature=800 °C, GHSV=150 L/h/g_{cat}, CH₄:CO₂:Ar/O₂ feed ratio=4:4:2.
- Figure 9.11:** Molar CO₂:CH₄ conversion ratio during CO₂ reforming over aged and fresh Pt/CeZrO₂ catalyst in both reactor types with no co-fed O₂. Reaction temperature=800 °C, GHSV=150 L/h/g_{cat}, CH₄:CO₂:Ar/O₂ feed ratio=4:4:2.
- Figure 9.12:** Molar ratio of water production-to-CH₄ conversion during CO₂ reforming over aged and fresh Pt/CeZrO₂ catalyst in both reactor types with no co-fed O₂. Reaction temperature=800 °C, GHSV=150 L/h/g_{cat}, CH₄:CO₂:Ar/O₂ feed ratio=4:4:2.

- Figure 9.13:** H₂:CO ratio during CO₂ reforming over aged and fresh Pt/CeZrO₂ catalyst in both reactor types with no co-fed O₂. Reaction temperature=800 °C, GHSV=150 L/h/g_{cat}, CH₄:CO₂:Ar/O₂ feed ratio=4:4:2.
- Figure 9.14:** Oxidation Factor during CO₂ reforming over a Pt/ZrO₂ and a Pt/CeZrO₂ catalyst in the PFR. Reaction temperature=800 °C, GHSV=150 L/h/g_{cat}, CH₄:CO₂:Ar/O₂ feed ratio=4:4:2.
- Figure 9.15:** Oxidation Factor during CO₂ reforming over a Pt/ZrO₂ and a Pt/CeZrO₂ catalyst in the QTMR. Reaction temperature=800 °C, GHSV=150 L/h/g_{cat}, CH₄:CO₂:Ar/O₂ feed ratio=4:4:2.
- Figure 9.16:** Oxidation Factor during CO₂ reforming over a Pt/CeZrO₂ catalyst in both reactors. Reaction temperature=800 °C, GHSV=150 L/h/g_{cat}, CH₄:CO₂:Ar/O₂ feed ratio=4:4:2.
- Figure 9.17:** RWGS extent during CO₂ reforming over a Pt/CeZrO₂ catalyst in both reactor types. Reaction temperature=800 °C, GHSV=150 L/h/g_{cat}, CH₄:CO₂:Ar/O₂ feed ratio=4:4:2.
- Figure 9.18:** Molar ratio of net carbon removed-to-net CH₄ converted from Pt/ZrO₂ and Pt/CeZrO₂ catalysts following CO₂ reforming in the improved QTMR. Obtained by oxidation at 800 °C using 500 µl injections of 10% O₂/Ar into Ar at 20 ccm.

Chapter 1: Introduction

1.1: Overview of the Topic

With the increasing global demand for cleaner energy, fuel cell hydrogen and ultraclean gas-to-liquid (GTL) fuels are receiving a great deal of attention as alternative energy sources. Mixtures of H₂ and CO known as synthesis gas serve as the intermediate between hydrocarbon feedstocks, and both hydrogen and GTL fuels. Synthesis gas can be produced by reforming reactions or partial oxidation reactions, both of which either require or can benefit from pure oxygen as a reactor feed. Among these reactions, partial oxidation requires the greatest amount of oxygen, and the requisite energy-intensive air separation unit represents a significant fraction of both the operating and capital costs of such a synthesis gas facility [1-4].

Because of the high economic, environmental, and safety costs associated with pure oxygen as a process feedstock, oxygen-conducting ceramic membranes have been explored as an alternative oxygen source for hydrocarbon conversion reactors [1-10]. These non-porous ceramic materials allow the transport of oxygen ions through the lattice of the solid material resulting in 100% selectivity for oxygen regardless of the source gas. The materials of interest for membrane reactor applications are mixed ionic-electronic conducting ceramic materials that conduct electrons as well as oxygen ions. As a result, they require only high temperature (typically 700 °C or higher) and an imposed oxygen potential gradient to transmit oxygen. Unlike solely ionic conducting materials such as those used in solid oxide fuel cells (SOFC's), mixed-conducting ceramics require no external circuitry. Like SOFC ceramics, they exhibit oxygen fluxes that generally increase with temperature above some threshold activation temperature.

In addition to the possible benefits to catalyst performance, membrane-supplied oxygen incorporates several significant environmental advantages over gas-phase oxygen supplies for synthesis gas operations: (1) the aforementioned substantial reduction in process energy consumption;

(2) safer oxygen (no hotspots or flammability concerns) [2, 9]; (3) inherently distributed oxygen introduction which can produce a more uniform and predictable reactor temperature profile and increase the selectivity of oxidation reactions [6, 11]; and (4) minimized occurrence of homogeneous thermochemical reactions involving O_2 which can produce soot-forming precursors [12].

Furthermore, if the resulting synthesis gas is used to produce Fischer-Tropsch liquids or oxygenated hydrocarbons via hydroformylation, CO_2 reforming provides a potential environmental benefit through its utilization of CO_2 as a feedstock.

Mixed-conducting ceramics have typically been investigated for use with the partial oxidation of methane (POM) because of the appropriately high operating temperatures and the strongly reducing environment created by the POM reactions. The high reactor temperature allows effective membrane oxygen transport with no additional energy requirement, while the reducing POM environment provides a large oxygen potential gradient even with atmospheric pressure air on the oxygen source side. POM is a desirable commercial reaction because its stoichiometric $H_2:CO$ ratio of two is ideal for Fischer-Tropsch synthesis of liquid hydrocarbons (F-T liquids) and, unlike steam and CO_2 reforming, it is an exothermic reaction which reduces energy costs. These incentives, coupled with the expense of the conventionally-produced oxygen currently required for partial oxidation, have led to its dominance of the membrane reactor field of inquiry. However, partial oxidation reactions may not be the most appropriate reaction for oxygen-conducting ceramic membranes because of the potentially irreconcilable requirements of high flux and high stability under the extreme oxygen gradients created by the hydrogen-containing environment on the reaction side of the membrane.

Many materials have been identified with measurable oxygen transport ability, but only minimal success fabricating membranes that might satisfy the requirements of commercial partial oxidation applications has been achieved to date. As a general rule, materials with sufficient flux to be of interest for partial oxidation reactions are not chemically or mechanically stable enough to be

used industrially in partial oxidation reactors. More stable materials may be available, but their ability to conduct oxygen is much more likely to be limited. The oxygen-conduction property requires a lack of chemical stability because it requires the repeated creation and filling of oxygen vacancies in the ceramic lattice. The easier these oxygen transitions are, the higher the flux but the greater the potential under extreme oxygen gradients for mechanical instability and/or transitions to phases with lower oxygen transport capability.

1.2: Scope of the Investigation

This investigation began with the proposition that lower oxygen fluxes that are currently attainable with more stable materials could benefit other reactions that do not require oxygen as a primary reactant but could benefit from small amounts of oxygen. Such reactions must also meet the necessary operating condition requirements of oxygen-conducting ceramic membranes: i.e., a reducing or oxygen-consuming reaction environment and a high-enough operating temperature. CO₂ reforming satisfies these operating constraints and has also been shown to benefit from oxygen in the feed [13-15].

As an additional incentive to use CO₂ reforming as the test reaction, some studies of oxygen-conducting ceramic membranes for partial oxidation of methane have shown that including CO₂ in the reaction feed or diluting the methane with small amounts of inert gas or oxygen creates a less reducing environment that can prolong membrane lifetime [16-17]. Thus, membranes that might not be capable of withstanding the severe reducing conditions of partial oxidation reactions could still be acceptable candidates for facilitating certain reactions. The use of very small amounts of oxygen (i.e., less than 10 mol% of the reactor feed) to enhance catalyst activity for CO₂ reforming is defined herein as “oxygen-assisted CO₂ reforming.”

A single membrane material was studied in this work: the non-perovskite SrFeCo_{0.5}O_x mixed oxide referred to henceforth as SFC. To evaluate the potential effect of an oxygen-conducting

ceramic membrane on CO₂ reforming, a variety of test scenarios were evaluated. SFC membranes were modified with micron-scale patterns and contiguous nano-scale layers of catalytic materials. They were tested with and without deposited materials and with and without conventional powder reforming catalysts. The deposited catalyst patterns required a flat membrane surface, so all tests were performed with disk-shaped membranes.

The membrane geometry and the desire to have the option of performing multiple tests with the same membrane required the development of a unique reactor system. Also, this was the inaugural project in the area of membrane reactors for the Stagg-Williams group. Reactor and analytical system development therefore constituted a major portion of the work for this project.

1.3: Objectives

This work encompasses five broad objectives:

- 1) Develop a reactor system for testing disk-shaped membranes
- 2) Test SFC membranes for flux
- 3) Test SFC membranes in methane conversion reactions (catalyst-patterned membranes and plain membranes with and without conventional powder catalysts)
- 4) Determine the effect of SFC membranes on CO₂ reforming, particularly on catalyst activity for methane conversion and on net reaction profiles as evaluated by product distribution and reactant conversion
- 5) Provide a sound experimental and theoretical foundation for future work to elucidate and improve the observed membrane effect.

The experimental techniques developed in this work will provide benefits that are directly transferable to other promising O-MIEC materials such as BaCo_{0.4}Fe_{0.4}Zr_{0.2}O_x [9] and Ba_{0.5}Sr_{0.5}Co_{0.8}Fe_{0.2}O_x [18] and to other membrane geometries. This dissertation presents the development and details of the membrane reactor system needed to perform this kind of work as well

as a thorough analysis of the initial results acquired with SFC membranes. The structure of the dissertation follows the development of the ideas involved rather than the chronological development of the daily work.

1.4: Structure of the Dissertation

Chapter 2 discusses the state of the art regarding O-MIEC membrane reactors for synthesis gas production in general and the SFC membrane material in particular. It also introduces the fundamental concepts for the work to follow, including a discussion of the decision to evaluate membrane reactors for CO₂ reforming rather than partial oxidation.

Chapters 3 and 4 provide an overview of the test materials and analytical equipment utilized in this work as well as the experimental approaches for both flux and reaction testing. An overview of the membrane fabrication process is included in Chapter 3. Chapter 4 focuses exclusively on reactor design and assembly.

Chapters 5 through 9 examine test results from all periods and modes of reaction testing. Chapters 5, 6, and 9 present and discuss reaction results as distinguished by reactor and catalyst used. Chapter 7 evaluates the potential mechanistic role of membrane oxygen, and Chapter 8 defends the proposition that the relationship between catalyst activity and reaction product distribution indicates catalyst oxidation state during reaction. The oxidation state hypothesis is derived from the possibility that the presence of the SFC membrane allows a powder catalyst to maintain a less oxidized state for a longer period of time.

Finally, the Appendices provide additional information about O-MIEC membranes, SFC, membrane fabrication, reactor operation, and reaction data analysis. As the main body of the dissertation focuses on CO₂ reforming reaction testing, the Appendices also contain a summary of oxygen flux testing without reaction.

References Cited in Chapter 1

1. Balachandran, U., J.T. Dusek, P.S. Maiya, B. Ma, R.L. Mieville, M.S. Kleefisch and C.A. Udovich, *Ceramic membrane reactor for converting methane to syngas*. Catal Today **36**, 1997, p.265-272.
2. Bouwmeester, H.J., *Dense ceramic membranes for methane conversion*. Catal Today **82**, 2003, p.141-150.
3. Dyer, P.N., R.E. Richards, S.L. Russek and D.M. Taylor, *Ion transport membrane technology for oxygen separation and syngas production*. Sol St Ionics **134**, 2000, p.21-33.
4. Feng, S.J., S. Ran, D.C. Zhu, W. Liu and C.S. Chen, *Synthesis gas production from methane with SrFeCo_{0.5}O_y membrane reactor*. Energy & Fuels **18**, 2004, p.385-389.
5. Maiya, P.S., U. Balachandran, J.T. Dusek, R.L. Mieville, M.S. Kleefisch and C.A. Udovich, *Oxygen transport by oxygen potential gradient in dense ceramic oxide membranes*. Sol St Ionics **99**, 1997, p.1-7.
6. Ritchie, J.T., J.T. Richardson and D. Luss, *Ceramic membrane reactor for synthesis gas production*. AIChE Jnl **47**(9), 2001, p.2092-2101.
7. Robinson, E.T., S. Aasland and J. Chen. *The application of oxygen transport membranes for syngas or hydrogen production*. in *2004 AIChE Spring Meeting*. 2004.
8. Sammells, A.F., M. Schwartz, R.A. Mackay, T.F. Barton and D.R. Peterson, *Catalytic membrane reactors for spontaneous synthesis gas production*. Catal Today **56**, 2000, p.325-328.
9. Tong, J., W. Yang, R. Cai, B. Zhu and L. Lin, *Novel and ideal zirconium-based dense membrane reactors for partial oxidation of methane to syngas*. Catal Letters **78**(1-4), 2002, p.129-137.
10. Tsai, C.-Y., A.G. Dixon, Y.H. Ma, W.R. Moser and M.R. Pascucci, *Dense perovskite La_{1-x}A'_xFe_{1-y}Co_yO_{3-δ} (A' = Ba, Sr, Ca) membrane synthesis, applications, and characterization*. J Amer Ceram Soc **81**(6), 1998, p.1437-1444.
11. Papp, H., P. Schuler and Q. Zhuang, *CO₂ reforming and partial oxidation of methane*. Topics in Catalysis **3**, 1996, p.299-311.
12. Spivey, J.J. in *232nd ACS National Meeting*. 2006. San Francisco.
13. O'Connor, A.M. and J.R.H. Ross, *The effect of O₂ addition on the carbon dioxide reforming of methane over Pt/ZrO₂ catalysts*. Catal Today **46**, 1998, p.203-210.
14. Souza, M.M.V.M. and M. Schmal, *Combination of carbon dioxide reforming and partial oxidation of methane over supported platinum catalysts*. Appl Cat A **255**, 2003, p.83-92.
15. Wang, W., S.M. Stagg-Williams, F.B. Noronha, L.V. Mattos and F.B. Passos, *Partial oxidation and combined reforming of methane of Ce-promoted catalysts*. Catal Today **98**, 2004, p.553-563.

16. Gu, X., L. Yang, L. Tan, W. Jin, L. Zhang and N. Xu, *Modified Operating Mode for Improving the Lifetime of Mixed-Conducting Ceramic Membrane Reactors in the POM Environment*. *Ind Eng Chem Res* **42**, 2003, p.795-801.
17. Tsai, C.-Y., A.G. Dixon, W.R. Moser and Y.H. Ma, *Dense perovskite membrane reactors for partial oxidation of methane to syngas*. *AIChE Jnl* **43**(11A), 1997, p.2741-2750.
18. Slade, D.A., Q. Jiang, K.J. Nordheden and S.M. Stagg-Williams, *A comparison of mixed-conducting oxygen-permeable membranes for CO₂ reforming*. *Catal Today* **148**, 2009, p.290-297.

Chapter 2: Motivation and State of the Art

2.1: Syngas from Methane

In recent decades, natural gas (i.e., mixtures of methane and other small hydrocarbons) has progressed from a low-value commodity that was commonly flared off during oil processing to one of our cleanest, most valuable, and most scrutinized natural resources. Although conventional natural gas combustion will undoubtedly continue to dominate consumption for the foreseeable future, two additional uses have renewed interest in natural gas. Methane's established role as a hydrogen source has led to investigations of natural gas as a feedstock for hydrogen production to support fuel cell applications, and the inconvenient location of many large natural gas reserves has generated great interest in the production of increasingly desirable liquid fuels via gas-to-liquids (GTL) synthesis processes. These two applications both depend on the production of mixtures of hydrogen and carbon monoxide known as “synthesis gas” (or *syngas*), which are the critical intermediates in the production of hydrogen and ultra-clean liquid fuels from hydrocarbons such as natural gas.

Diminishing global oil reserves and increasing public desire for “clean” energy sources have led to a recent upsurge in interest in expanding hydrogen production and also in increasing natural gas utilization in general. Natural gas is difficult to transport cheaply and safely from remote locations, which has allowed the continued existence of large and largely untapped reservoirs around the world. GTL technologies such as Fischer-Tropsch synthesis and methanol synthesis have thus received renewed attention for their ability to create conveniently transported—and extremely clean—synthetic liquid fuels in stand-alone natural gas processing facilities.

Syngas-based hydrogen production and GTL technologies are not new, but the inefficiencies of the conventional processes indicate they are not as optimized as more competitive industries tend to be, particularly in the syngas production step. It has been estimated that syngas production alone accounts for 60% or more of the cost of such natural gas upgrading processes [1]. The prospects of

both a major inroad into the developing hydrogen economy and a promising means of safely utilizing remote natural gas reserves therefore depend greatly on improving syngas production efficiency.

2.1.1: Overview of reforming reactions

Several net reactions are commonly used to produce syngas from hydrocarbons (Table 2.1). The choice of reaction(s) depends on the feedstock and the desired H₂:CO ratio in the products. Only methane will be discussed in this work as the hydrocarbon feedstock, but syngas can be produced from any hydrocarbon using the same basic set of reactions. The stoichiometry of the reactants and products will vary with the hydrocarbon feedstock but the net reaction categories are the same.

NOTE: the use of the term “net reactions” is a reference to the fact that these are not fundamental reactions but are rather the stoichiometric manifestations of multiple fundamental reactions such as methane decomposition, carbon oxidation, etc.

Table 2.1: Summary of relevant net reactions

| Net Reaction | Chemical Equation | ΔH_{298K}° [$\frac{kJ}{mol}$] | Product H ₂ :CO Ratio |
|---------------------------|--|--|----------------------------------|
| Partial oxidation | $CH_4 + \frac{1}{2} O_2 \rightarrow CO + 2H_2$ | -36 | 2 |
| Steam reforming | $CH_4 + H_2O \rightarrow CO + 3H_2$ | +206 | 3 |
| CO ₂ reforming | $CH_4 + CO_2 \rightarrow 2CO + 2H_2$ | +247 | 1 |
| Water-Gas Shift | $CO + H_2O \rightleftharpoons CO_2 + H_2$ | -41 | NA |
| Combustion | $CH_4 + 2O_2 \rightarrow CO_2 + 2H_2O$ | -802 | NA |

Partial oxidation has an H₂:CO ratio of 2:1 that is ideal for the Fischer-Tropsch and methanol GTL syntheses of liquid fuels [2], but this reaction requires a large amount of oxygen. The nitrogen in air precludes its direct use as the oxygen supply, and pure gas-phase oxygen is an expensive—and hazardous—feedstock. In the conventional industrial process for partial oxidation of methane (or *POM*), the cryogenic air separation unit is typically the most expensive aspect of the *POM* syngas production facility [3]. Any reduction in the cost of supplying oxygen to such a system would

directly lower its production costs and thus increase its competitiveness. Dyer et al. estimated in 2000 that a 25% reduction in the cost of current GTL technology would make GTL products competitive with oil at \$20/barrel and pointed out that such price parity would substantially increase GTL production [4].

Steam reforming's higher product $H_2:CO$ ratio makes it the most desirable for hydrogen production, but its endothermicity is an expensive attribute, even more so because the target temperatures for these reactions with methane are at least 750 °C. One solution is to combine steam reforming with partial oxidation in a process known as *autothermal reforming*. Although the oxygen requirement for autothermal reforming is less than that for partial oxidation, it is still substantial. Compared to straight steam reforming for hydrogen production, autothermal reforming nevertheless provides an attractive energy savings.

CO₂ reforming has not received as much industrial attention to date as the aforementioned reactions, largely because of the tendency for carbon deposition but also because of its unfavorable energetics. However, hydroformylation processes require the 1:1 $H_2:CO$ ratio produced by CO_2 reforming, and CO_2 is an increasingly undesirable byproduct of our fossil fuel energy industries. Both of these circumstances encourage an investigation into techniques to make CO_2 reforming a more feasible alternative.

As syngas is conventionally produced by steam reforming or partial oxidation reactions that produce $H_2:CO$ ratios of two or greater, CO_2 reforming with its stoichiometric $H_2:CO$ ratio of one is a potentially useful sidestream reaction for decreasing the overall $H_2:CO$ ratio in a synthesis gas product to meet target ratios less than two. Ratios between one and two are needed for both hydroformylation and certain Fischer-Tropsch reactions.

Another potential approach to producing $H_2:CO$ ratios between one and two is the use of *combined reforming* (i.e., a combination of partial oxidation and CO_2 reforming). Combined

reforming has been explored with the intention of decreasing the endothermicity from straight CO₂ reforming and increasing catalyst life by reducing carbon deposition [5-17]. It also offers the potential for “tuning” the H₂:CO ratio via manipulation of the ratio of O₂ and CO₂ in the reactor feed. Adding small amounts of oxygen to promote catalyst performance and decrease the energy requirements of CO₂ reforming could bring this potentially valuable syngas production reaction closer to mainstream industrial application.

Unfortunately, combined reforming requires pure oxygen as a feedstock, and an energy-intensive air separation unit represents a substantial capital and operating cost. For example, about one-third of a methane partial oxidation (POM) synthesis gas facility’s operating costs and up to 45% of its capital costs can come from the air separation unit alone [18]. Improving the oxygen supply route for syngas production processes appears to offer an excellent opportunity to revolutionize the syngas-dependent sector of the burgeoning clean energy industry. Once they are robust enough, high flux O-MIEC membranes offer the potential to replace separated oxygen gas in future combined reforming processes.

Using even smaller amounts of oxygen, such as those readily supplied by currently available lower flux O-MIEC ceramic membranes, is a realistic option today. Very small amounts of oxygen (e.g., less than 2% of the feedstream) would not affect the H₂:CO ratio significantly, but they could improve catalyst performance sufficiently to make *oxygen-assisted CO₂ reforming* a feasible alternative for producing syngas with an H₂:CO ratio of approximately one. This work investigates the potential benefits of this approach to syngas production.

2.2: Oxygen Conducting Ceramic Membranes (O-MIEC ceramics)

The high costs associated with pure oxygen have provided the motivation to explore the use of mixed ionic-electronic conducting ceramic membranes (O-MIECs) as an alternative oxygen source for syngas production reactors [1-4, 19-25]. Unlike the oxygen-conducting ceramic membranes used

in solid-oxide fuel cells such as yttria-stabilized zirconia (YSZ), the ability of O-MIECs to conduct electron and oxygen ions simultaneously enables these membranes to operate without an external electron circuit. O-MIEC ceramic membranes require only an imposed oxygen potential gradient and sufficiently high temperatures to transport oxygen from the high oxygen content side to the low oxygen content side.

In addition to syngas production applications, O-MIECs are being investigated for use as oxygen sensors and in safer, lower-cost oxygen supply systems [4, 26], as well as to improve methane coupling and selective ethane oxidation reactors [27-30]. At temperatures above their effective activity thresholds (typically greater than 600 °C [20]), dense oxygen-conducting ceramics can be characterized in general as exhibiting

- highly mobile lattice oxygen ions
- continuously variable oxygen content (i.e., oxygen nonstoichiometry) via the ability to support lattice oxygen defects and/or undergo gradual, dispersed phase changes
- the surface abilities to dissociate molecular oxygen while incorporating oxygen ions and to re-associate oxygen ions while evolving molecular oxygen.

Under an oxygen potential gradient and above some threshold temperature a perfectly sealed, fully densified mixed-conducting oxygen-conducting ceramic would exhibit perfectly selective oxygen production [2]. At temperatures between their respective activity threshold and degradation temperatures, O-MIEC ceramic membranes exhibit oxygen fluxes that generally increase with both temperature and the imposed oxygen gradient. If an O-MIEC membrane were used in place of co-fed gaseous oxygen, the benefits of combined reforming or oxygen-assisted CO₂ reforming could be obtained while minimizing the associated costs.

The major challenge in developing these membranes and transferring them to the field involves the incompatible requirements of high oxygen transport and high material stability. These requirements have proven particularly difficult to reconcile in the strongly reducing environments of

methane conversion reactors. This work provides new insight into the effect of O-MIEC ceramic membranes on CO₂ reforming with a conventional powder catalyst and also evaluates the effect of catalytic material deposition on O-MIEC membrane performance.

2.2.1: O-MIECs for methane conversion

The aforementioned need to improve the oxygen supply situation for syngas production reactions coincides well with the capabilities of dense ceramic O-MIECs. The high temperature required for effective oxygen transport can be a significant drawback for currently available O-MIECs in other possible applications, but it represents an advantage for syngas production reactors. Methane partial oxidation and reforming reactions require a temperature of 800 °C or greater for acceptable syngas selectivity [23], which matches the lower end of the temperature range for high oxygen conduction rates through ceramic O-MIECs. The potential for 100% selectivity for oxygen over nitrogen also offers a compelling improvement on conventional equilibrium-limited cryogenic air separation, providing, among other advantages, a corresponding decrease in NO_x emissions [20].

Other advantages include the inherent distributed delivery of oxygen in an O-MIEC reactor, including avoidance of the hotspot and flammability issues that can be a problem with co-fed methane and oxygen [2, 22]. Gradual oxygen introduction can also improve the yield of partially and/or easily oxidized products such as carbon monoxide and hydrogen [23]. The absence of gas-phase oxygen could even minimize the occurrence of homogeneous thermochemical reactions involving O₂ that can produce soot precursors [31].

Although these are all compelling incentives, the most publicized benefit of membrane-based syngas reactors is the obviation of the expensive air separation unit required in a conventional syngas production facility. In addition to reducing capital costs by up to 35% [20], O-MIEC reactors can reduce operating costs as well, most dramatically in a self-heating POM facility. Regarding industrial emissions, Robinson et al. estimate that an O-MIEC based autothermal steam reformer could increase

hydrogen yields by up to 21% over those from a conventional industrial plant while simultaneously reducing NO_x emissions by more than 50% and CO₂ emissions by about 20% [20].

A large number of ceramic O-MIEC materials have been and continue to be developed, but the concurrent needs for high oxygen transport and high material stability in the harsh environment of a methane conversion reactor have been difficult to satisfy. In spite of more than two decades of work on this problem, no published evidence is available that O-MIEC technology for synthesis gas production has been implemented on a commercial scale. However, a body of knowledge on O-MIECs in general has been amassed over the years and a number of promising techniques have been developed for improving membrane performance in less demanding environments such as air separation systems. These developments may eventually lead to a membrane with sufficient oxygen transport and mechanical integrity for partial oxidation reactor applications. In particular, the deposition of micro- or nano-scale patterns or layers of active materials on the surface of an acceptably stable O-MIEC offers an intriguing means of improving membrane performance without compromising mechanical stability.

2.2.2: O-MIEC compositions

Because the vast majority of O-MIEC ceramics examined in the literature belong to the perovskite category of metal oxides, while others contain significant perovskite phase percentages, discussions herein will focus on perovskite oxygen transport characteristics. Any metal oxide with the general formula ABO₃, where A is the larger cation with a 12-fold oxygen ion coordination and B is the smaller cation with a 6-fold coordination, is considered to be a perovskite oxide. A-site choices in the literature include La, Sr, and Ba, while B-site choices include Fe, Co, Cr, Cu, Mn, Ga, and Ni. Table 2.2 in Section 2.5 contains several examples of O-MIEC compositions that have been tested as part of POM membrane reactors. The oxygen conduction phenomenon exhibited by certain perovskite oxides is believed to arise from their ability to support oxygen vacancies and lattice

disorder, allowing the relatively rapid and sustainable transport of oxygen ions and holes under the appropriate conditions.

An important closely related metal oxide structure is the orthorhombic brownmillerite structure ($ABO_{2.5}$). This is essentially a highly ordered perovskite derivative with high oxygen vacancy that can appear when a variable oxygen content perovskite phase approaches an oxygen deficiency of 16.7% (i.e., one-sixth) [2]. It is generally believed that the highly ordered oxygen ion vacancies in brownmillerites lead to low oxygen flux because the brownmillerite phase is more stable than the related perovskite and does not support oxygen hole transport. However, at high enough temperature brownmillerite phases may disorder sufficiently to return the material to a high-vacancy perovskite structure with higher oxygen transport capability [3, 26, 32-34]. To state this concept another way, oxygen flux can suffer if perovskite oxygen deficiency reaches a level that encourages the formation of highly-ordered low-oxygen phases.

2.3: In situ Membrane Behavior

2.3.1: Oxygen nonstoichiometry and membrane fracture

Membrane fracture, which is the common shortcoming of ceramic O-MIEC materials, particularly in partial oxidation applications [2], can result from chemical decomposition in the form of phase conversion and segregation or from lattice expansion mismatch within either a single phase or stable set of phases [3, 35]. It is well established that equilibrium oxygen ion content in these materials varies with both temperature and ambient oxygen partial pressure, and oxygen content losses beyond a material's phase stability limit can cause the aforementioned chemical decomposition. Under a constant oxygen partial pressure, equilibrium oxygen ion content decreases with increasing temperature until some constituents, particularly cobalt but also iron, can even be reduced to their metallic state by temperature alone [36]. A reducing atmosphere (e.g., one

containing hydrogen and/or methane or, according to Ma et al., one with an oxygen partial pressure $< 10^{-6}$ atm [37]) can produce the same effect at even lower temperatures [32, 38].

Contrary to mass balance-oriented intuition, dense O-MIECs actually expand as their oxygen content decreases. Lowered oxygen content increases lattice oxygen vacancies and reduces the oxidation states of a portion of the membrane's metal ions, both of which diminish the material's overall binding forces and allow it to expand even under isothermal conditions [39-42]. To illustrate the potential extent of this expansion, the brownmillerite-to-perovskite phase transition described in Section 2.2.2 has been observed to produce a unit cell volume increase of up to 6% for $\text{SrCo}_{0.8}\text{Fe}_{0.2}\text{O}_x$ (or *SCFO*) [40]. Adler has proposed that this "chemical expansivity" should be considered a new physical property for these materials, concluding that chemical expansion from oxygen content decrease can be significantly greater than pure thermal expansion and arguing that labeling as thermal expansion the volume increases of oxygen-conducting MIECs during temperature increases oversimplifies the phenomenon [39].

A chemical expansion gradient is also a much more likely explanation for a fracture-inducing density gradient than a thermal expansion gradient. Electronic conductivity is a characteristic feature of these mixed-conducting materials at functional temperatures and is necessary to their oxygen transport function. The Wiedemann-Franz Law states that the ratio of thermal conductivity to electronic conductivity increases with temperature for solid materials. At temperatures high enough to conduct electrons (i.e., approaching 1000 K), these materials should therefore exhibit sufficient thermal conductivity to make reasonable an assumption of nearly isothermal behavior at steady state.

The membrane's lattice oxygen content, on the other hand, is clearly not isocratic, so a chemical expansion gradient is inevitable. The likelihood that an imposed chemical gradient will be more extreme than a possible thermal gradient further supports the argument that chemical expansion

under operating conditions is both greater and more important than thermal expansion. It also undermines the idea that thermal expansion might be a primary cause of membrane fracture.

2.3.2: Self-adjusting phase equilibria

For metal oxide materials with such labile oxygen ions, phase adjustments are to be expected following changes in oxygen environment and/or temperature. Studies using *in situ* x-ray diffraction (XRD) have confirmed the ubiquity of responsive phase adjustments in O-MIEC ceramics, from Pei et al. in 1995 [35] to Wang et al. in 2005 [43]. Depending on both the material and the new environment, a change can occur throughout the entire membrane or it can be highly localized (e.g., only at a surface or as distributed pockets of a newly formed phase in an equilibrium mixture of phases) [24, 32, 38]. For a material with a large variety of phase options that is exposed to a persistent oxygen partial pressure gradient, it is reasonable to expect the formation of a phase composition gradient that reflects the electrochemical oxygen potential gradient in the membrane.

Numerous researchers have confirmed that certain materials—most notably SFC—can consist entirely of intimately intermixed phases (see Figure B.1 in Appendix B). Such mixtures are referred to as “phase assemblages” or “solid solutions” and they will adjust their phase distribution according to their environment [44-47]. Phase distribution changes in O-MIEC ceramics have been observed to be readily reversible [22, 35, 37], making their equilibrium phase compositions highly sensitive to temperature and gaseous environment [45]. However, phase transition kinetics for solid phase equilibrium transitions may be slow enough at lower temperatures that phase change reversibility can be masked or suspended [48]. The O-MIEC phase change attribute with perhaps the broadest ramifications is the possibility for reduced oxygen environments to allow phase transitions to occur at lower temperatures than were observed in higher oxygen environments [47]. This final phenomenon confirms that equilibrium phase compositions are determined by membrane oxygen content, which, as discussed earlier, depends on both temperature and oxygen partial pressure.

2.3.3: Reforming reactor conditions

An isothermal membrane exposed simultaneously to two different oxygen partial pressures experiences non-uniform chemical expansion (or contraction) to a degree that depends on the material phases present and the ratio of the oxygen partial pressures [35, 42]. The oxygen concentration gradient across a partial oxidation reactor membrane with a permeate side oxygen partial pressure of between 10^{-17} and 10^{-30} atm at 850 °C [1, 19, 23] is much more extreme than the gradient during a typical oxygen flux test with a permeate-side sweep gas oxygen partial pressure of 10^{-3} – 10^{-5} atm [23, 34, 48]. Considering the much larger chemical expansion gradient in a membrane reactor, among other differences, it is not surprising that a greater number of successful oxygen flux studies have been reported than successful POM membrane reactor studies. The very properties that give some materials high oxygen diffusivity can make them unfit for use in methane conversion applications [20].

The largest practical challenge facing designers of oxygen-conducting ceramic membranes is clearly the need to simultaneously maximize oxygen conduction—which should correlate positively with bulk oxygen absorption/desorption capacity and lattice contractions/expansions—and membrane mechanical stability, which should exhibit an inverse correlation with these characteristics.

2.4: Membrane Performance Criteria

A long-standing oxygen flux target for industrial application of dense O-MIEC membranes is 1 standard $\text{cm}^3/\text{min}/\text{cm}^2$ (i.e., 1 sccm/ cm^2) [26]. Published studies have reported a wide variety of oxygen flux results ranging from 0.001 to ~ 1 sccm/ cm^2 under an air:inert gradient, and this range has been increased to 0.1 to 10 sccm/ cm^2 with the assistance of a catalyst-facilitated oxygen-consuming reaction on the permeate side (Table 2.2 in Section 2.5 provides examples). In addition to high oxygen transport, a successful membrane material must also exhibit long-term physical and chemical stability in the high temperature environments it will encounter. In the case of membrane reactors for

synthesis gas production from methane, the material will be used continuously at temperatures as high as 1000 °C with its oxygen source side exposed to air and its permeate side exposed to a highly reducing environment containing variable mole fractions of methane and hydrogen. The membrane material must therefore withstand simultaneously two very different external environments as well as the resulting internal oxygen potential gradient that drives the diffusion of oxygen ions.

2.5: Oxygen Flux in Membrane Reactors

Table 2.2 provides an overview of published oxygen flux results for ceramic O-MIEC materials tested as dense membranes under similar conditions.

Table 2.2: Oxygen flux results for various membrane materials; test temperature of 850 °C and membrane thickness of ~1 mm unless noted otherwise

| O-MIEC Material | Air:Inert Gradient [sccm/cm ²] | Air:POM Gradient [sccm/cm ²] |
|--|--|--|
| SrFeCo _{0.5} O _x [3, 44-45, 48-49] | 0.001 – 0.13 | 0.3 (80% CH ₄ feed; no catalyst; 350 hrs) [3] 3 (80% CH ₄ ; Rh catalyst; 500 hrs; 900 °C) [3] |
| SrCo _{0.8} Fe _{0.2} O _x [3, 22, 34] | 0.1 – 0.9 | Fractured quickly [3, 22] |
| La _{0.6} Sr _{0.4} Co _{0.8} Fe _{0.2} O _x [38] | 0.1 (900 °C) | 0.1 (25% CH ₄ ; no catalyst; 900 °C) |
| La _{0.2} Ba _{0.8} Fe _{0.8} Co _{0.2} O _x [24] | 0.8 | 4 (5% CH ₄ feed; Ni catalyst; 500 hrs) |
| La _{0.5} Sr _{0.5} Fe _{0.8} Ga _{0.2} O _x [23] | 0.14 (2 mm thick) | NA |
| | 0.23 (150 μm) | 0.34 (100% CH ₄ feed; Rh catalyst; 10 hrs) |
| BaCo _{0.4} Fe _{0.4} Zr _{0.2} O _x [22] | 0.6 | 5.5 (50% CH ₄ feed; Ni catalyst; > 2000 hrs) |
| Ba _{0.5} Sr _{0.5} Co _{0.8} Fe _{0.2} O _x [25, 50] | 1.15 – 1.5 (1.8 mm thick) | 10.45 (50% CH ₄ feed; LiLaNi catalyst; 500 hrs) [25] |
| | | 8.5 (43% CH ₄ , 14% CO ₂ , 43% He feed; LiLaNi catalyst; 100 hrs; 900 °C) [50] |
| Ba _{0.5} Sr _{0.5} Co _{0.8} Fe _{0.2} O _x (bilayer membrane w/ 400 μm dense layer) [51] | 0.8 (800 °C) | 2.2 (40% CH ₄ , 40% CO ₂ , 20% Ar; Pt catalyst; 800 °C) |
| proprietary [4, 21], but possibly Sr _{0.85} La _{0.15} Fe _{0.7} Ga _{0.3} O _x [22] | NA | 10 (80% CH ₄ ; proprietary catalysts (both reaction and source sides); > 1 yr; 900 °C) [21] |

Although a few laboratory successes have been reported, membrane reactor work has often either been limited to short run times [23] or employed undesirable mitigating factors such as methane feed stream dilution with inert gas or even gas-phase oxygen to increase the effective oxygen potential on the permeate side [22, 24, 52]. Additionally, published accounts tend not to acknowledge the extent of the membrane integrity issues encountered [53-54].

2.6: CO₂ Reforming with O-MIEC Membranes

Published studies of mixed-conducting ceramic membranes have typically focused on partial oxidation of methane (POM) because of its appropriately high operating temperatures and the large oxygen gradient created by the strongly reducing environment of the POM reaction. These are the appropriate conditions for high oxygen flux through the membrane material, but they can also destabilize the membrane through the mechanisms discussed in Section 2.3. The absence of a commercial membrane partial oxidation facility emphasizes the difficulty of achieving both high oxygen flux and high mechanical stability.

However, mechanically stable but lower flux membranes could benefit other reactions with appropriate operating conditions for membrane activity, and CO₂ reforming is an obvious example of such a reaction. CO₂ reforming shares the reducing reaction environment and high operating temperature of POM but is so prone to catalyst deactivation by carbon deposition that much of the published work on CO₂ reforming focuses on increasing useful catalyst life by decreasing or modifying carbon deposits [55-61]. If an oxygen-conducting ceramic membrane could be used in place of co-fed gas-phase oxygen, the benefits of oxygen-assisted CO₂ reforming (for low flux membranes) or combined reforming (for high flux membranes) could be obtained without the costs and operational disadvantages associated with gas-phase oxygen.

In addition to the potential benefit of membrane oxygen on catalyst deactivation, CO₂ in a membrane reactor feed might also have a beneficial effect on membrane stability. Studies of low

stability O-MIEC ceramics have shown that adding CO₂ to the permeate-side feed stream can reduce the likelihood of membrane fracture [52, 62]. The potential for mutual benefits indicates that CO₂ reforming might be the most appropriate reaction choice in general for ceramic membrane syngas reactors. Furthermore, the smaller oxygen requirement of oxygen-assisted CO₂ reforming brings a selection of lower flux but mechanically stable membrane materials into consideration as candidates.

2.6.1: Overview of published work on combined reforming

As discussed in Section 2.1.1, including oxygen in a CO₂ reforming feed has been explored with the objectives of decreasing carbon deposition and thereby increasing catalyst activity and useful lifespan, manipulating H₂:CO ratio, and manipulating the energetics of the reaction system to achieve a self-sustaining operating temperature [5-17]. Table 2.3 provides an overview of the molar reactor feed compositions used in published combined reforming work.

Table 2.3: Overview of molar reactor feed compositions in published combined reforming studies

| Investigators (Year) [Ref] | CO₂:CH₄ | O₂:CH₄ | O:C | Inert dilution |
|---|--------------------------------------|-------------------------------------|--------------------|-----------------------|
| Vernon, et al. (1992) [15] | 0.05 – 0.98 | 0.03 – 0.5 | 0.98 – 1.05 | none |
| O'Connor, et al. (1998) [5] | 0.11 – 0.67 | 0.17 – 0.44 | 1 | 60 – 70% He |
| Souza and Schmal (2003) [6] | 0.5 | 0.25 – 0.5 | 1 – 1.33 | 80 – 83% He |
| Wang, et al. (2004) [7] | 0.33 – 0.75 | 0.25 – 0.33 | 1 – 1.2 | none |
| Choudhary, et al. (2006) [8-10] | 0.14 – 0.39 | 0.34 – 0.5 | 1.05 – 1.12 | none |
| Jing, et al. (2004, 2006) [11-12] | 0.2 – 0.5 | 0.25 – 0.4 | 1 | none |
| Guo, et al. (2008) [16] | 0.15 – 0.83 | 0.09 – 0.43 | 1 | none |
| He, et al. (2009) [13-14] | 0.4 | 0.3 | 1 | none |
| Michael, et al. (2009) [17] | 1 – 1.75 | 0.38 – 0.61 | 1 – 1.64 | 35 – 70% Ar |
| Shao, et al. [50] (<i>membrane oxygen</i>) | 0.33 | 0.32 | 0.98 | 38% He |
| Range of published work | 0.05 – 1.75 | 0.03 – 0.61 | 0.98 – 1.64 | 0 – 83% |
| <i>Stoichiometric partial oxidation</i> | -- | 0.5 | 1 | -- |
| <i>Stoichiometric CO₂ reforming</i> | 1 | -- | 1 | -- |
| <i>Proposed range for “oxygen-assisted CO₂ reforming”</i> | ≥ 0.8 | ≤ 0.1 | 1 – 1.2 | -- |

As predicted by both thermodynamics and stoichiometry, these studies all show increasing methane conversion with increasing oxygen content in the feed. They also consistently observe lower (or no) carbon deposition with the inclusion of oxygen in the reactor feed. As a general rule, atomic O:C ratios greater than one allow the possibility of significant hydrogen and/or carbon monoxide oxidation, while ratios less than one can allow coke deposition via excess methane decomposition.

All of the referenced studies used a small amount of CO₂ relative to the stoichiometric CO₂ reforming ratio of one—typically 50% or less of the stoichiometric ratio—and at least 50% of the stoichiometric O₂:CH₄ ratio for partial oxidation. Several studies include lone exceptions to this rule, with more CO₂ and less O₂ in the feed. The two most extreme exceptions are a single test by Vernon et al. that used a CO₂:CH₄ ratio of 0.98 and only 1.4 mol% O₂ in the feed [15] and a single test by Guo et al. with CO₂:CH₄ ratio of 0.83 and an O₂:CH₄ ratio of 0.09 [16]. Other than these two individual tests, the available published work falls into the category of “combined reforming,” in that the amounts of CO₂ and O₂ fed are fairly balanced and the studies generally emphasize partial oxidation over CO₂ reforming. Also, the majority of the oxygen feed rates are greater than the amount of oxygen that an SFC membrane could be expected to provide.

Table 2.3 provides a preliminary definition for a new reforming reaction category referred to herein as “oxygen-assisted CO₂ reforming.” As distinguished from combined reforming, this term refers to reaction sets that are dominated by CO₂ reforming, with oxygen added only as needed to enhance or maintain catalyst activity. Oxygen-assisted CO₂ reforming is not intended to manipulate H₂:CO ratio (other than attaining and maintaining a ratio near unity) or to provide an energetically-neutral reaction set. It would instead be useful when a H₂:CO ratio of one is desired and catalyst life is a performance issue and/or when feed streams with excess CO₂ need to be utilized. As a starting point, it is suggested that oxygen-assisted CO₂ reforming of methane should be limited to feed compositions with CO₂:CH₄ ratios of 0.8 and higher and O₂:CH₄ ratios of 0.1 or less.

Only two of the 39 individual tests covered by Table 2.3 fit into the oxygen-assisted CO₂ reforming category: one each by Vernon et al. and Guo et al. It is worth noting that the high CO₂:CH₄ ratio, low O₂ test by Vernon et al. shows the highest hydrogen and carbon monoxide yields of any of their tests and nearly the highest methane conversion. They also observed no carbon deposition in any of their tests.

2.6.2: Conclusions from published work on combined reforming

Although increases in H₂:CO ratios with increasing oxygen feed are reported in the studies in Table 2.3, ratios do not approach the theoretical limits for their respective feed compositions. Hydrogen selectivity (i.e., hydrogen production relative to methane conversion) tends to decrease with increasing oxygen in the feed. This reflects either increased hydrogen oxidation relative to methane conversion as oxygen in the reactor feed is increased or more reverse Water-Gas Shift reaction (rWGS) when both oxygen (which leads to higher hydrogen levels) and CO₂ (which is a rWGS reactant) are included in the reactor feed.

O'Connor et al. measured platinum dispersion by hydrogen chemisorption before and after reaction testing and found that dispersion on a 1% Pt/ZrO₂ catalyst decreases more during reaction as oxygen content in the reactor feed is increased, with straight CO₂ reforming showing the smallest decrease in dispersion and straight POM the largest [5]. Interestingly, catalyst activity decreased faster over time with less oxygen in the feed. Coking therefore impacts Pt/ZrO₂ catalyst activity more than metal sintering, which justifies the inclusion of feed oxygen in CO₂ reforming applications.

Finally, the recently published work of Michael et al. offers several valuable insights into reaction priority in combined reforming and autothermal reforming scenarios [17]. The Michael study used an adiabatic reactor with relatively large quantities of high-load supported rhodium catalysts (5 wt% Rh) to approach equilibrium conversions with feeds comprised of various combinations of methane, oxygen, CO₂, and steam (their combined reforming tests are included in

Table 2.3). Through an impressive catalyst bed-depth analysis, the authors conclude that partial oxidation, steam reforming, and the water-gas shift reactions (forward and reverse) determine product composition in mixed reforming scenarios. They also conclude that net CO₂ reforming only occurs in the absence of water or oxygen (i.e., either when they are not included in the reactor feed or after they have been entirely consumed). When net CO₂ reforming does occur in mixed reforming conditions, the authors further propose that it is actually a combination of rWGS and steam reforming.

2.6.3: Published work on CO₂ reforming with O-MIEC membranes

Only one previous study was found in the literature that reports including CO₂ in the feed stream of an O-MIEC membrane reactor for methane reforming (Shao et al. in Table 2.3 [50]). However, their test was conducted to determine the effect of CO₂ on the O-MIEC membrane during partial oxidation of methane rather than the effect of an O-MIEC membrane on CO₂ reforming.

Shao and co-workers tested a combination of partial oxidation and CO₂ reforming of methane with a high flux Ba_{0.5}Sr_{0.5}Co_{0.8}Fe_{0.2}O_x (BSCF) membrane and an alumina-supported LiLaNiO catalyst in a single 100 hour test at 900 °C. The test was intended to determine if the presence of CO₂ in the reactor feed inhibited membrane oxygen flux via the formation of carbonates on the membrane surface. The authors observed 15% lower oxygen flux than during partial oxidation, but this can be attributed to the dilution of the feed with CO₂ and the resulting lower hydrogen production in the reactor. The test confirmed that both membrane and catalyst can function effectively with CO₂ in the reactor feed.

Only one reaction test was reported by Shao et al., so the effect of the membrane on catalyst performance could not be ascertained. Other work published by the same group indicates that—other than this one test with CO₂ in the feed—they have focused entirely on partial oxidation reactions in their ongoing membrane reactor research [25, 63-64]. Fortunately, this lone precedent supports the feasibility of using O-MIEC membranes in CO₂ reforming applications. However, with a CO₂:CH₄

ratio of 1:3 and equimolar amounts of CO₂ and dioxygen entering the reactor, CO₂ reforming cannot be considered the dominant methane conversion reaction, and the reported steady state H₂:CO ratio of 1.46 confirms that it was not.

2.6.4: O-MIEC membrane oxygen-assisted CO₂ reforming

Although work suggesting the potential industrial benefits of oxygen-assisted CO₂ reforming has been published, no work is available in the literature exploring the effect of either small amounts of oxygen (e.g., less than 10 mol% O₂ equivalent on a methane basis) or an O-MIEC membrane reactor on CO₂ reforming. CO₂ reforming with O-MIEC membranes therefore appears to be an unexplored field of study. The studies in Table 2.3 show that high flux O-MIEC membranes might be able to enhance the cost-effectiveness of combined reforming. By extension, conventional CO₂ reforming could also be enhanced by the inclusion of smaller amounts of oxygen and higher amounts of CO₂ than studied to date. Low flux/high stability membrane materials such as SFC could be valuable in such applications.

Depending on membrane oxygen flux and reactor operating conditions, O-MIEC membranes could therefore play a valuable role in certain syngas production applications for either combined reforming or oxygen-assisted CO₂ reforming. By serving as a safe, distributed, and cheap oxygen supply, they could remove the need for costly gas-phase oxygen, improve oxygen distribution and temperature control within a reactor, and provide a more desirable product distribution than co-fed gas-phase O₂.

2.7: Net Reaction Profiles as a Critical Performance Indicator

The work presented in this dissertation explores the novel proposition of using mechanically stable, lower flux O-MIEC membranes for oxygen-assisted CO₂ reforming by using catalysts that have been studied previously for CO₂ reforming and partial oxidation of methane in conventional

plug-flow reactors (PFRs). Published work on CO₂ reforming and combined reforming has focused largely on methane conversion and H₂:CO ratio as performance indicators and has typically not evaluated comprehensively the overall reactions that might actually be occurring. This is somewhat understandable when a common reactor such as a quartz-tube PFR is used for a straightforward set of catalyst comparison experiments. However, with a chemically-active membrane reactor, every clue that can be acquired regarding the potential reactions that occur during operation is essential to determining the effect (and thus the potential utility) of the membrane. A more rigorous analytical approach than is typically used for such experiments is required to even begin to understand what might be occurring in a membrane reactor.

This work focuses closely on the set of net reactions that can occur under oxygen-assisted and straight CO₂ reforming conditions (i.e., those listed in Table 2.1). Net reaction profiles (i.e., which net reactions are occurring and in what proportions) are critically important for determining the appropriateness of a catalyst or membrane for a particular application and for optimizing a reactor system once it has been selected. In this case, because an entirely new reactor type is being evaluated for CO₂ reforming of methane, net reaction profile trends will provide the key evidence needed to establish the comprehensive effect of the SFC membranes utilized in this work, as well as the effect of small amounts of co-fed O₂.

The traditional reforming reaction analysis of methane conversion and H₂:CO ratio data is insufficient to determine these effects completely. Combustion, for example, registers as methane conversion and has no effect on H₂:CO ratio but is clearly not a desirable reaction in a syngas production reactor. This investigation will therefore extend beyond the common metrics. Reactor effluent composition will be evaluated thoroughly throughout each reaction test to determine as closely as possible the individual effects of SFC membranes and co-fed O₂ on product distribution and reactant conversion over time on stream. This product distribution and reactant conversion information will then be used to evaluate trends for the net reactions in Table 2.1. This information in

turn will provide the necessary foundation to determine the true advantages, disadvantages, and potential value of both approaches to CO₂ reforming applications.

The “big picture” focus described above represents the appropriate first step in the evaluation of this novel strategy for CO₂ reforming. A comprehensive evaluation of the molecular-level effects of incorporating O-MIEC membranes into CO₂ reforming reactors is essential both to justify and to provide guidance to the more focused fundamental work that should follow if this strategy merits further pursuit.

References Cited in Chapter 2

1. Maiya, P.S., U. Balachandran, J.T. Dusek, R.L. Mieville, M.S. Kleefisch and C.A. Udovich, *Oxygen transport by oxygen potential gradient in dense ceramic oxide membranes*. Sol St Ionics **99**, 1997, p.1-7.
2. Bouwmeester, H.J., *Dense ceramic membranes for methane conversion*. Catal Today **82**, 2003, p.141-150.
3. Balachandran, U., J.T. Dusek, P.S. Maiya, B. Ma, R.L. Mieville, M.S. Kleefisch and C.A. Udovich, *Ceramic membrane reactor for converting methane to syngas*. Catal Today **36**, 1997, p.265-272.
4. Dyer, P.N., R.E. Richards, S.L. Russek and D.M. Taylor, *Ion transport membrane technology for oxygen separation and syngas production*. Sol St Ionics **134**, 2000, p.21-33.
5. O'Connor, A.M. and J.R.H. Ross, *The effect of O₂ addition on the carbon dioxide reforming of methane over Pt/ZrO₂ catalysts*. Catal Today **46**, 1998, p.203-210.
6. Souza, M.M.V.M. and M. Schmal, *Combination of carbon dioxide reforming and partial oxidation of methane over supported platinum catalysts*. Appl Cat A **255**, 2003, p.83-92.
7. Wang, W., S.M. Stagg-Williams, F.B. Noronha, L.V. Mattos and F.B. Passos, *Partial oxidation and combined reforming of methane of Ce-promoted catalysts*. Catal Today **98**, 2004, p.553-563.
8. Choudhary, V.R. and K.C. Mondal, *CO₂ reforming of methane combined with steam reforming or partial oxidation of methane to syngas over NdCoO₃ perovskite-type mixed metal-oxide catalyst*. Applied Energy **83**, 2006, p.1024-1032.
9. Choudhary, V.R., K.C. Mondal and T.V. Choudhary, *Oxy-CO₂ Reforming of Methane to Syngas over CoO_x/CeO₂/SA-5205 Catalyst*. Energy & Fuels **20**(5), 2006, p.1753-1756.
10. Choudhary, V.R., K.C. Mondal and T.V. Choudhary, *Partial oxidation of methane to syngas with or without simultaneous steam or CO₂ reforming over a high-temperature stable NiCoMgCeO_x supported on zirconia-hafnia catalyst*. Appl Cat A **306**, 2006, p.45-50.

11. Jing, Q., H. Lou, L. Mo, J. Fei and X. Zheng, *Combination of CO₂ reforming and partial oxidation of methane over Ni/BaO-SiO₂ catalysts to produce low H₂/CO ratio syngas using a fluidized bed reactor*. J of Molecular Catal A: Chemical **212**, 2004, p.211-217.
12. Jing, Q.S. and X.M. Zheng, *Combined catalytic partial oxidation and CO₂ reforming of methane over ZrO₂-modified Ni/SiO₂ catalysts using fluidized-bed reactor*. Energy **31**, 2006, p.2184-2192.
13. He, S., Q. Jing, W. Yu, L. Mo, H. Lou and X. Zheng, *Combination of CO₂ reforming and partial oxidation of methane to produce syngas over Ni/SiO₂ prepared with nickel citrate precursor*. Catal Today **148**, 2009, p.130-133.
14. He, S., H. Wu, W. Yu, L. Mo, H. Lou and X. Zheng, *Combination of CO₂ reforming and partial oxidation of methane to produce syngas over Ni/SiO₂ and Ni-Al₂O₃/SiO₂ catalysts with different precursors*. Int J of Hydrogen Energy **34**, 2009, p.839-843.
15. Vernon, P.D.F., M.L.H. Green, A.K. Cheetham and A.T. Ashcroft, *Partial oxidation of methane to synthesis gas, and carbon dioxide as an oxidising agent for methane conversion*. Catal Today **13**, 1992, p.417-426.
16. Guo, J., Z. Hou, J. Gao and X. Zheng, *Syngas production via combined oxy-CO₂ reforming of methane over Gd₂O₃-modified Ni/SiO₂ catalysts in a fluidized-bed reactor*. Fuel **87**, 2008, p.1348-1354.
17. Michael, B.C., A. Donazzi and L.D. Schmidt, *Effects of H₂O and CO₂ addition in catalytic partial oxidation of methane on Rh*. Jnl of Catal **265**, 2009, p.117-129.
18. Wilhelm, D.J., D.R. Simbeck, A.D. Karp and R.L. Dickenson, *Syngas production for gas-to-liquids applications: technologies, issues, and outlook*. Fuel Processing Technology **71**, 2001, p.139-148.
19. Feng, S.J., S. Ran, D.C. Zhu, W. Liu and C.S. Chen, *Synthesis gas production from methane with SrFeCo_{0.5}O_y membrane reactor*. Energy & Fuels **18**, 2004, p.385-389.
20. Robinson, E.T., S. Aasland and J. Chen. *The application of oxygen transport membranes for syngas or hydrogen production*. in 2004 AIChE Spring Meeting. 2004.
21. Sammells, A.F., M. Schwartz, R.A. Mackay, T.F. Barton and D.R. Peterson, *Catalytic membrane reactors for spontaneous synthesis gas production*. Catal Today **56**, 2000, p.325-328.
22. Tong, J., W. Yang, R. Cai, B. Zhu and L. Lin, *Novel and ideal zirconium-based dense membrane reactors for partial oxidation of methane to syngas*. Catal Letters **78**(1-4), 2002, p.129-137.
23. Ritchie, J.T., J.T. Richardson and D. Luss, *Ceramic membrane reactor for synthesis gas production*. AIChE Jnl **47**(9), 2001, p.2092-2101.
24. Tsai, C.-Y., A.G. Dixon, Y.H. Ma, W.R. Moser and M.R. Pascucci, *Dense perovskite La_{1-x}A'_xFe_{1-y}Co_yO_{3-δ} (A' = Ba, Sr, Ca) membrane synthesis, applications, and characterization*. J Amer Ceram Soc **81**(6), 1998, p.1437-1444.
25. Dong, H., Z. Shao, G. Xiong, J. Tong, S. Sheng and W. Yang, *Investigation on POM reaction in a new perovskite membrane reactor*. Catal Today **67**, 2001, p.3-13.

26. Steele, B.C.H., *Oxygen ion conductors and their technological applications*. Material Science and Engineering **B13**, 1992, p.79-87.
27. Akin, F.T., Y.S. Lin and Y. Zeng, *Comparative study on oxygen permeation and oxidative coupling of methane on disk-shaped and tubular dense ceramic membrane reactors*. Ind Eng Chem Res **40**, 2001, p.5908-5916.
28. Lin, Y.S. and Y. Zeng, *Catalytic properties of oxygen semipermeable perovskite-type ceramic membrane materials for oxidative coupling of methane*. Jnl of Catal **164**, 1996, p.220-231.
29. Omata, K., O. Yamazaki, K. Tomita and K. Fujimoto, *Oxidative Coupling of Methane on an ABO_3 Type Oxide with Mixed Conductivity*. J Chem Soc, Chem Commun **14**, 1994, p.1647-1648.
30. Rebeilleau-Dassonneville, M., S. Rosini, A.C. van Veen, D. Farrusseng and C. Mirodatos, *Oxidative activation of ethane on catalytic modified dense ionic oxygen conducting membranes*. Catal Today **104**, 2005, p.131-137.
31. Spivey, J.J. in *232nd ACS National Meeting*. 2006. San Francisco.
32. Xu, S.J. and W.J. Thomson, *Stability of $La_{0.6}Sr_{0.4}Co_{0.2}Fe_{0.8}O_{3-\delta}$ perovskite membranes in reducing and nonreducing environments*. Ind Eng Chem Res **37**, 1998, p.1290-1299.
33. Ma, Y.H., *Dense palladium and perovskite membranes and membrane reactors*. MRS Bulletin **March**, 1999, p.46-49.
34. Qiu, L., T.H. Lee, L.-M. Liu, Y.L. Yang and A.J. Jacobson, *Oxygen permeation studies of $SrCo_{0.8}Fe_{0.2}O_{3-\delta}$* . Sol St Ionics **76**, 1995, p.321-329.
35. Pei, S., M.S. Kleefisch, T.P. Kobylinski, J. Faber, C.A. Udovich, V. Zhang-McCoy, B. Dabrowski, U. Balachandran, R.L. Mieville and R.B. Peoppel, *Failure mechanisms of ceramic membrane reactors in partial oxidation of methane to synthesis gas*. Catal Letters **30**, 1995, p.201.
36. Berry, F.J., J.F. Marco and X. Ren, *Reduction properties of phases in the system $La_{0.5}Sr_{0.5}MO$ ($M = Fe, Co$)*. Sol St Ionics **178**, 2005, p.961-969.
37. Ma, B. and U. Balachandran, *Phase stability of $SrFeCo_{0.5}O_x$ in reducing environments*. Mat Res Bull **33**(2), 1998, p.223-236.
38. ten Elshof, J.E., H.J. Bouwmeester and H. Verweij, *Oxidative coupling of methane in a mixed-conducting perovskite membrane reactor*. Appl Cat A **130**, 1995, p.195-212.
39. Adler, S.B., *Chemical expansivity of electrochemical ceramics*. J Am Ceram Soc **84**(9), 2001, p.2117-2119.
40. Hodges, J.P., J.D. Jorgensen, D.J. Miller, B. Ma, U. Balachandran and J.W. Richardson, *Crystal structures of mixed-conducting oxides present in the Sr-Fe-Co-O system*. Mat Res Soc Symp Proc **496**, 1998, p.173-178.

41. Ullmann, H., N. Trofimenko, F. Tietz, D. Stoeber and A. Ahmad-Khanlou, *Correlation between thermal expansion and oxide ion transport in mixed conducting perovskite-type oxides for SOFC cathodes*. Sol St Ionics **138**, 2000, p.79-90.
42. Atkinson, A. and T.M.G.M. Ramos, *Chemically-induced stresses in ceramic oxygen ion-conducting membranes*. Sol St Ionics **129**, 2000, p.259-269.
43. Wang, H., C. Tablet, W. Yang and J. Caro, *In situ high temperature X-ray diffraction of mixed ionic and electronic conducting perovskite-type membranes*. Materials Letters **59**, 2005, p.3750-3755.
44. Armstrong, T., F. Prado, Y. Xia and A. Manthiram, *Role of perovskite phase on the oxygen permeation properties of the $Sr_4Fe_{6-x}Co_xO_{13+\delta}$ system*. J Electrochem Soc **147**(2), 2000, p.435-438.
45. Xia, Y., T. Armstrong, F. Prado and A. Manthiram, *Sol-gel synthesis, phase relationships, and oxygen permeation properties of $Sr_4Fe_{6-x}Co_xO_{13+\delta}$ ($0 \leq x \leq 3$)*. Sol St Ionics **130**, 2000, p.81-90.
46. Fossdal, A., L.T. Sagdahl, M.-A. Einarsrud, K. Wiik, T. Grande, P.H. Larsen and F.W. Poulsen, *Phase equilibria and microstructure in $Sr_4Fe_{6-x}Co_xO_{13}$ ($0 \leq x \leq 4$) mixed conductors*. Sol St Ionics **143**, 2001, p.367-377.
47. Ma, B., N.I. Victory, U. Balachandran, B.J. Mitchell and J.W. Richardson, *Study of the mixed-conducting $SrFeCo_{0.5}O_y$ system*. J Am Ceram Soc **85**(11), 2002, p.2641-2645.
48. Kim, S., Y.L. Yang, R. Christoffersen and A.J. Jacobson, *Determination of oxygen permeation kinetics in a ceramic membrane based on the composition $SrFeCo_{0.5}O_{3.25-\delta}$* . Sol St Ionics **109**, 1998, p.187-196.
49. Ikeguchi, M., K. Yoshino, K. Kanie, M. Nomura, E. Kikuchi and M. Matsukata, *Effects of preparation method on oxygen permeation properties of $SrFeCo_{0.5}$ membrane*. Sep & Pur Tech **32**, 2003, p.313-318.
50. Shao, Z.P., H. Dong, G.X. Xiong and W.S. Yang, *Syngas Production Using an Oxygen-Permeating Membrane Reactor with Cofeed of Methane and Carbon Dioxide*. Chinese Chemical Letters **11**(7), 2000, p.631-634.
51. Slade, D.A., Q. Jiang, K.J. Nordheden and S.M. Stagg-Williams, *A comparison of mixed-conducting oxygen-permeable membranes for CO_2 reforming*. Catal Today **148**, 2009, p.290-297.
52. Gu, X., L. Yang, L. Tan, W. Jin, L. Zhang and N. Xu, *Modified Operating Mode for Improving the Lifetime of Mixed-Conducting Ceramic Membrane Reactors in the POM Environment*. Ind Eng Chem Res **42**, 2003, p.795-801.
53. Dixon, A.G., *personal communication*. 2004: Austin, TX (AIChE Annual Meeting).
54. Gerdes, K., *personal communication*. 2005: Cincinnati, OH (AIChE Annual Meeting).
55. Bitter, J.H., K. Seshan and J.A. Lercher, *Deactivation and Coke Accumulation during CO_2/CH_4 Reforming over Pt Catalysts*. Jnl of Catal **183**, 1999, p.336-343.

56. Nagaoka, K., K. Seshan, K. Aika and J.A. Lercher, *Carbon Deposition during Carbon Dioxide Reforming of Methane--Comparison between Pt/Al₂O₃ and Pt/ZrO₂*. Jnl of Catal **197**, 2001, p.34-42.
57. O'Connor, A.M., Y. Schuurman, J.R.H. Ross and C. Mirodatos, *Transient studies of carbon dioxide reforming of methane over Pt/ZrO₂ and Pt/Al₂O₃*. Catal Today **115**, 2006, p.191-198.
58. Pompeo, F., N.N. Nichio, M.M.V.M. Souza, D.V. Cesar, O.A. Ferretti and M. Schmal, *Study of Ni and Pt catalysts supported on α -Al₂O₃ and ZrO₂ applied in methane reforming with CO₂*. Appl Cat A **316**, 2007, p.175-183.
59. Souza, M.M.V.M., D.A.G. Aranda and M. Schmal, *Coke Formation of Pt/ZrO₂/Al₂O₃ Catalysts during CH₄ Reforming with CO₂*. Ind Eng Chem Res **41**, 2002, p.4681-4685.
60. Stagg-Williams, S.M., F.B. Noronha, G. Fendley and D.E. Resasco, *CO₂ Reforming of CH₄ over Pt/ZrO₂ Catalysts Promoted with La and Ce Oxides*. Jnl of Catal **194**, 2000, p.240-249.
61. Ashcroft, A.T., A.K. Cheetham, M.L.H. Green and P.D.F. Vernon, *Partial oxidation of methane to synthesis gas using carbon dioxide*. Nature **352**, 1991, p.225-226.
62. Tsai, C.-Y., A.G. Dixon, W.R. Moser and Y.H. Ma, *Dense perovskite membrane reactors for partial oxidation of methane to syngas*. AIChE Jnl **43**(11A), 1997, p.2741-2750.
63. Lu, H., Y. Cong and W.S. Yang, *Oxygen permeability and stability of Ba_{0.5}Sr_{0.5}Co_{0.8}Fe_{0.2}O_{3- δ} as an oxygen-permeable membrane at high pressures*. Sol St Ionics **177**, 2006, p.595-600.
64. Lu, H., J. Tong, Y. Cong and W.S. Yang, *Partial oxidation of methane in Ba_{0.5}Sr_{0.5}Co_{0.8}Fe_{0.2}O_{3- δ} membrane reactor at high pressure*. Catal Today **104**(154-159), 2005, p.154.

Chapter 3: Experimental Methodology

Sets of experiments were planned around the objectives outlined in Chapter 1. The particular analytical focus of this work for both membrane flux testing and reaction testing is the accurate assessment of reactor effluent composition. The experimental scope can be broadly categorized as determining the effect of SFC membranes on CO₂ reforming with multiple catalyst types with simultaneous evaluation of the effect of the CO₂ reforming reaction environment on the SFC membranes. The major branches of the experimental work were:

- 1) membrane fabrication
- 2) reactor system design and production
- 3) membrane flux testing
- 4) catalytic reaction testing (CO₂ reforming and oxygen-assisted CO₂ reforming)

Membrane fabrication and reactor system design are discussed in Appendix C and Chapter 4, respectively. The flux testing procedure is summarized in Section 3.1 and additional details and test results are provided in Appendices E and F. The remainder of this chapter and the main body of the dissertation focus on reaction testing—specifically, on the individual effects of SFC membranes and co-fed O₂ on CO₂ reforming catalyst performance.

3.1: Flux Testing

Membranes are tested for oxygen flux using the same reactors as for reaction testing and follow similar set-up procedures, although with no powder catalyst. For flux testing, argon is fed to the reaction chamber as an inert sweep gas to remove any oxygen that evolves from the membrane's upper surface. To maintain a constant O₂ partial pressure at the lower surface (i.e., the oxygen source surface), air flows continuously at a flowrate at least 40 times that of reactor feed (the air flow rate exceeds the maximum flowrate that can be measured by the flowmeter of 1000 mL/min). Permeate side effluent composition is evaluated using a Balzers Omnistar quadrupole mass spectrometer.

Oxygen flux was estimated from mass spectrometer data for oxygen and nitrogen. Leaked air is quantified with the nitrogen signal. Net membrane oxygen flux is then calculated from the difference between the actual oxygen signal and the signal predicted for air from the nitrogen signal. Prior to testing, at least two different amounts of air in argon are used to determine the signal ratio for oxygen and nitrogen in air as well as the expected signal ratios for argon and oxygen and argon and nitrogen. As oxygen, nitrogen, and argon are the only species present in detectable quantities during flux testing, membrane oxygen contribution can be consistently assessed using the signal ratios of these three species.

Membrane oxygen flux is then calculated using the known flowrate of argon into the reactor, the measured flowrate out of the reactor, and the concentration of membrane oxygen calculated from the mass spectrometer signal ratios. A series of temperatures was used for most flux tests and the system was allowed to equilibrate at each temperature for at least 30 minutes and up to 2 hours if needed. Flux values were only calculated at the end of an equilibration period. Figure 3.1 provides an example of the results calculated from mass spectrometer data for a flux test in the SSMR.

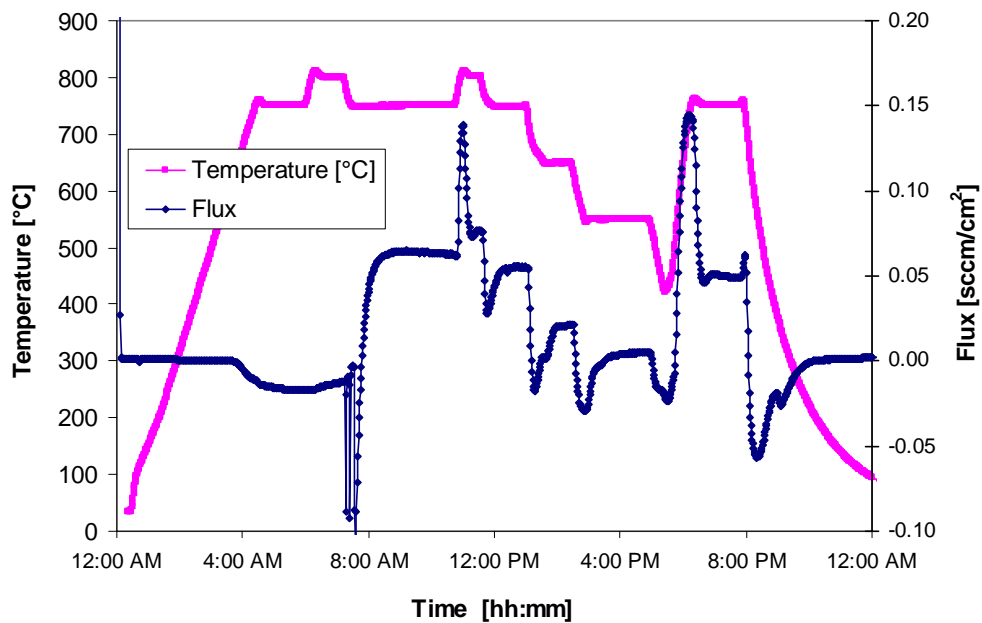


Figure 3.1: Example output from an SSMR flux test with a plain SFC membrane (7/14/05)

The dark blue line in Figure 3.1 representing the calculated oxygen flux (as gas-phase O₂) exhibits significant transient behavior with every temperature change above approximately 400 °C. This is attributed to the SFC material's ability to quickly evolve or incorporate oxygen as part of its phase equilibration when heated or cooled under a low oxygen environment (argon, in this case).

NOTE: Because of signal drift, exact calibrations could not be performed with this mass spectrometer. However, signal ratios were confirmed to be consistent even though signal levels were not. The signal drift phenomenon was obvious and was investigated extensively, but the mass spectrometer manufacturer repeatedly denied that it was possible. No adjustments to the instrument prevented it.

3.2: Reaction Testing

Two different membrane reactors were used for reaction and flux testing: one fabricated from stainless steel (the SSMR) and one from quartz tubing (the QTMR). A quartz-tube PFR-type reactor was also used for reaction testing to provide baseline catalyst results. In addition to the SFC membranes, membrane reactor tests were conducted with an inert-coated stainless steel blank (the inert coating is Boron Nitride Aerosol Lubricat Blue from ZYP Coating Inc.). The blank tests provide baseline results for the membrane reactors.

3.2.1: Test reactions and parameters

CO₂ reforming was chosen as the test reaction for this work, although small amounts of oxygen were also included in the feed in some tests. In all reaction tests, a molar CH₄:CO₂ ratio of 1:1 was used and CH₄ and CO₂ comprised 80% of the feed. For SFC membrane experiments, the remaining 20% of the feed was pure argon, while specific percentages of O₂ in argon were used in the stainless steel blank membrane tests. In addition to true CO₂ reforming (i.e., no oxygen), the co-fed O₂ amounts tested with the blank included 0.2%, 1%, and 2% of the total volumetric feed flowrate. Co-fed gas-phase oxygen was used to distinguish any unique effects of the SFC membranes.

Other than in a series of tests evaluating the effect of space velocity, reactor feed flowrates correspond to a modified space velocity of 150 L/hr/gram catalyst in all tests, regardless of reactor type. Atmospheric pressure air is used as the oxygen source for the lower membrane surface. With the QTMR, membranes were tested for cracks or porosity at the reaction temperature of 800 °C using slightly pressurized helium. No quantifiable helium penetration was detected at 800 °C before or after reaction.

3.2.2: Powder catalysts

Two different catalysts were used: 0.42% Pt/ZrO₂ and 0.43% Pt/CeZrO₂. Catalyst from a single batch was used in all tests for a given catalyst. The Pt/ZrO₂ catalyst was chosen because it has been studied previously in conventional quartz tube PFR reactors [1-12] and has shown relatively quick deactivation which allows differences in catalyst performance to be observed expeditiously. The Pt/CeZrO₂ catalyst was selected because it has exhibited improved activity and slower deactivation than the Pt/ZrO₂ catalyst in previous work [3, 12-14].

Catalyst powders were prepared by depositing platinum on commercially available support materials via the incipient wetness impregnation technique with an aqueous solution of H₂PtCl₆·6H₂O. Prior to deposition, substrates were calcined at 800 °C; after deposition they were dried overnight at 120 °C and then calcined at 400 °C for 2 hours in flowing air. BET single point surface area analysis indicated a surface area of 29 m²/g for the Pt/ZrO₂ catalyst (assessed using a Micromeritics Gemini II 2370 surface area analyzer available in Professor Bala Subramaniam's lab). Platinum dispersion was not determined for the actual catalysts used, but previous studies with the same catalyst types indicated a post-reduction and post-heating dispersion of 11% [15].

3.2.3: Reaction tests in the membrane reactors

After fully establishing the reaction test methodology (i.e., from Chapter 6 on), a total reactor feed flowrate of 25 mL/min with 20% argon or argon/O₂ in the feed is used in all membrane reactor

tests. As described above, the 20% argon feed contribution can include co-fed oxygen in tests with the stainless steel blank. Porter mass flow controllers maintain the target gas flows into the membrane reactor using control signals from the Camile™ operation and data acquisition program. A 6-inch-long cylindrical Watlow furnace provides uniform reactor heating for the membrane as well as approximately 3 inches of gas pre-heat zone for the quartz tube membrane reactor. Reactor temperature is controlled and monitored along with feed gas flowrates by the fully programmable Camile™ system.

Typical membrane reactor experiments use 10 mg of powder catalyst which is spread in a thin layer (~1 mm) across the portion of the membrane surface (SFC or blank) within the inner diameter of the sealing gasket. The thin catalyst layer ensures good proximity between the membrane and the entire catalyst bed and minimizes transport resistance within the catalyst layer on both the SFC membrane and the blank. A small amount of catalyst has the additional advantage of immediately exposing catalyst deactivation trends by allowing the reactors to operate well below equilibrium conversion levels. The primary disadvantage of the small catalyst quantities is a minimal opportunity for post-reaction recovery and analysis. Figure 3.2 provides a schematic depiction of the SFC membrane under operating conditions.

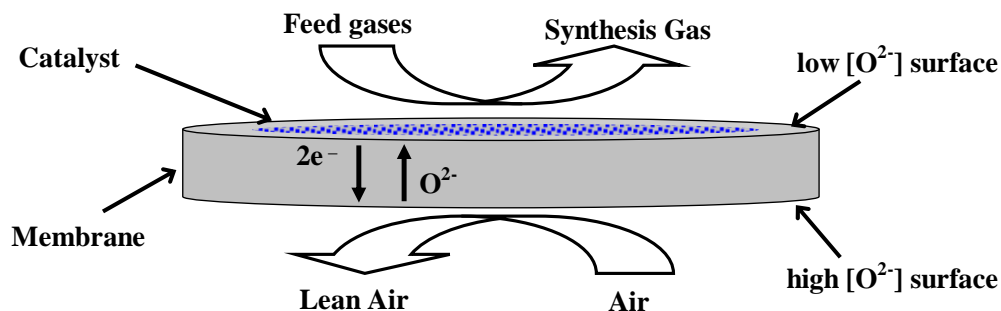


Figure 3.2: Schematic of an O-MIEC membrane under reaction conditions

The reactor is initially heated to reaction temperature (750 °C with the SSMR and 800 °C with the QTMR) with an argon-only feed. It is then held at reaction temperature with the same argon-only feed for two hours while the gold seals seat themselves and the membrane equilibrates under the

air:argon oxygen potential gradient. This two-hour hold at 800 °C is also imposed during experiments with the stainless steel blank membrane to ensure comparable pre-reaction conditions for the catalyst.

Steady state oxygen production from the SFC membranes under these conditions is assessed using the flux testing methodology described in Section 3.1. Pre-reaction oxygen production results varied but on average were around 0.007 mL/min O₂ at 800 °C, or 0.03% of the standard membrane reactor feed of 25 ml/min. The corresponding O₂ flux is about 0.004 sccm/cm². This oxygen production occurs under an air:argon oxygen gradient. Membranes are expected to produce more oxygen under reaction conditions.

After the two hour equilibration period, the reaction feed mixture is started through the reactor. SFC membrane tests used 10 ml/min each methane and carbon dioxide and 5 mL/min argon. Stainless steel membrane tests used the same feed as a basis, but oxygen was substituted for a small portion of the argon in a set of tests. The amounts of co-fed oxygen used represented 0.2, 1.0, and 2.0% of the total reactor feed on a mole (volume) basis or 1%, 5%, and 10% displacements of the argon portion of the reactor feed.

A GC injection series is initiated approximately five minutes after the reaction is started. Reactor effluent flowrates are monitored as closely as possible, but the Agilent flowmeter is sensitive to water and can therefore only be used intermittently during reaction tests. Pre-reaction catalyst reduction was removed from the basic membrane reactor test procedure after early attempts produced large quantities of water from hydrogen oxidation on the SFC membrane.

3.2.4: Reaction product analysis

Reactor effluent composition is analyzed simultaneously with the Balzers Omnistar quadrupole mass spectrometer and an SRI 8610C gas chromatograph with a Supelco Carboxen 1010

PLOT column. The GC determines composition accurately but intermittently while the mass spectrometer permits continuous assessment of reactor effluent. The mass spectrometer provides important additional information including pre-reaction oxygen flux data and also helps confirm and interpolate trends observed in the GC data. The GC has both a flame ionization detector (FID) for accurate CO, CO₂, and CH₄ quantification and a thermal conductivity detector (TCD) for hydrogen, air/N₂, and redundant CO, CO₂, and CH₄ data. In addition, effluent flowrate and oxygen concentration are monitored using an Agilent ADM 2000 flowmeter and an AMI Model 60 oxygen sensor, respectively. Effluent water is calculated from a hydrogen atom balance (trends are confirmed by mass spectrometer data) and membrane oxygen flux is calculated from an oxygen atom balance.

3.2.5: Plug-flow reactor (PFR) tests

The purpose of the PFR testing was to help interpret the results from the membrane reactor tests. Typical PFR tests use 20 mg of powder catalyst and a total feed flowrate of 50 mL/min, both of which are twice the values for the membrane reactor tests. All PFR tests were conducted at 800 C, and the catalyst is diluted 40:1 with quartz powder to provide isothermal conditions in the catalyst bed. Bed dilution also increases catalyst contact time.

The two hour pre-reaction hold was included in a few PFR experiments, but not as a general strategy. Catalyst in the PFR was therefore not exposed to exactly the same conditions as in the membrane reactors. Catalyst reduction and other pretreatment issues were explored using the PFR, as well as some co-fed oxygen testing.

3.2.6: Post-reaction catalyst analysis

Catalyst from the SSMR and PFR tests couldn't be recovered for post-reaction analysis, but the QTMR did allow post-reaction catalyst collection. For certain QTMR tests, carbon deposition was assessed by post-reaction oxidation testing.

After careful disassembly of the membrane reactor, the used catalyst can be collected from the membrane and transferred to a quartz tube for carbon oxidation. Because small amounts of catalyst were used in these tests, small amounts of oxygen must be used for the oxidation. A 50 μL injection loop was used with 5% oxygen in argon, allowing oxygen to be added in 2.5 μL pulses. Pulses were monitored and quantified with mass spectrometer data. The resulting oxygen peak areas were assessed using Origin and converted to unreacted oxygen volumes based on the known peak area for a full 2.5 μL pulse. CO_2 peak areas were quantified to determine the point at which carbon oxidation had ended, which also provided a redundant means of quantifying carbon removal.

References Cited in Chapter 3

1. Bitter, J.H., K. Seshan and J.A. Lercher, *The State of Zirconia Supported Platinum Catalysts for CO_2/CH_4 Reforming*. Jnl of Catal **171**, 1997, p.279-286.
2. O'Connor, A.M. and J.R.H. Ross, *The effect of O_2 addition on the carbon dioxide reforming of methane over Pt/ZrO₂ catalysts*. Catal Today **46**, 1998, p.203-210.
3. Stagg-Williams, S.M., F.B. Noronha, G. Fendley and D.E. Resasco, *CO_2 Reforming of CH_4 over Pt/ZrO₂ Catalysts Promoted with La and Ce Oxides*. Jnl of Catal **194**, 2000, p.240-249.
4. Nagaoka, K., K. Seshan, K. Aika and J.A. Lercher, *Carbon Deposition during Carbon Dioxide Reforming of Methane--Comparison between Pt/Al₂O₃ and Pt/ZrO₂*. Jnl of Catal **197**, 2001, p.34-42.
5. Souza, M.M.V.M., D.A.G. Aranda and M. Schmal, *Reforming of Methane with Carbon Dioxide over Pt/ZrO₂/Al₂O₃ Catalysts*. Jnl of Catal **204**, 2001, p.498-511.
6. Bitter, J.H., K. Seshan and J.A. Lercher, *Deactivation and Coke Accumulation during CO_2/CH_4 Reforming over Pt Catalysts*. Jnl of Catal **183**, 1999, p.336-343.
7. Souza, M.M.V.M. and M. Schmal, *Combination of carbon dioxide reforming and partial oxidation of methane over supported platinum catalysts*. Appl Cat A **255**, 2003, p.83-92.
8. Wei, J. and E. Iglesia, *Mechanism and Site Requirements for Activation and Chemical Conversion of Methane on Supported Pt Clusters and Turnover Rate Comparisons among Noble Metals*. J Phys Chem B **108**, 2004, p.4094-4103.
9. O'Connor, A.M., Y. Schuurman, J.R.H. Ross and C. Mirodatos, *Transient studies of carbon dioxide reforming of methane over Pt/ZrO₂ and Pt/Al₂O₃*. Catal Today **115**, 2006, p.191-198.
10. Pompeo, F., N.N. Nichio, M.M.V.M. Souza, D.V. Cesar, O.A. Ferretti and M. Schmal, *Study of Ni and Pt catalysts supported on $\alpha\text{-Al}_2\text{O}_3$ and ZrO₂ applied in methane reforming with CO_2* . Appl Cat A **316**, 2007, p.175-183.

11. Souza, M.M.V.M., D.A.G. Aranda and M. Schmal, *Coke Formation of Pt/ZrO₂/Al₂O₃ Catalysts during CH₄ Reforming with CO₂*. Ind Eng Chem Res **41**, 2002, p.4681-4685.
12. Wang, W., S.M. Stagg-Williams, F.B. Noronha, L.V. Mattos and F.B. Passos, *Partial oxidation and combined reforming of methane of Ce-promoted catalysts*. Catal Today **98**, 2004, p.553-563.
13. Noronha, F.B., A. Shamsi, C. Taylor, G. Fendley, S.M. Stagg-Williams and D.E. Resasco, *Catalytic performance of Pt/ZrO₂ and Pt/Ce-ZrO₂ catalysts on CO₂ reforming of CH₄ coupled with steam reforming or under high pressure*. Catal Lett **90**(1-2), 2003, p.13-21.
14. Mattos, L.V., E. Rodino, D.E. Resasco, F.B. Passos and F.B. Noronha, *Partial oxidation and CO₂ reforming of methane on Pt/Al₂O₃, Pt/ZrO₂, and Pt/Ce-ZrO₂ catalysts*. Fuel Processing Technology **83**, 2003, p.147-161.
15. Stagg-Williams, S.M., *personal communication*. 2005: University of Kansas (weekly advisor meeting).

Chapter 4: Reactor Design and Assembly

The original scope of this work was to apply dual conducting mixed metal oxide membranes, specifically $\text{SrFeCo}_{0.5}\text{O}_x$ (SFC), with structured patterns of metal and multi-component catalytic sites to the production of hydrogen via reforming reactions. The catalyst patterns were to be deposited by photolithography techniques used in the semiconductor industry. These techniques require a planar surface, and deposited feature size is limited by surface roughness.

Catalytic metal dispersion is a critical catalyst performance parameter and photolithographic features tend to be much larger than catalytic metal particles on conventional supported catalysts, so the smallest deposited particles possible were desired. A flat and smooth membrane surface was therefore required. Disk-shaped membranes were chosen to accommodate the requirement of a planar surface for photolithography, and reactors were designed and fabricated accordingly.

Additional design constraints included high temperature resistance, ideally to 900 °C but at least to 800 °C; inertness to oxidation and reduction reactions; effective sealing against outside air incursions; ease of assembly and disassembly; and intact membrane recovery. Membrane reactors require a gasket or seal of some kind as an intermediate between the membranes and the reactor surfaces, and gasket selection is an important enough topic to warrant its own section in the discussion that follows.

4.1: Stainless Steel Membrane Reactor (SSMR)

4.1.1: SSMR construction

The first membrane reactor used was a two-piece CSTR-type reactor designed by Ed Atchison and Ian Palko and fabricated from 316 stainless steel. In this design, the membrane is placed into a deep hole in the larger bottom piece of the reactor to cover a hemispherical chamber that was machined out of the bottom. As depicted in Figure 4.1, the smaller top piece, which has a mirror-

image hemispherical chamber at the end of its shaft, is inserted on top of the membrane. The two reactor pieces are compressed against the membrane surfaces by three machine screws that pass through unthreaded holes in the top piece into threaded holes around the perimeter of the bottom piece.

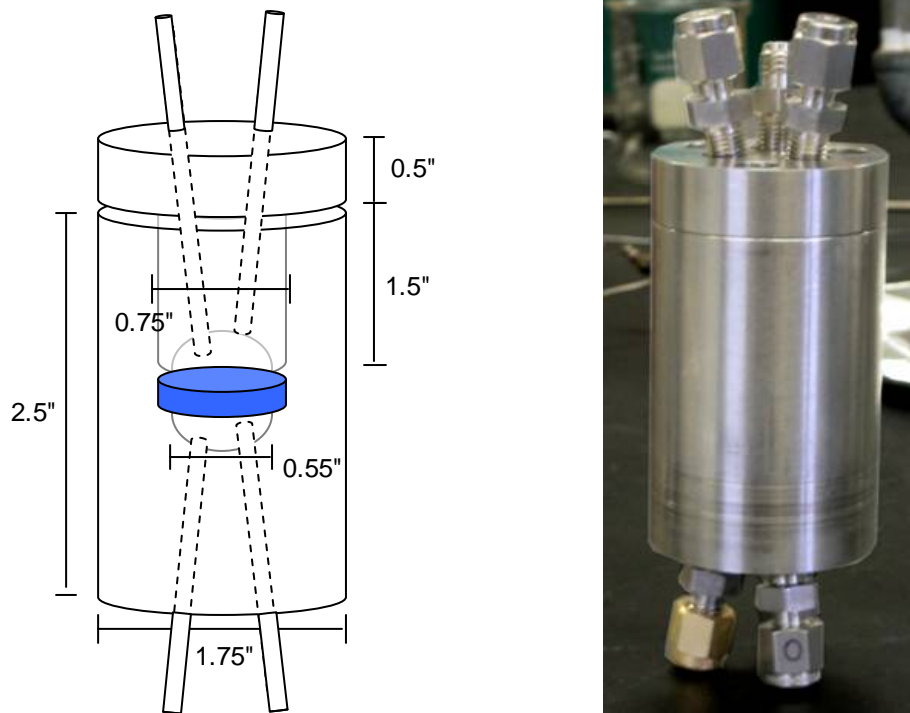


Figure 4.1: Stainless steel membrane reactor (SSMR) internal schematic and photograph

The red lines in Figure 4.2 represent signals to and from the Camile™ control system and the light blue lines represent gas flow lines. The red circles indicate thermocouple positions and the blue boxes are control devices or instruments. The hemispherical chamber in each reactor piece has three holes that are bored through the piece. On the opposite surface of each piece, three stainless steel Swagelok™ fittings are permanently installed in the holes: one for the gas inlet, one for the outlet, and one for a thermocouple. A thermocouple and two short 1/8” stainless steel gas lines are permanently installed in these Swagelok™ fittings. The thermocouples are positioned such that the tips extend a small distance into the hemispherical chambers, as depicted in Figure 4.1. Type K thermocouples

(12" long with 1/8" diameter sheath, from Omega) are used in all three reactor systems (SSMR, QTMR, and PFR).

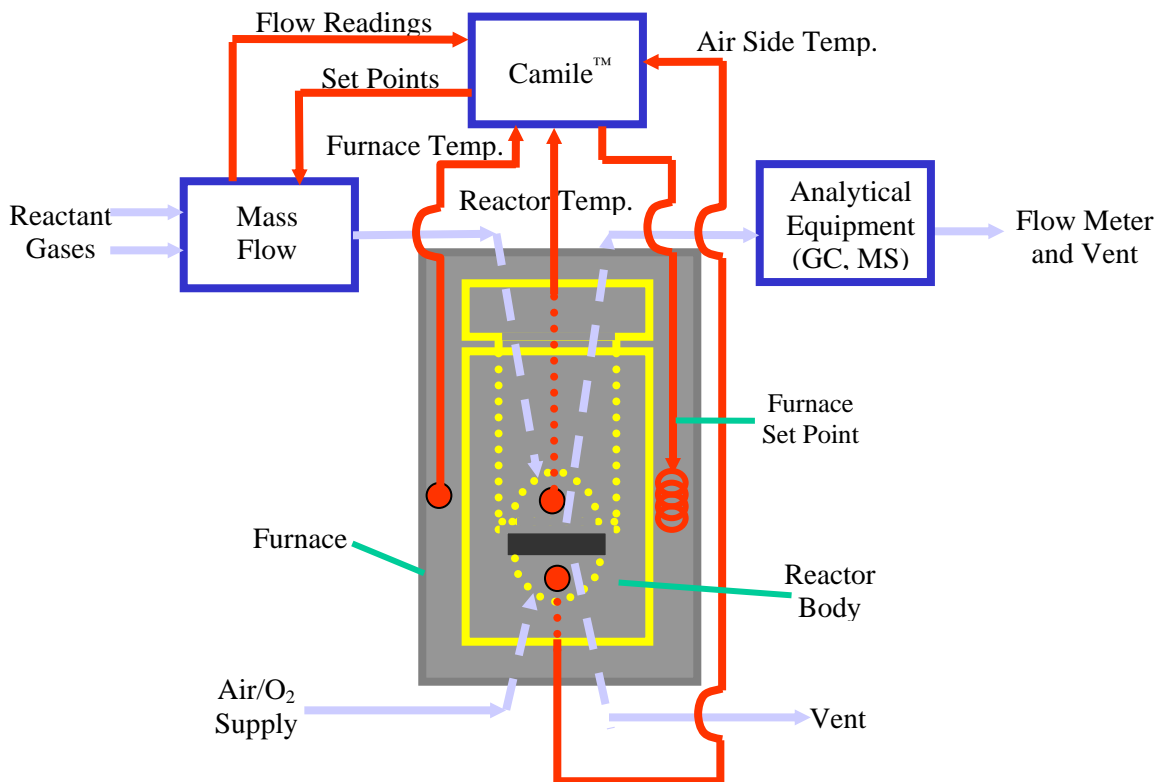


Figure 4.2: Stainless steel membrane reactor (SSMR) system

4.1.2: SSMR assembly

Before inserting the top reactor piece, the membrane (or blank) and gaskets are positioned carefully in the hole in the bottom piece and powder catalyst (if used) is added and distributed as evenly as possible across the area circumscribed by the inner diameter of the gasket on the top surface. Care is taken to avoid disturbing the position of the gaskets or the distribution of the powder catalyst while inserting and aligning the top reactor piece and tightening the screws. Prior to assembly, the interior reactor surfaces are sprayed with the same inert boron nitride (BN_3) paint used to coat the stainless steel blank membrane to prevent reaction on the steel surfaces (Boron Nitride

Aerosol Lubricoat Blue, ZYP Coating Inc.). The machine screws are tightened using a torque wrench to ensure even compression around the membrane perimeter. Before insertion, the screws are coated with an anti-seize paste to lubricate the threads during initial assembly and to facilitate removal after the test is complete (SAF-T-EZE nickel Anti-sieze, STL Compound Corporation).

Because both the top and the bottom of the SSMR have a thermocouple and two stainless steel lines protruding from them, the reactor cannot sit on a flat surface without a stand. A piece of 2" diameter stainless steel tubing is used to support the body of the reactor with a groove in the bottom to allow the tubing and thermocouple to access their respective connections. Sections of copper tubing are attached to the reactor's permanent stainless steel gas lines because copper is flexible and allows the assembled reactor to be moved as needed. However, stainless steel tubing is used again on the reactor outlet line downstream of the copper section so that the line can be heated without oxidizing. Line heating reduces water condensation in the reactor outlet line.

After all lines are attached and the reactor is properly positioned and supported, a clamshell annular ceramic furnace is installed around the reactor body. A third thermocouple is inserted into the space between the furnace and the exterior surface of the reactor, as indicated by the left-most red circle in Figure 4.1. Quartz-wool insulation is packed around the top and bottom openings of the furnace and as needed around the top portion of the reactor.

4.1.3: SSMR conclusions

The SSMR provided a good starting point for initial oxygen flux and reaction studies because of its ease of assembly and the high thermal stability caused by its large mass. However, the stainless steel body oxidized during sustained operation at temperatures above 750 °C, so early testing did not exceed 750 °C for extended periods of time. The machine screw sealing mechanism also appeared to lose compression somewhat at high temperature such that the seal was insufficient for conclusive

assessment of the effect of the SFC membrane on the reaction tests. Unfortunately, target temperatures for methane reforming and oxygen flux studies were 800 °C or higher.

A new reactor was required for high temperature testing, but the SSMR could be very useful for lower temperature testing, particularly in conjunction with the pneumatic press as the compression mechanism.

SSMR advantages:

- Easy to assemble
- Durable all-metal construction
- Excellent thermal stability (large thermal mass)

SSMR disadvantages:

- Poor seal at high temperatures (large leak, plus oxidized gaskets)
- Difficult to position gaskets and distribute catalyst evenly
- Difficult to remove membrane intact
- Catalyst cannot be recovered without contamination
- Relatively low maximum operating temperature of 750 °C

4.2: Quartz Tube Membrane Reactor (QTMR)

4.2.1: QTMR construction

The stainless steel reactor was replaced by a quartz tube membrane reactor (QTMR) with a more effective sealing mechanism and capable of operating at temperatures above 800 °C. The QTMR consists of concentric quartz tubes with tube diameters and wall thicknesses selected to provide comparable linear gas velocities in the feed (between the tubes) and product (through the inner tube) flow paths. Tube dimensions and part details are provided in Appendix O. Control, data recording, and analytical equipment are otherwise the same as shown in Figure 4.1 for the SSMR,

with one exception: a digital volumetric flowmeter (Agilent ADM 2000) was acquired for continuous monitoring and recording of reactor effluent flowrates.

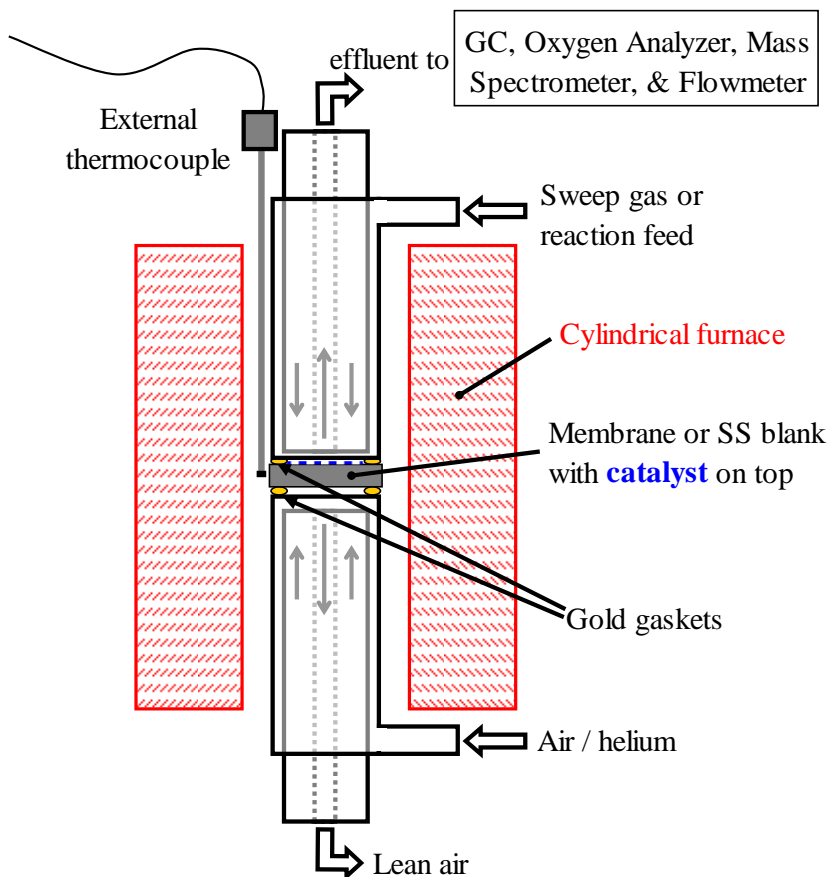


Figure 4.3: Quartz Tube Membrane Reactor (QTMR) system

As shown in Figure 4.3, reactants flow into the top part of the reactor through the annular space between the two concentric quartz tubes, and effluent leaves the reactor through the inner tube after passing through the catalyst layer on the membrane's top surface. The inner tube has a thick wall and is positioned as close to the membrane surface as possible (within 2 mm) to maximize contact of the gas stream with the catalyst layer (i.e., to minimize "bypass"). In addition to the SFC ceramic membranes, a stainless steel "blank" membrane was used to examine the effect of co-fed molecular oxygen on catalyst performance in the QTMR and to provide baseline data for the SFC membrane experiments in both membrane reactors.

Initially, only one thermocouple was available for the QTMR. It was positioned external to the reactor within 1/16" of the membrane's outside edge. The QTMR was installed so that the membrane (and thermocouple) was positioned slightly below the midpoint of the furnace (the same 6" long annular furnace used with the SSMR). Modifications were later made to the QTMR to allow the installation of an interior thermocouple down the center of the inner quartz tube to monitor the reaction chamber temperature. The tip of this thermocouple was placed within ~2 mm of the reaction-side membrane surface.

To minimize lateral forces on the assembled reactor, a 6-inch section of 1/8" Teflon tubing was added as a flexible connector between the top outlet of the reactor and the original 1/8" outlet line. The Teflon piece is also translucent, which allows condensed water in the reactor outlet stream to be observed directly. Prior to this, water condensation could only be inferred from GC and mass spectrometer results.

The QTMR seals against the membrane using an external pneumatic press to maintain constant compressive force regardless of reactor temperature. The bottom portion of the pneumatic press consists of a piston in a cylinder with a gas supply line. A three-way valve on the gas supply line allows the cylinder to be charged with air either from a conventional regulated gas cylinder for continuous operation or from a foot-operated bicycle tire pump for reactor assembly. The constant force from the gas cylinder regulator holds the two parts of the reactor together firmly at a delivery pressure of 5 psi. *NOTE: The pneumatic press was actually developed and implemented with the SSMR before the QTMR was constructed, as were the gold ring gaskets. The final tests with the SSMR benefitted from these improvements.*

In this preliminary work with the QTMR, the feed gases flow through the annular space and the reaction chamber effluent flows out through the inner quartz tube (Figure 4.4). The primary justification for this decision was the desire to use the outer quartz tube, which is directly heated by

the cylindrical furnace and in close proximity to the external thermocouple, as a feed gas pre-heat zone to control the reactor feed temperature at the target temperature.

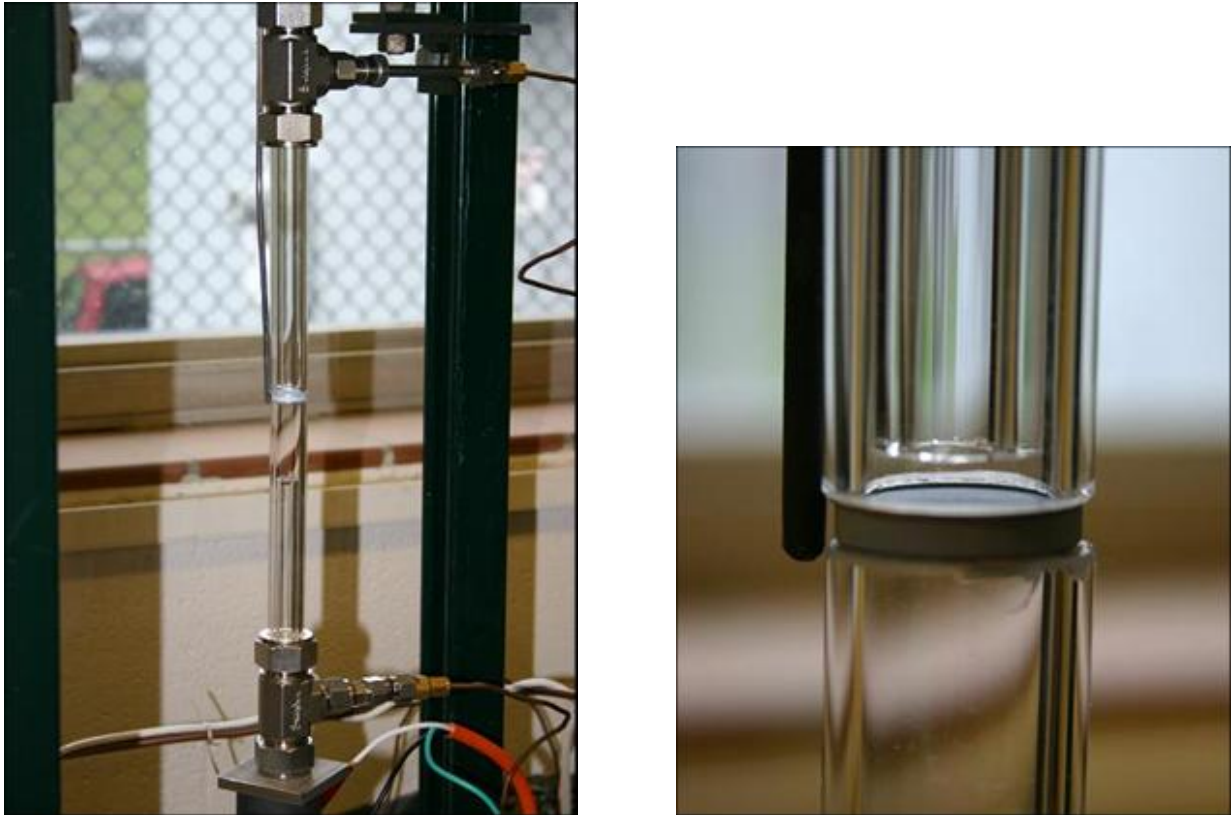


Figure 4.4: Photographs of the QTMR prior to furnace and insulation installation

4.2.2: QTMR assembly

During installation, a removable sleeve is used to align the two pieces of the reactor with the membrane sandwiched between them. The pneumatic press is then used with the foot pump to compress the top and bottom reactor pieces against the membrane. A gas cylinder with a low pressure regulator is then engaged to compress the reactor parts at constant pressure.

Gold ring seals (Item No. GG060020, Scientific Instrument Service) allow the outer quartz tubes to seal against the top and bottom membrane surfaces. Prior to installation, gold seals are attached to the membrane with three small drops of Crazy Glue (chemical composition: ethyl 2-

cianoacrylate) prior to installation. The glue burns off early in the heating process (by 400 °C), but the gold seals do not soften until 800 °C. An airtight seal forms when the seals soften at 800 °C. After the seal has formed, it endures both increases and decreases in temperature within the temperature range of interest (400 to 900 °C) as long as it remains under compression. The drops of glue used to hold the gaskets in place during assembly burn away long before the seal forms and therefore have no effect on seal integrity.

Once the reactor has been stabilized by the constant compressive force provided by the regulated gas supply, the alignment sleeve is removed and the inlet and outlet lines are attached. The clamshell annular ceramic furnace is then installed around the reactor body with the membrane located approximately one-third of the way up the 6" furnace, leaving approximately 4" of the reactor inlet tube within the span of the furnace as a pre-heat zone.

The external thermocouple is inserted into the space between the furnace and the reactor, as indicated in Figure 4.3, with the tip touching the exposed edge of the membrane. Quartz-wool insulation is then packed around the top and bottom openings of the furnace and around the top portion of the reactor.

4.2.3: QTMR Conclusions

The QTMR can endure sustained operation at temperatures of 800 °C or higher and the external pneumatic compression mechanism works well at high temperatures. The reactor seals effectively at reaction temperatures with both the SFC membranes and the stainless steel blank. Low temperature sealing was not as good as with the SSMR and the earlier gaskets (copper and graphite), but low temperature sealing was not considered an area of critical importance for this work.

QTMR advantages:

- Easy to assemble

- Excellent seal at high temperatures
- High maximum operating temperature (at least 900 °C)
- Membranes may be recovered intact
- Used catalyst may be recovered

QTMR disadvantages:

- Poor seal at low temperatures
- Quartz tubes are fragile and difficult to refinish if damaged

4.3: Reactor Sealing

4.3.1: Copper gaskets

Copper was the first gasket material selected for use with the SSMR. The copper gaskets were thin disks that were sized to fit the SSMR.

Copper provided a reasonably good seal across the effective temperature range of the SSMR (i.e., room temperature to 750 °C). However, copper oxidized extensively under membrane testing conditions wherein air was continuously fed to the bottom chamber of the SSMR. Gasket oxidation helped fuse the membrane or blank to the reactor body.

The copper gasket also required high compressive force (i.e., high torque on the SSMR's compression screws) to seal at low temperature and the high temperature seal was not as good as desired. Copper's melting point is also too low for effective use at the high end of the target temperature range (i.e., hotter than 800 °C).

4.3.2: Graphite gaskets

With the goal of reducing the compressive force required at low temperatures and facilitating membrane removal after testing, high-purity graphite gaskets were auditioned (0.5" ID x 0.75" OD

Grafoil GTK and GTJ gaskets, Sealing Devices, Inc.). The graphite used in the gasket construction was specified as nuclear grade and was found to be as heat-resistant as claimed by the manufacturer. The reaction side gaskets, which were exposed to very little oxygen held up remarkably well during reaction testing.

Even nuclear-grade graphite is not oxidation resistant at the test temperatures of interest, however, so it was hoped that the compression of the gasket and the resulting small exposed surface area would protect the bottom (or air side) gasket from oxidation.. The continuous air flow on the oxygen supply side of the membrane eroded the bottom gasket significantly and continuously. The longer the test, the less gasket material remained at the end, although the reaction side gaskets consistently appeared to be undiminished.

Graphite gaskets offered the best low temperature seal, but the seal generally deteriorated with increasing temperature. With the screw-compression SSMR, this phenomenon was initially attributed to gasket erosion because the screw-compression mechanism was incapable of adjusting to the loss of membrane thickness. However, the pneumatic press was introduced while the SSMR was still in use, and even with the constant-compression pneumatic press the graphite gasket seal diminished with increasing temperature. Because the graphite gaskets are not made of a dense material like gold or copper (they are formed by pressing a large number of very thin graphite sheets together), they do allow gas transport. For the graphite material in question, higher temperature operation appears to increase gas diffusion through the gaskets. One unique problem with the graphite gaskets was the appearance of CO₂ from air-side gasket oxidation at temperatures above approximately 500 °C. The CO₂ was formed on the air side of the membrane, but detectable quantities must diffuse through the reaction-side gasket because the analytical instruments are on the outlet line from the reaction side.

4.3.3: Gold gaskets

Before switching to the QTMR, gold wire gaskets were tested with the SSMR and were found to offer improved high temperature sealing ability and dramatically greater oxidation resistance and durability over the graphite gaskets, particularly on the air side of the membrane. The gold gaskets were initially used on both sides of the membrane in the QTMR, but the bottom gasket was later abandoned to save money because leaks are not an issue on the air side of the membrane.

On assembly, the gold gaskets do not provide as good a seal as either the graphite gaskets or the copper gaskets. The gold gaskets are rings (i.e., they have a cylindrical cross-section) while the copper gaskets are flat, and the difference in cross-sectional shape is significant for a rigid material. However, the gold seals soften as the reactor system approaches its 800 °C reaction temperature and the seal is fully formed within 30 minutes at 800 °C. After testing, the gold gaskets are flattened and thus have a similar cross-section to the copper gaskets. Gold gaskets tend to stick to the membranes after reaction (as did the other two gasket materials), but they were re-used successfully if they weren't compressed excessively the first time.

In all cases, the leak with the gold rings during operation at 800 °C was estimated as less than 0.2% of the reactor feed flowrate based on elemental nitrogen in the reactor effluent. This was viewed as a noteworthy accomplishment, but it is important to reiterate that leakage during reactor heat-up is unavoidable before the gold seals soften sufficiently near 800 °C. As a result of the poor initial seal, the air content of the effluent during heat-up averages approximately 5% of the reactor's pre-reaction argon feed.

4.3.4: Reactor sealing conclusions

In general, the combination of the pneumatic compression mechanism and the gold gaskets provides the best seals with both the SSMR and the QTMR. However, either copper or graphite

gaskets would be superior for low temperature testing (~700 °C or less for copper and ~500 °C or less for graphite). Because the membrane sits at the bottom of a deep cavity in the SSMR, graphite gaskets might offer the best chance of an easy membrane extraction post-reaction. Table 4.1 provides a quick performance comparison of the three gasket materials tested in this work.

Table 4.1: Gasket material performance comparison

| Gasket Property | Copper | Graphite | Gold |
|--|---------------|-----------------|-------------|
| Low temperature seal quality | Fair | Good | Poor |
| High temperature seal quality | Good | Fair | Excellent |
| Oxidation resistance | Fair | Poor | Excellent |
| Ease of membrane removal (post-reaction) | Poor | Good | Fair |
| General durability | Fair | Poor | Excellent |
| Average rating (Poor = 0, Fair = 1, Good = 2, Excellent = 3) | 1.0 | 1.2 | 2.0 |

If used, the alternative gasket materials would require higher compressive forces than required by gold at 800 °C, as gold softens sufficiently at 800 °C that only modest compressive force is required to flatten the gasket and provide an excellent seal. At low enough operating temperatures and with mechanical durable membranes, the screw-compression mechanism in the SSMR could be used with the graphite or copper gaskets. Unlike the pneumatic compression mechanism, the screw-compression option requires no outside parts or additional equipment, which could be an important benefit in some circumstances.

Chapter 5: Initial Reaction Studies: The SSMR and Patterned Membranes

This chapter presents and analyzes the reaction test results obtained with the SSMR. This initial investigation of the concept of membrane oxygen-assisted CO₂ reforming used SFC membranes with and without deposited platinum patterns and also a platinum on zirconia powder catalyst (0.43 wt% Pt/ZrO₂) that exhibited rapid deactivation in previous CO₂ reforming work [1]. The SSMR has a relatively high leak rate (i.e., oxygen from leaked air on the order of the oxygen provided by the SFC membranes), and the effect of leakage oxygen in this early work confounds the effect of the SFC membrane on catalyst activity. Although operational issues prevented a quantitative assessment of the improvement imparted by the SFC membrane, it clearly enhanced the stability of the powder catalyst.

Reaction tests were performed at 700 °C with and without the powder Pt/ZrO₂ catalyst and at 750 °C with both platinum patterned and plain membranes. Moving beyond the conventional approach to assessing reforming reactions by methane conversion and H₂:CO ratio, several additional product and reactant ratios are introduced as tools to evaluate the possible net reaction profiles for the various tests. In tests with patterned membranes or no catalyst, water and CO₂ production levels implicate combustion as the dominant methane conversion reaction, whereas CO₂ reforming appears to account for most of the methane conversion in the presence of the powder Pt/ZrO₂ catalyst.

Under SEM evaluation, the patterned SFC membranes showed significant surface restructuring that is attributed to phase changes caused by the highly reducing reaction environment (see Appendix D for images and discussion). Patterned membranes were abandoned for reaction testing after the work described in this chapter because of the dramatic phase change behavior and the high incidence of combustion they exhibited. All subsequent reaction tests use conventional powder catalysts.

5.1: Initial SSMR Tests

5.1.1: Methane conversion

This early work with the stainless steel reactor confirmed the potential benefit of a low flux membrane reactor for CO₂ reforming. Figure 5.1 presents the first set of reaction data obtained with the membrane reactor. These results were obtained at 700 °C with 8 mg catalyst and a 10 cm³/min (ccm) feed of 50% each methane and carbon dioxide. Feed flowrates were increased to a minimum of 20 ccm following these first four tests, and the corresponding modified space velocity of 150 L/h/g_{cat} was used as the standard feed rate for all subsequent tests with powder catalyst. The exposed membrane surface area is 1.53 cm².

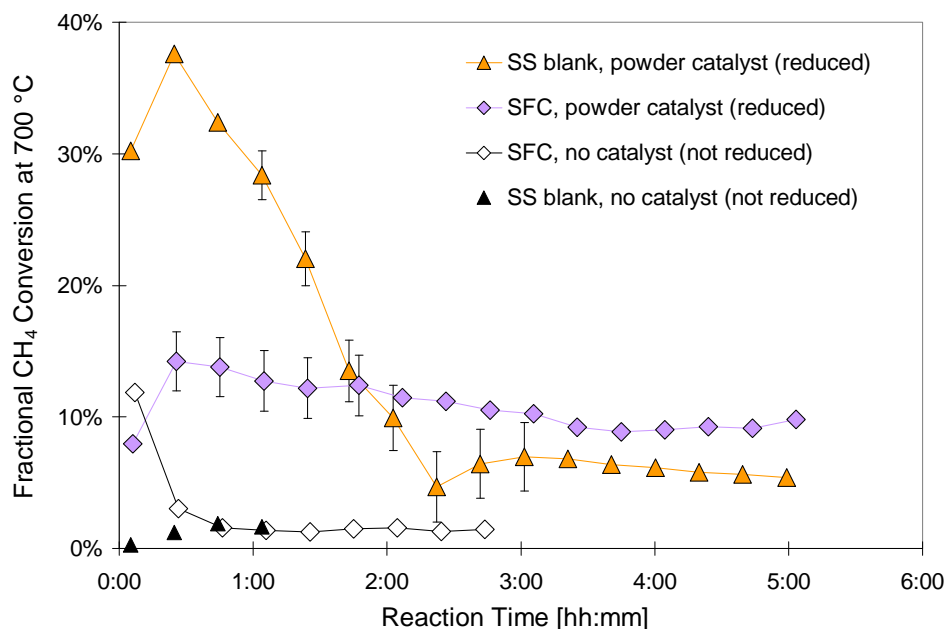


Figure 5.1: Fractional CH₄ conversion during CO₂ reforming over a Pt/ZrO₂ catalyst in the original SSMR. Reaction temperature=700 °C, GHSV=75 L/h/g_{cat}, CH₄:CO₂ feed ratio=1:1 with no Ar/O₂ dilution.

Although the membrane seems to have a detrimental effect on catalyst activity initially, the catalyst sustains its activity much more effectively on the membrane. Also, the SFC membrane and the painted steel blank without catalyst exhibit a similarly low amount of activity for methane

conversion, indicating that the sustained activity in the membrane test with powder is not caused by methane conversion on the SFC surface itself.

Regarding the lower early activity, it was discovered on disassembly that the powder catalyst in this membrane test had been pushed away from the reactor inlet and was therefore not distributed evenly over the exposed surface as intended (and as was done successfully in the stainless steel blank test). The catalyst bunching certainly occurred during pre-reaction flushing with argon when flowrates as high as 100 ccm were used, compared to 20 ccm total during the reaction test. *NOTE: a pad of quartz wool and a reactor feed flow rate limit of 50 mL/min maximum were used successfully in future SSMR tests with powder catalyst to prevent this from reoccurring. No catalyst redistribution was observed in any subsequent tests. The SS blank with catalyst test in Figure 5.1 was the first test performed with these precautions in place.*

Poor catalyst distribution could explain the lower average activity of the catalyst on the membrane, but it does not explain the decreased deactivation rate relative to the blank test. If anything, the poor catalyst distribution should have diminished any effect of the membrane by decreasing the amount of catalyst in contact with the membrane. The fact that an effect was observed even with minimal catalyst/membrane contact presages the eventual hypotheses about the mechanism of the synergistic activity between catalyst and membrane.

5.1.2: CO₂ conversion

Another noteworthy observation from this first set of tests is the effect of the membrane on CO₂ conversion. As Figure 5.2 depicts, CO₂ conversion was actually negative for the tests with no catalyst, indicating that CO₂ was produced rather than consumed in these tests. CO₂ production in conjunction with methane conversion generally indicates combustion, which is not surprising given the absence of a catalyst capable of promoting CO₂ reforming and the presence of oxygen in the reaction chamber (from leaked air in the blank test and from both leaked air and membrane oxygen in

the SFC test). The symmetrical relationship between methane and CO₂ conversion reinforces the suggestion of methane combustion in the tests without catalyst.

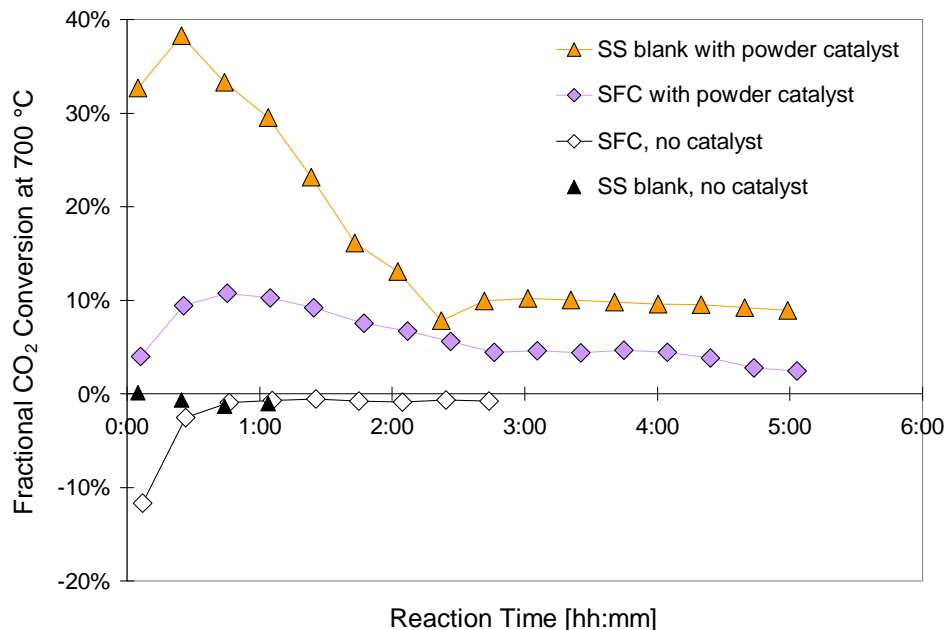


Figure 5.2: Fractional CO₂ conversion during CO₂ reforming over a Pt/ZrO₂ catalyst in the original SSMR. Reaction temperature=700 °C, GHSV=75 L/h/g_{cat}, CH₄:CO₂ feed ratio=1:1 with no Ar/O₂ dilution.

In spite of the catalyst redistribution problem, methane conversion in the membrane test with catalyst exceeded methane conversion in the blank test with catalyst after approximately two hours on stream. Even as this occurred, CO₂ conversion in the membrane test with catalyst remained lower than CO₂ conversion in the blank test with catalyst. This is the first conclusive evidence that the SFC membrane has an effect on the net reaction profile in a membrane reactor with a CO₂ reforming feed.

5.1.3: H₂:CO ratio

The hydrogen to carbon monoxide ratio (H₂:CO ratio) in the reactor effluent is a common “single parameter” used to evaluate the net reaction profile in a reforming reactor. However, this ratio cannot distinguish between complete combustion and reforming reactions because complete combustion produces neither hydrogen nor carbon monoxide. For CO₂ reforming with the 1:1 feed

ratio used in this work, the theoretical maximum $H_2:CO$ ratio is one. $H_2:CO$ ratios less than the stoichiometric maximum are generally attributed to reverse Water-Gas Shift (rWGS) [2-4].

For this initial set of tests, Figure 5.3 demonstrates that the $H_2:CO$ ratios are in the expected range for CO_2 reforming of one or less. CO_2 reforming thus appears to be the dominant methane conversion reaction in the tests with catalyst. The fact that the two tests with no catalyst are indistinguishable in Figure 5.3 from the two tests with catalyst confirms the inability of the $H_2:CO$ ratio to distinguish the effect of combustion in a reforming reaction set.

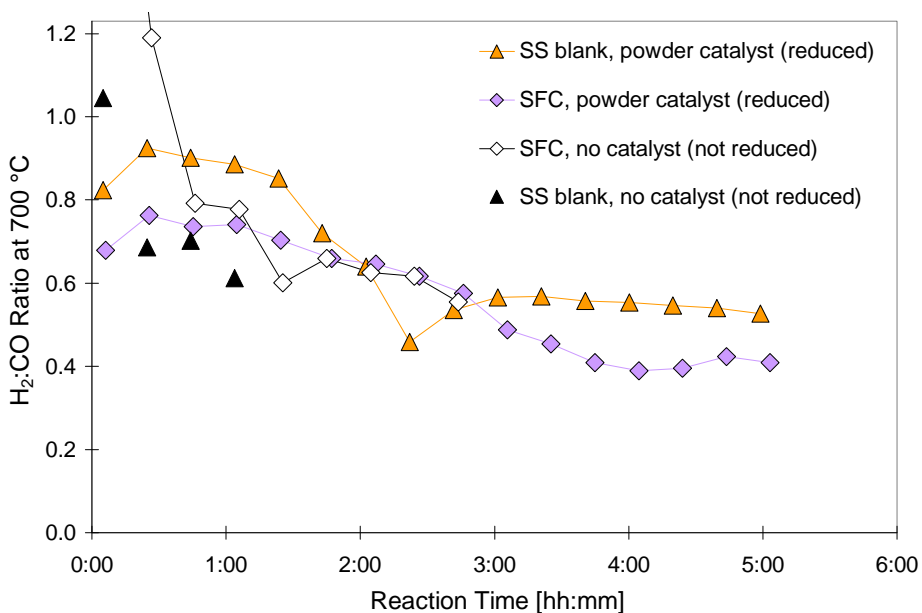


Figure 5.3: $H_2:CO$ ratio during CO_2 reforming over a Pt/ZrO_2 catalyst in the original SSMR. Reaction temperature= $700\text{ }^\circ\text{C}$, $GHSV=75\text{ L/h/g}_{cat}$, $CH_4:CO_2$ feed ratio=1:1 with no Ar/O_2 dilution.

5.1.4: Hydrogen selectivity

In general, the negative CO_2 conversions depicted in Figure 5.2 for the tests without catalyst indicate clearly that CO_2 reforming does not occur to a significant extent without the powder catalyst, and the first data point in particular indicates that complete carbon oxidation occurs at the beginning of the test period. The general failure of the membrane alone to support CO_2 reforming is not surprising since this reaction requires the assistance of an appropriately selective reforming catalyst.

Because the H₂:CO ratio results provide little insight in this situation, it is worth looking at the ratio of the amount of H₂ produced to the amount of CH₄ converted. This metric has a theoretical maximum value of two for both CO₂ reforming and methane partial oxidation. A value under two indicates some amount of hydrogen oxidation, which can occur either directly or as part of rWGS.

The rWGS reaction also produces CO from CO₂ and therefore does two things: 1) it dramatically reduces the H₂:CO ratio by simultaneously increasing CO and decreasing H₂ and 2) it decreases the amount of CO₂ in the reactor effluent which registers as additional CO₂ conversion. The data in Figures 5.2 and 5.3 manifest neither of these trends, and, as the hydrogen production-to-methane conversion ratio (i.e., hydrogen selectivity) trends demonstrate in Figure 5.4, the amount of hydrogen produced per methane reacted is lower than the theoretical value for CO₂ reforming in all cases and is lower on the membrane than on the stainless steel blank. Direct hydrogen oxidation is likely the most significant cause of the reduced H₂:CO ratio with the SFC membrane.

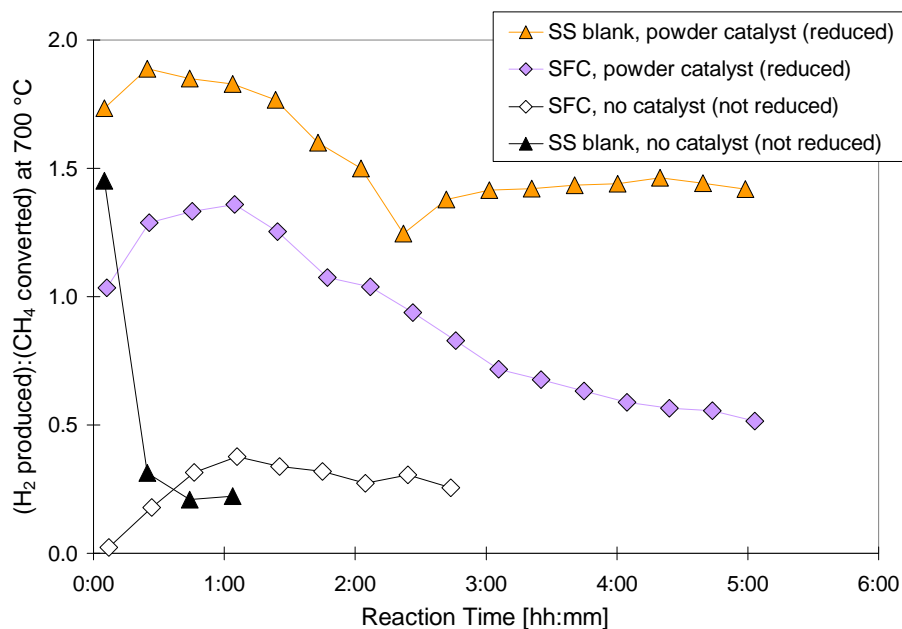


Figure 5.4: Molar ratio of H₂ production-to-methane conversion during CO₂ reforming over a Pt/ZrO₂ catalyst in the original SSMR. Reaction temperature=700 °C, GHSV=75 L/h/g_{cat}, CH₄:CO₂ feed ratio=1:1 with no Ar/O₂ dilution.

Observations of mass spectrometer signals during pre-reaction reduction processes indicate that hydrogen oxidation occurs readily on the membrane surface and the lower hydrogen selectivity values in Figure 5.4 for the membrane case reinforce this observation. The sum of the evidence obtained throughout this work strongly indicates that hydrogen oxidation is the principal mechanism for membrane oxygen extraction under reforming reaction conditions. This will be proposed in the next chapter as a fundamental hypothesis of this work.

5.2: Methane Conversion Assessment with Patterned Membranes

Patterned membranes produced by Sean Murphy for his Master's thesis work were evaluated for CO₂ reforming in the SSMR [5]. Flux testing preceded these reaction tests, so the membranes had already been exposed to multiple temperatures and oxygen gradients prior to reaction testing. Because the initial set of tests was performed at 700 °C without a temperature-related mishap, the reaction test temperature was increased to 750 °C for these tests. This temperature increase was a significant step toward the target reaction test temperature of 800 °C, but 750 °C was ultimately determined to be the maximum temperature for sustained operation of the SSMR.

5.2.1: Fractional conversion

SFC membranes patterned with 20 nm thick platinum particles of 3 micron diameter and 5 micron spacing (edge-to-edge) were tested at 750 °C with a 50:50 feed of CH₄ and CO₂ at higher flowrates than 10 mL/min. Figure D.3 in Appendix D includes SEM images of a membrane of this type before and after testing. Fractional methane conversion results for an unreduced patterned membrane, a reduced patterned membrane, a reduced unpatterned membrane, and the stainless steel blank without catalyst are presented in Figure 5.5. The membrane with powder catalyst results from Figure 5.1 are included for comparison. With the exception of the 700 °C membrane with powder catalyst test, the membrane reaction tests were preceded by a multi-temperature flux testing process

under an argon sweep gas. All tests except the indicated Pt-patterned membrane test also included a pre-reaction hydrogen reduction step.

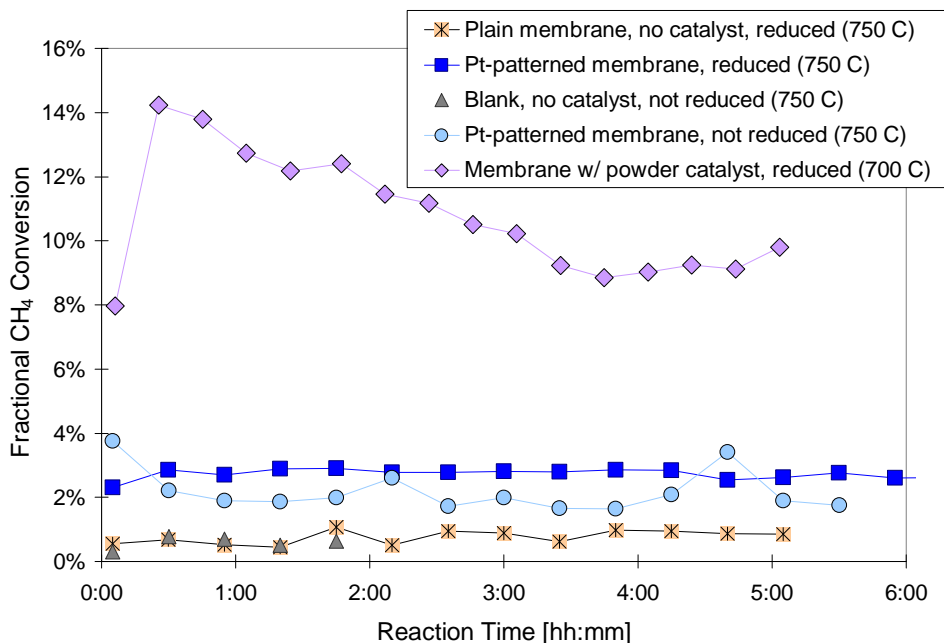


Figure 5.5: Fractional CH₄ conversion during CO₂ reforming over a Pt/ZrO₂ catalyst and Pt-patterned membranes in the original SSMR. Reaction temperature as indicated, CH₄:CO₂ feed ratio=1:1 with no Ar/O₂ dilution, various feed flowrates.

5.2.2: Molar conversion rate

At first glance, the fractional conversion data imply that the patterned membranes are not as effective as the conventional powder catalyst. However, the total flowrate in the 700 °C test with the powder catalyst was 10 ccm while the flowrate in the two tests with the reduced membranes was 40 ccm and the flowrate in the unreduced patterned membrane test and the blank test was 20 ccm. Presenting the results as millimoles of CH₄ converted per second removes the flowrate effect and depicts a different relationship between the tests. From the molar conversion rate perspective provided by Figure 5.6, the patterned membrane compares more favorably to the traditional catalyst, particularly given the lack of a catalyst bed for the reactants to pass through. With the patterned membranes, the reaction chamber contents only flow around a pattern on a polished horizontal surface (i.e., a two-dimensional catalyst).

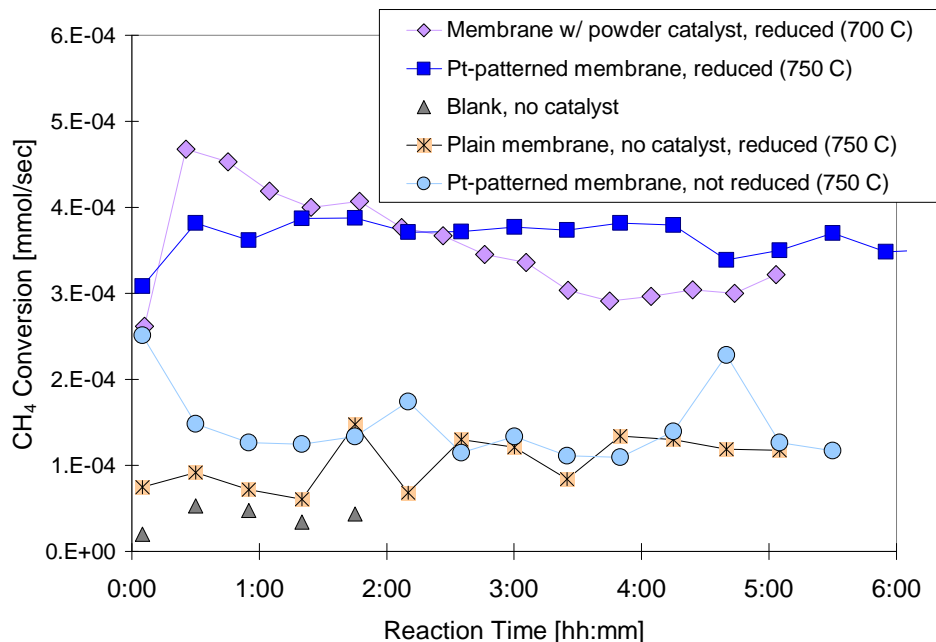


Figure 5.6: Molar CH₄ conversion during CO₂ reforming over a Pt/ZrO₂ catalyst and Pt-patterned membranes in the original SSMR. Reaction temperature as indicated, CH₄:CO₂ feed ratio=1:1 with no Ar/O₂ dilution, various feed flowrates.

Interestingly, methane conversion rates on the unreduced patterned membrane and the reduced plain membrane converged somewhat at steady state. Given their low conversion relative to the reduced patterned membrane, it is possible that the unreduced platinum has little effect and that the early difference was actually the result of the higher initial membrane oxygen content of the unreduced membrane.

5.2.3: Turnover frequency (TOF)

The patterned membrane tests were performed at 750 °C instead of 700 °C and therefore should exhibit relatively greater activity, yet in Figure 5.6 they show comparable or lesser activity on a molar conversion rate basis. A comparison of turnover frequency (TOF) values, or moles of methane reacted per mole of exposed platinum per time, is the next step to achieving a true comparison of the catalyst pattern to the conventional supported platinum catalyst.

Exposed platinum must be determined for the two different catalyst types and the two tests with no catalyst of either kind cannot be included. Moles of exposed platinum can be calculated for the powder catalyst using the known catalyst dispersion [1] and for the patterned membranes using the known geometries of the platinum pattern (calculations provided in Appendix D). Turnover frequencies calculated using these values are presented in Figure 5.7.

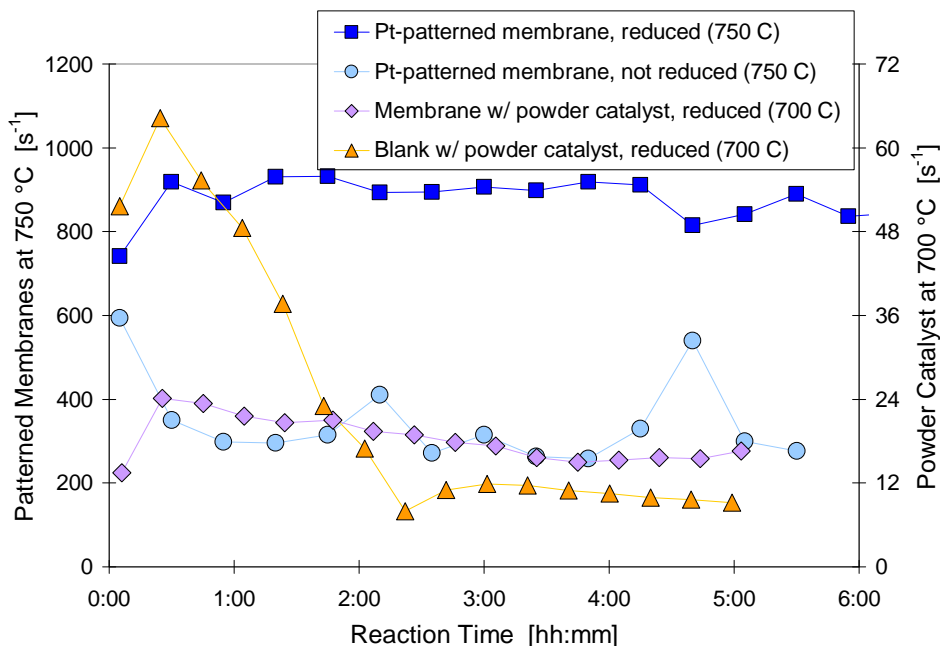


Figure 5.7: CH₄ conversion turnover frequency (TOF) during CO₂ reforming over a Pt/ZrO₂ catalyst and Pt-patterned membranes in the original SSMR. Reaction temperature as indicated, CH₄:CO₂ feed ratio=1:1 with no Ar/O₂ dilution, various feed flowrates.

The TOF approach to methane conversion shows the patterned membranes in a much more positive light: their efficiency per exposed platinum atom is dramatically higher than that of the conventional powder catalyst—so much so that they cannot be presented on the same scale. The primary y-axis in Figure 5.7 applies to the two patterned membrane tests and the secondary y-axis applies to the two powder catalyst tests. TOF cannot be used as the default methane conversion metric for this work because not all tests include catalyst, but TOF will be considered whenever possible.

5.2.4: Reaction temperature

Although temperature is the remaining factor to be addressed to allow a proper comparison of the methane conversion results for the plain and patterned membranes, it appears to account for only a fraction of the difference in scale in Figure 5.7.

The data in Figure 5.7 show that the steady state turnover frequency of the reduced patterned membrane is about fifty times that of the reduced powder catalyst. However, Wei and Iglesia and Maestri et al. demonstrate that the rate constants for the forward CO₂ reforming reaction over platinum and rhodium double with each 50 °C increase in temperature [6-8]. After applying a factor of two to the methane conversion results for the powder catalyst on SFC test to account for the temperature difference, the TOFs for the patterned membrane are still about 25 times those of the powder catalyst. *NOTE: the effect of temperature on equilibrium product composition for these reaction conditions is summarized in Table N.2 in Appendix N.*

It is also worth noting here that Wei and Iglesia and Maestri et al. determined that CO₂ reforming reaction rates over platinum and rhodium is first order in CH₄ and zero order in CO₂ and that steam reforming and methane decomposition are both first order in CH₄ as well. Because methane decomposition is also generally accepted to be the first step in partial oxidation, the conclusion can be drawn that methane reforming reactions in general are first-order in methane.

5.2.5: Catalyst powder distribution

The redistribution of the powder catalyst on the membrane surface that was described in Section 5.1.1 also needs to be accounted for. The corresponding blank test with powder catalyst was chosen as a reference reaction with which to align the the initial activity of the catalyst on the membrane (later testing proves this to be a reliable estimate). Multiplying the membrane test conversion results by five aligns them initially with the blank test results. However, even after

including this factor of five, the patterned membrane still shows a fivefold increase in TOF over the powder catalyst. This is a dramatic difference.

5.2.6: Other factors affecting the comparison of patterned membranes and powder catalyst

Other significant factors underlying the powder catalyst and the patterned membrane tests generally reinforce rather than undermine the conclusion that the patterned membranes have higher methane conversion activity than a powder catalyst on top of a membrane. For example, the estimated amount of oxygen from air leakage into the system during the powder catalyst test was around 1% of the feed while leak oxygen in the patterned catalyst test was less than 0.2%. Additional leaked oxygen was therefore not responsible for the higher relative methane conversion on the patterned membrane. If it had had any effect, it would have favored the powder catalyst test.

Another important operational factor is catalyst bed volume (or depth). Although the catalyst bed in the powder catalyst test is intentionally thin to minimize transport limitations and maximize the fraction of the catalyst in contact with the membrane, the bed had significantly more depth than the patterned membrane surface. The 3 micron platinum features were deposited at a target thickness of 20 nm (0.02 microns), so the effective “bed depth” for these membranes is only 20 nm. This represents a much smaller fraction of the reaction chamber volume than the ~1 mm deep powder catalyst bed. Once again, any advantage in methane-catalyst contact should accrue to the powder catalyst, not the patterned membranes.

It is worth noting that, despite the overall difference in magnitude, the activity trends in Figure 5.7 for the two SFC membrane tests with a pre-reaction reduction step and catalyst of either kind are similar: both test types exhibit an immediate increase in methane conversion from an initial low value over the first 30 minutes of reaction and then display a relatively steady and modest decline in activity over the next 5 hours of reaction.

5.3: Available Oxygen and Catalyst Activity

To determine the effect of oxygen on catalyst activity, both membrane oxygen and leaked oxygen must be considered in the evaluation. Total oxygen into the reactor (i.e., the combined oxygen from air leakage and membrane flux) can be calculated with an oxygen balance, but membrane flux cannot be estimated without first quantifying the air leakage. Also, if leaks are large relative to membrane oxygen flux, the effect of oxygen from the leaked air on catalyst activity can overwhelm the effect of the smaller amount of membrane oxygen.

5.3.1: Total oxygen

Because of the interdependence between leaked and membrane oxygen and the fact that these early SSMMR tests experienced relatively large leak rates, the least speculative approach to evaluating the effect of oxygen on catalyst activity for these tests is to relate total oxygen to methane conversion as shown in Figure 5.8. In the case of the patterned membranes and their lower leak rate relative to feed rate (0.2% leaked oxygen in the overall feed compared to 1% in the powder catalyst test), a majority of the oxygen in question is likely provided by the membrane. *NOTE: with the four-fold increase in feed rate for the patterned membrane test compared to the powder membrane test, the absolute leak rates for these tests are closer than the % leak comparison implies: the leak rate in the patterned membrane tests is ~0.8ccm vs. 1.0 ccm in the membrane test with powder catalyst.*

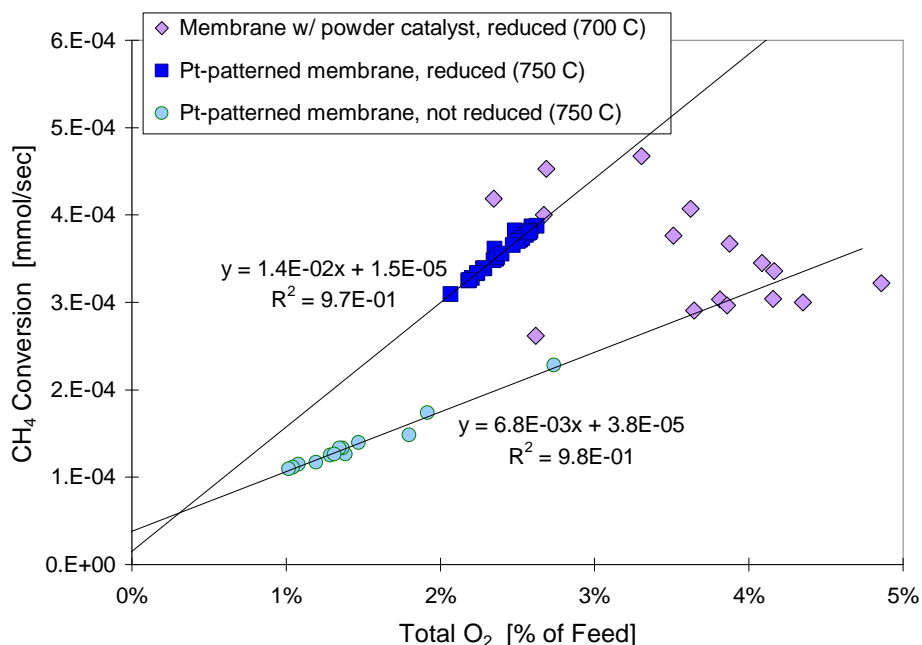


Figure 5.8: Molar CH₄ conversion vs. total available oxygen during CO₂ reforming over a Pt/ZrO₂ catalyst and Pt-patterned membranes in the original SSMR. Reaction temperature as indicated, CH₄:CO₂ feed ratio=1:1 with no Ar/O₂ dilution, various feed flowrates.

Figure 5.8 provides the following conclusions: (1) reduction improves patterned membrane activity; (2) under CO₂ reforming conditions, patterned membrane activity depends linearly on oxygen, regardless of the source; (3) despite their different slopes, the trend lines for the reduced and unreduced patterned membranes converge to almost the same point on the y-axis; and (4) the methane conversion activity of the Pt/ZrO₂ powder catalyst on an SFC membrane does not initially appear to be related to oxygen concentration. *NOTE: the trendlines in Figure 5.8 were assigned using Microsoft Excel's "Add Trendline" feature. The initial sample from each set was not included.*

Both lines in Figure 5.8 intersect the y-axis above zero, indicating that a small amount of methane conversion should occur on a patterned membrane with or without reduction even in the absence of oxygen. As it happens, the steady state rate of methane conversion without catalyst on both the stainless steel blank and plain, unreduced membrane averaged approximately 5×10^{-5} mmol/sec, which coincides exactly with the projected baseline methane conversion for the unreduced patterned membrane (i.e., the y-intercept of the fitted line for that test) in Figure 5.8.

Figure 5.8 also indicates that methane conversion on the patterned membranes is largely determined by oxygen availability and exhibits a first-order dependence on oxygen. This contrasts with the apparent insensitivity of methane conversion to oxygen with the powder catalyst, implying a primary methane-conversion reaction with the Pt/ZrO₂ catalyst that does not depend on oxygen. In the conditions provided for these tests, CO₂ reforming is the most likely candidate.

5.3.2: Membrane oxygen flux

Flux estimates for the reduced patterned membrane were two to four times higher than estimates for the unreduced patterned membrane and the 700 °C powder catalyst test membrane. However, membrane oxygen contributions are comparable on a feed volume percentage basis for the two reduced tests because of the higher feed flow rate in the patterned membrane tests (40 ccm vs. 10 ccm). Figure 5.9 demonstrates the similarity of the average reactor feed composition for the two tests with pre-reaction reduction steps.

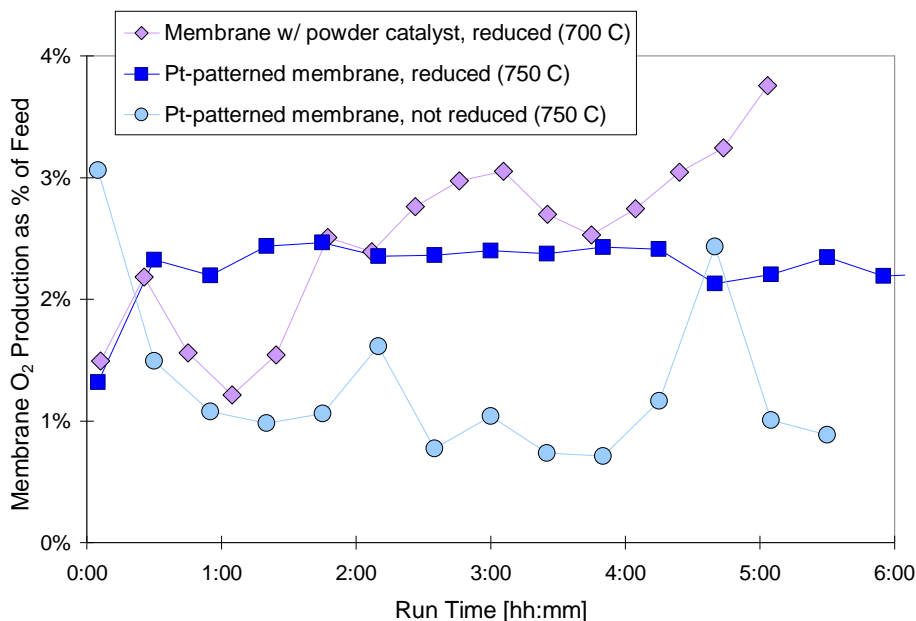


Figure 5.9: Membrane oxygen production during CO₂ reforming over a Pt/ZrO₂ catalyst and Pt-patterned membranes in the original SSMR. Reaction temperature as indicated, CH₄:CO₂ feed ratio=1:1 with no Ar/O₂ dilution, various feed flowrates.

Figure 5.9 also exemplifies the effect of reduction on membrane oxygen flux trends: the unreduced membrane starts with a high oxygen production value that begins to drop immediately, while the reduced membranes have the opposite early response to the reaction environment. The unreduced membrane is likely displaying a quick release of oxygen as the top surface of the membrane moves abruptly toward a lower equilibrium oxygen content in the reforming reaction environment. The reduced membranes appear initially to be somewhat depleted in oxygen on the reaction-side surface. They then recover as oxygen demand continues throughout the reaction period and the relatively slow oxygen flux process is able to catch up to the rate of surface oxygen consumption. The initial oxygen depletion in the reduced membranes is attributed to hydrogen exposure in the pre-reaction reduction steps, which have a much higher hydrogen content than the reaction environments (100% hydrogen in the 700 °C test reduction step and 10% in the 750 °C reduction step, compared to maximum hydrogen concentrations of 8% and 0.4%, respectively, during the 700 °C and 750 °C tests).

5.4: The Effect of Reduction on Membrane Activity

Because Figure 5.6 shows that the platinum particles are essential for methane conversion on an SFC membrane with no powder catalyst and because membrane oxygen correlates highly with methane conversion in Figure 5.8, any set of reactions considered for the patterned membranes should focus on the interface between the platinum particles and the membrane material itself. This mechanistic approach has also been proposed and defended in the literature for conventional supported catalysts in CO₂ reforming [9-10]. The oxidation state of the membrane surface becomes an important factor for patterned membrane catalytic activity.

5.4.1: Methane conversion and oxygen flux

The patterned membrane tests confirm another interesting trend from the first set of 700 °C tests: membranes that have been reduced exhibit low initial methane conversion activity followed by

an increase within the first 30 minutes. Figure 5.7 also reinforces the converse observation from Figure 5.1 that methane conversion over an unreduced membrane is generally at its highest at the beginning of a test and then tends to decrease immediately. These catalyst activity observations can all be linked directly to the membrane oxygen flux observations in Figure 5.9. In the early part of the reaction period, methane conversion reflects the membrane equilibration process, which in turn depends on pre-reaction conditions.

5.4.2: CO₂ conversion and membrane reduction

The low initial methane conversion with a reduced membrane is believed to result from oxygen depletion in the membrane's exposed surface during the reduction step. As Figures 5.2 and 5.10 show, CO₂ conversion also appears to depend on membrane reduction: it is initially positive for membrane tests with a pre-reaction reduction step and negative for membrane tests without pre-reaction reduction. As used earlier in Figures 5.7 and 5.9, polynomial trendlines were added to help distinguish the trends in Figure 5.10. *NOTE: negative CO₂ conversion indicates CO₂ production.*

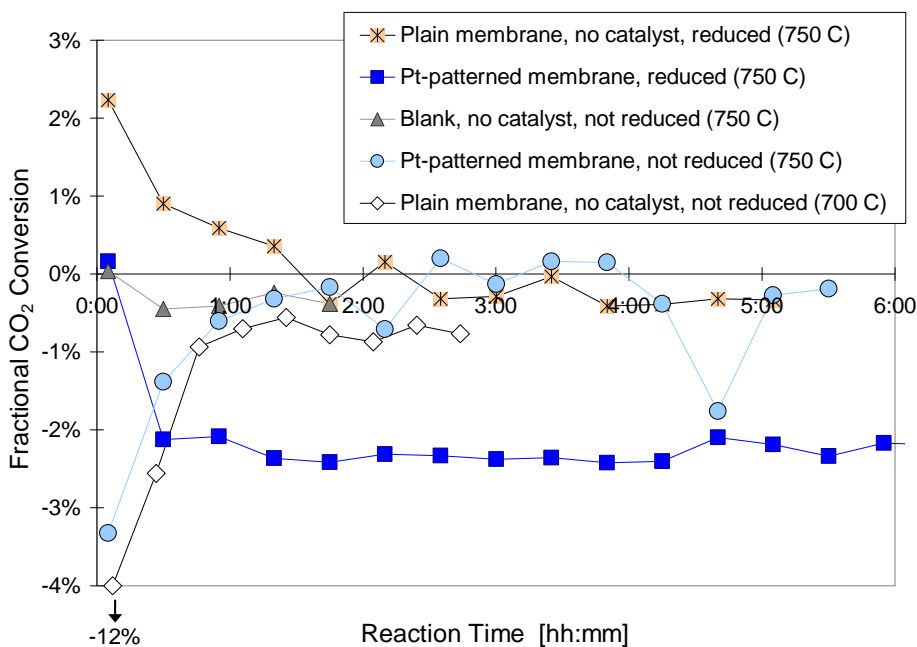


Figure 5.10: Fractional CO₂ conversion during CO₂ reforming over a Pt/ZrO₂ catalyst and Pt-patterned membranes in the original SSMR. Reaction temperature as indicated, CH₄:CO₂ feed ratio=1:1 with no Ar/O₂ dilution, various feed flowrates.

Figure 5.11 provides the respective methane conversion results for the CO₂ conversion results in Figure 5.10, also with trendlines to facilitate trend distinction.

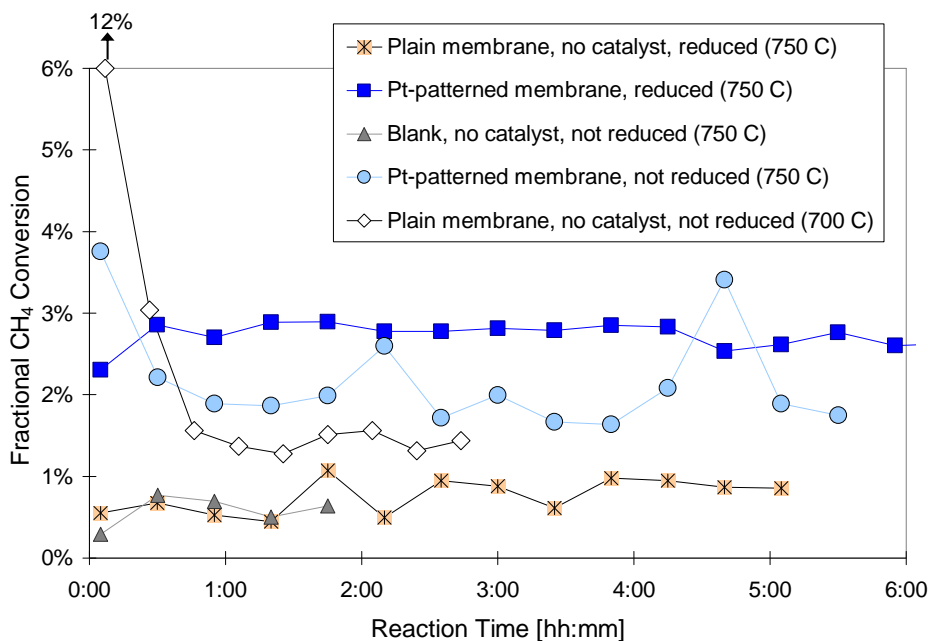


Figure 5.11: Fractional CH₄ conversion during CO₂ reforming over a Pt/ZrO₂ catalyst and Pt-patterned membranes in the original SSMR. Reaction temperature as indicated, CH₄:CO₂ feed ratio=1:1 with no Ar/O₂ dilution, various feed flowrates.

The reduced membrane with no catalyst shows initial CO₂ conversion more than four times as great as methane conversion. Because there is no supported catalyst to interact with CO₂ and only the SFC membrane surface available, this initial CO₂ conversion discrepancy falls into a region where reaction with the reduced membrane is the only possible explanation. Coupled with the oxygen depletion evidence for reduced membranes from the flux estimates, these observations lead to the conclusion that CO₂ will react on the surface of a membrane that has been reduced by hydrogen but not on an unreduced membrane.

If the increasing CO₂ conversion observed in the unreduced membrane tests were from rWGS, there would be commensurate amounts of water and CO produced, but water levels exactly mirror methane conversion for these tests and are correspondingly low throughout. Figure 5.12

demonstrates clearly that carbon monoxide levels trend with CO₂ conversion while methane conversion remains low and flat. Additionally, the two reduced membrane tests show a significant amount of apparent conversion of CO₂ to CO in the early part of the tests while the unreduced membrane initially exhibits low CO and high CO₂ levels. The one hypothesis that explains all of the trends is that the reduced membranes initially convert CO₂ to CO and the unreduced membrane (and the blank) do not.

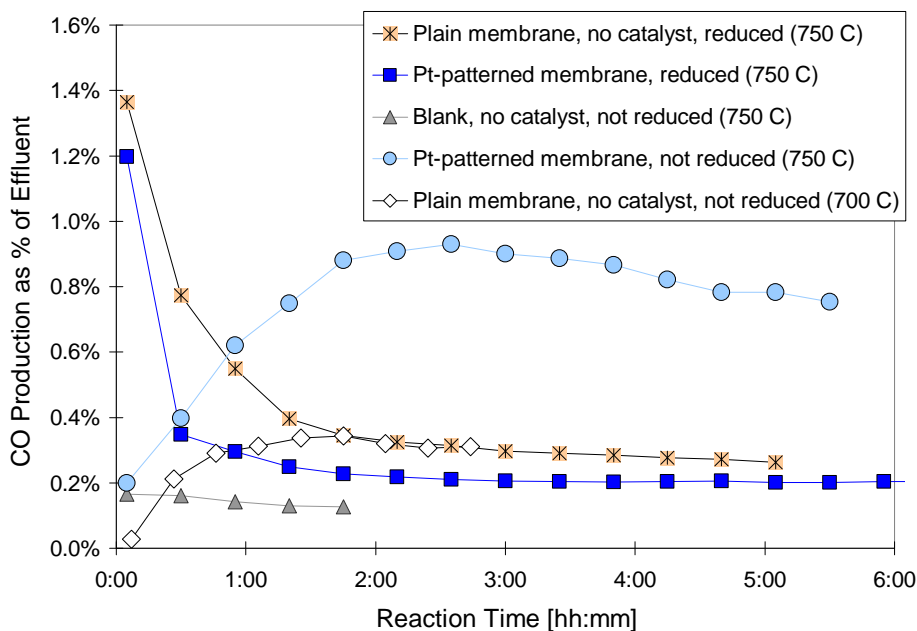


Figure 5.12: CO production during CO₂ reforming over a Pt/ZrO₂ catalyst and Pt-patterned membranes in the original SSMR. Reaction temperature as indicated, CH₄:CO₂ feed ratio=1:1 with no Ar/O₂ dilution, various feed flowrates.

The final pieces of supporting evidence are the membrane oxygen production estimates (Figure 5.13), which show low initial values for the two reduced membranes and a relatively high value for the one unreduced membrane. These results lead to the hypotheses that a negative flux is the result of CO₂ reduction on the membrane surface and that this only occurs after the SFC has been exposed to hydrogen.

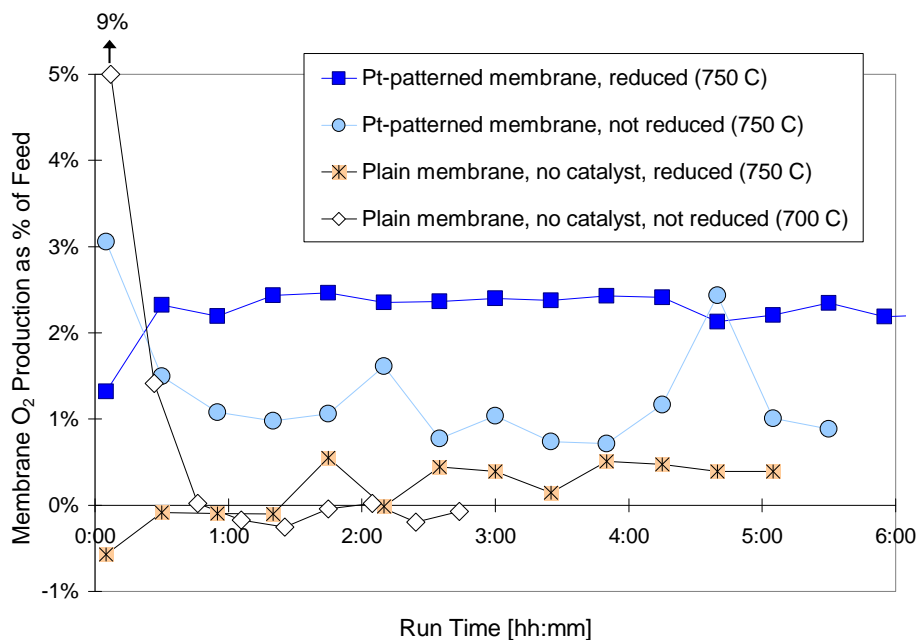


Figure 5.13: Membrane oxygen production during CO₂ reforming over a Pt/ZrO₂ catalyst and Pt-patterned membranes in the original SSMR. Reaction temperature as indicated, CH₄:CO₂ feed ratio=1:1 with no Ar/O₂ dilution, various feed flowrates.

5.4.3: Motivation for reactant and product ratio analysis

The complexity of the above discussion reinforces the need for a more convenient and efficient strategy for evaluating reforming reaction profiles in non-traditional reactor systems. The overall effect of an O-MIEC membrane on CO₂ reforming reaction sets is not known, but the traditional focus on methane conversion and H₂:CO ratio is clearly inadequate to determine the reactions that occur on a membrane surface and in a powder catalyst bed. This is challenging because of the need to evaluate simultaneously trends for multiple species as the membrane and catalyst themselves change over time on stream. Product and reactant ratios represent potentially powerful tools for distinguishing among multiple reaction pathway options. The remainder of this chapter and the subsequent chapters will focus on using such ratios to determine the mechanistic effect of SFC membranes on supported catalyst activity.

5.5: Combustion Analysis with the Patterned Membranes

Methane decomposition on platinum particles is believed to be the critical initiation step in reforming scenarios [6-11], so the reaction mechanism on a patterned SFC membrane is likely to be initiated by the adsorption and decomposition of CH_4 on the platinum particles. Two hydrogen molecules are released in this process and the adsorbed carbon atom either removes oxygen from the membrane surface (which serves as the catalyst support in this application) or reacts with a gas-phase oxygen molecule, if available. The oxidized carbon is then released as CO or CO_2 , and the apparent methane conversion reactions are partial oxidation and combustion, or a combination of the two. In any of these scenarios, CO_2 does not participate as a reactant in the rate-determining step, which is consistent with the argument by Wei and Iglesia and Maestri et al. that CO_2 reforming is zero-order in CO_2 [6-8]. This mechanism requires that the carbon oxidation reactions occur at the platinum-support or platinum-SFC boundary.

5.5.1: CO_2 evaluation

With the platinum particles in direct contact with the highly reducible and self-replenishing SFC membrane, CO_2 may be unnecessary as a reactant for methane conversion on the patterned membrane (although it may play a valuable role in stabilizing the membrane material as mentioned in Section 2.6 [12-13]). To examine the relationship between net CO_2 conversion and CH_4 conversion more carefully, Figure 5.14 present the molar net conversion ratio of the two reactants.

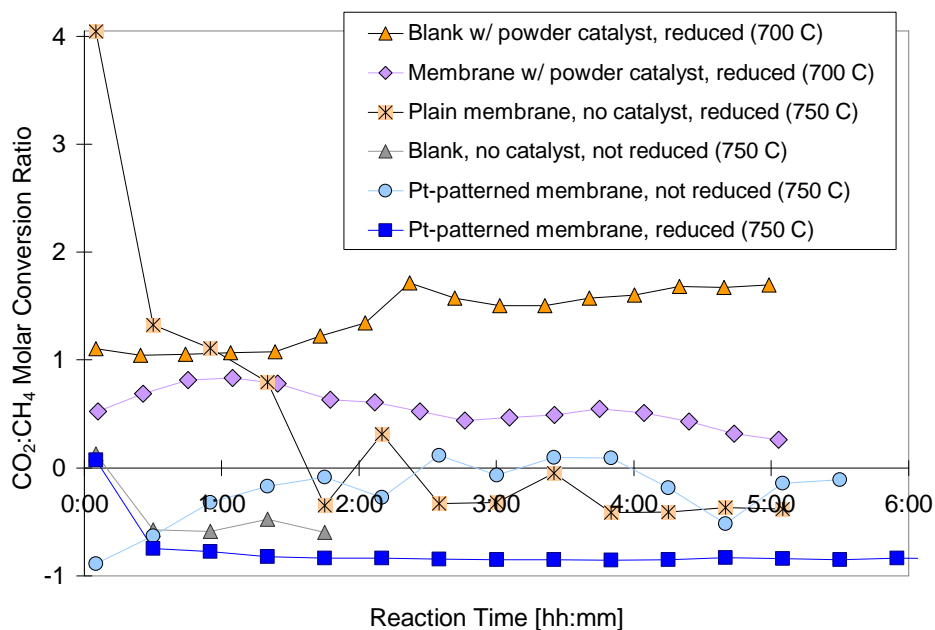


Figure 5.14: Molar $\text{CO}_2:\text{CH}_4$ conversion ratio during CO_2 reforming over a Pt/ZrO_2 catalyst and Pt-patterned membranes in the original SSMR. Reaction temperature as indicated, $\text{CH}_4:\text{CO}_2$ feed ratio=1:1 with no Ar/O_2 dilution, various feed flowrates.

Figure 5.14 confirms that CO_2 conversion on the patterned membranes is not positively correlated with methane conversion. In fact, CO_2 conversion is negatively correlated with methane conversion with the platinum patterned membranes, indicating that CO_2 is produced as methane is consumed. CO_2 production rather than consumption points to combustion rather than CO_2 reforming. The steady-state ratio of CO_2 production to CH_4 consumption for the reduced patterned membrane is about 0.8—i.e., four CO_2 molecules are produced for every five methane molecules converted. Combustion could account for a minimum 80% of methane conversion on the reduced patterned membrane, and even more than 80% if simultaneous rWGS masks additional combustion by consuming CO_2 .

5.5.2: Methane conversion and molar oxygen supply rate

A modified version of Figure 5.8 using a molar rate for both total oxygen feed and methane conversion yields valuable insight into the possible reaction mechanism on the patterned membranes.

Figure 5.15 includes the results from the blank counterpart to the membrane with powder catalyst test and provides strong evidence that the dominant reaction on the patterned membranes is combustion.

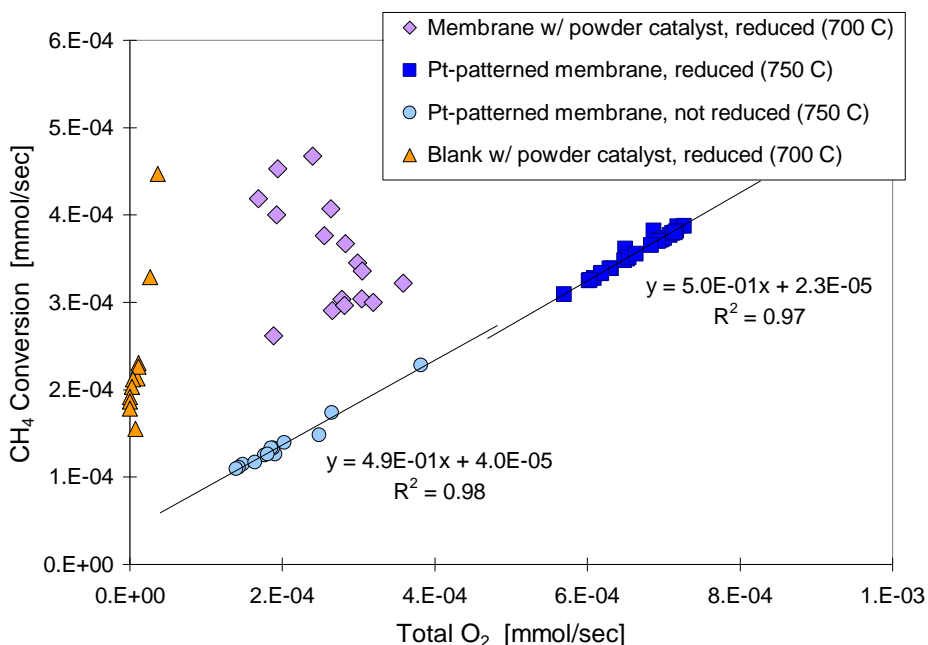


Figure 5.15: Molar CH₄ conversion vs. total available oxygen during CO₂ reforming over a Pt/ZrO₂ catalyst and Pt-patterned membranes in the original SSMR. Reaction temperature as indicated, CH₄:CO₂ feed ratio=1:1 with no Ar/O₂ dilution, various feed flowrates.

The slope of the methane conversion vs. total oxygen line is 0.5 for both the reduced and unreduced cases (i.e., one mole of methane consumed for every two moles of oxygen supplied). This is the stoichiometric relationship expected for methane combustion. The positive y-intercept term indicates that a small amount of another methane consuming reaction must be occurring also. This could be either CO₂ or steam reforming, given the significant amounts of both water and CO₂ available in the reaction chamber, with CO₂ reforming once again the more likely candidate because of the higher CO₂ levels.

Although the patterned membranes follow the stoichiometric oxygen-methane consumption relationship for combustion, the powder catalyst on membrane test exhibits an average relationship of almost 1.5 moles of methane converted per mole of oxygen available. This is closer to the 2:1 ratio for partial oxidation than the combustion ratio of 1:2. If combustion is occurring with the powder

catalyst, it is occurring at a much lower level than with the patterned membranes. Because multiple reactions can and do occur, water production is a key parameter for determining the type and extent of the methane conversion reactions on the SFC membranes.

5.5.3: Water production

Water in the reactor effluent was not measured directly but was calculated by hydrogen atom balance. For the patterned membrane tests, water is produced at about a 1:1 ratio to the amount of O_2 present (Figure 5.16). This is once again consistent with the combustion hypothesis, as methane combustion produces one mole of water for every mole of oxygen consumed. In all three cases, net water production scales linearly with available oxygen, the majority of which is provided by the membranes, but the powder catalyst system produced more water than can be explained by combustion, let alone partial oxidation. However, Figure 5.14 shows that the powder catalyst reaction also consumes CO_2 , which implicates either a combination of partial oxidation and rWGS or a combination of CO_2 reforming and direct hydrogen oxidation as the explanation for the additional water.

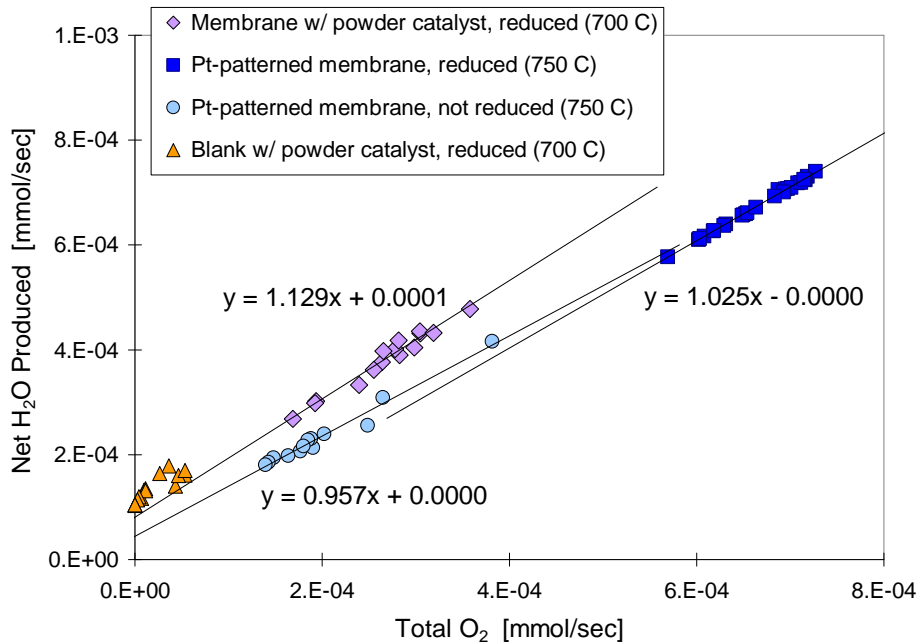


Figure 5.16: Molar H₂O production vs. total available oxygen during CO₂ reforming over a Pt/ZrO₂ catalyst and Pt-patterned membranes in the original SSMR. Reaction temperature as indicated, CH₄:CO₂ feed ratio=1:1 with no Ar/O₂ dilution, various feed flowrates.

With a patterned membrane, the deposited platinum particles guarantee proximity of the reaction products to the membrane surface, so a significant fraction of the hydrogen produced by methane decomposition can spill over onto the membrane surface and form water. This action creates oxygen vacancies in the exposed portion of the SFC lattice. Hydrogen can also oxidize readily at the membrane surface via gas-phase transport with any SFC membrane. Thus, direct hydrogen oxidation is a highly probable reaction.

Figure 5.17 shows that water production on the patterned membranes conforms to combustion stoichiometry (two moles of water produced for every mole of methane reacted), while the plain membrane with powder catalyst moves away from combustion with an average water produced-to-methane consumed ratio of 1:1. Even more telling is the amount of water produced on the stainless steel blank: with no membrane oxygen available, water production plateaus at about 0.00015 mmol/sec. The leak estimate for this test was 0.00013 mmol/sec of O₂, so hydrogen oxidation could account for about half of the oxygen in the system. It seems reasonable to assume

that the remainder of the gas-phase oxygen is consumed by some combination of combustion and partial oxidation, with some CO oxidation possible as well.

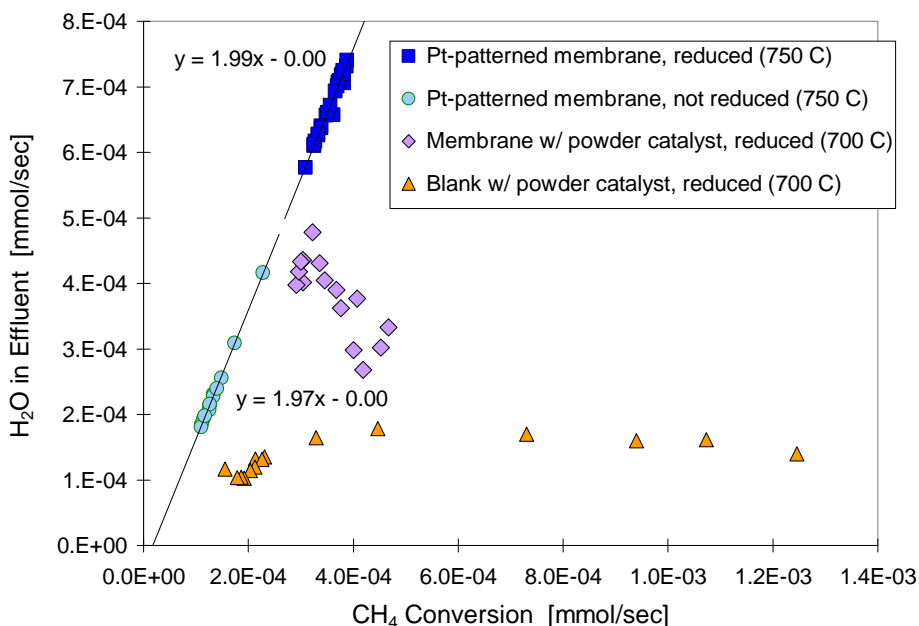


Figure 5.17: Molar H₂O production vs. molar CH₄ conversion during CO₂ reforming over a Pt/ZrO₂ catalyst and Pt-patterned membranes in the original SSMR. Reaction temperature as indicated, CH₄:CO₂ feed ratio=1:1 with no Ar/O₂ dilution, various feed flowrates.

5.5.4: Hydrogen selectivity

The hydrogen production-to-methane conversion ratio is directly related to the preceding water production discussion and provides a straightforward assessment of the fate of hydrogen in the various scenarios. The theoretical maximum ratio is two, but hydrogen oxidation and rWGS reduce the value in reality. Assuming no hydrogen-containing products other than water and hydrogen are produced, hydrogen from converted methane must go to either elemental hydrogen or water.

Figure 5.18 demonstrates the validity of the hypothesis that hydrogen is converted to water on the SFC membranes. The effect is more pronounced when the platinum is deposited directly on the membrane with a patterned membrane than when it resides on a powder support that is then spread across the membrane. The blank test shows the hydrogen selectivity; the membrane with the powder

catalyst shows less, particularly as the catalyst degrades; and the patterned membranes yield only a small minority of the potential hydrogen. The reduced patterned membrane converts almost 95% of the released hydrogen to water.

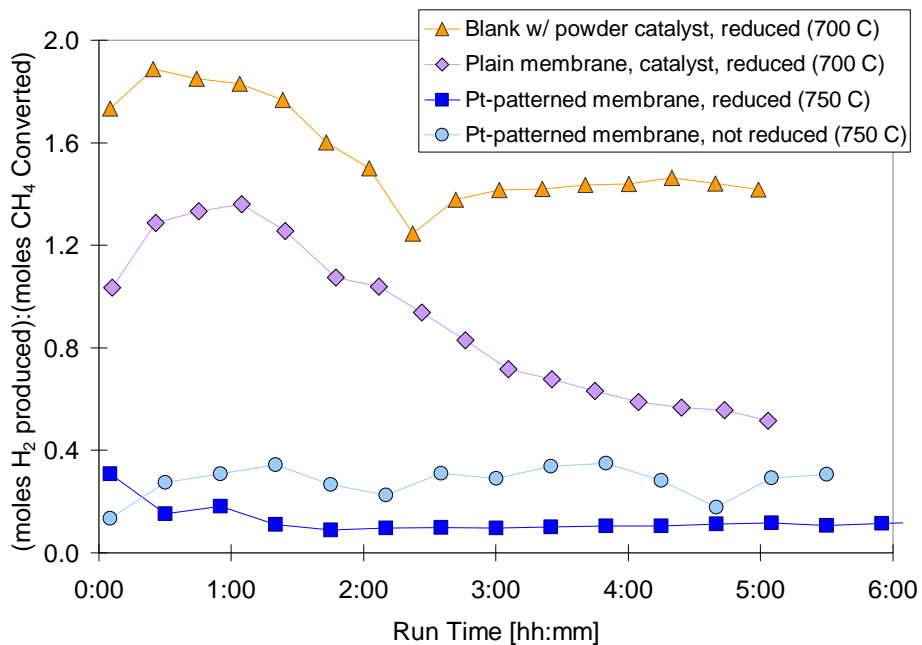


Figure 5.18: Molar ratio of H₂ production-to-CH₄ conversion during CO₂ reforming over a Pt/ZrO₂ catalyst and Pt-patterned membranes in the original SSMR. Reaction temperature as indicated, CH₄:CO₂ feed ratio=1:1 with no Ar/O₂ dilution, various feed flowrates.

Presenting the same information in another format provides a different perspective on the role of hydrogen oxidation in the membrane reactor. Figure 5.19 displays the molar production rate of hydrogen as a function of the molar conversion rate of methane. *NOTE: Figure 5.19 has two y-axes, one for each catalyst type.*

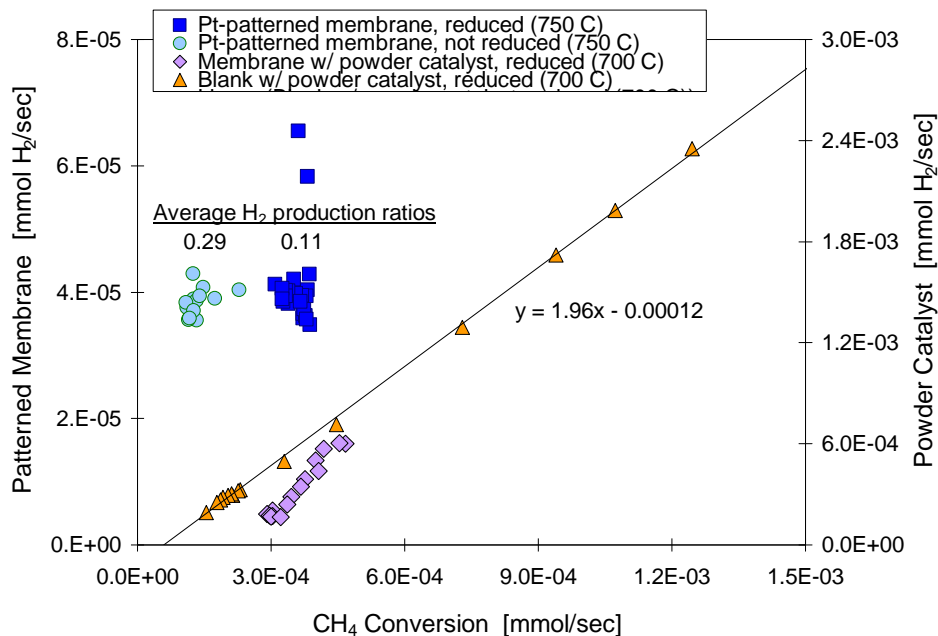


Figure 5.19: Molar H₂ production vs. molar CH₄ conversion during CO₂ reforming over a Pt/ZrO₂ catalyst and Pt-patterned membranes in the original SSMR. Reaction temperature as indicated, CH₄:CO₂ feed ratio=1:1 with no Ar/O₂ dilution, various feed flowrates.

In this format, the patterned membrane results are clustered together, indicating a low correlation between methane conversion and hydrogen production. This contrasts sharply with the high correlation between water production and methane conversion they exhibited in Figure 5.17 and thus demonstrates conclusively that combustion is the dominant reaction on the patterned membranes, particularly the reduced patterned membrane. As mentioned earlier, an appropriately selective catalyst is required for CO₂ reforming or partial oxidation. An SFC membrane with deposited platinum particles does not appear to constitute such a catalyst.

5.5.5: Hydrogen selectivity with no membrane

The results for the blank test in Figure 5.19 are linear with a slope almost equal to the theoretical maximum value of two, yet the actual point-by-point results in Figure 5.18 are clearly not in this ratio. The difference between the actual and theoretical amounts of hydrogen production is very consistent and corresponds to the steady water production levels observed in Figure 5.17 for this test. It also corresponds to the uniform methane conversion offset in the data in Figure 5.19.

The $\text{H}_2:\text{CO}$ ratio for this test is initially close to one, which supports the idea of high hydrogen selectivity, but it then drops to a steady state value of approximately 0.55 (Figure 5.3). Figure 5.14 shows a steady state $\text{CO}_2:\text{CH}_4$ conversion ratio of about 1.6, which in conjunction with the steady water production accounts for the low $\text{H}_2:\text{CO}$ ratio. These observations and stoichiometry indicate that rWGS is the cause of the water and CO production and the CO_2 conversion. The baseline water production in Figure 5.17 could therefore imply either a phenomenon of increasing rWGS activity as methane conversion activity decreases or a constant amount of the rWGS reaction that is independent of methane conversion activity and becomes more prominent only because methane conversion decreases. Whatever the cause, the phenomenon accrues to the Pt/ ZrO_2 catalyst but not to the platinum patterned membranes, implying that the Pt/ ZrO_2 catalyst might be prone to rWGS as its activity declines.

5.5.6: $\text{H}_2:\text{CO}$ ratio evaluation

The baseline water production displayed in Figure 5.17 for the blank test with catalyst seems likely to have been produced by a constant level of the rWGS reaction. If so, the $\text{H}_2:\text{CO}$ ratio should decrease as methane conversion decreases and the relative contribution of rWGS to the $\text{H}_2:\text{CO}$ becomes more significant. This negative contribution should be more pronounced at lower methane conversions than at higher, once again because it is assumed to be fairly constant. Figure 5.20 confirms these two predictions for the blank test: the $\text{H}_2:\text{CO}$ ratio is less than one and it declines more steeply at lower methane conversions. With no membrane effect to consider in the blank test, it can be concluded that the Pt/ ZrO_2 catalyst appears to support a certain amount of rWGS activity regardless of methane conversion activity. The amount of this rWGS activity likely depends on the oxidation state of the catalyst.

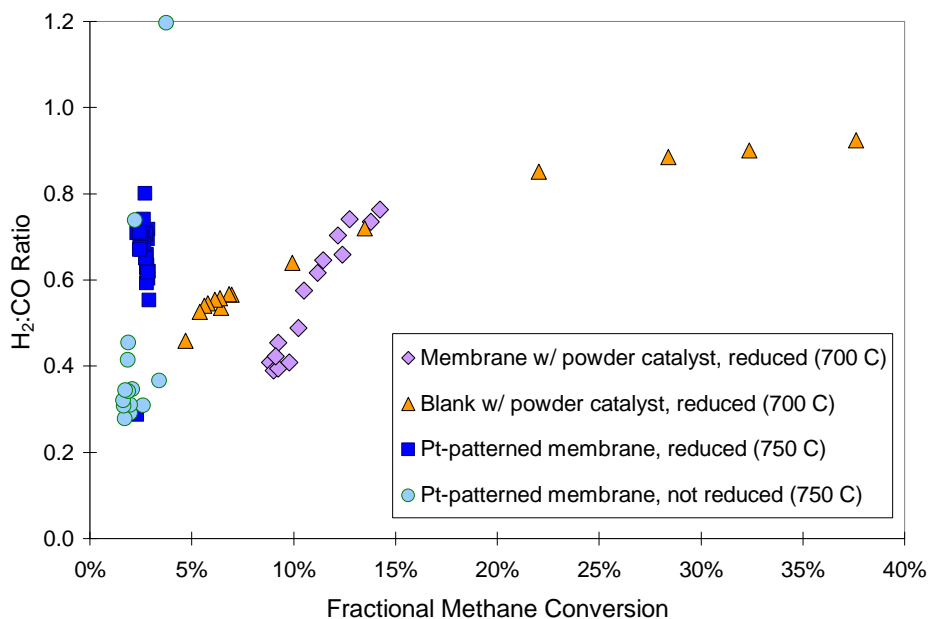


Figure 5.20: H₂:CO ratio vs. fractional CH₄ conversion during CO₂ reforming over a Pt/ZrO₂ catalyst and Pt-patterned membranes in the original SSMR. Reaction temperature as indicated, CH₄:CO₂ feed ratio=1:1 with no Ar/O₂ dilution, various feed flowrates.

With the potentially large contribution of combustion in the reaction set, the H₂:CO ratio is less helpful than usual for deconvoluting the reforming reaction scheme. However, the generally low H₂:CO ratios do confirm that partial oxidation is not the dominant oxygen-consuming reaction in any of the membrane tests and also that WGS is not the explanation for the increase in CO₂ in the patterned membrane tests (Figure 5.14). While WGS produces CO₂, it also produces hydrogen and consumes carbon monoxide and thus would lead to higher H₂:CO ratios than exhibited in Figure 5.20. Rather than resulting from RWG, the high CO₂ levels with the patterned membranes is most likely the result of combustion.

5.5.7: The effect of oxygen over time

The distinct trends displayed by the powder catalyst in Figures 5.16, 5.19, and 5.20 confirm that the “Membrane w/ powder catalyst” data are not as randomly distributed as they appear in Figures 5.8, 5.15, and 5.17. The relationship between oxygen and methane conversion with the

powder catalyst can be evaluated further by plotting the ratio of the methane conversion rate and the total oxygen supply rate vs. time, as shown in Figure 5.21.

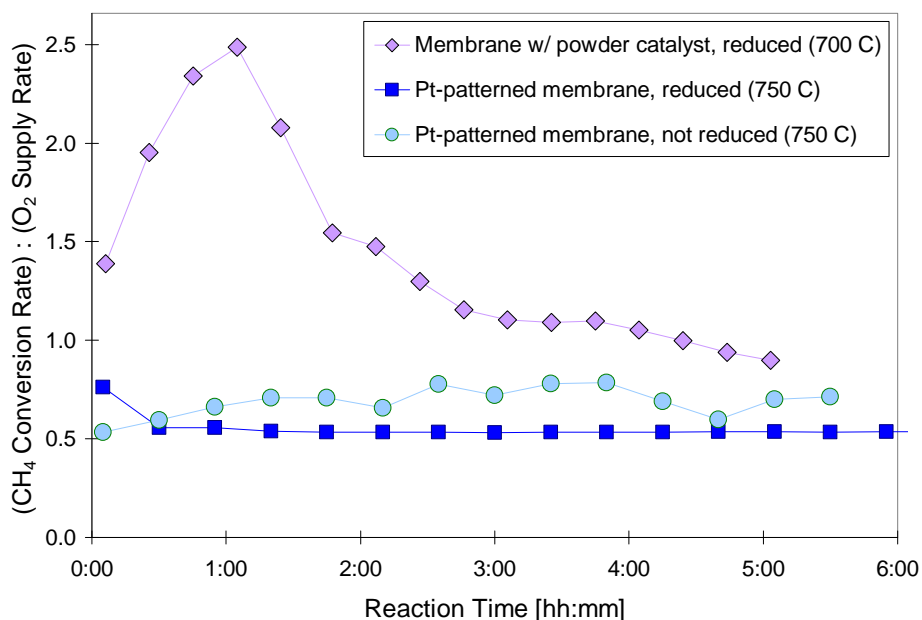


Figure 5.21: Molar ratio of CH₄ conversion-to-oxygen supply during CO₂ reforming over a Pt/ZrO₂ catalyst and Pt-patterned membranes in the original SSMR. Reaction temperature as indicated, CH₄:CO₂ feed ratio=1:1 with no Ar/O₂ dilution, various feed flowrates.

As expected, the results from the patterned membrane tests hover around the 0.5 mark representing methane combustion. However, before the Pt/ZrO₂ catalyst performance degrades in the blank test, the methane conversion-to-oxygen ratio for the powder catalyst exceeds the partial oxidation value of two, indicating the presence of a significant amount of other methane consuming reactions. As the the reduced powder catalyst deactivates, it actually approaches the same relationship with oxygen as the patterned membranes. With Figure 5.14 showing that the CO₂:CH₄ conversion ratio also decreases over time for this test, it is possible that combustion becomes more significant as catalyst performance degrades.

Combustion clearly accounts for some of the observed methane conversion—particularly on the patterned membranes. The likelihood of this is enhanced by the presence of both oxygen, which is necessary for combustion, and platinum, which is a common combustion catalyst. However, even

on the patterned membranes combustion cannot be the only methane-consuming reaction in the reaction set. First, combustion does not produce H_2 and CO and both are present in the products from all tests, and second, there is not enough oxygen present for combustion to account for all of the observed methane conversion. One or more additional methane consuming reactions must occur from a list of candidates that includes CO_2 reforming, steam reforming, and partial oxidation.

If, as proposed herein, membrane oxygen is consumed entirely by hydrogen oxidation on the membrane surface under reaction conditions, the most probable additional methane conversion reactions are CO_2 and steam reforming. Water produced at the membrane surface could participate in steam reforming in the catalyst layer as it passes back through after leaving the membrane surface. However, this is only possible when there is a catalyst layer on top of the membrane. The apparent dominance of combustion with the patterned membranes coupled with their lack of a powder catalyst layer supports the hypotheses that, in the presence of a powder catalyst bed, hydrogen converts to water on the membrane surface and water produced on the membrane surface participates in steam reforming in the catalyst bed.

5.6: Alternative Approach to Turnover Frequency

While exposed platinum is the conventional basis for laboratory catalyst analysis, an important economic consideration for precious metal catalysts in industrial processes is the total amount of precious metal used. The patterned membranes appear to have a dramatic advantage in precious metal efficiency over the conventional powder catalyst, but the method of deposition produces much larger metal particles than those typically found in powder catalysts (e.g., 3 micron diameters instead of 3 nanometer). An alternative turnover frequency was therefore considered on the assumption that it is more economically relevant. Figure 5.22 presents methane conversion per total platinum loading as opposed to methane conversion per available surface platinum (as in Figure 5.8).

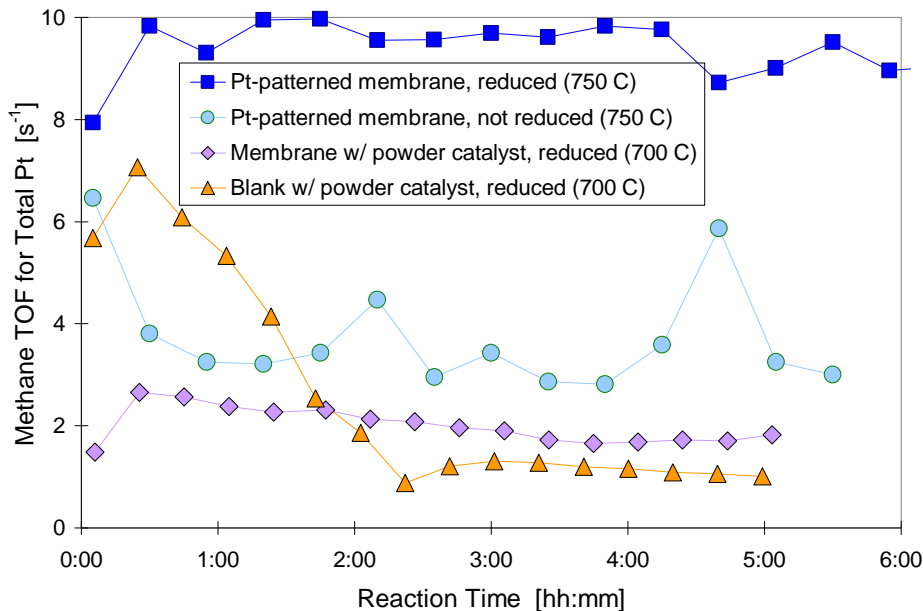


Figure 5.22: CH₄ conversion turnover frequency (TOF) based on total Pt mass during CO₂ reforming over a Pt/ZrO₂ catalyst and Pt-patterned membranes in the original SSMR. Reaction temperature as indicated, CH₄:CO₂ feed ratio=1:1 with no Ar/O₂ dilution, various feed flowrates.

Even with this conservative approach, Figure 5.22 shows that the patterned membranes are more efficient for methane conversion, although in this analysis the difference has decreased sufficiently that the comparison can at least be made with a single y-axis. By any standard, platinum-patterned SFC membranes are clearly efficient at converting methane. However, they fail to produce proportionally high hydrogen yields and do not appear to be selective enough to serve as reforming catalysts.

5.7: Revisiting the Earliest Tests

The original 700 °C test results can be re-evaluated using the reactant and product ratios introduced above. The CO₂:CH₄ conversion ratios in Figure 5.23 show that combustion is the initial reaction on the SFC membrane with no catalyst because of the 1:1 ratio between methane conversion and CO₂ production. This conclusion is supported by the near zero hydrogen production in these initial data points depicted in Figure 5.4 (hydrogen production-to-methane conversion ratio vs.

reaction time). Although the net reaction profile changes quickly to a mixture of combustion and reforming, the methane conversion levels are low enough that all activity is believed to arise from oxygen from the relatively large leak with the SSMR.

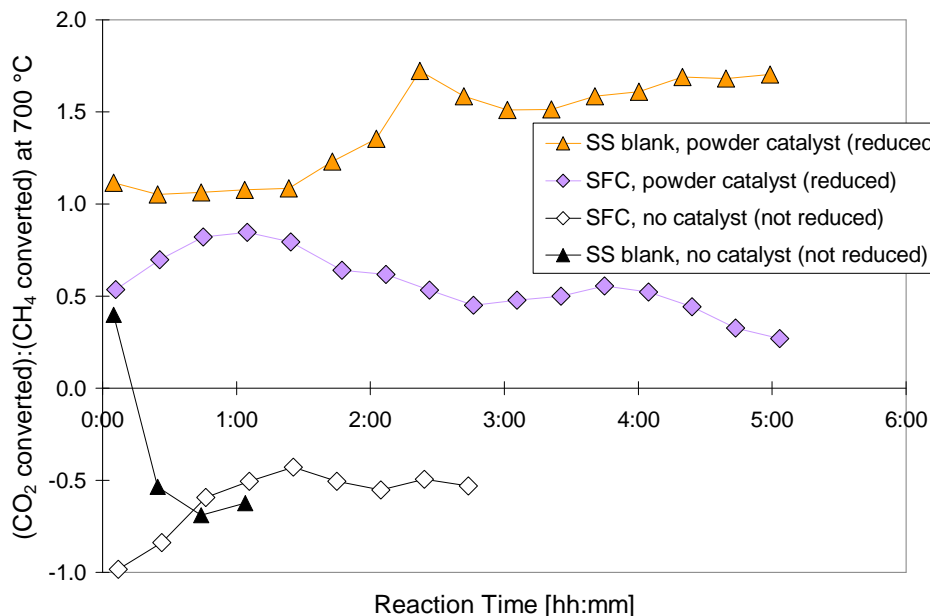


Figure 5.23: Molar $\text{CO}_2:\text{CH}_4$ conversion ratio during CO_2 reforming over a Pt/ZrO_2 catalyst in the original SSMR. Reaction temperature= $700\text{ }^\circ\text{C}$, $\text{GHSV}=75\text{ L/h/g}_{\text{cat}}$, $\text{CH}_4:\text{CO}_2$ feed ratio= $1:1$ with no Ar/O_2 dilution.

The $\text{CO}_2:\text{CH}_4$ conversion ratios in Figure 5.23 for the two tests with catalyst are in a range that indicates a significant amount CO_2 reforming, but the results for the blank test without catalyst indicate a quick transition from a reforming to a combustion scenario after the initial data point. The membrane test without catalyst undergoes an opposite transition: the initial $\text{CO}_2:\text{CH}_4$ conversion ratio of negative one indicates methane combustion only, but this ratio then increases over time to approximately the same level as the blank test with no catalyst.

Methane conversion-to-oxygen supply ratio is another ratio introduced in this chapter. Figure 5.24 provides these ratios for the early $700\text{ }^\circ\text{C}$ SSMR tests.

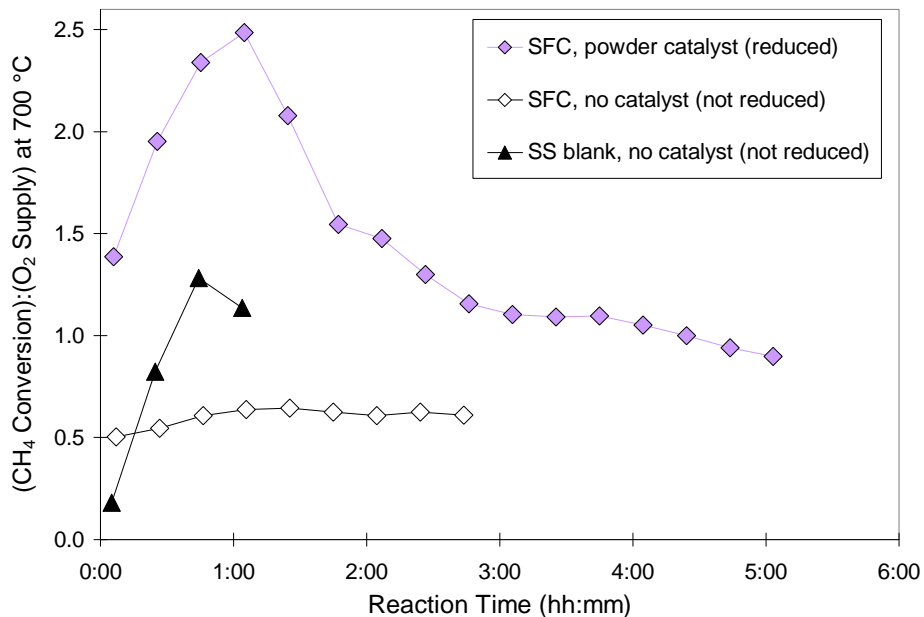


Figure 5.24: Molar ratio of CH₄ conversion-to-oxygen supply during CO₂ reforming over a Pt/ZrO₂ catalyst in the original SSMR. Reaction temperature=700 °C, GHSV=75 L/h/g_{cat}, CH₄:CO₂ feed ratio=1:1 with no Ar/O₂ dilution.

For the membrane test without catalyst, the ratio of moles of methane converted to moles of oxygen supplied starts exactly at the combustion value of 0.5 and stays close to that mark for the duration of the test. For the blank test with no catalyst and for the membrane test with catalyst, methane conversion exceeds the potential contribution from combustion only, indicating at least one other methane consuming reaction. Figure 5.23 supports CO₂ reforming as a contributing reaction for the blank test and as the majority reaction for the membrane test with catalyst.

Considering the total evidence from Figures 5.4, 5.23, and 5.24, it seems clear that combustion occurs immediately on the membrane without catalyst but then diminishes somewhat, as evidenced by an increase in moles of hydrogen produced and a decrease in the moles of CO₂ produced per mole of methane converted. Hydrogen production increases to about 30% of the moles of methane converted over the final two hours of the test, while CO production increases to about 50% of methane converted to match the amount of CO₂ production. By the end of the test, the carbon

in methane is therefore being converted in roughly equal proportions to CO and CO₂ while about 85% of the hydrogen from methane is converted to water.

Figure 5.25 presents the ratio of moles of water produced to moles of methane converted. In conjunction with Figure 5.23, Figure 5.25 reinforces the conclusions that combustion is the dominant methane conversion reaction in the absence of powder catalyst and that the contribution of combustion increases slowly over time on the SFC membrane with powder catalyst.

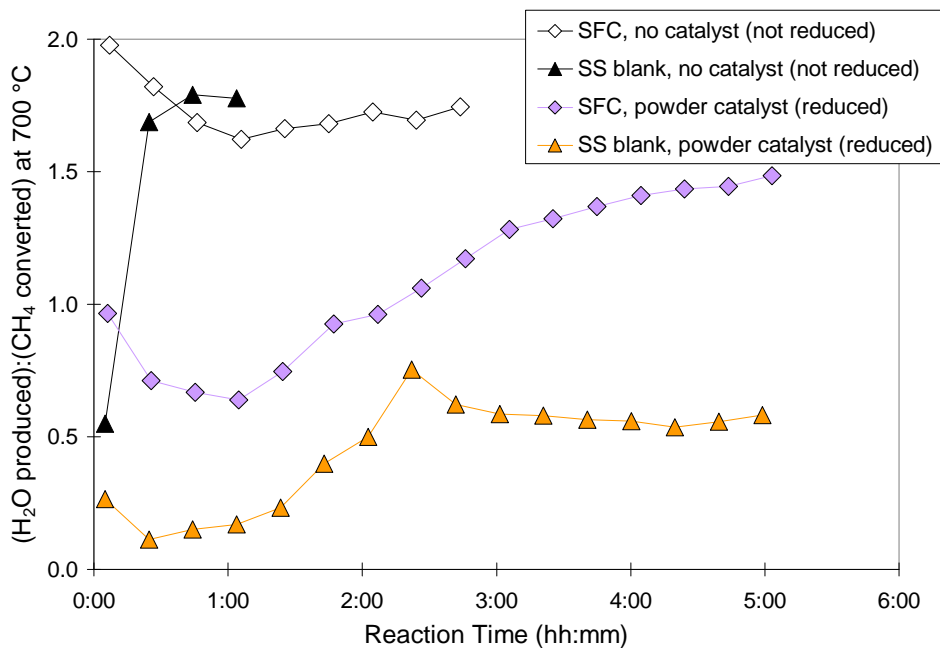


Figure 5.25: Molar ratio of water production-to-CH₄ conversion during CO₂ reforming over a Pt/ZrO₂ catalyst in the original SSMR. Reaction temperature=700 °C, GHSV=75 L/h/g_{cat}, CH₄:CO₂ feed ratio=1:1 with no Ar/O₂ dilution.

The powder catalyst on the SS blank shows increasing water production in conjunction with increasing CO₂ conversion as the catalyst activity degrades over time, indicating an increase in the relative amount of rWGS with decreased overall catalyst activity rather than an increase in combustion. If combustion were increasing proportionally as the catalyst degraded, CO₂ conversion would drop rather than increase.

5.8: Observations and Conclusions from Chapter 5

- (1) Reactant and product ratios other than the H₂:CO ratio are valuable tools in determining the likely net reaction profiles in O-MIEC membrane reactor testing
- (2) In small quantities as part of a CO₂ reforming feed, gas-phase oxygen (from system leaks, in this case) contributes significantly to methane combustion
- (3) Tests with no catalyst of any kind exhibit a similar and very low amount of methane conversion with both the blank and SFC membranes. The amount of methane conversion that does occur appears to be related directly to the relative size of the air leak into the reactor for both the blank and the SFC membrane and is thus believed not to occur on the SFC surface.
- (4) Platinum-patterned SFC membranes exhibit high methane conversion activity with a CO₂ reforming feed compared to a powder Pt/ZrO₂ supported catalyst, but they act as combustion catalysts rather than as CO₂ reforming catalysts
- (5) With a powder Pt/ZrO₂ catalyst in place, methane conversion is dominated by CO₂ reforming
- (6) Hydrogen oxidation is most likely the primary mode of removing oxygen from an SFC membrane surface under CO₂ reforming reaction conditions
- (7) CO₂ may be converted to CO on the surface of an SFC membrane that has been reduced by hydrogen
- (8) Steam reforming may occur in a powder catalyst layer from water produced on a membrane surface by hydrogen oxidation. *NOTE: the apparent net reaction for a combination of steam reforming and hydrogen oxidation is partial oxidation, but the combined mechanism is believed to occur because of the unlikelihood of direct partial oxidation in an O-MIEC membrane reactor.*
- (9) With the Pt/ZrO₂ catalyst on the blank membrane at 700 °C, the amount of rWGS relative to the amount of methane conversion appears to increase as the methane conversion activity of the catalyst decreases over time on stream. Combustion rates might also increase as the catalyst degrades.
- (10) With the Pt/ZrO₂ catalyst on an SFC membrane at 700 °C, the proportion of combustion appears to increase slightly as the methane conversion activity of the catalyst decreases over time on stream.

References Cited in Chapter 5

1. Wang, W., S.M. Stagg-Williams, F.B. Noronha, L.V. Mattos and F.B. Passos, *Partial oxidation and combined reforming of methane of Ce-promoted catalysts*. Catal Today **98**, 2004, p.553-563.
2. Donazzi, A., A. Beretta, G. Groppi and P. Forzatti, *Catalytic partial oxidation of methane over a 4% Rh/ α -Al₂O₃ catalyst, Part II: Role of CO₂ reforming*. Jnl of Catal **255**, 2008, p.259-268.
3. Michael, B.C., A. Donazzi and L.D. Schmidt, *Effects of H₂O and CO₂ addition in catalytic partial oxidation of methane on Rh*. Jnl of Catal **265**, 2009, p.117-129.
4. Lin, Y.-C., K.L. Hohn and S.M. Stagg-Williams, *Hydrogen generation from methanol oxidation on supported Cu and Pt catalysts: Effects of active phases and supports*. Appl Cat A **327**, 2007, p.164-172.
5. Murphy, S., *Fabrication and Catalytic Patterning of Non-porous Ion and Electron Dual-Conducting Membranes Using Electron Beam Evaporation*, in *Department of Chemical and Petroleum Engineering*. 2005, University of Kansas: Lawrence, KS.
6. Wei, J. and E. Iglesia, *Structural requirements and reaction pathways in methane activation and chemical conversion catalyzed by rhodium*. Jnl of Catal **225**, 2004, p.116-127.
7. Maestri, M., D.G. Vlachos, A. Beretta, G. Groppi and E. Tronconi, *Steam and dry reforming of methane on Rh: Microkinetic analysis and hierarchy of kinetic models*. Jnl of Catal **259**, 2008, p.211-222.
8. Wei, J. and E. Iglesia, *Mechanism and Site Requirements for Activation and Chemical Conversion of Methane on Supported Pt Clusters and Turnover Rate Comparisons among Noble Metals*. J Phys Chem B **108**, 2004, p.4094-4103.
9. Bitter, J.H., K. Seshan and J.A. Lercher, *The State of Zirconia Supported Platinum Catalysts for CO₂/CH₄ Reforming*. Jnl of Catal **171**, 1997, p.279-286.
10. Nagaoka, K., K. Seshan, K. Aika and J.A. Lercher, *Carbon Deposition during Carbon Dioxide Reforming of Methane--Comparison between Pt/Al₂O₃ and Pt/ZrO₂*. Jnl of Catal **197**, 2001, p.34-42.
11. Noronha, F.B., A. Shamsi, C. Taylor, G. Fendley, S.M. Stagg-Williams and D.E. Resasco, *Catalytic performance of Pt/ZrO₂ and Pt/Ce-ZrO₂ catalysts on CO₂ reforming of CH₄ coupled with steam reforming or under high pressure*. Catal Lett **90**(1-2), 2003, p.13-21.
12. Gu, X., L. Yang, L. Tan, W. Jin, L. Zhang and N. Xu, *Modified Operating Mode for Improving the Lifetime of Mixed-Conducting Ceramic Membrane Reactors in the POM Environment*. Ind Eng Chem Res **42**, 2003, p.795-801.
13. Tsai, C.-Y., A.G. Dixon, W.R. Moser and Y.H. Ma, *Dense perovskite membrane reactors for partial oxidation of methane to syngas*. AIChE Jnl **43**(11A), 1997, p.2741-2750.

Chapter 6: QTMR Reaction Studies: the SFC Membrane Effect

After the quartz tube membrane reactor system (QTMR) was designed and constructed it was used for all remaining tests. This reactor allows higher temperature testing and produces significantly better seals at reaction temperatures than the SSMR system. The target CO₂ reforming temperature of 800 °C is attainable with the QTMR and is therefore used with all subsequent tests.

The QTMR was also designed so that powder catalyst could be recovered from the membrane or blank after a reaction test, which allowed some post-reaction catalyst analysis. Because of the different sealing mechanism and the use of gold seals, the QTMR allows larger leaks at lower temperatures than the SSMR. As a result, membrane and catalyst are exposed to oxygen on the order of 1% of the argon sweep gas during initial heat-up prior to flux or reaction testing. A high quality seal forms at 800 °C within 30 minutes of arriving at that temperature, at which point the leak oxygen content of the reaction chamber is minimal.

The minimal leak oxygen allows the effect of the SFC membrane to be assessed independently of the levels of gas-phase oxygen that are present in the tests discussed in Chapter 5. The lower background oxygen levels also dramatically increases the differences between tests with the stainless steel blank and tests with the SFC membranes, enabling a more rigorous analysis of the effect of SFC membranes on catalyst activity based on the principal effects identified in Chapter 5. In addition to the reaction tests with catalyst, a summary of tests without catalyst is discussed with a focus on determining the influence of air leaks on observed activity in tests without catalyst.

This chapter begins with a list of the hypotheses derived from the initial SSMR testing. It then analyzes the initial QTMR tests with powder catalyst on SFC by comparing them to analogous tests with the stainless steel blank. The standard test conditions for the remainder of the reaction tests in this work are established in the initial QTMR tests. The following standard test conditions apply to all reaction tests that follow:

- CO₂ reforming with a modified space velocity of 150 L/h/g_{cat} (corresponds to a feed flowrate of 25 ccm in the QTMR and 50 ccm in the PFR)
- feed composition of 40 mol% CH₄, 40 mol% CO₂, and 20 mol% argon (the argon diluent is included as a placeholder to allow future testing with co-fed oxygen in argon/oxygen blends)
- 800 °C reaction temperature
- no pre-reaction catalyst reduction step

The following two conditions apply only to tests in the QTMR:

- 10 mg of powder catalyst spread evenly in a ~1 mm thick layer across the membrane surface within the circumference of the gold seal
- two hour pre-reaction hold time at 800 °C to allow SFC membranes to equilibrate (this is also done in blank tests to maintain equivalent conditions between the two types of tests).

One confounding factor for comparing the QTMR tests to the SSMR tests is the source of the SFC membranes. The original membranes tested in the SSMR were fabricated by the group of Dr. Utham Balachandran at Argonne National Lab using SFC powder procured at Superconductive Components, Inc., while the membranes tested in the QTMR were fabricated in-house from SFC powder procured from Praxair Specialty Ceramics. Although the effect was generally similar, the in-house membranes exhibited substantially lower flux than the Balachandran membranes in independent flux tests. This phenomenon is summarized in Appendix F and is believed to depend more on the change in SFC powder than on the fabrication procedure.

6.1: Hypotheses and Reaction Pathways

After considering the entire body of data from this work, a set of hypotheses has been developed that collectively explain all of the observed trends in the net reactions. Because the evidence is highly interrelated and is thus dispersed throughout the various parts of this work, the hypotheses are presented here and are supported and referenced throughout the remaining chapters.

6.1.1: Proposed hypotheses

- (1) In the presence of H₂ at high temperature, an SFC membrane does not evolve any gas-phase O₂ but rather oxidizes hydrogen exclusively. SFC does evolve gas-phase O₂ in a non-reducing high temperature environment.
- (2) Only two reactions occur to a significant extent on the SFC surface under CO₂ reforming reaction conditions: H₂ oxidation and CO₂ reduction. The surface must be reduced by H₂ for CO₂ reduction to occur. *NOTE: under the appropriate conditions, CO oxidation will also occur on an SFC surface, but these tests have too much CO₂ in the feed to observe this.*
- (3) Pt/ZrO₂ catalyst exposed to gas-phase oxygen while at high temperature promotes H₂ oxidation (and possibly complete combustion) more readily than catalyst exposed only to inert or reducing environments which is more likely to promote CO₂ reforming. Platinum oxidation state is therefore affected by gas-phase oxygen even under CO₂ reforming conditions and is a key determining factor for both catalyst activity and reaction selectivity.
- (4) The use of an SFC membrane as a powder catalyst substrate may promote *in situ* catalyst reduction and/or decrease *in situ* oxidation under CO₂ reforming conditions.
- (5) If oxygen is available, combustion is the dominant methane-consuming reaction in the presence of a non-selective catalyst such as oxidized Pt/ZrO₂ or a platinum-patterned SFC membrane.
- (6) A plain SFC surface promotes rWGS in a process referred to as “membrane-facilitated rWGS.” The Pt/ZrO₂ catalyst also promotes rWGS, with the amount of rWGS relative to methane conversion increasing as the catalyst degrades. These related but distinct phenomena are the cause of the low H₂:CO ratios observed in the later stages of all tests with the Pt/ZrO₂ catalyst.
- (7) Steam reforming can occur in a membrane reactor with a CO₂ reforming feed when a powder reforming catalyst layer is added to an SFC membrane. Water produced on the membrane surface by hydrogen oxidation can participate in steam reforming as it passes through the powder catalyst layer after leaving the membrane surface. The combined reaction is stoichiometrically indistinguishable from partial oxidation with membrane oxygen but is substantially more likely.

6.1.2: Reaction pathways

The following fundamental and net (i.e., combined) reactions are proposed as the relevant reaction pathways for this work. For simplicity, any reaction with a single reactant or product is

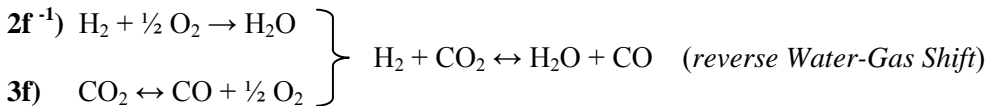
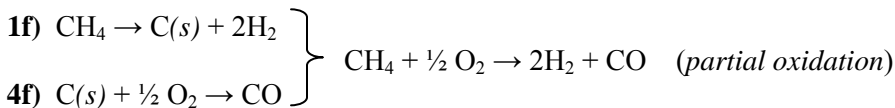
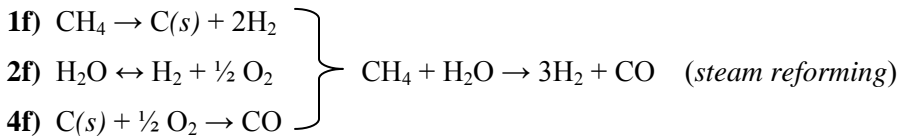
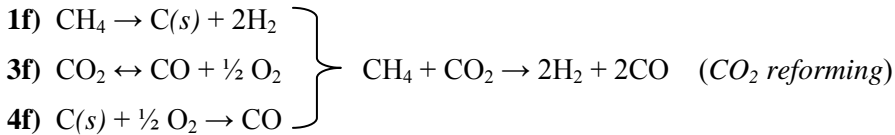
considered fundamental. Two-sided arrows indicate reactions with the potential for significant reversibility under the relevant operating conditions.

| <u>Fundamental reactions</u> | <u>$\Delta H_{298 K}$ [kJ/mol]</u> |
|---|---|
| 1f) $\text{CH}_4 \rightarrow \text{C}(s) + 2\text{H}_2$ | +74.6 |
| 2f) $\text{H}_2\text{O} \leftrightarrow \text{H}_2 + \frac{1}{2} \text{O}_2$ | +241.8 |
| 3f) $\text{CO}_2 \leftrightarrow \text{CO} + \frac{1}{2} \text{O}_2$ | +283.0 |
| 4f) $\text{C}(s) + \frac{1}{2} \text{O}_2 \rightarrow \text{CO}$ | -110.5 |

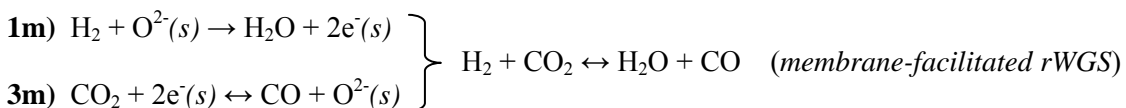
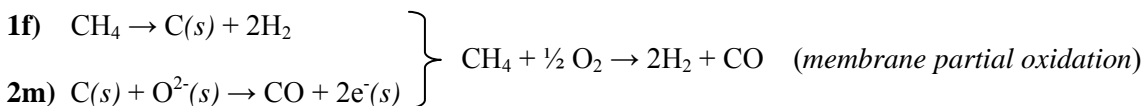
Fundamental membrane oxygen reactions (ΔH unknown)

- 1m)** $\text{H}_2 + \text{O}^{2-}(s) \rightarrow \text{H}_2\text{O} + 2\text{e}^-(s)$
- 2m)** $\text{C}(s) + \text{O}^{2-}(s) \rightarrow \text{CO} + 2\text{e}^-(s)$
- 3m)** $\text{CO}_2 + 2\text{e}^-(s) \leftrightarrow \text{CO} + \text{O}^{2-}(s)$

Net reactions (combinations of fundamental reactions)



Net membrane oxygen reactions



6.2: Initial Baseline QTMR Tests (#1)

The following discussions focus exclusively on comparing Pt/ZrO₂ catalyst performance in the QTMR with an SFC membrane to catalyst performance with the inert blank membrane and then on clarifying the potential explanations for any differences. The QTMR system was improved significantly after some tests had already been performed. Tests referred to as “#1” of a certain type occurred before the improvements; the same type of test accompanied by a “#2” refers to a repeated incidence after the improvements. Appendix G includes an overview of the system improvements and their potential effect on the data analysis.

6.2.1: Methane conversion

Under the standard reaction conditions with the blank membrane, the Pt/ZrO₂ catalyst loses most of its activity within the first two hours of operation (Figure 6.1). The increase in activity between 6 and 7 hours with the blank in Figure 6.1 corresponds to the temporary addition of 1.0 mol% oxygen to the reactor feed. This amount of oxygen was chosen to represent an average oxygen flow rate from the SFC membrane during reaction, as estimated from the original SSMR testing. Methane conversion on the blank increases only slightly with the addition of the co-fed oxygen, which was added by switching from a pure argon gas cylinder to a cylinder of 5% oxygen in argon at the same flowrate.

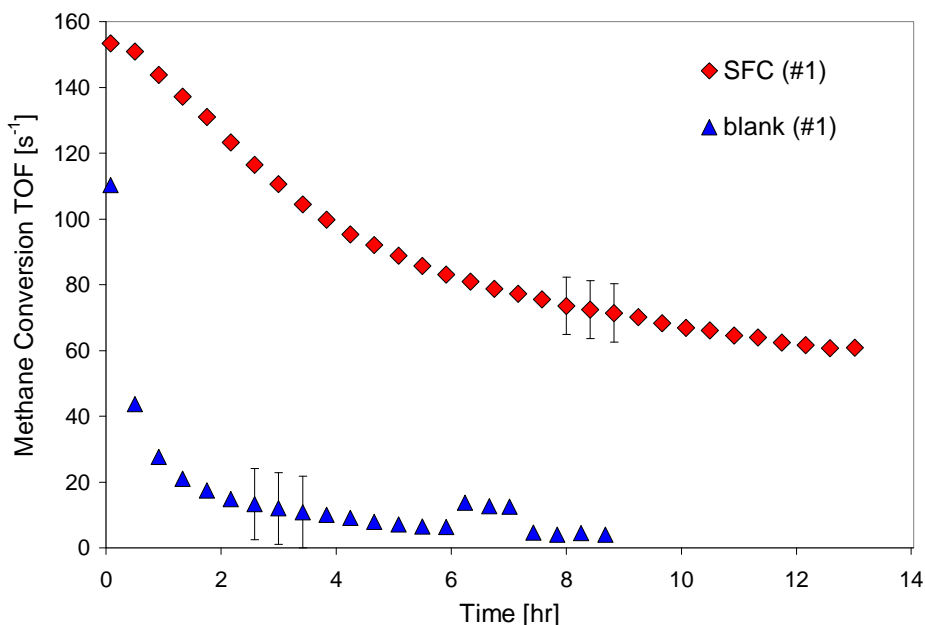


Figure 6.1: CH₄ conversion turnover frequency (TOF) during CO₂ reforming over a Pt/ZrO₂ catalyst in the original QTMR. Reaction temperature=800 °C, GHSV=150 L/h/g_{cat}, CH₄:CO₂:Ar feed ratio=4:4:2.

With the SFC membrane, the catalyst exhibits slower and less extensive deactivation as well as higher initial activity. It was confirmed post-test that the catalyst remained well-distributed across the membrane face—in contrast to the catalyst redistribution in the original test of powder catalyst on an SFC membrane in Chapter 5. The results in Figure 6.1 are therefore more representative of the membrane effect than the results for the original SFC membrane test with powder catalyst.

Gas-phase oxygen is added to the feed in the blank test to evaluate its effect, partly because of the high leak rates experienced in previous tests in the SSMR. The additional oxygen clearly has only a minor effect on catalyst activity compared to the effect of the SFC membrane. This implies that the catalyst has degraded significantly relative to the catalyst in the SFC membrane test.

The membrane test in Figure 6.1 uses an SFC membrane made in-house that exhibits significantly less oxygen flux than the membranes tested in Chapter 5. Given the dramatic

improvement depicted in Figure 6.1 with such a low-flux membrane, it is possible that a higher flux membrane could enhance catalyst stability even more dramatically.

6.2.2: Oxygen flux during reaction

Oxygen flux through the SFC membrane during the reaction test in Figure 6.1 was estimated from the effluent composition results. Figure 6.2 shows the flux estimates as equivalent O₂ flowrates along with the levels of key reactor constituents. The average membrane oxygen feed contribution over the first three hours of this test is approximately 1% (gas-phase O₂ equivalent), which vindicates the choice of 1% for the co-fed oxygen interlude in Figure 6.1. An average value is obviously not representative of the entire test period because of the steady decline in oxygen flux, but the greatest changes in activity occur in the first few hours in tests without an SFC membrane. The first three hours can therefore be considered the most influential period for catalyst activity in a membrane reactor test.

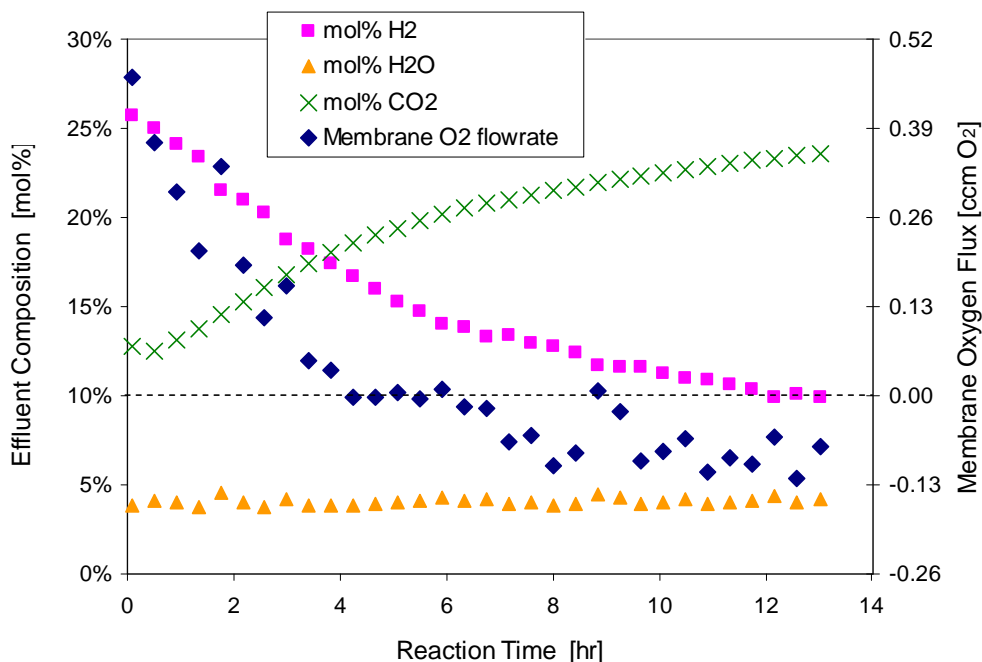


Figure 6.2: Reactor effluent composition and membrane oxygen flux (as O₂) during CO₂ reforming over a Pt/ZrO₂ catalyst in the original QTMR with an SFC membrane. Reaction temperature=800 °C, GHSV=150 L/h/g_{cat}, CH₄:CO₂:Ar feed ratio=4:4:2.

Under the CSTR approximation, the effluent composition is assumed to be the same as the reaction chamber composition, and membrane oxygen flux varies in Figure 6.2 in a way that is consistent with the reactions that are believed to occur on the surface of the SFC membrane. Namely, hydrogen oxidation removes oxygen from the SFC lattice and CO₂ reduction returns some oxygen to a lattice that is depleted after being reduced by hydrogen.

CO₂ can adsorb simultaneously or subsequently on the surface of a membrane that is exposed to hydrogen. It is believed to donate an oxygen atom to the SFC lattice, resulting in the release of a CO molecule from the surface. This aspect of the proposed mechanism is limited only by oxygen vacancies. As concluded in Chapter 5, the low CO₂ conversion activity of unreduced membranes indicates that CO₂ reduction does not occur without prior or simultaneous reduction of the SFC by hydrogen. Oxygen uptake by SFC from CO₂ reduction is proposed as the explanation for the negative flux values in Figure 6.2.

6.2.3: Membrane recharge and reaction re-start

The membrane test in Figure 6.1 was stopped after 13 hours, but the reactants were briefly started again after a five-hour break during which only argon flowed through the reactor system. This pause was implemented to see if oxygen from the membrane could act to rejuvenate the catalyst through coke removal. Figure 6.3 is Figure 6.1 with an expanded time scale, and Figure 6.4 is the equivalent expansion of Figure 6.2. It should be noted that the catalyst is only exposed to a small amount of oxygen during the break, from both the 0.026 ccm average air leak and the ~0.007 ccm oxygen flux (O₂ equivalent), and that later testing showed that high temperature gas-phase oxygen exposure reduces the activity of this Pt/ZrO₂ catalyst.

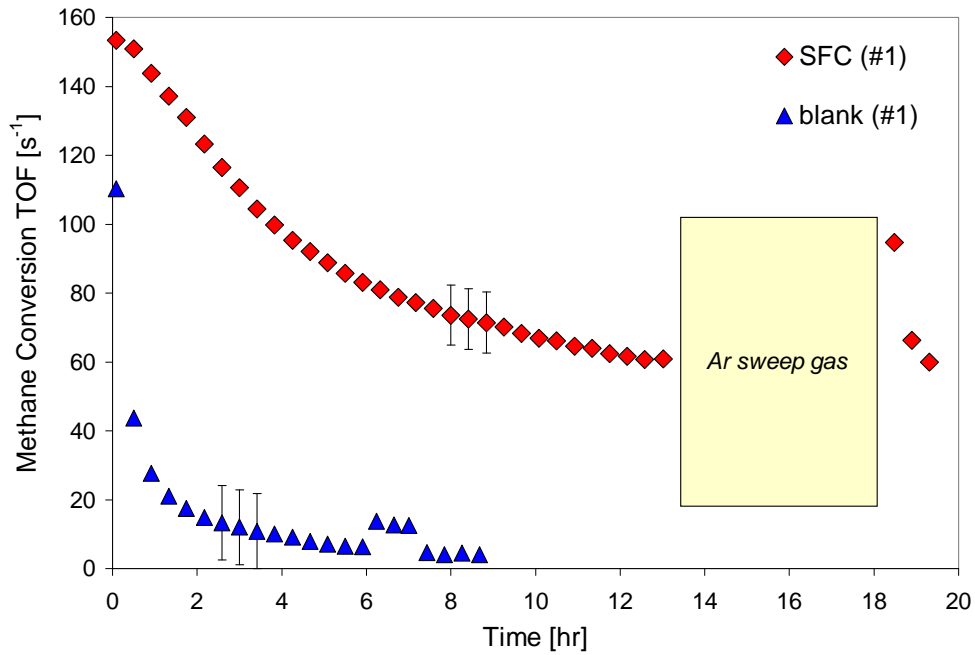


Figure 6.3: CH₄ conversion turnover frequency (TOF) during CO₂ reforming over a Pt/ZrO₂ catalyst in the original QTMR. Reaction temperature=800 °C, GHSV=150 L/h/g_{cat}, CH₄:CO₂:Ar feed ratio=4:4:2. With pause and re-start.

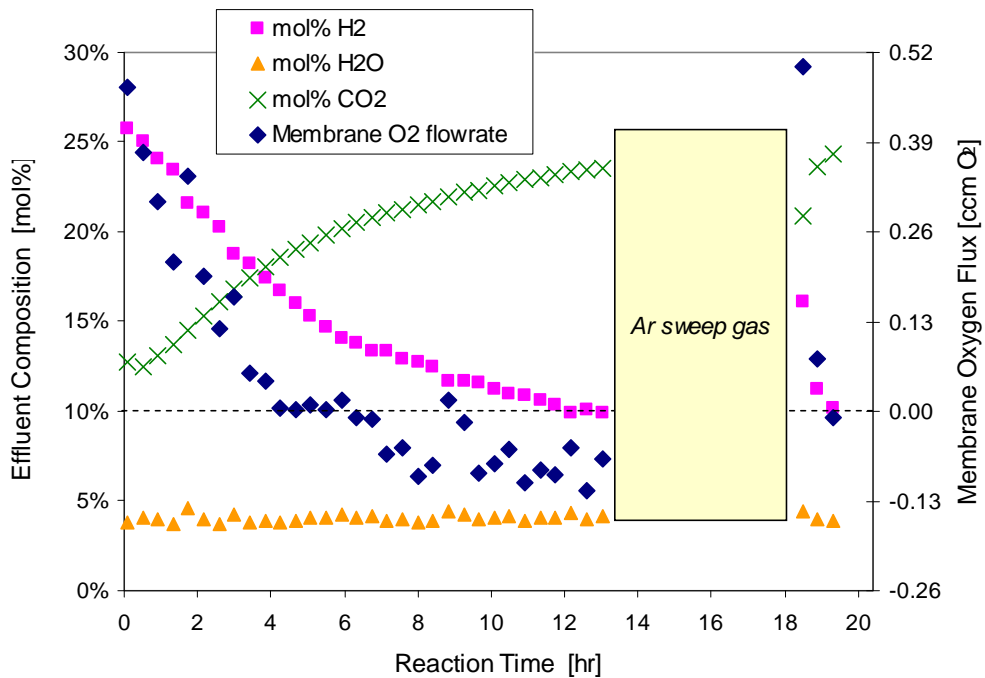


Figure 6.4: Reactor effluent composition and membrane oxygen flux (O₂ equivalent) during CO₂ reforming over a Pt/ZrO₂ catalyst in the original QTMR with an SFC membrane. Reaction temperature=800 °C, GHSV=150 L/h/g_{cat}, CH₄:CO₂:Ar feed ratio=4:4:2. With pause and re-start.

The catalyst rejuvenation period had a beneficial effect on the membrane in that initial oxygen flux on re-start matches the original initial value. However, the catalyst itself is obviously degraded from its original starting condition, as both methane and CO₂ conversion and hydrogen production are significantly lower after the re-start than after the original start and catalyst activity drops more steeply after the re-start. However, it is worth noting that catalyst methane conversion on the membrane after the break and re-start is still substantially higher than at any time on the blank after the first hour on stream. It is possible that the catalyst rejuvenation period was too short to remove enough carbon to make a significant improvement, but it is also possible that a certain amount of irreversible degradation occurred during the first 13 hour test period.

The relatively low ambient hydrogen level and high CO₂ level after the re-start are a result of the lower methane conversion, and they could explain the quick drop in net flux. If so, these observations support the theory that hydrogen is necessary to extract oxygen from SFC at higher rates than can be achieved in a flux test with an inert sweep gas. They also strongly support the idea that the catalyst and membrane must act in concert to achieve the observed effects.

6.2.4: Membrane surface reaction hypothesis evaluation

Figure 6.2 clearly demonstrates that net membrane oxygen production decreases as reactor hydrogen content decreases and CO₂ content increases. This is consistent with the proposed membrane interactions with hydrogen and CO₂. Under the hypothesized membrane surface reaction scheme, the SFC lattice incorporates oxygen atoms while reducing CO₂ to CO. Depending on the reaction environment and the membrane's current equilibrium oxygen requirements, this surface reaction system could easily produce negative flux estimates. Also, if the proposed scheme is correct, net membrane oxygen flux should vary directly with reactor hydrogen content and inversely with reactor CO₂ content (assuming the SFC is sufficiently reduced at the time of evaluation to be able to reduce CO₂).

Figure 6.5 provides additional evidence for this hypothesis by comparing the estimated membrane flux to the mole ratio of hydrogen and CO₂ in the reactor effluent. Membrane oxygen production shows clear but different correlations with the H₂:CO₂ ratio for both the initial test and the brief re-start test.

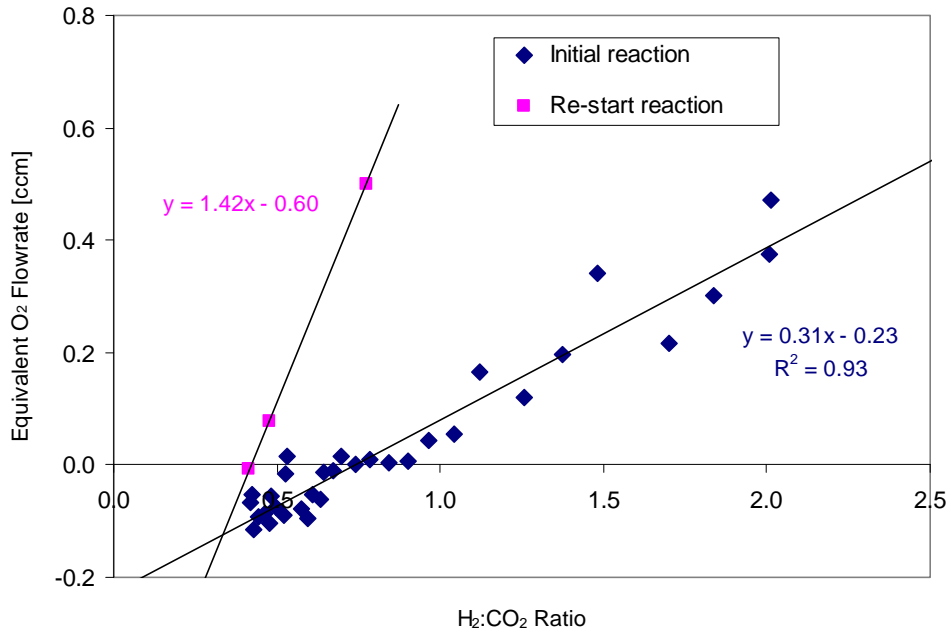


Figure 6.5: Membrane oxygen flux (O₂ equivalent) vs. H₂:CO₂ ratio during CO₂ reforming over a Pt/ZrO₂ catalyst in the original QTMR with an SFC membrane. Reaction temperature=800 °C, GHSV=150 L/h/g_{cat}, CH₄:CO₂:Ar feed ratio=4:4:2.

The H₂:CO₂ ratio fits the flux estimate better than either of the individual component mole fractions (an R² of 0.93 compared to 0.89 and 0.88 for H₂ and CO₂, respectively, according to Excel’s “line fit” algorithm). This gives credibility to the idea that both reactions occur simultaneously on the membrane surface. The higher slope on the re-start reaction line supports the idea that the catalyst is in a different state after the five-hour break.

Unlike the catalyst, the membrane surface is “recharged” somewhat during the break, as evidenced by the increasing O₂:N₂ ratios in the argon sweep gas during the break and the high membrane oxygen production estimate after the break. When the reaction feed is re-introduced, the

membrane is primed to release a significant amount of oxygen, which the flux estimates confirm, but the powder catalyst is no longer active enough to produce the same methane conversion activity.

6.3: Additional QTMR Test Results

6.3.1: Improved system baseline tests (#2)

The initial tests were repeated after improving the QTMR system as described in Appendix G. Among other improvements, line heating was increased and GC data analysis was improved substantially. Figure 6.6 provides the analogous results for the improved testing to the initial testing results in Figure 6.1.

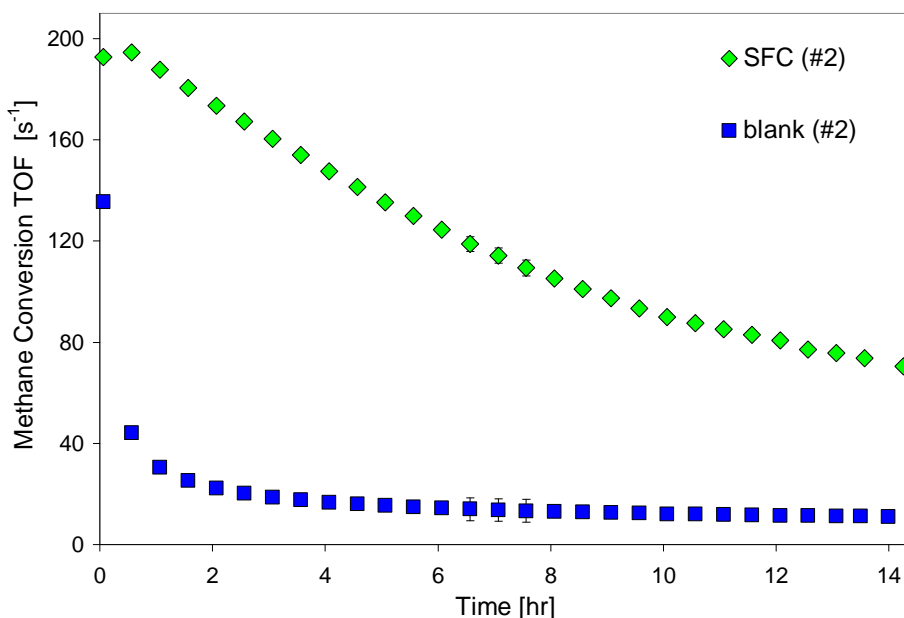


Figure 6.6: CH₄ conversion turnover frequency (TOF) during CO₂ reforming over a Pt/ZrO₂ catalyst in the improved QTMR. Reaction temperature=800 °C, GHSV=150 L/h/g_{cat}, CH₄:CO₂:Ar/O₂ feed ratio=4:4:2.

As expected from earlier results, Figure 6.6 shows a dramatic decrease in both rate and extent of catalyst deactivation with the SFC membrane under the same reaction conditions. These results confirm both the conclusion that oxygen supplied via a ceramic membrane both enhances and preserves the activity of the Pt/ZrO₂ catalyst and the repeatability of the QTMR test procedure. A

similar catalyst activity preservation effect has been reported for a Ni/ γ -Al₂O₃ catalyst in a POM membrane reactor system [1].

6.3.2: Membrane oxygen flux overview

Regardless of the actual oxygen activity mechanism(s) of the SFC membrane, methane conversion results confirm that SFC alone does not convert a significant amount of methane under CO₂ reforming feed conditions. They also demonstrate that the catalyst and the membrane work in concert to achieve the observed improvement with the Pt/ZrO₂ catalyst. However, more details about the chemical activity of the membrane is needed to determine its mode of action.

One membrane attribute that can be assessed quantitatively is the amount of oxygen produced. Figure 6.7 presents membrane oxygen production estimates during reaction for four QTMR membrane tests with the Pt/ZrO₂ catalyst, including one modified membrane. The modified membrane has a very thin layer of platinum (~7 angstroms) deposited on the air (oxygen supply) side.

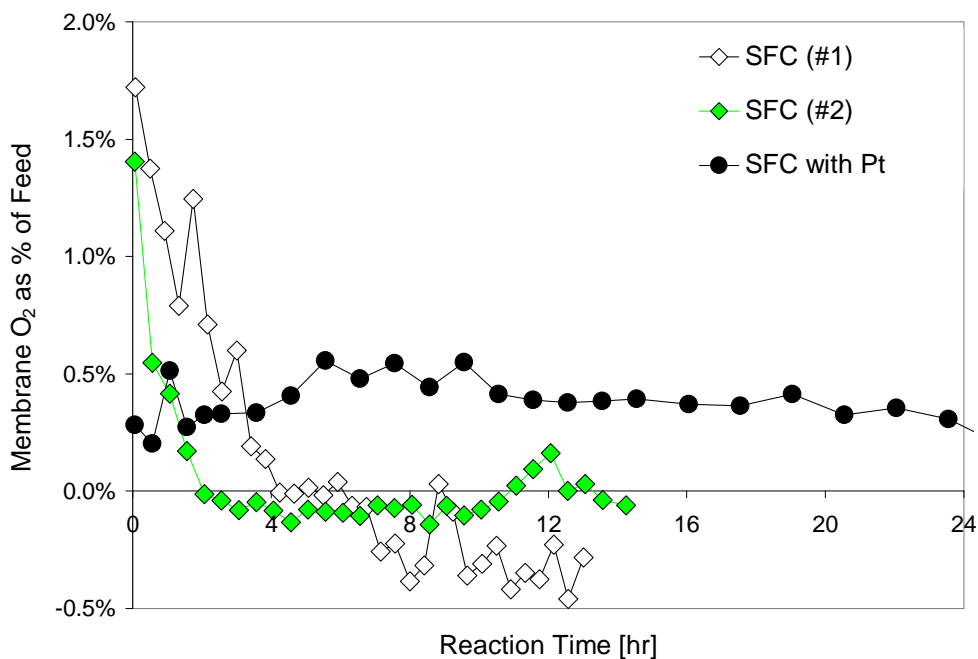


Figure 6.7: Membrane oxygen flux (O₂ equivalent) as mole% of feed during CO₂ reforming over a Pt/ZrO₂ catalyst in both QTMRs with SFC membranes. Reaction temperature=800 °C, GHSV=150 L/h/g_{cat}, CH₄:CO₂:Ar feed ratio=4:4:2.

Interestingly, the membrane with the lowest initial oxygen production (the platinum-coated membrane) exhibits the highest net oxygen production over the course of the test, and the membrane with the highest initial production ends with the lowest oxygen production (in this case, lowest actually means the most negative). As discussed earlier, the negative values are ascribed to CO₂ reduction on the depleted SFC, most likely because of a slow solid-state transport response to the initial oxygen “dumping” that is attributed to rapid hydrogen oxidation on the fresh SFC surface.

NOTE: the layer of deposited platinum is too thin to cover the SFC entirely. The SFC surfaced is polished to a 1-micron scale, but is quite rough on the nanometer scale. It is therefore expected that the platinum coating is not at all contiguous.

6.3.3: Methane conversion in membrane tests

The platinum-coated membrane does not provide the largest amount of oxygen initially, but it clearly provides the most consistent amount of oxygen. Its average oxygen production over the first 24 hours of the test is 0.4% on a molar feed basis. Figure 6.8 provides a comparison of the methane conversion activity for the same four membrane tests. The blank tests with no oxygen are included for reference.

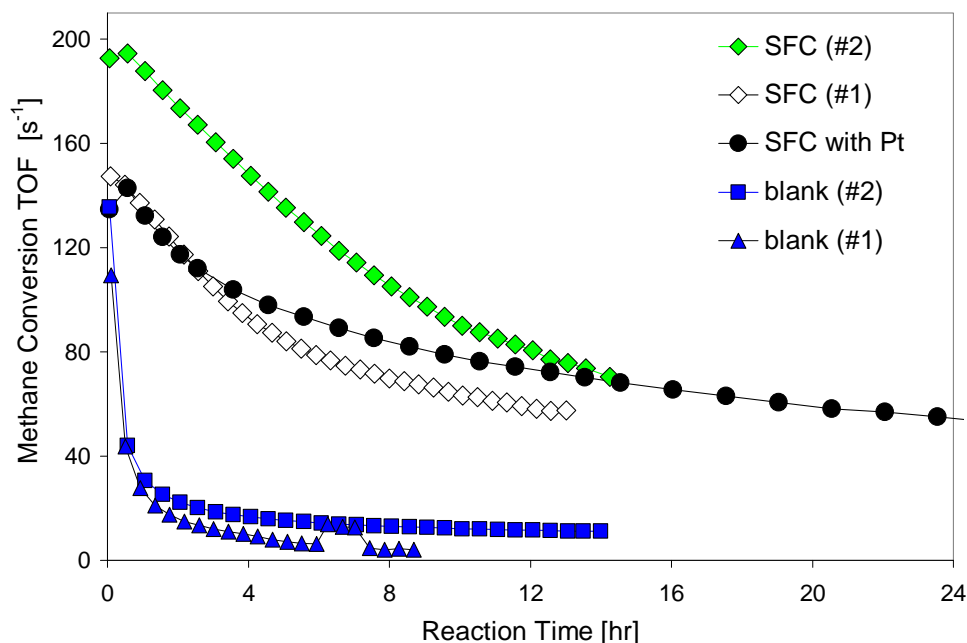


Figure 6.8: CH₄ conversion turnover frequency (TOF) during CO₂ reforming over a Pt/ZrO₂ catalyst in both QTMRs. Reaction temperature=800 °C, GHSV=150 L/h/g_{cat}, CH₄:CO₂:Ar feed ratio=4:4:2.

The catalyst on the platinum-coated membrane doesn't exhibit as much methane conversion initially as the membranes, particularly SFC (#2), but the catalyst in that test also deactivates less extensively. Methane conversion with the platinum-coated membrane actually parallels oxygen flux, and the membrane appears to have the potential to outperform even SFC (#2) over an extended period in spite of its early activity deficit. The platinum-coated membrane is from the same batch as SFC (#2), so head-to-head comparisons should be meaningful.

6.3.4: H₂:CO ratio in membrane tests

The steadily decreasing H₂:CO ratios for all of the membrane tests in Figure 6.9 indicate that hydrogen oxidation and/or carbon monoxide production increase on the membrane over time. Because this same effect is not observed in the blank tests, it appears to be related to the SFC membranes. As such, this phenomenon must be accounted for in any discussions of net reaction profiles and mechanisms for membrane activity.

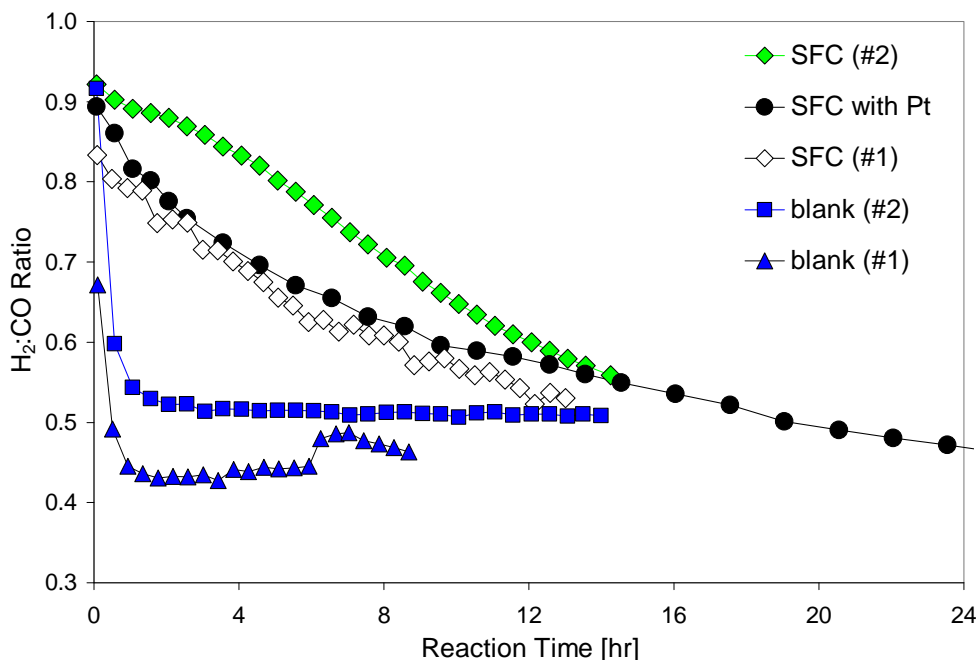


Figure 6.9: H₂:CO ratio during CO₂ reforming over a Pt/ZrO₂ catalyst in both QTMRs. Reaction temperature=800 °C, GHSV=150 L/h/g_{cat}, CH₄:CO₂:Ar feed ratio=4:4:2.

In spite of the counterproductive trends in H₂:CO ratio, Figure 6.8 provides a reminder that methane conversion after 14 hours is significantly higher (i.e., more than twice as high) in the worst QTMR membrane test than with the blank and no oxygen. The relative amount of undesirable side reactions may increase over time on the SFC membrane, but methane conversion remains substantially higher with the membrane than without.

6.4: Reactor and Membrane Testing without Catalyst

The SSMR results discussed in Chapter 5 for tests without catalyst indicate that only small amounts of combustion and even smaller amount of reforming reactions occur over either the SS blank or the SFC membranes without catalyst. Later tests show even less activity, but the QTMR also allows less leaked air. This observation provided the motivation to investigate the true effect of leaked air on methane conversion. Fortunately, there was a wide range of leak rates, as demonstrated in Table 6.1.

Table 6.1: Summary of tests with no catalyst; CH₄ conversions as [mol_{converted} / mol_{fed}]

| Test details | Average steady state CH ₄ conversion | Pre-reaction leak [% of feed] |
|-------------------------------------|---|-------------------------------|
| Blank, 700 °C (10/18/04) | 1.26% | 3.37% |
| Blank, 750 °C (6/2/05) | 0.58% | 0.99% |
| Blank, 800 °C (9/22/05) | 0.25% | 0.43% |
| Blank + 1% O ₂ (2/22/06) | 1.87% | 0.57% |
| PFR + 1% O ₂ (2/2/06) | 0.60% | 0% |
| PFR (2/2/06) | 0.21% | 0% |
| PFR (4/7/06) | 0.17% | 0% |
| SFC, 700 °C (10/14/04) | 2.77% | 5.66% |
| SFC, 750 °C (5/7/05) | 0.76% | 1.11% |
| SFC, 750 °C (5/13/05) | 0.69% | 1.11% |
| SFC, 800 °C (10/8/05) | 0.39% | 0.19% |

6.4.1: Oxygen and methane conversion without catalyst

To evaluate the differences in the various “no catalyst” tests, average methane conversions over the duration of the tests are correlated with air leak estimates. As shown in Figure 6.10, leak level clearly determines methane conversion on the stainless steel blank. The effect is less distinct with the SFC membrane, but this is to be expected because of the membrane’s ability to interact with oxygen. A membrane can add or remove its own oxygen to the system, including the direct uptake of leaked oxygen before it has a chance to react if the leak occurs along the membrane surface.

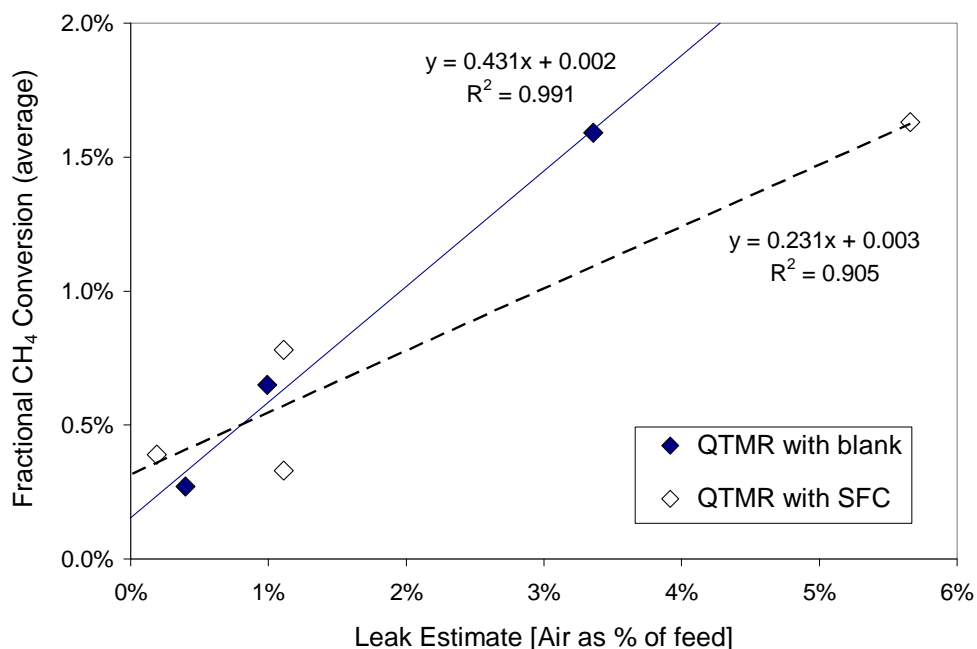


Figure 6.10: Average fractional CH₄ conversion vs. air leak estimate during CO₂ reforming with no catalyst in both QTMRs. Reaction temperature=800 °C, GHSV=150 L/h/g_{cat}, CH₄:CO₂:Ar feed ratio=4:4:2.

To sidestep the issue of membrane-oxygen interactions, the total amount of oxygen entering the reactor (other than the oxygen in CO₂) can be compared with the average methane conversion for the test as shown in Figure 6.11. For this comparison, the average oxygen value is represented by its mole ratio to the methane feed, putting oxygen on the same basis as fractional methane conversion (fractional conversion is the mole ratio of methane converted-to-methane fed). This representation also allows convenient evaluation of the reaction stoichiometry.

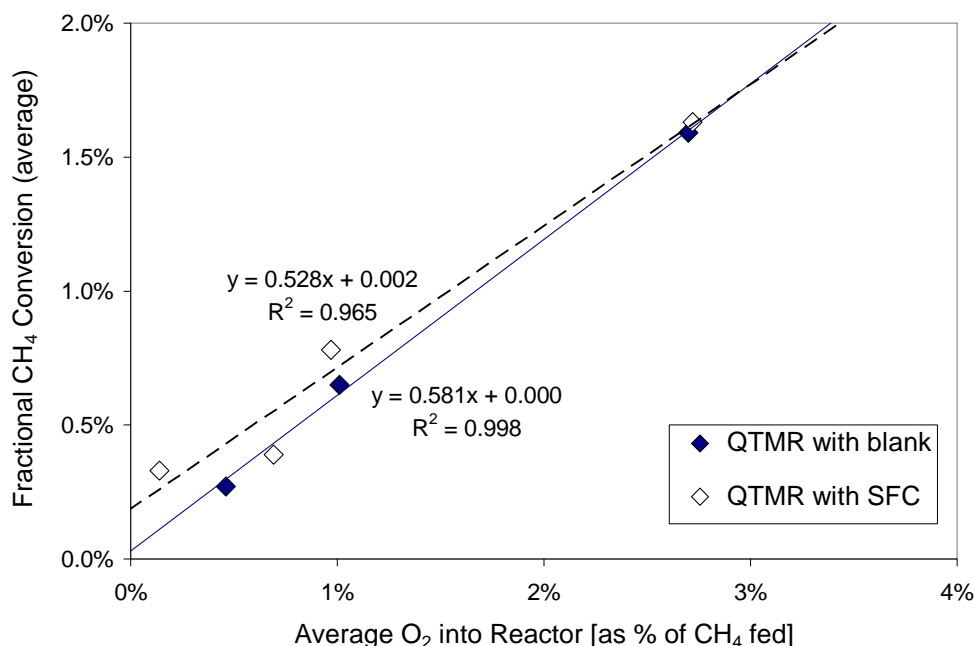


Figure 6.11: Average fractional CH₄ conversion vs. average total oxygen into reactor during CO₂ reforming with no catalyst in both QTMRs. Reaction temperature=800 °C, GHSV=150 L/h/g_{cat}, CH₄:CO₂:Ar feed ratio=4:4:2.

The stainless steel blank and the SFC membrane tests exhibit similar trends, confirming that methane conversion is not significantly affected by the SFC membrane itself and that both catalyst and membrane are needed to produce the desired benefit from an SFC membrane. The slope of the lines is nearly 0.5, which is the theoretical value for combustion, and both lines are close enough to 0.5 to conclude that combustion accounts for the majority of the methane conversion with no catalyst.

6.4.2: Water production without catalyst

Figure 6.12 shows the relative water production values for the QTMR “no catalyst” tests. Pure combustion would yield a slope of two, so the water production data confirm that combustion causes the majority of the methane conversion on both the blank and the SFC membranes when no catalyst is present. The fact that both lines intersect the x-axis at positive values can be interpreted as evidence that a very small amount of another methane consuming reaction occurs as well (CO₂ reforming, steam reforming, or partial oxidation). This interpretation is consistent with the fact that

the slopes for the lines in Figure 6.12 are both less than two. Not only is there a slight offset, but slopes less than two indicate that the amount of the side reaction increases along with the amount of combustion as more oxygen is made available.

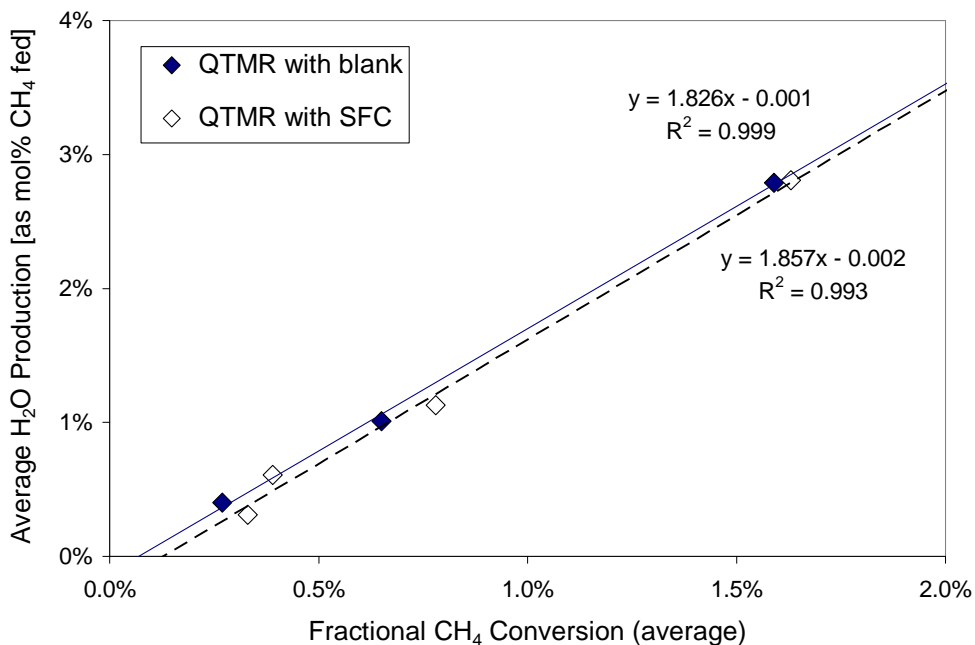


Figure 6.12: Average relative water production vs. average fractional CH₄ conversion during CO₂ reforming with no catalyst in both QTMRs. Reaction temperature=800 °C, GHSV=150 L/h/g_{cat}, CH₄:CO₂:Ar feed ratio=4:4:2.

In general, methane conversion with no catalyst trends very closely with the amount of available oxygen, and leaked gas-phase O₂ and membrane oxygen are largely indistinguishable with no catalyst present. It appears that the intrinsic activities of both the SFC membrane and the stainless steel blank are similarly low and that both depend on the availability of gas-phase oxygen.

6.5: Membrane Mechanism Hypothesis

6.5.1: Possible activity mechanisms for membrane oxygen

Three possibilities for the exact role of membrane oxygen in the reaction mechanism have been considered. First, oxygen ions could recombine to form molecular oxygen after they diffuse through the membrane material and these molecules would then desorb from the membrane surface

before reacting as gas-phase oxygen. This molecular oxygen would be introduced at the bottom of the catalyst bed and might thus compete less with CH₄ for some of the platinum sites than co-fed O₂ which would lead to less *in situ* catalyst oxidation. Although this scenario is consistent with the increased activity observed with the ceramic membrane, it is unlikely that oxygen ions on the surface of the membrane would preferentially recombine to form molecular oxygen and desorb from the surface before reacting with the readily available hydrogen in the reaction environment.

An alternate and more probable explanation is that the oxygen ions on the surface of the membrane react directly with hydrogen produced by catalytic methane decomposition. Membrane oxygen is not expected to react directly with CH₄ to a significant extent since, as previously demonstrated, CH₄ conversion on the membrane is negligible in the absence of catalyst. However, water produced by the oxidation of hydrogen at the membrane surface could increase CH₄ conversion by participating in steam reforming as it passes out through the catalyst layer. The net effect of hydrogen oxidation followed by steam reforming is stoichiometrically indistinguishable from methane partial oxidation.

A final possibility which has been proposed is that the oxygen ions in the SFC might be mobile enough to transfer to the powder catalyst from the membrane surface. While this is an intriguing idea, it is the least likely of the three given the substantial transport barriers and distances for solid state ion migration from the SFC membrane surface to the individual platinum particles in the pores of the ZrO₂-supported catalyst. In addition to being the least likely of the three options, the oxygen ion migration theory is impossible to verify or disprove from the available data, so only the first two possibilities were evaluated in this work.

6.5.2: Proposed SFC activity mechanism

Any performance discrepancy between co-fed oxygen and membrane oxygen supports the hypothesis that, under reforming reaction conditions with low net oxygen production, membrane

oxygen is consumed at the membrane surface rather than leaving the membrane as molecular O₂. Compelling evidence also exists that membrane oxygen production can become negative at times, implying that an SFC membrane surface can extract oxygen from the reaction environment. Based on the evidence, hydrogen oxidation is proposed as the only significant oxygen-consuming surface reaction and CO₂ reduction is proposed as the oxygen-replenishing surface reaction for SFC

This hypothesis represents a significant departure from the explicit or implicit assumption by previous researchers in this field that membrane oxygen participates in partial oxidation of methane in its molecular state (i.e., as O₂) [1-11]. Only one published statement that hydrogen oxidation on the membrane surface is a possible pathway for oxygen flux enhancement was found [12]. It is theoretically possible that other, higher flux membrane materials could transport oxygen so quickly under reaction conditions that the oxygen could leave the membrane via a different mechanism in the presence of hydrogen, but no explicit evidence could be found for this. In any case, given the overwhelming thermodynamic impetus for hydrogen oxidation, it seems extremely unlikely methane reacts directly with molecular oxygen evolved from a membrane surface in the presence of hydrogen. It is therefore the position of this author that under reaction conditions in the presence of hydrogen, oxygen is removed from the SFC membrane surface exclusively by hydrogen oxidation.

Supporting this perspective, Ikeguchi et al. found no increase in oxygen flux when methane was fed along with argon to an O-MIEC membrane reactor [12]. However, adding CO and hydrogen to the argon sweep gas resulted in increased oxygen flux, with hydrogen having the more significant effect. In the presence of a supported rhodium catalyst powder, the methane feed did cause a dramatic increase in flux. This increase was attributed to the diffusion of hydrogen released by methane decomposition on the catalyst to the membrane surface where it was oxidized to water and could then participate in steam reforming in the catalyst bed—exactly the reaction pathway endorsed by this dissertation.

The tests Ikeguchi et al. conducted with the methane/argon and a reforming catalyst feed created an environment where hydrogen availability increased as more oxygen was supplied to the reactor by the membrane. The tests where hydrogen was supplied directly, on the other hand, were self-limiting, as any increase in oxygen supply would decrease the partial pressure of hydrogen and thus undermine the oxygen supply mechanism.

Hydrogen oxidation at the membrane followed by steam reforming in the catalyst bed is stoichiometrically identical to partial oxidation with evolved molecular oxygen. However, there are critical implications for membrane reactor design and optimization as well as both membrane and catalyst choice if the alternate reaction pathway endorsed herein is correct.

6.5.3: Trace oxygen uptake by SFC

Post-reaction mass spectrometer data demonstrate that as the reactor cools and exhibits the presence of increasing nitrogen levels as leakage increases, low oxygen is observed until the membrane has replenished the oxygen content of the top surface. The length of time for this replenishment depends on the membrane material and the duration and intensity of the oxygen-depleting reaction period. Figure 6.13 depicts the post-reaction period following the brief second reaction in the “SFC #1” test. The pre-reaction oxygen flux trend for the same test is included for comparison as Figure 6.14.

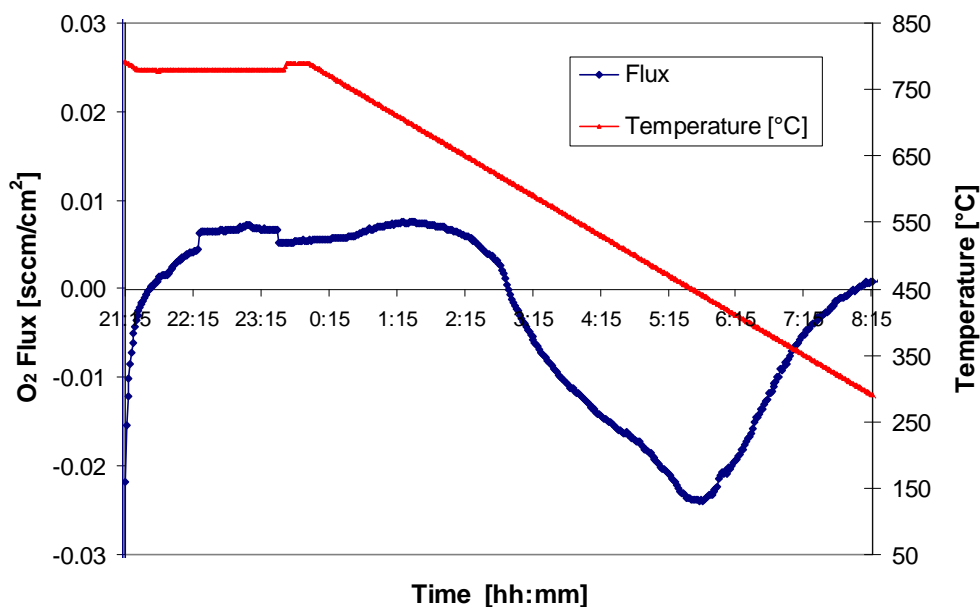


Figure 6.13: Membrane oxygen flux (O₂ equivalent) during cool-down following CO₂ reforming over a Pt/ZrO₂ catalyst in the original QTMR with an SFC membrane. Ar sweep gas flowrate=25 ccm.

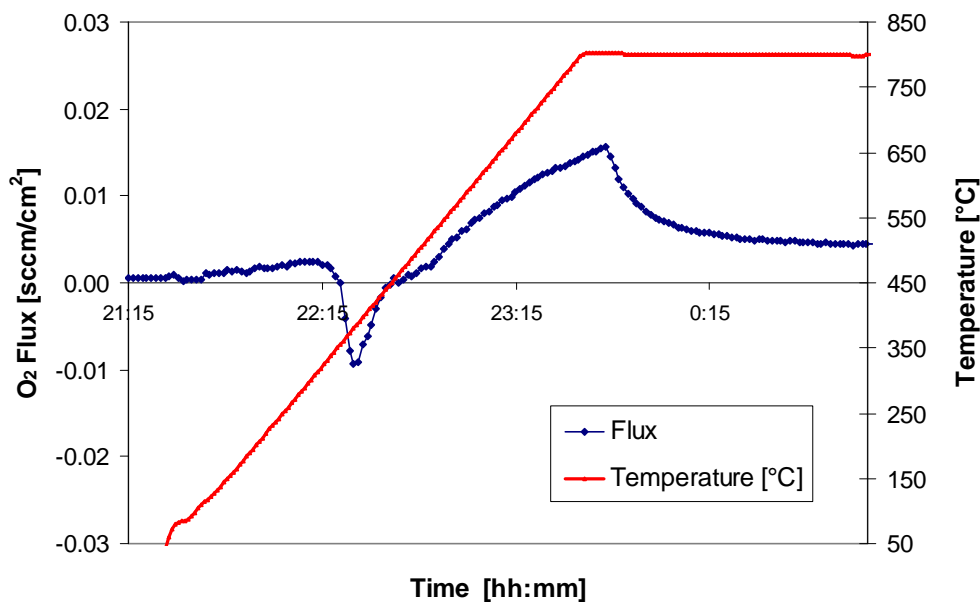


Figure 6.14: Membrane oxygen flux (O₂ equivalent) during heat-up prior to CO₂ reforming over a Pt/ZrO₂ catalyst in the original QTMR with an SFC membrane. Ar sweep gas flowrate=25 ccm.

It appears that the reaction side surface of the membrane is so depleted of oxygen that it absorbs oxygen from the leaked air, stopping either when it approaches saturation or when the membrane cools to the point that solid state reactions cease. If this interpretation of the missing oxygen (i.e., negative flux) phenomenon is correct and a membrane can absorb significant amounts of scarce molecular oxygen under an inert argon environment following a reaction test, it is implausible that molecular oxygen could evolve from a membrane surface under a highly reducing reaction environment. It becomes more plausible, however, that an SFC membrane that has been reduced to less than its equilibrium oxygen content for a given temperature could extract oxygen from CO₂.

6.6: Observations and Conclusions from Chapter 6

- (1) Membrane oxygen flux under reaction conditions represents the net oxygen transferred to the reaction chamber from the SFC as determined by the relative amounts of hydrogen oxidation and CO₂ reduction on the membrane surface. Negative flux values indicate an operating state wherein the membrane is converting more CO₂ to CO than hydrogen to water.
- (2) Using an SFC membrane as a substrate for a conventional powder catalyst (Pt/ZrO₂, in this case) in a CO₂ reforming reactor dramatically improves catalyst activity both initially and over time.
- (3) The catalyst layer and the SFC membrane act in concert to produce the observed effects.
- (4) H₂:CO ratio decreases more gradually on an SFC membrane than on the blank, but it could decrease further with the SFC membrane even while methane conversion remains higher.
- (5) Methane conversion activity on both the blank and the SFC membrane with a CO₂ reforming feed correlates closely with the amount of leaked air and the reaction products correlate closely with combustion products. The SFC and blank exhibit equally low activity in the absence of a catalyst, and it is therefore believed that the SFC surface does not convert a significant amount of methane.
- (6) Following a change in environment (e.g., a temperature change), an SFC membrane that is depleted in oxygen relative to its equilibrium composition in its new environment will incorporate oxygen from the gas-phase to equilibrate itself, even if only very small amounts of oxygen are available.

- (7) A very thin (approximately two atomic monolayers) coating of platinum on the oxygen supply side of an SFC membrane appears to have a beneficial effect on the amount of oxygen the membrane can supply under reaction conditions. It also improves flux persistence.

References Cited in Chapter 6

1. Feng, S.J., S. Ran, D.C. Zhu, W. Liu and C.S. Chen, *Synthesis gas production from methane with SrFeCo_{0.5}O_y membrane reactor*. Energy & Fuels **18**, 2004, p.385-389.
2. Zhu, D.C., X.Y. Xu, S.J. Feng, W. Liu and C.S. Chen, *La₂NiO₄ tubular membrane reactor for conversion of methane to syngas*. Catal Today **82**, 2003, p.151-156.
3. Jin, W., X. Gu, S. Li, P. Huang, N. Xu and J. Shi, *Experimental and simulation study on a catalyst packed tubular dense membrane reactor for partial oxidation of methane to syngas*. Chem Eng Science **55**, 2000, p.2617-2625.
4. Balachandran, U., J.T. Dusek, P.S. Maiya, B. Ma, R.L. Mieville, M.S. Kleefisch and C.A. Udovich, *Ceramic membrane reactor for converting methane to syngas*. Catal Today **36**, 1997, p.265-272.
5. Tsai, C.-Y., A.G. Dixon, Y.H. Ma, W.R. Moser and M.R. Pascucci, *Dense perovskite La_{1-x}A'_xFe_{1-y}Co_yO_{3-δ} (A' = Ba, Sr, Ca) membrane synthesis, applications, and characterization*. J Amer Ceram Soc **81**(6), 1998, p.1437-1444.
6. Dong, H., Z. Shao, G. Xiong, J. Tong, S. Sheng and W. Yang, *Investigation on POM reaction in a new perovskite membrane reactor*. Catal Today **67**, 2001, p.3-13.
7. Gu, X., L. Yang, L. Tan, W. Jin, L. Zhang and N. Xu, *Modified Operating Mode for Improving the Lifetime of Mixed-Conducting Ceramic Membrane Reactors in the POM Environment*. Ind Eng Chem Res **42**, 2003, p.795-801.
8. Lu, H., J. Tong, Y. Cong and W.S. Yang, *Partial oxidation of methane in Ba_{0.5}Sr_{0.5}Co_{0.8}Fe_{0.2}O_{3-δ} membrane reactor at high pressure*. Catal Today **104**(154-159), 2005, p.154.
9. Zhang, P., X. Chang, Z. Wu, W. Jin and N. Xu, *Effect of the Packing Amount of Catalysts on the Partial Oxidation of Methane Reaction in a Dense Oxygen-Permeable Membrane Reactor*. Ind Eng Chem Res **44**, 2005, p.1954-1959.
10. Bouwmeester, H.J., *Dense ceramic membranes for methane conversion*. Catal Today **82**, 2003, p.141-150.
11. Frade, J.R., V.V. Kharton, A. Yaremchenko and E. Naumovich, *Methane to syngas conversion Part 1: Equilibrium conditions and stability requirements of membrane materials*. Jnl of Power Sources **130**, 2004, p.77-84.
12. Ikeguchi, M., T. Mimura, Y. Sekine, E. Kikuchi and M. Matsukata, *Reaction and oxygen permeation studies in Sm_{0.4}Ba_{0.6}Fe_{0.8}Co_{0.2}O_{3-δ} membrane reactor for partial oxidation of methane to syngas*. Appl Cat A **290**, 2005, p.212-220.

Chapter 7: The Role of Membrane Oxygen

In addition to initiating the investigation of the hypotheses derived from this work, Chapter 6 provided conclusive confirmation of the beneficial effect of SFC membranes on the Pt/ZrO₂ catalyst under CO₂ reforming conditions. This chapter begins to examine the nature of the membrane's contribution to methane conversion by evaluating tests performed in the QTMR with co-fed O₂. The use of reactant and product ratios recommended in Chapter 5 is employed to compare the effects of co-fed O₂ and the SFC membrane. The first carbon deposition data acquired by a small volume oxygen injection technique are also reported for catalyst from both blank and SFC membrane tests.

7.1: Initial QTMR Testing with 1% Co-Fed Oxygen

To determine if Pt/ZrO₂ interacts differently with membrane oxygen than with molecular oxygen, the continuous addition of 1% co-fed oxygen was tested with the stainless steel blank. As discussed in Section 6.2.2, 1% oxygen is believed to be a suitable representative value. While early SSMR tests with membranes fabricated by the Balachandran group exhibited oxygen contributions at least this high throughout a reaction test period, later tests with membranes fabricated in-house yielded less than 1% at steady state but averaged approximately this much in the early part of their reaction tests. With the first few hours (if not the first fifteen minutes) of a test period believed to be have the greatest impact on catalyst performance, 1% co-fed oxygen represents an appropriate co-fed oxygen level to begin examining the effect of co-fed oxygen on catalyst performance. It also has already been tested as part of a brief co-fed oxygen interlude in the first blank test with catalyst performed in the QTMR.

7.1.1: Methane conversion

The results of the first complete 1% co-fed oxygen test are provided in Figure 7.1. This figure is an expansion of Figure 6.3. While the 1% co-fed oxygen test shows a small improvement in methane conversion over the blank test without oxygen, it does not show a significant improvement

in catalyst deactivation rate. This indicates clearly that oxygen alone is not responsible for the decreased deactivation rate with the SFC membrane.

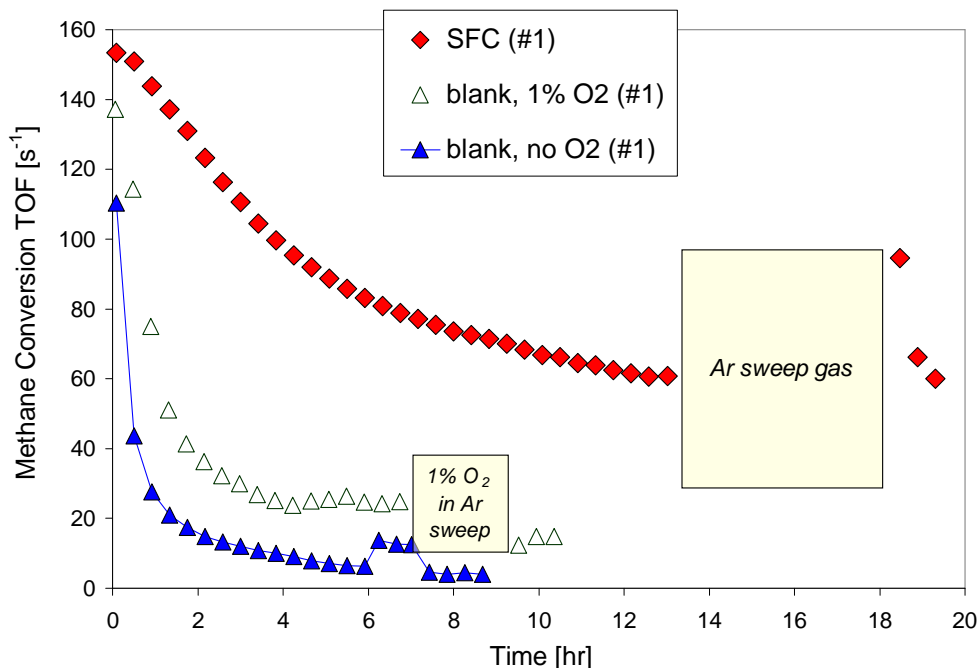


Figure 7.1: CH₄ conversion turnover frequency (TOF) during CO₂ reforming over a Pt/ZrO₂ catalyst in the original QTMR. Reaction temperature=800 °C, GHSV=150 L/h/g_{cat}, CH₄:CO₂:Ar/O₂ feed ratio=4:4:2.

As discussed in Section 6.2.3 with Figure 6.3, the SFC membrane test was paused for five hours of argon-only feed before the original reactant feed was re-started. It was hoped that membrane oxygen could improve catalyst activity by removing deposited carbon, and the result is a significant but short-lived increase in methane conversion. The brief improvement after the break could result either from the oxidation of deposited carbon or from the membrane replenishing its oxygen content while under the air/argon gradient and then releasing the accumulated oxygen on returning to a reducing reaction environment. For comparison with this, the blank test with 1% co-fed oxygen was also paused and re-started, as indicated in Figure 7.1.

During this 45 minute break, the catalyst was exposed to 1% oxygen in argon at the same flowrate as the reaction feed (25 ccm). The desired effect of the 1% oxygen/argon period was to

remove any deposited carbon while limiting the oxygen content of the reaction chamber to that to which it is exposed during the reaction portion of the test. The oxidizing interlude clearly fails to increase catalyst activity and actually decreases methane conversion somewhat. The original deactivation appears to be irreversible and thus could be caused by platinum sintering, but there also appears to have been additional deactivation over the 1% oxygen/argon interlude. Either additional sintering occurs during this period or small amounts of oxidation cause this catalyst to lose activity.

7.1.2: Catalyst deactivation

Catalyst deactivation is commonly assumed to result either from loss of catalyst surface area via platinum particle sintering (i.e., physical deactivation) or from carbon deposition and/or adsorption of other species (i.e., chemical deactivation). However, there is a subcategory to the chemical deactivation option that could occur in any oxygen-containing reaction environment: platinum oxidation state could also affect catalyst activity. The pauses and re-starts in the tests presented in Figure 7.1 provide potential insight into the effect of platinum oxidation state on Pt/ZrO₂ catalyst activity. If valid, this insight will help explain deactivation mechanism(s) at work in these tests.

7.1.3: H₂:CO ratio

The H₂:CO ratio is significantly higher with the SFC membrane than in the blank test with no oxygen, which sees the ratio drop from its initial value of almost 0.7 to a somewhat stable value of ~0.45 within the first hour of reaction (Figure 7.2). The blank test with 1% co-fed oxygen shows a parallel trend to that of the blank test with no oxygen, but the overall levels are higher throughout by 0.2 to 0.3 and indicate a steady state value higher than that of the SFC membrane test. The difference between the two blank tests is consistent with the amount of partial oxidation that corresponds with the amount of co-fed oxygen added, given a baseline amount of rWGS.

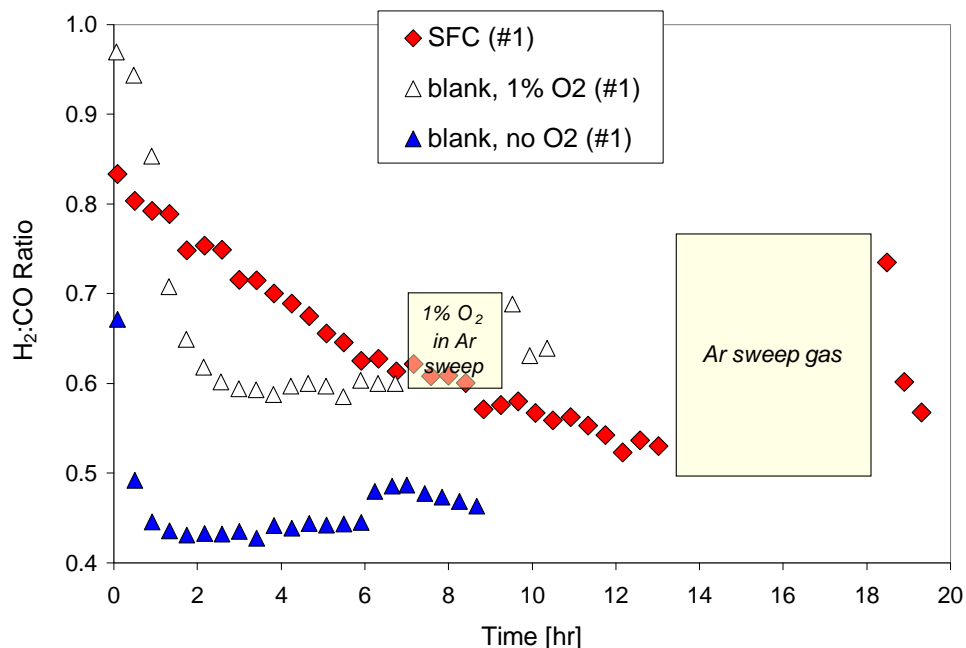


Figure 7.2: H₂:CO ratio during CO₂ reforming over a Pt/ZrO₂ catalyst in the original QTMR. Reaction temperature=800 °C, GHSV=150 L/h/g_{cat}, CH₄:CO₂:Ar/O₂ feed ratio=4:4:2.

As in Chapter 6, H₂:CO ratios with the SFC membrane show a gradual decline and are generally low in spite of high methane conversion. The increase after the 5-hour break in the reaction drops as quickly as the methane conversion. However, the increase after the break is slightly more pronounced than the increase in methane conversion which could result from the temporarily elevated membrane-provided oxygen level as opposed to renewed catalyst activity in general.

In general, the H₂:CO ratio in all tests tends to track with methane conversion. As Figure 7.3 shows, the SFC test results are somewhat in line with the blank test with no oxygen, while the blank test with co-fed oxygen trends higher at all methane conversions. In conjunction with the low oxygen flux estimates for this membrane test from Chapter 6, this discrepancy indicates either that the oxygen flux for this particular test is much lower than 1% or that the membrane effect is fundamentally different than the effect of gas-phase oxygen.

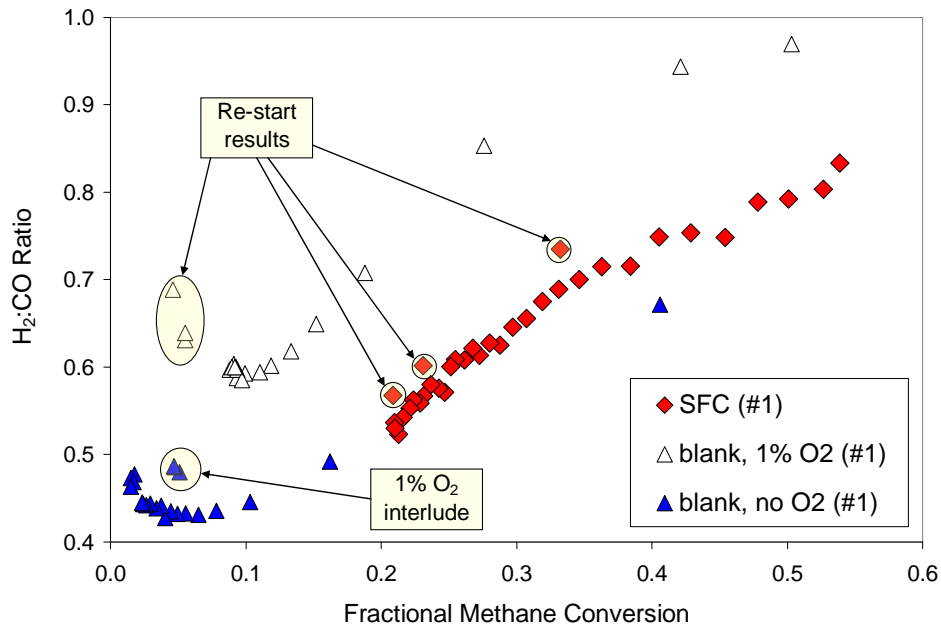


Figure 7.3: H₂:CO ratio during CO₂ reforming over a Pt/ZrO₂ catalyst in the original QTMR. Reaction temperature=800 °C, GHSV=150 L/h/g_{cat}, CH₄:CO₂:Ar/O₂ feed ratio=4:4:2.

Although the increase in H₂:CO ratio on re-starting the reaction with the SFC membrane does not approach the corresponding level for the blank test with 1% oxygen, it is both persistent and consistent with the other trends exhibited with the blank. Further testing is needed to see if the increased methane conversion and H₂:CO ratio on the SFC membrane after the break is related to carbon removal from the catalyst or simply the result of increased oxygen content of the membrane.

7.2: Improved System with 1% Co-Fed Oxygen

After improving the reactor system and the GC calibration approach as described in Appendix G, the QTMR testing described above was repeated. The strategy of using the stainless steel blank with co-fed oxygen to help elucidate the role of membrane oxygen was ultimately expanded to include other amounts of co-fed oxygen.

7.2.1: Methane conversion

With the stainless steel blank membrane in the improved system, a 1% co-fed O₂ test scenario exhibits a similar relationship to the no oxygen case as in the initial set of tests. CH₄ conversion is

higher with 1% O₂ than with no co-fed O₂, but, as in Figure 7.1, the deactivation trends are the same with and without co-fed oxygen. As Figure 7.4 shows, steady deactivation rates are reached after about six hours of reaction for the blank tests, although conversion levels are low in both cases.

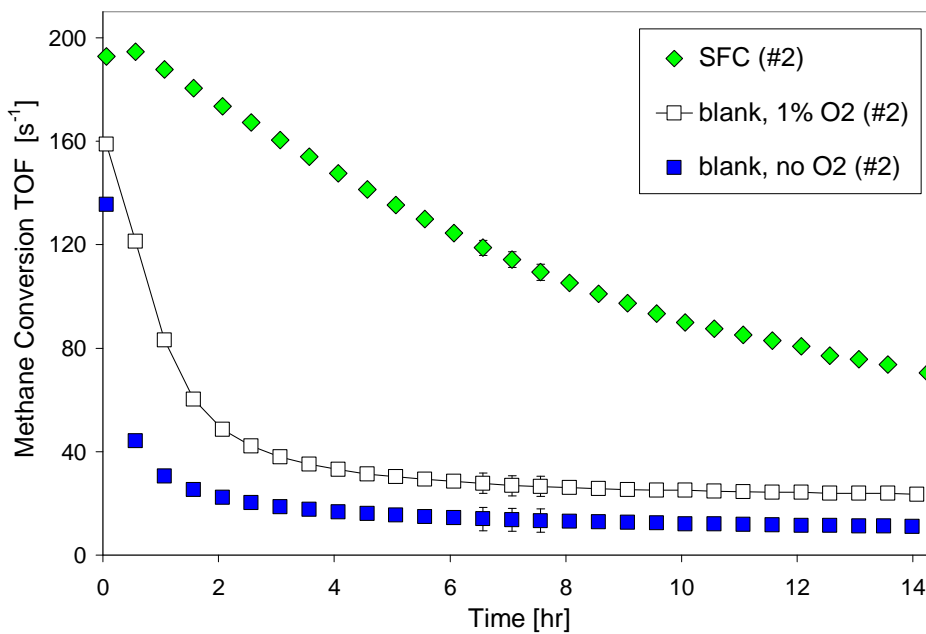


Figure 7.4: CH₄ conversion turnover frequency (TOF) during CO₂ reforming over a Pt/ZrO₂ catalyst in the original QTMR. Reaction temperature=800 °C, GHSV=150 L/h/g_{cat}, CH₄:CO₂:Ar/O₂ feed ratio=4:4:2.

Over the final seven hours, the difference in methane conversion between the blank tests with 1% oxygen and with no oxygen is very close to the theoretical contribution of partial oxidation from the co-fed oxygen. The average actual TOF difference is 12.8 sec⁻¹, which coincides with a theoretical stoichiometric partial oxidation contribution of 13.3 sec⁻¹ for 1% co-fed O₂. Equating co-fed oxygen with partial oxidation stoichiometry in this case leads to the possibility that partial oxidation with the co-fed oxygen could be responsible for the entire difference between the quasi-steady state conversions of the two blank tests. As combustion requires four times as much oxygen per mole of methane converted compared to partial oxidation, the available oxygen would only allow combustion to account for 26% of the incremental 12.8 sec⁻¹ of conversion over the second half of the test period. By looking only at methane conversion, it appears that partial oxidation is the most

plausible explanation for the increase in catalyst activity with 1% co-fed oxygen. This preliminary conclusion will be revisited later in this chapter by evaluating other reactant product and reactant ratios for these tests.

7.2.2: H₂:CO ratio

The H₂:CO ratio results in Figure 7.5 provide a final corroboration of the similarity of the two baseline test sets with the QTMR (i.e., before and after the system improvements) and also of the beneficial effects of the improvements. The general relationships between the three tests are the same as in Figure 7.2, but the trends are cleaner as a result of the systemic improvements.

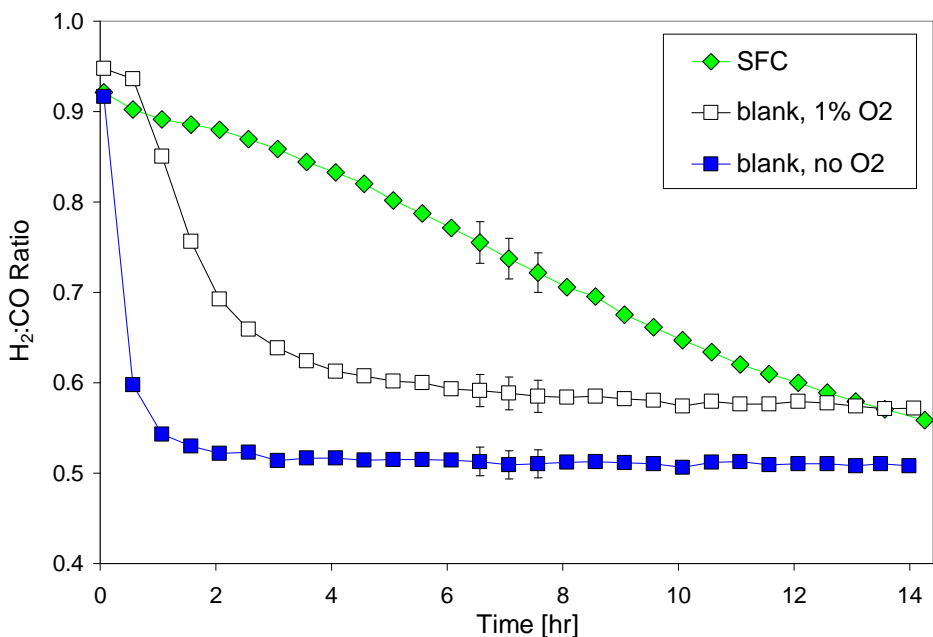


Figure 7.5: H₂:CO ratio during CO₂ reforming over a Pt/ZrO₂ catalyst in the improved QTMR. Reaction temperature=800 °C, GHSV=150 L/h/g_{cat}, CH₄:CO₂:Ar/O₂ feed ratio=4:4:2.

7.3: Improved System with Other Co-Fed Oxygen Amounts

7.3.1: Selection of additional co-fed oxygen amounts

Although 1% co-fed oxygen is somewhat representative of the average amount of oxygen supplied by the SFC membrane in this membrane test, the effect of the co-fed oxygen was minimal

compared to the effect of the membrane. However, the oxygen output from this membrane material varies significantly across a test, particularly in the early stages. In most reaction tests, SFC membrane oxygen production is initially high, drops fairly quickly, undergoes minor fluctuations, and ultimately ends up at a low value relative to the initial transitional value. Using an average oxygen flux for the co-fed O₂ amount does not represent the full range of oxygen levels to which the catalyst may be exposed on the membrane. The possibility that either the higher or lower oxygen levels from the membrane could be beneficial must be explored before the apparent unique benefits of the SFC membrane can be accepted.

The high initial flux estimates under reaction conditions are not believed to represent true oxygen flux through the membrane but rather a “dumping” of oxygen from the membrane as it equilibrates with its new environment. This is not true, sustainable oxygen flux, but the oxygen is supplied by the membrane and is therefore indistinguishable from true flux to the reaction chamber. With an unreduced membrane, changing the environment over the top surface of the membrane from pure argon to a hydrogen-containing mixture leads to unsustainably high initial oxygen output, which then drops quickly as the membrane equilibrates with the reaction environment. The membrane even appears to uptake oxygen from the environment if the membrane has recently been—or is currently being—exposed to high enough levels of hydrogen.

To evaluate the effect of the various oxygen outputs to which the catalyst was exposed during the SFC membrane test in Figure 7.4, other co-fed O₂ levels of interest were identified from estimates of membrane oxygen production during that reaction. Based on the information available at the time, two additional levels of co-fed O₂ were selected to test with the stainless steel blank: 2% co-fed O₂ to reproduce the initial surge of oxygen from the membrane and 0.2% O₂ to represent the eventual steady state flux under reaction conditions with the second generation SFC membranes.

7.3.2: Additional co-fed oxygen amount testing

The next two co-fed oxygen tests were intended to determine whether the catalyst activity enhancement and preservation effects that were seen with the SFC membrane could be achieved with co-fed oxygen at any of the likely membrane supply levels. Figure 7.6 provides an emphatic answer: the four stainless steel blank tests all exhibited the same deactivation curve shape regardless of oxygen amount. It can be concluded that gas-phase oxygen does not offer a significant improvement in catalyst longevity and higher levels may actually have a detrimental effect on Pt/ZrO₂ catalyst activity.

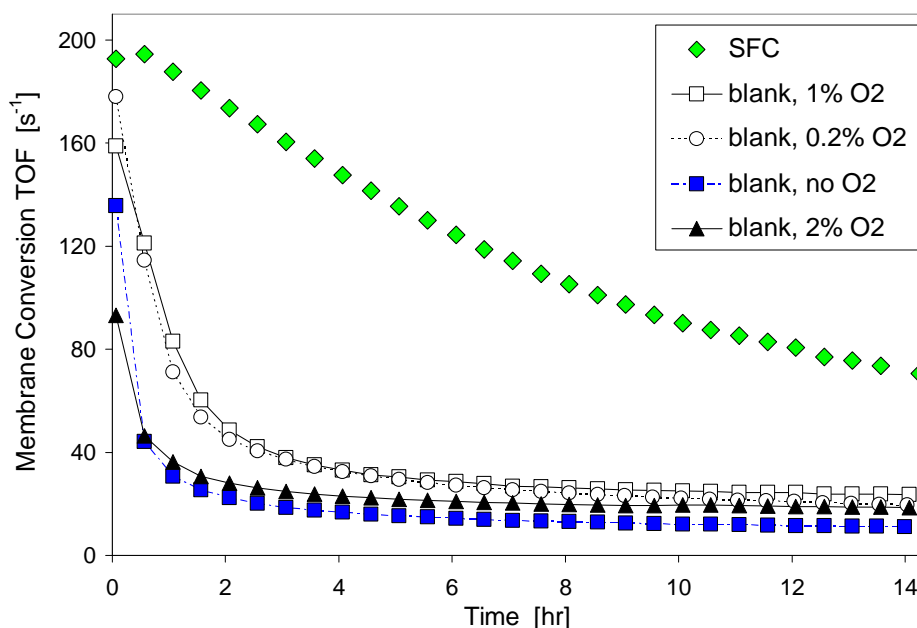


Figure 7.6: CH₄ conversion turnover frequency (TOF) during CO₂ reforming over a Pt/ZrO₂ catalyst in the improved QTMR. Reaction temperature=800 °C, GHSV=150 L/h/g_{cat}, CH₄:CO₂:Ar/O₂ feed ratio=4:4:2.

Table 7.1 is provided to help distinguish between the four blank tests in Figure 7.6 by clarifying the initial and final CH₄ conversion values for each quantity of co-fed oxygen. Surprisingly, the 2% O₂ test showed the lowest initial activity of any of the tests. This observation seemingly eliminates the possibility that an initial release of gas-phase oxygen from the SFC material is responsible for the high catalyst activity with the SFC membrane while simultaneously bolstering a

new hypothesis that *in situ* catalyst reduction is a critical factor in the SFC membrane’s success at promoting catalytic methane conversion.

By the second analysis point (i.e., after 35 minutes of reaction time), methane conversion with 2% co-fed O₂ exceeds that of the “no oxygen” case. It continues to exceed the no oxygen case throughout the 14 hour test period

but remains significantly less than the conversion levels in the 0.2% and 1% co-fed O₂ cases. In a similar pattern, the 0.2% co-fed O₂ test shows an initially higher CH₄ conversion than the 1% O₂ test but then drops below it for the remainder of the test period. The crossover in the 0.2% and 1% O₂ data and the relationships in the results for the four blank tests are consistent with the proposals that (1) co-fed oxygen can oxidize the catalyst *in situ* and/or hinder any *in situ* catalyst reduction that might otherwise occur and (2) catalyst oxidation state is important and can be negatively affected by co-fed oxygen even as gas-phase oxygen contributes to catalyst activity.

Table 7.1: Oxygen effect comparison; results as TOF [$\text{mol}_{\text{CH}_4 \text{ converted}} / \text{mol}_{\text{exposed Pt}}/\text{sec}$]

| Oxygen addition | Initial CH ₄ Conversion | Conversion after 14 hr |
|-----------------|------------------------------------|------------------------|
| SFC membrane | 196 | 71 |
| 2% co-fed | 93 | 19 |
| 1% co-fed | 163 | 24 |
| 0.2% co-fed | 175 | 20 |
| None | 137 | 11 |

7.4: Product Ratio Analysis for All Co-Fed Oxygen Tests

Co-fed oxygen appears to play dual and contradictory roles in a CO₂ reforming scenario with the Pt/ZrO₂ catalyst—a small amount of oxygen can be beneficial yet too much can inhibit catalyst activity. The benefit arises from the conversion of additional methane and is observed over an extended time period while the inhibiting action occurs immediately but can be compensated for somewhat over time by the tendency for higher activity with co-fed oxygen. It appears that higher oxygen levels initially decrease catalyst activity—most likely through platinum oxidation or diminished *in situ* platinum reduction—but later support methane conversion by promoting partial oxidation and combustion. However, as demonstrated with the patterned membranes in Chapter 5,

more methane conversion does not translate to improved synthesis gas production if water supplants hydrogen in the product stream. It is therefore necessary to evaluate the reaction by more than just methane conversion.

7.4.1: H₂:CO ratio

After methane conversion, the conventional next step in reforming reaction analysis is to examine the H₂:CO ratio of the products. For the collected blank tests, Figure 7.7 shows H₂:CO ratio results that largely conform to the prediction that more oxygen leads to more partial oxidation which produces higher H₂:CO ratios. With one notable exception, H₂:CO ratios in the blank tests are higher with more co-fed oxygen. The exception is the 2% O₂ case, which never reaches the level of the 1% O₂ catalyst test.

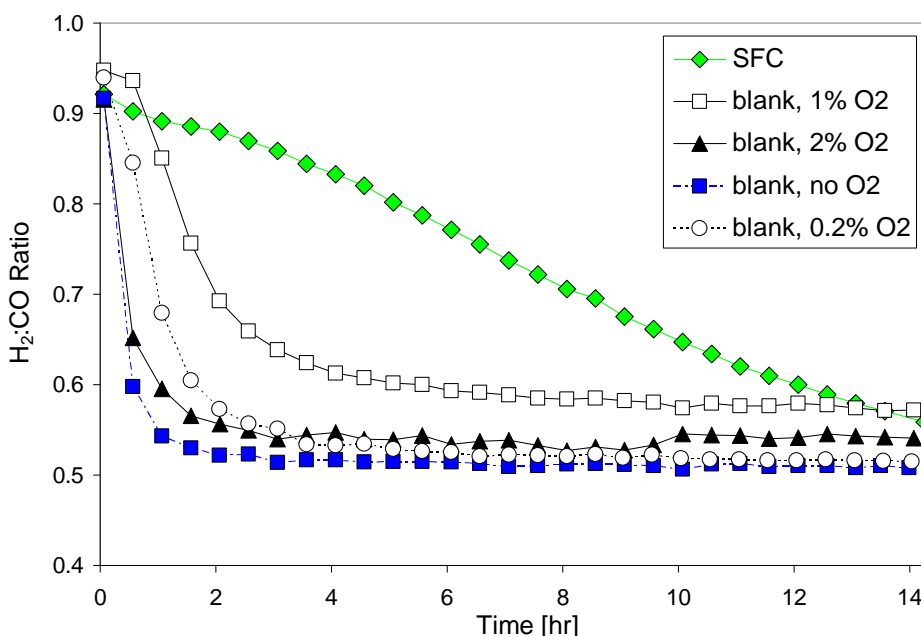


Figure 7.7: H₂:CO ratio during CO₂ reforming over a Pt/ZrO₂ catalyst in the improved QTMR. Reaction temperature=800 °C, GHSV=150 L/h/g_{cat}, CH₄:CO₂:Ar/O₂ feed ratio=4:4:2.

It is worth noting that the selective hydrogen oxidation that has been proposed for the SFC membrane should produce lower H₂:CO ratios than expected from methane conversion levels. In other words, if the selective hydrogen oxidation hypothesis is correct, the H₂:CO ratio should not be

elevated by the membrane as significantly as methane conversion is. Figures 7.6 and 7.7 uphold this prediction.

7.4.2: Relative water production

The $H_2:CO$ ratios in the 2% co-fed O_2 case are also lower than expected, and this too can be explained by the relative amount of water produced in the tests. The molar ratios of water produced to methane reacted presented in Figure 7.8 clearly indicate that substantially more water is produced in the 2% co-fed O_2 test per quantity of methane converted. Water formation directly decreases the amount of elemental hydrogen in the product stream, as H_2 and H_2O are the only two products considered in the hydrogen atom balance and therefore depend only on each other and the amount of methane reacted. Water can be formed by direct hydrogen oxidation (as is proposed for the SFC membrane tests), by the rWGS reaction, and by combustion. The amount of CO_2 conversion relative to methane conversion and the relative production of hydrogen and CO can be used to determine the relative prominence of the three water production options.

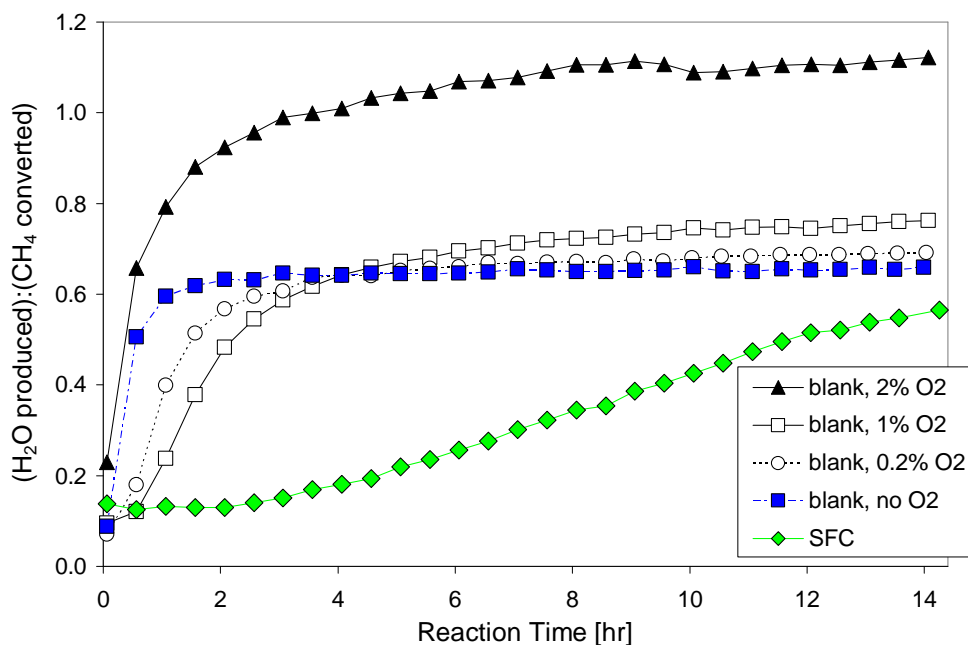


Figure 7.8: Molar ratio of water production-to- CH_4 conversion during CO_2 reforming over a Pt/ZrO₂ catalyst in the improved QTMR. Reaction temperature=800 °C, GHSV=150 L/h/g_{cat}, $CH_4:CO_2:Ar/O_2$ feed ratio=4:4:2.

Relative water production increases more dramatically over time with the SFC membrane than with the blank. By itself, this trend could be interpreted as evidence of combustion. However, combustion would not cause the simultaneous decrease in H₂:CO ratio observed in this test. Increasing relative water production with decreasing H₂:CO implies rWGS.

7.4.3: Relative CO₂ consumption

Figure 7.9 provides relative CO₂ conversion results (i.e., the molar ratio of CO₂-to-methane consumed). This ratio is lowest (and drops most dramatically) during the 2% O₂ test, for which Figure 7.8 shows disproportionately high (and gradually increasing) water production. The combination of high water production and low CO₂ conversion indicates a significant amount of combustion in the net reaction profile for this reaction. Because the 2% co-fed O₂ test also has the greatest amount of gas-phase oxygen, these results collectively support the hypothesis that the Pt/ZrO₂ catalyst could be oxidized *in situ* by gas-phase oxygen if it can be otherwise confirmed that oxidized catalyst promotes combustion over partial oxidation when co-fed O₂ is available. With no pre-reaction catalyst reduction process, exposure to 2% co-fed O₂ has a unexpected negative influence on Pt/ZrO₂ catalyst performance compared to lower amounts of co-fed O₂.

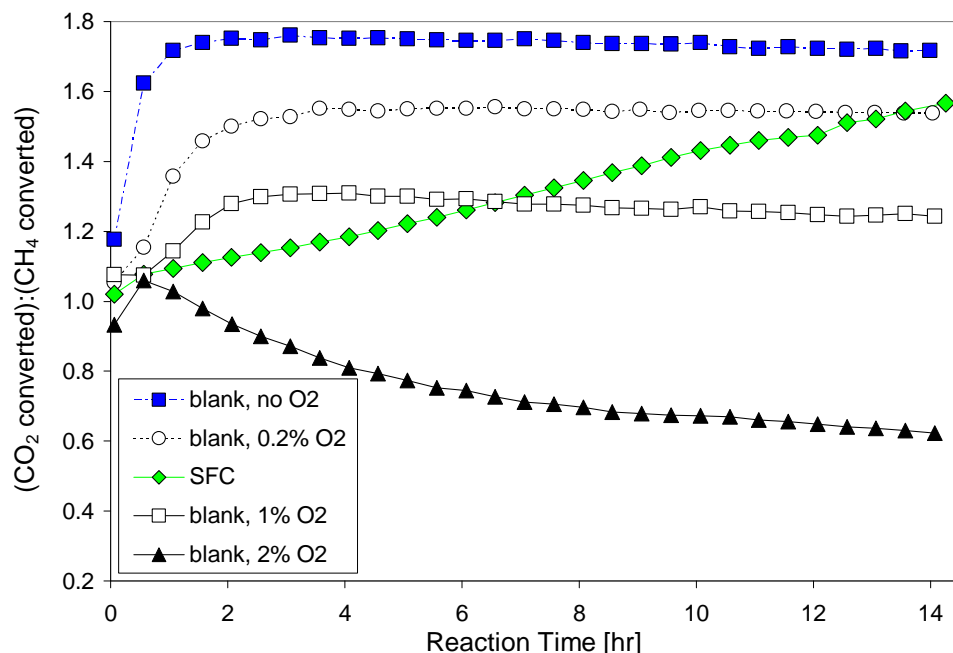


Figure 7.9: Molar $\text{CO}_2:\text{CH}_4$ conversion ratio during CO_2 reforming over a Pt/ZrO_2 catalyst in the improved QTMR. Reaction temperature= 800°C , GHSV= $150\text{ L/h/g}_{\text{cat}}$, $\text{CH}_4:\text{CO}_2:\text{Ar}/\text{O}_2$ feed ratio= $4:4:2$.

Unlike the platinum-patterned membranes on which combustion dominated and CO_2 conversion was actually negative, the powder Pt/ZrO_2 catalyst always exhibits positive CO_2 conversion, so CO_2 reforming appears to be occurring at some level throughout the powder catalyst tests. Nevertheless, relative CO_2 conversion drops over time in the presence of co-fed oxygen. If accompanied by an increase in relative water production, a trend of decreasing relative CO_2 consumption is attributed to a transition from CO_2 reforming, which consumes CO_2 , to combustion, which produces CO_2 . This is the case for the 2%, 1%, and 0.2% co-fed oxygen tests in Figures 7.8 and 7.9; the two exceptions to the increasing combustion trend are the “no oxygen” case and the SFC membrane case.

7.4.4: The blank test with no oxygen

The $\text{CO}_2:\text{CH}_4$ conversion ratio, the $(\text{H}_2\text{O production}):(\text{CH}_4\text{ conversion})$ ratio, and the $\text{H}_2:\text{CO}$ ratio show uniquely stable behavior for the “no oxygen” test (Figures 7.7, 7.8, and 7.9). All three

ratios stabilize within two to three hours of the beginning of the reaction while the methane conversion continues slowly downward for a much longer time (Figure 7.6). The conclusion from this is that the net reaction profile remains constant even as the overall methane conversion decreases over the final 80% of the test period. However, reaction profile stability is inversely related to the amount of co-fed oxygen, indicating that the presence of gas-phase oxygen under reaction conditions may affect the oxidation state of the Pt/ZrO₂ catalyst, which then affects the reaction profile. It is reasonable to assume that this effect might only be apparent because of the generally low methane conversion levels in these tests (which are intentional, as discussed in Chapter 3, and not meant to represent realistic operating conditions) and thus the relatively low ambient hydrogen levels. Regardless of the explanation, they are detectable and consistent and represent an interesting phenomenon that is not observed in reaction tests with higher catalyst loading.

7.4.5: Relative CO production

Over the latter part of the 1% and 2% co-fed O₂ tests, the (H₂O production):(CO₂ conversion) ratios change the most while the H₂:CO ratio changes the least. This reinforces the conclusion that combustion is displacing CO₂ reforming in these tests because combustion produces only water and CO₂, which would not affect the H₂:CO ratio but would affect the other two ratios of interest, including the ratio of carbon monoxide produced to methane converted (Figure 7.10). The trends in Figures 7.9 and 7.10 confirm for the blank tests that combustion is displacing some portion of the CO₂ reforming rather than some other side reaction such as rWGS.

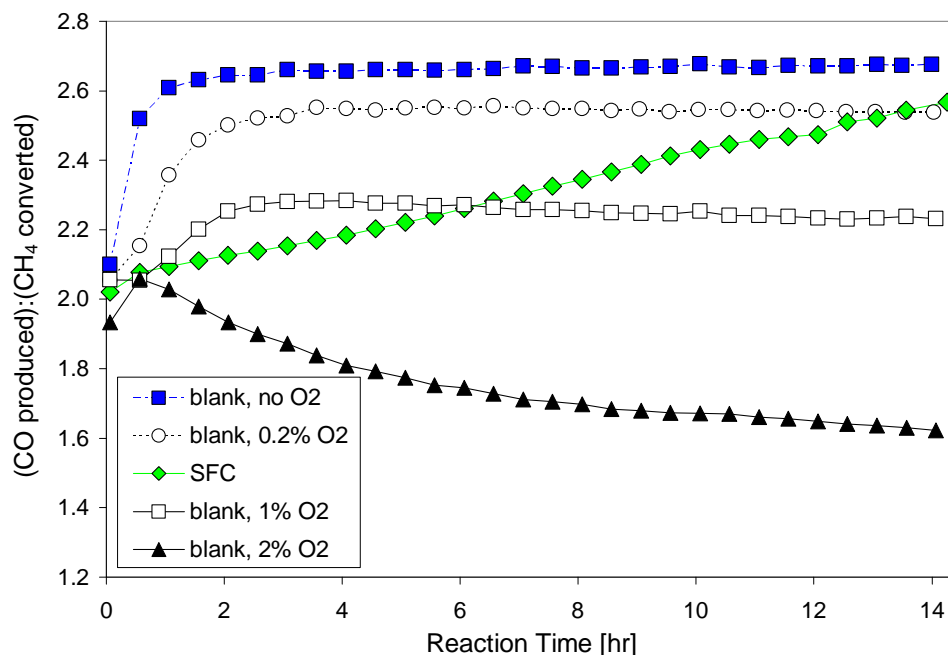


Figure 7.10: Molar ratio of CO production-to-CH₄ conversion during CO₂ reforming over a Pt/ZrO₂ catalyst in the improved QTMR. Reaction temperature=800 °C, GHSV=150 L/h/g_{cat}, CH₄:CO₂:Ar/O₂ feed ratio=4:4:2.

For the SFC membrane test, on the other hand, relative CO₂ conversion and relative CO production increase concomitantly over the reaction period along with relative water production. This appears to be evidence of rWGS. However, if the effect were predominantly a result of rWGS occurring in the powder catalyst bed, the same effect should be seen in the blank tests, particularly the blank test with no oxygen. This is not the case.

7.4.6: The SFC membrane test

The data imply that the lower relative CO₂ conversion in the blank tests with co-fed oxygen is caused by an increasing contribution from combustion rather than by increasing rWGS, particularly in the 2% co-fed O₂ test. Thus, rWGS in the catalyst bed seems unlikely to be the cause of the anomalous results from the SFC membrane test. The possibility must be entertained that there is another cause for the observed drop in H₂:CO ratio in Figure 7.7 as well as for the identical trends for CO₂ conversion and CO production (Figures 7.9 and 7.10). These trends eliminate combustion,

partial oxidation, steam reforming, and CO₂ reforming as options and point to the rWGS reaction in spite of the conclusions drawn from the blank tests. An alternative explanation may bridge the apparent contradiction.

The collective membrane test evidence indicates that selective hydrogen oxidation at the SFC membrane surface is the most likely source of the increase in relative water production, but the increase in relative CO₂ conversion must still be explained. In this SFC membrane test, the increase in CO₂ conversion and H₂O production coincide with net membrane oxygen production values equal to or less than zero (see Figure 6.7). Assuming that the membrane continues to provide oxygen to oxidize hydrogen to water, negative net oxygen production values require the conversion of CO₂ on the membrane surface. This leads to a proposed reaction combination that can be referred to as “membrane-facilitated rWGS.” In this scenario, the proposed ability of the membrane to convert CO₂ to CO after the membrane surface has been reduced by H₂ leads to an indirect version of the rWGS reaction. Hydrogen first reduces the membrane and CO₂ then replenishes the oxygen removed by hydrogen.

The net effect of this combination of membrane surface reactions is an increased tendency toward rWGS stoichiometry in the reaction products, with the resulting reduction in H₂:CO ratio. If this hypothesis is correct, the H₂:CO ratio should be lower on the SFC membrane for equivalent methane conversion than the H₂:CO ratio in the blank tests. Figure 7.11 shows that this is the case (the lines are added to improve the visibility of the trends).

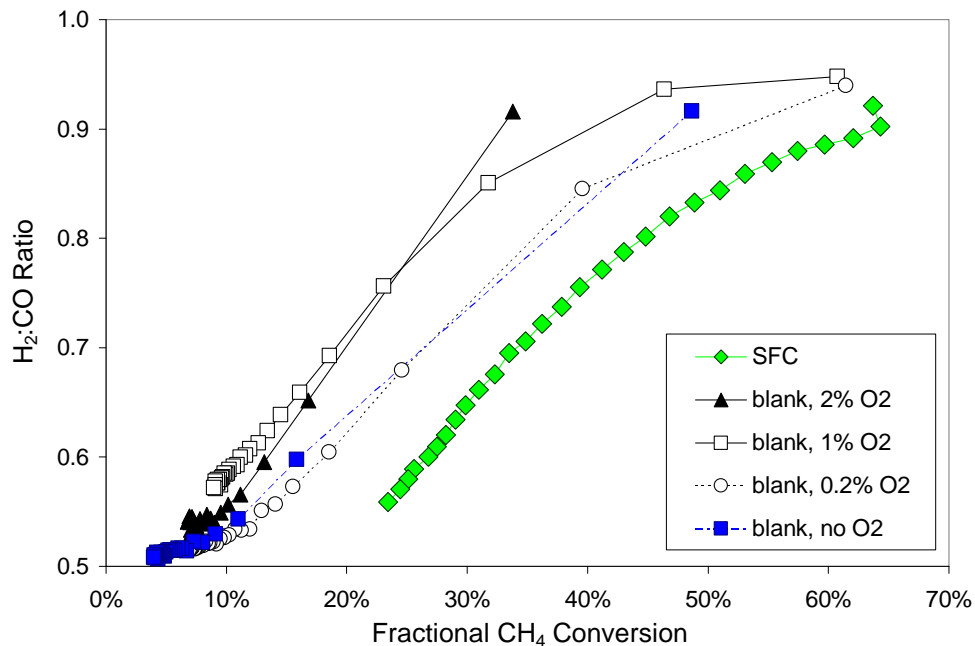


Figure 7.11: H₂:CO ratio vs. fractional CH₄ conversion during CO₂ reforming over a Pt/ZrO₂ catalyst in the improved QTMR. Reaction temperature=800 °C, GHSV=150 L/h/g_{cat}, CH₄:CO₂:Ar/O₂ feed ratio=4:4:2.

Comparing the SFC membrane results to the blank with no oxygen results in Figures 7.4 through 7.10 provides a final important observation. Although methane conversion remains substantially higher after 14 hours on the membrane than on the blank (Figure 7.6), all of the product and conversion ratios for the SFC membrane test (Figures 7.4 through 7.10) approach those of the blank with no oxygen as the membrane test progresses. The net reaction profiles for the two tests thus converge over time, which is consistent with the observation from Chapter 6 that the membrane flux also approaches zero over time. This combination indicates that the instantaneous effect of the SFC membrane diminishes substantially over time, even as the higher methane conversion values demonstrate a persistent enhancement of overall catalyst activity with the SFC membrane. In other words, the same reaction profile as with the blank with no oxygen begins to appear in the same proportions late in the membrane test but the overall activity level is much higher with the membrane than with the blank. Either the membrane has a persistent effect on the Pt/ZrO₂ catalyst even with no

apparent oxygen flux or the initial effect has persistent ramifications, such as self-sustaining higher hydrogen levels.

7.5: Equilibrium Conversions and Product Ratios

As a reference, thermodynamic equilibrium compositions were determined for each of the co-fed O₂ cases using the Thermosolver program [1]. The reaction enthalpies in Table 7.2 were calculated using the equilibrium quantities of the products and reactants and their standard enthalpies of formation at 25 °C. The guidelines described in Appendix K were used to determine the molar extent of the rWGS reaction at equilibrium, and the results were confirmed via enthalpy balance.

Table 7.2: Equilibrium data for isothermal CO₂ reforming. Reaction temperature = 800 °C; pressure = 1 atm; CH₄:CO₂:Ar/O₂ feed ratio = 4:4:2.

| Oxygen in Reaction Feed | No O₂ | 0.2% O₂ | 1% O₂ | 2% O₂ |
|--|-------------------------|---------------------------|-------------------------|-------------------------|
| CH ₄ conversion | 91.3% | 91.7% | 93.3% | 94.7% |
| H ₂ :CO ratio | 0.958 | 0.961 | 0.968 | 0.977 |
| CO ₂ :CH ₄ conversion ratio | 1.045 | 1.036 | 1.005 | 0.970 |
| Relative H ₂ O production | 0.044 | 0.047 | 0.059 | 0.075 |
| ΔH _{rxn} [kJ/mol CH ₄ converted] | 249 | 246 | 234 | 220 |
| Ratio of rWGS-to-CH ₄ converted | 4.5% | 4.7% | 5.9% | 7.6% |

In general, the theoretical equilibrium data in Table 7.2 reinforce the observations from the experimental co-fed O₂ results. The 2% co-fed O₂ case represents the only major deviation from expectations. It is worth noting again in the context of these equilibrium data that co-fed oxygen greater than 1% has a negative effect on catalyst activity and selectivity that is not predicted by the reactor feed composition and thermodynamics.

Perhaps the most interesting trend in Table 7.2 is the increase in relative rWGS activity with increasing O₂. This provides thermodynamic support to the previously discussed idea that oxygen increases the extent of rWGS in combined reforming and oxygen-assisted CO₂ reforming scenarios.

7.6: Product Ratio Analysis for All SFC Membrane Tests

As in Chapter 6, the SFC membrane results are analyzed together for convenient comparison, including the original 700 °C SSMR test. As a starting point, Figure 7.12 provides an overview of methane conversion presented as turnover frequencies. *NOTE: the blank with no oxygen and the blank with 2% O₂ tests are included as references.*

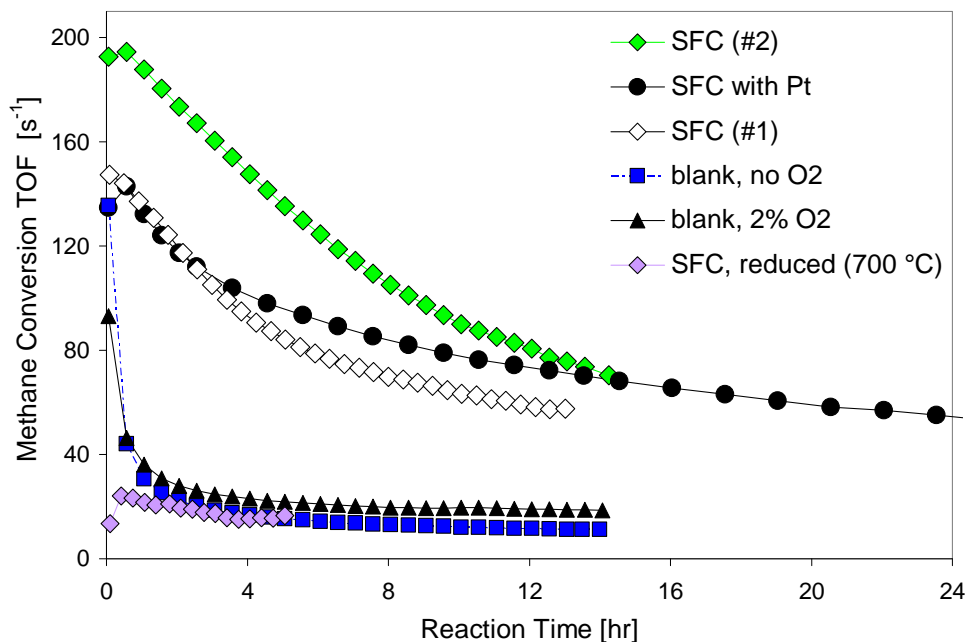


Figure 7.12: CH₄ conversion turnover frequency (TOF) during CO₂ reforming over a Pt/ZrO₂ catalyst in both QTMRs. Reaction temperature=800 °C, GHSV=150 L/h/g_{cat}, CH₄:CO₂:Ar/O₂ feed ratio=4:4:2.

The low TOFs for the 700 °C SSMR test are easily explained by the reaction temperature. The difference in quasi-steady state conversion is perfectly consistent with the kinetic parameter prediction discussed in Chapter 5. A 100 °C difference should give a four-fold difference in reaction rates, as depicted in Figure 7.12.

7.6.1: Relative CO₂ conversion

The initial membrane test (700 °C in the SSMR) showed a decreasing relative CO₂ conversion trend and increasing relative water production trend, as did the co-fed oxygen blank tests

in Figures 7.8 and 7.9. This combination indicates combustion. Oppositely, the later QTMR membrane tests exhibited increasing relative CO₂ conversion with decreasing relative water production, which indicates rWGS. This difference can be explained by the much larger leaks experienced by the initial SSMR tests. In Figure 7.13, the higher CO₂ conversion late in the SFC (#1) membrane test coincides with lower (i.e., more negative) oxygen production from this membrane.

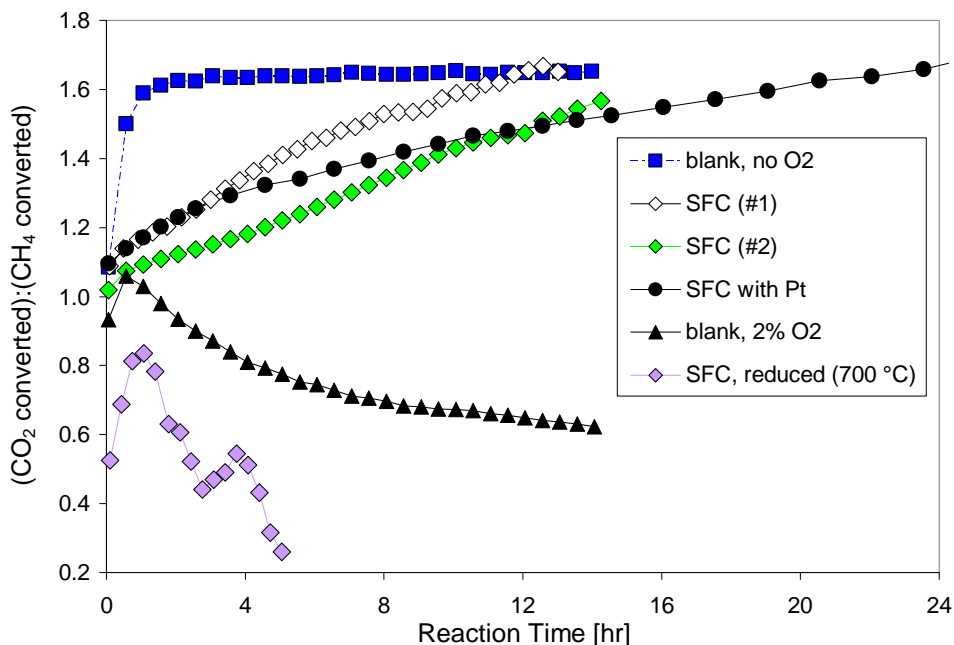


Figure 7.13: Molar CO₂:CH₄ conversion ratio during CO₂ reforming over a Pt/ZrO₂ catalyst in both QTMRs. Reaction temperature=800 °C, GHSV=150 L/h/g_{cat}, CH₄:CO₂:Ar/O₂ feed ratio=4:4:2.

In the 700 °C SSMR test, the air leak was more than 5% of the feed rate compared to ~0.05% of feed in the QTMR tests. Because of the larger total amount of available oxygen in the 700 °C membrane test (membrane oxygen plus at least 1% gas-phase O₂), the Pt/ZrO₂ catalyst should have performed in the SSMR more like it does in a 1% or 2% co-fed oxygen test than in a QTMR membrane test. Figure 7.13 shows that this is the case for CO₂ conversion.

7.6.2: Relative water production

In addition to the gas-phase oxygen present in the 700 °C SSMR test, thermodynamics also makes a major contribution to the greater relative amount of combustion: in increasing the reaction

temperature from 700 °C to 800 °C, the equilibrium constant for CO₂ reforming increases by a factor of twenty (from 7.7 to 153) and the equilibrium constant for combustion decreases by four orders of magnitude (from 7.6x10⁴² to 7.5x10³⁸) [1]. Predictably then, the 700 °C membrane test also exhibits greater relative water production than any of the other tests (Figure 7.14). The combination of low CO₂ conversion and high water production make it clear that the 700 °C SSMR test with the high leak produces a significant amount of combustion. *NOTE: Figures N.1 and N.2 in Appendix N depict equilibrium constants vs. temperature for the reactions of interest between 550 °C and 850 °C.*

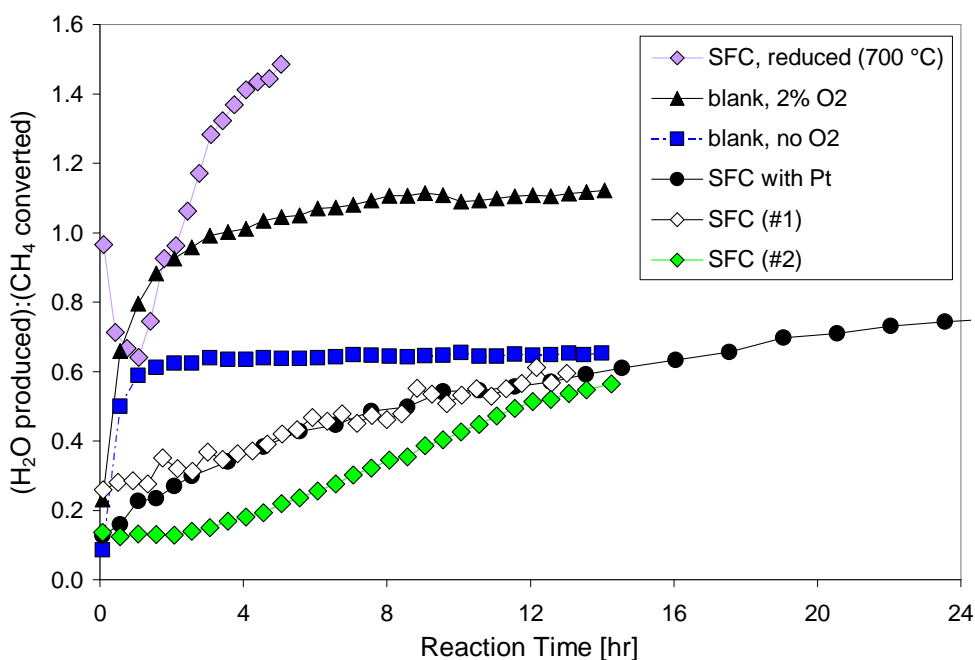


Figure 7.14: Molar ratio of water production-to-CH₄ conversion during CO₂ reforming over a Pt/ZrO₂ catalyst in both QTMRs. Reaction temperature=800 °C, GHSV=150 L/h/g_{cat}, CH₄:CO₂:Ar/O₂ feed ratio=4:4:2.

On the other hand, relative water production and CO₂ conversion in the three QTMR SFC membrane tests start low and then approach the level of the “no oxygen” test by moving in the direction of increasing rWGS (or “membrane-facilitated rWGS”). Although relative water production extends above the blank control for only one of the QTMR SFC membrane tests, it appears that all three would match or exceed the level for the no oxygen test if allowed more reaction time.

7.7: Post-Reaction Carbon Analysis

For the later tests with the QTMR, catalyst beds are cooled under flowing argon after reaction to preserve the final catalyst state as much as possible. After removal from the membrane reactor, used catalyst samples can then be transferred to a quartz tube reactor for carbon oxidation testing. The tubular reactor, which contains only a quartz wool pad to support the catalyst sample, is heated to 800 °C and the sample is then exposed to small pulses of oxygen (50 µl each) in an argon sweep gas to oxidize any carbon deposits. Mass spectrometer data are integrated to estimate the amount of CO₂ and CO produced, and these estimates are then used to approximate the amount of carbon deposited on the catalyst. The small quantities of spent catalyst add a degree of difficulty to this controlled oxidation procedure, but the ability to inject small and discrete amounts of oxygen and to monitor very small changes in gas stream composition permit the acquisition of usable results.

Although the amount of carbon is negligible from a reactor mass balance perspective (never greater than 0.0003% of the total carbon fed), it might have an effect on catalyst activity. The absence of any clear trends between catalyst activity and post-reaction carbon removal discourages speculation as to the effect of deposited carbon. However, the effect of net oxygen on catalyst carbon accumulation is more conclusive. Net oxygen is the time-averaged sum of the leaked oxygen and the co-fed or membrane oxygen over the duration of the test.

As Figure 7.15 demonstrates, relative carbon accumulation on powder catalyst on the stainless steel blank appears to trend nicely with the total amount of oxygen present during the test. Because test duration is not constant among the tests, the carbon accumulation ratio is calculated by dividing the moles of carbon removed by the net moles of methane converted over the duration of the test. Net methane converted and net oxygen available are each calculated by summing the estimates from each GC data point over the subsequent time interval. The individual values in the sum are

obtained by multiplying the current mole fractions of methane converted and total oxygen available by the current molar flowrate and the elapsed time between the previous and current GC data points.

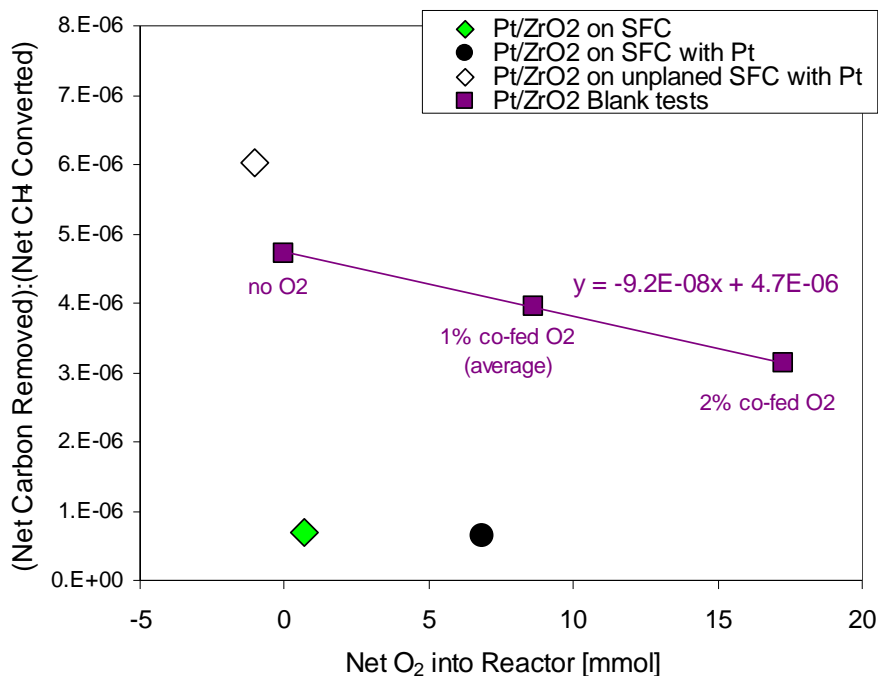


Figure 7.15: Molar ratio of net carbon removed-to-net CH₄ converted from Pt/ZrO₂ catalyst following CO₂ reforming in the improved QTMR. Obtained by oxidation at 800 °C using 500 µl injections of 10% O₂/Ar into Ar at 20 ccm.

Carbon accumulation with the SFC membrane also depends on net oxygen availability, although less continuously than with the blank. The “SFC with Pt” test received ten times more net oxygen from its membrane than the “SFC” test and approximately 6% less carbon was oxidized from its catalyst. On the other hand, the “unplaned SFC with Pt” test exhibited a net negative oxygen flux over its duration and its catalyst yielded almost nine times the amount of carbon as the “SFC” test. Net negative flux means the membrane took in more oxygen than it produced. One conclusion that can be drawn from this is that net membrane oxygen affects the amount of catalyst coking. A more speculative interpretation is that CO₂ reduction on the membrane (which is believed to be the source of the negative flux estimates) is related to carbon deposition on the powder catalyst in addition to CO production on the membrane. In any case, it can be concluded as a general rule that carbon

deposition occurs in inverse proportion to the amount of oxygen available throughout the reaction, whether the oxygen is co-fed or membrane oxygen.

7.8: Observations and Conclusions from Chapter 7

- (1) Catalyst oxidation state is an important predictive factor for Pt/ZrO₂ catalyst activity and deactivation rate. It appears to be influenced by co-fed gas-phase oxygen
- (2) *In situ* catalyst oxidation appears likely with a combination of co-fed oxygen and low methane conversion such as observed with the unreduced Pt/ZrO₂ catalyst.
- (3) Oxidized Pt/ZrO₂ catalyst is more likely to cause combustion in the presence of gas-phase O₂ than fresh or reduced catalyst.
- (4) Zero (or negative) net membrane oxygen flux in conjunction with high methane conversion activity could indicate a reaction set on the SFC surface that is analogous to rWGS. This will be referred to herein as “membrane-facilitated reverse Water-Gas Shift.”
- (5) Over time on stream, the net reaction profile on the SFC membrane approaches that of the blank test with no oxygen, but the overall activity remains substantially higher than in the no oxygen test.
- (6) Carbon deposition was generally low in all tests as a fraction of methane converted and was very low in SFC membrane tests with net positive oxygen flux. A net negative oxygen flux test showed the largest relative amount of carbon deposition
- (7) Carbon deposition on the Pt/ZrO₂ catalyst in the blank tests was found to be inversely proportional to the amount of co-fed oxygen in the feed.

References Cited in Chapter 7

1. Barnes, C. and M. Koretsky, *Thermosolver*, 1.0 (2003), John Wiley & Sons, Inc.

Chapter 8: The Effect of Catalyst Oxidation State

The novel approach to evaluating reaction profiles under CO₂ reforming conditions using various mole ratios of reactant and products is explored and expanded upon, culminating in a single selectivity parameter for oxygen-assisted CO₂ reforming or combined reforming: the Oxidation Factor. The Oxidation Factor is intended to provide a simple way to distinguish between desirable (i.e., CO₂ reforming) and undesirable (i.e., hydrogen oxidation, carbon monoxide oxidation, and methane combustion) catalyst activity to facilitate the investigation of potential modes of catalyst activity with the SFC membrane and the determination of the causes of Pt/ZrO₂ catalyst activity degradation.

In addition to additional testing in the QTMR, a conventional plug-flow reactor (PFR) is used to provide baseline performance results for the Pt/ZrO₂ catalyst. In particular, the PFR is used to evaluate the effect of different pre-reaction conditions on catalyst activity, including both reduction and pre-reaction oxygen exposure.

8.1: Catalyst Pretreatment Tests in the QTMR

The diminished activity in the 2% co-fed O₂ blank test and the increased activity with similar initial quantities of membrane oxygen leads to the suggestions that gas-phase oxygen can inhibit *in situ* catalyst reduction while the SFC membrane somehow facilitates *in situ* reduction or, conversely, that gas-phase oxygen in a CO₂ reforming environment can oxidize catalytic metal particles over time while membrane oxygen does not. As presented earlier, a reasonable conjecture from these complementary suggestions is the largely overlooked idea that membrane oxygen does not evolve into the gas phase under reaction conditions and thus allows the catalyst to maintain a higher activity level than if it were continually exposed to gas-phase co-fed oxygen. Additional tests were conducted to explore the *in situ* reduction/oxidation hypothesis.

8.1.1: Catalyst reduction prior to loading

First, CO₂ reforming was performed using a portion of Pt/ZrO₂ catalyst that had been reduced prior to loading into the membrane reactor. The catalyst was heated in a quartz tube PFR to 400 °C under flowing hydrogen and held for one hour then cooled to room temperature in argon. At room temperature, it was removed from the PFR and loaded into the membrane reactor on the stainless steel blank where it was heated to 800 °C in argon (along with the inevitable leaked air) and then used for CO₂ reforming with a feed containing 1% co-fed O₂. As Figure 8.1 depicts, this pre-reduction step does not have a beneficial effect on either the initial or final catalyst activity in the membrane reactor. Exposure to leaked air during pre-heating in the membrane reactor clearly reverses any benefits of preliminary catalyst reduction. Given that the catalyst in the 1% co-fed O₂ test without pre-reduction was exposed to similar oxygen levels during temperature ramp-up, it even appears that pre-reduction decreases catalyst activity slightly.

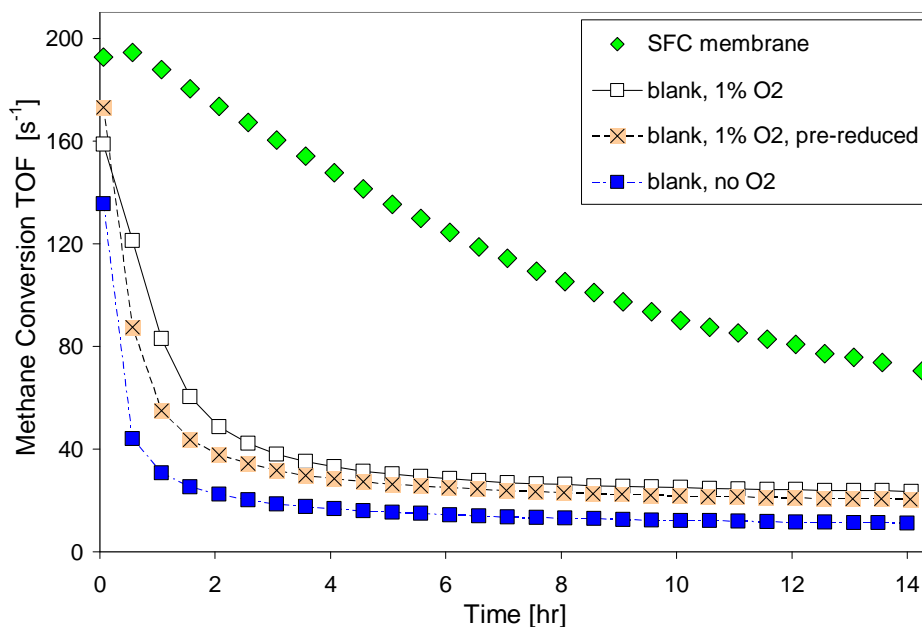


Figure 8.1: CH₄ conversion turnover frequency (TOF) during CO₂ reforming over a Pt/ZrO₂ catalyst in the improved QTMR. Reaction temperature=800 °C, GHSV=150 L/h/g_{cat}, CH₄:CO₂:Ar/O₂ feed ratio=4:4:2.

Figure 8.1 discourages the option of reducing catalyst prior to loading into the membrane reactor. It also lends support to the idea of *in situ* reduction during CO₂ reforming in catalyst beds on an SFC membrane. The catalyst beds in all SFC membrane tests are exposed to similar quantities of leaked oxygen during heat-up yet still exhibit higher activity than either of the 1% O₂ blank tests. The relatively low (and occasionally negative) amount of oxygen provided by the membrane therefore cannot account for the increase in activity on the SFC membrane. Something else must be responsible for the higher activity on the membrane, and the only compelling possibility is an improvement in the condition of the catalyst. This improvement could arise from one or more of the following three possibilities for catalyst on the membrane: 1) smaller platinum particles (i.e., less sintering and higher platinum surface area), 2) less carbon deposition, and/or 3) less oxidation of the platinum particles. The possibility that *in situ* reduction somehow occurs during the early stages of CO₂ reforming in the membrane reactor was tested next.

8.1.2: Pre-reaction catalyst reduction

In general, it was decided that catalyst reduction over the SFC membrane at temperatures above 400 °C could be an undesirable option because of the affinity of the membrane material for hydrogen and the resulting high rates of water production and accompanying membrane surface phase changes. However, it is possible to conduct a high-temperature catalyst reduction step with the stainless steel blank with no undue consequences. In the test depicted in Figure 8.2, hydrogen (5 % by volume) is added to the pre-reaction argon feed for 15 minutes immediately prior to the introduction of the reactant gases. A short argon flush period is used to minimize residual hydrogen and then the reaction feed is started with 0.2% co-fed O₂. This test exhibits an immediate and persistent increase in methane conversion levels relative to the unreduced test with 0.2% co-fed O₂ and all other blank tests.

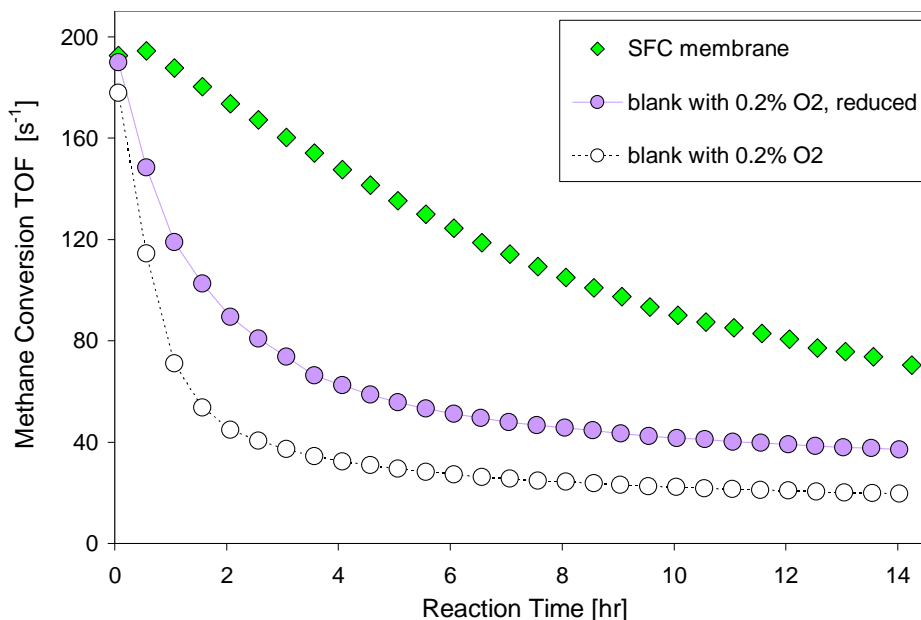


Figure 8.2: CH₄ conversion turnover frequency (TOF) during CO₂ reforming over a Pt/ZrO₂ catalyst in the improved QTMR. Reaction temperature=800 °C, GHSV=150 L/h/g_{cat}, CH₄:CO₂:Ar/O₂ feed ratio=4:4:2.

Although the effect is less dramatic than that of the SFC membrane, this brief initial reduction improved catalyst performance in a similar manner to the ceramic membrane by increasing both the initial and the longer-term activity of the catalyst. Since the proposed *in situ* effect of the SFC membrane would entail a more sustained exposure to an oxygen-free hydrogen-containing environment than the pre-reaction hydrogen exposure test presented in Figure 8.2, the membrane effect should be more protracted than that of a brief initial reduction. The methane conversion data for the SFC membrane exhibit just such a trend, with the maximum conversion not occurring until a short time into the reaction and the maintenance of even higher conversion over the duration of these tests. Both of these effects are consistent with the suggested idea of *in situ* reduction in the early portion of the reaction test: early methane conversion should decrease less quickly if catalyst reduction is ongoing, and an extended reducing period should lead to higher methane conversion over the duration of the test.

8.1.3: Water production and CO₂ conversion

In the absence of significant solid state interactions between the membrane and the Pt/ZrO₂ catalyst, the higher sustained conversion with the SFC membrane in Figure 8.2 indicates improved catalyst activity because of either a different gas-phase environment or a more reduced/less oxidized catalyst bed or both. To help evaluate these options, Figures 8.3 and 8.4 overlay results from the catalyst pretreatment tests and from the two most recent SFC membrane tests.

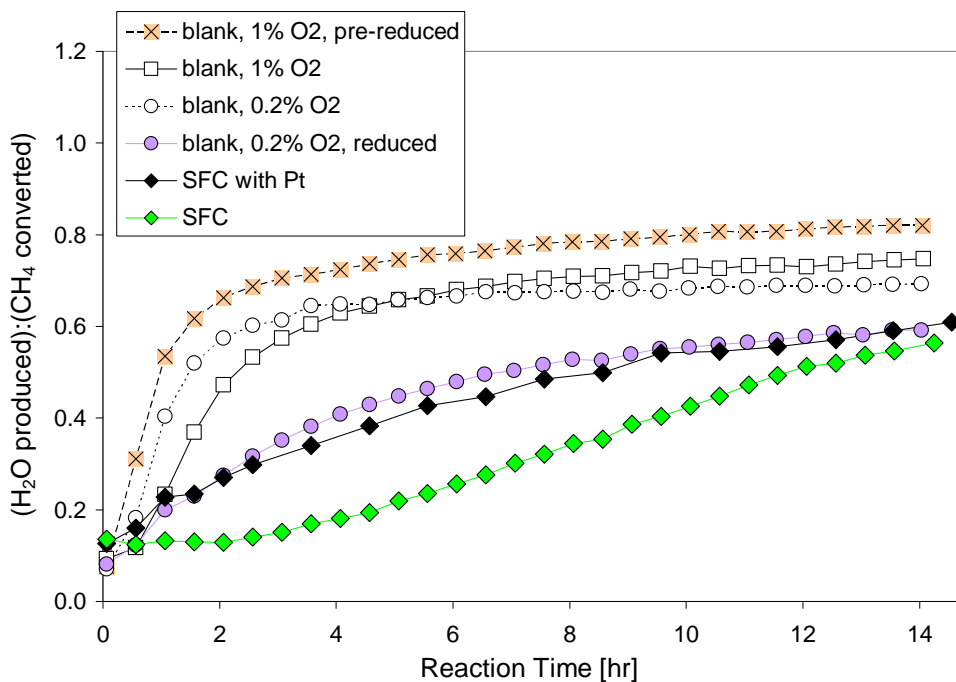


Figure 8.3: Molar ratio of water production-to-CH₄ conversion during CO₂ reforming over a Pt/ZrO₂ catalyst in the improved QTMR. Reaction temperature=800 °C, GHSV=150 L/h/g_{cat}, CH₄:CO₂:Ar/O₂ feed ratio=4:4:2.

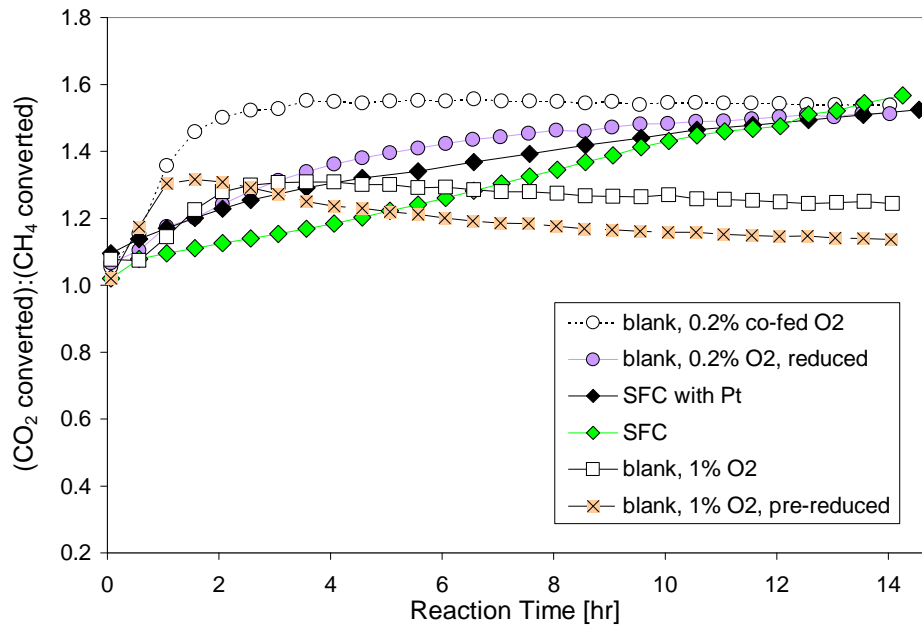


Figure 8.4: Molar CO_2 : CH_4 conversion ratio during CO_2 reforming over a Pt/ ZrO_2 catalyst in the improved QTMR. Reaction temperature= $800\text{ }^\circ\text{C}$, GHSV= $150\text{ L/h/g}_{\text{cat}}$, CH_4 : CO_2 :Ar/ O_2 feed ratio= $4:4:2$.

In general, Figures 8.3 and 8.4 show that water production increases and CO_2 conversion decreases with increasing oxygen into the reactor, regardless of its source. The one exception is the blank test with reduced catalyst and 0.2% oxygen, which produces by the least water relative to methane conversion among the blank reaction tests by a significant margin. The two SFC membrane tests show similar relative CO_2 conversion levels, but plain membrane shows markedly less relative water production, indicating the possibility of more steam reforming in that test. The pre-reduced catalyst test, on the other hand, exhibits the most evidence of combustion.

8.1.4: H_2 :CO ratio

The H_2 :CO ratio responds likewise over the reaction period. In Figure 8.5, the plain SFC membrane exhibits the highest values overall, which reinforces the possibility of the greatest amount of steam reforming in the catalyst bed. The reduced catalyst bed with 0.2% oxygen performs best among the blank tests, confirming the value of reduction as a means of producing a more desirable reaction profile in addition to more activity overall.

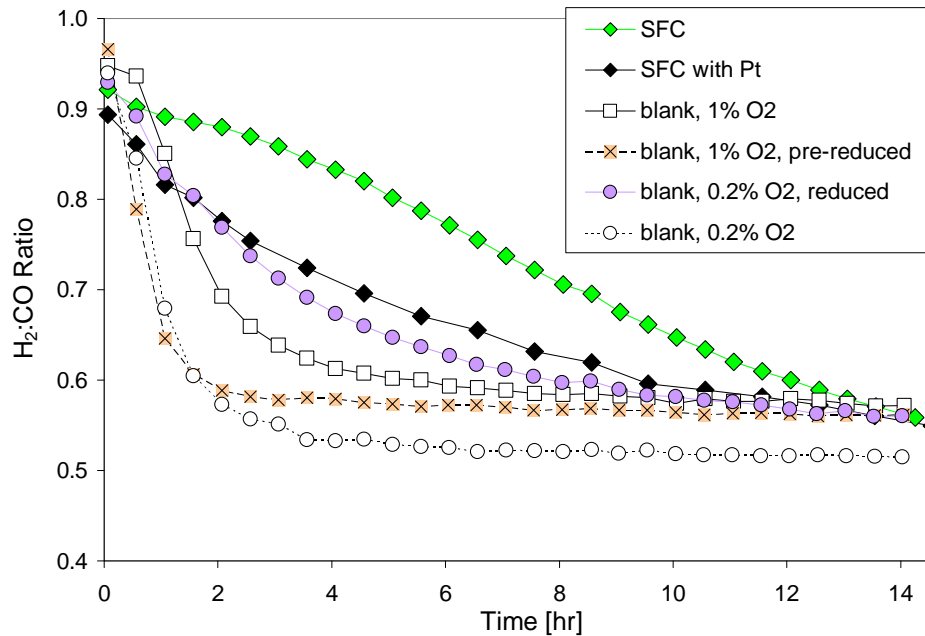


Figure 8.5: H₂:CO ratio during CO₂ reforming over a Pt/ZrO₂ catalyst in the improved QTMR. Reaction temperature=800 °C, GHSV=150 L/h/g_{cat}, CH₄:CO₂:Ar/O₂ feed ratio=4:4:2.

It is worth noting that by the end of the 14-hour reaction period, the H₂:CO ratio for both SFC membrane tests is still decreasing with the apparent potential to get lower than the majority of the blank tests. Nevertheless, methane conversion remains high in the membrane tests compared to all of the blank tests, including the 0.2% O₂ with reduction test, even as the H₂:CO ratios of the membrane tests drop steadily below those of the comparable blank tests. Other than the 0.2% O₂ with reduction test, the ratios for the blank tests have all reached steady state by the end of the reaction period.

There is an interesting combination of differences between the relative water production and relative CO₂ conversion results for the two blank tests with 0.2% O₂. The unreduced test shows significantly more CO₂ conversion and more water production, indicating rWGS rather than combustion. The H₂:CO results confirm this. However, the water production discrepancy is disproportionately higher than the CO₂ conversion discrepancy and the reduced test approaches the unreduced value more slowly. It appears that the unreduced catalyst with 0.2% O₂ exhibits both

rWGS and some combustion or other complete product oxidation, while the reduced catalyst exhibits mostly rWGS.

8.1.5: Methane conversion

Although they have distinct differences in methane conversion (Figure 8.6), the 0.2% O₂ with reduction test and the platinum-coated SFC test show remarkably similar product profiles (i.e., similar reaction profiles). The reactions appear to have occurred in the same proportions but the platinum-coated membrane caused more of them to occur. The platinum-coated SFC test also exhibited the only consistent oxygen production values among the membrane tests (equivalent to 0.4% co-fed O₂ at steady state). It therefore may be truly more comparable with the co-fed oxygen tests which use a constant oxygen feed. If so, the similarities between the platinum-coated SFC test and the 0.2% O₂ with reduction test imply that the SFC membrane allows *in situ* catalyst reduction to occur early in the reaction period. This conclusion is accompanied by the earlier conclusions that reduced catalyst converts methane more effectively with less combustion and less rWGS than unreduced catalyst.

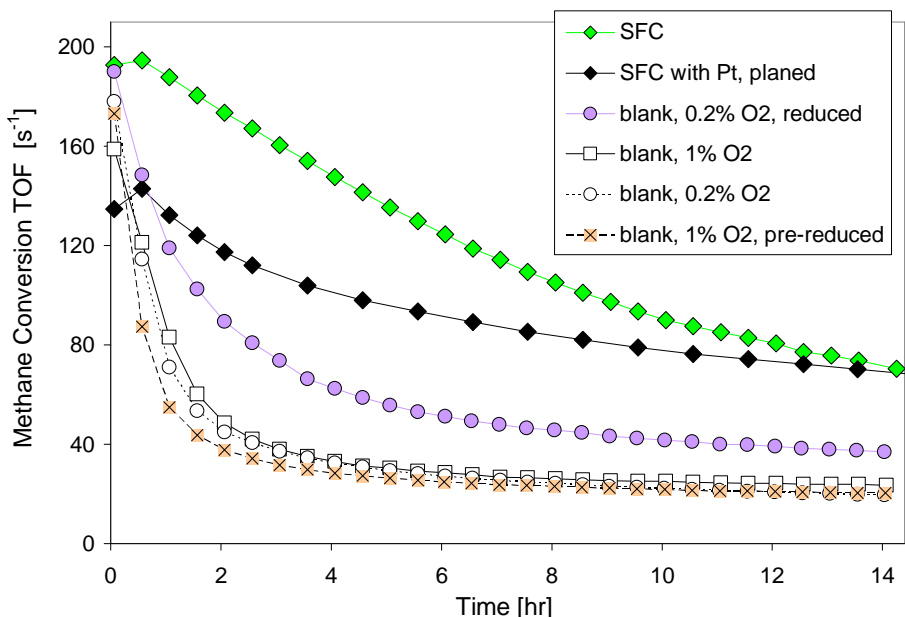


Figure 8.6: CH₄ conversion turnover frequency (TOF) during CO₂ reforming over a Pt/ZrO₂ catalyst in the improved QTMR. Reaction temperature=800 °C, GHSV=150 L/h/g_{cat}, CH₄:CO₂:Ar/O₂ feed ratio=4:4:2.

In general, the biggest distinctions between membrane and blank tests appear in the methane conversion results (Figure 8.6), with less dramatic differences in the metrics that indicate reaction profile (e.g., Figures 8.3 through 8.5). By bridging the gap somewhat for every metric, the 0.2% O₂ with reduction test provides valuable insight into the potential effect of the SFC membrane on the Pt/ZrO₂ catalyst.

8.2: Assessing Reaction Selectivity: the Oxidation Factor

8.2.1: Defining a selectivity expression

To help distinguish reaction data by the relative amounts of undesirable oxidation reactions versus CO₂ reforming, a dimensionless selectivity parameter, the “Oxidation Factor,” has been defined. This factor represents the relative quantities of reaction products from CO₂ reforming and from undesirable oxidation reactions (i.e., CO and H₂ oxidation individually and combustion, which is simply a combination of the first two). Although rWGS is not desirable in CO₂ reforming because of its negative effect on H₂:CO ratio, in the context of this analysis it is not considered an “undesirable oxidation reaction” because CO₂ is reduced to CO as H₂ is oxidized to water. It therefore causes no net gain in the undesirable oxidation products, water and CO₂.

The larger the Oxidation Factor, the greater the extent of undesirable oxidation reactions in the reaction mix. It is defined as

$$\text{Oxidation Factor} = \frac{\left[\left(\text{CO}_2 \text{ produced} \right) \cdot \left(\text{H}_2\text{O produced} \right) \right]}{\left[\left(\text{H}_2 \text{ produced} \right) \cdot \left(\text{CO produced} \right) \right]} \quad \text{Equation 8.1}$$

Assessing CO₂ production is complicated by the fact that CO₂ is both produced and consumed. CO₂ produced by combustion equals methane consumed by combustion, but CO₂ is also consumed by CO₂ reforming on a one-to-one basis with methane. The portion of methane conversion

accounted for by combustion in a binary reaction set of CO₂ reforming and combustion is therefore half the difference between net methane conversion and net CO₂ conversion. The factor of 0.5 was omitted from the selectivity expression for simplicity. However, the H₂:CO ratio was included as a multiplier for net CO₂ conversion because side reactions—other than combustion—that decrease CO₂ conversion also increase H₂:CO ratio, and vice-versa. According to these decisions, the expression for Oxidation Factor (OF) in terms of moles of species consumed and produced can be written

$$OF = \left[(CH_4 \text{ conversion}) - (CO_2 \text{ conversion}) \cdot \left(\frac{H_2}{CO} \right)^x \right] \cdot \left(\frac{H_2O}{CO \cdot H_2} \right) \quad \text{Equation 8.2}$$

where the first factor (in square brackets) is intended to scale with moles of CO₂ produced by combustion (or stand-alone CO oxidation) but not necessarily to reflect it exactly.

Finally, all factors can be expressed relative to CH₄ conversion by dividing numerator and denominator by the molar CH₄ conversion:

$$OF = \left[1 - (\text{relative } CO_2 \text{ conversion}) \cdot \left(\frac{H_2}{CO} \right)^x \right] \cdot \left[\frac{(\text{relative } H_2O)}{(\text{relative } CO) \cdot (\text{relative } H_2)} \right] \quad \text{Equation 8.3}$$

The utility of using the H₂:CO ratio to modulate the net CO₂ conversion term can be demonstrated using reverse Water-Gas Shift as an example. All analyses have indicated that rWGS is the most significant side reaction in many of these tests, whether in the catalyst bed or because of “membrane-facilitated rWGS” as discussed earlier. RWGS can mask combustion because it increases relative CO₂ conversion. However, it also decreases the H₂:CO ratio. Including the H₂:CO ratio as a multiplier of the net CO₂ conversion term thus diminishes the impact of rWGS on the Oxidation Factor. *NOTE: The exponent “x” has been added to the H₂:CO ratio to allow optimization of the selectivity expression by fine tuning the effect of the H₂:CO multiplier. Appendix G discusses the Oxidation Factor expression optimization as well as the effect of side reactions including rWGS on the Oxidation Factor.*

In its assigned position, the H₂:CO ratio also acts to mitigate the false evidence of combustion that would result from partial oxidation, steam reforming, and Water-Gas Shift. These three reactions all decrease net CO₂ consumption relative to methane consumption which the Oxidation Factor expression would interpret as greater CO₂ production and thus a larger combustion proportion. However, because these reactions also increase the theoretical H₂:CO ratio—which would equal one if CO₂ reforming were the only reforming reaction—using the H₂:CO ratio as a multiplier counterbalances to some extent the reduction in net CO₂ consumption that would otherwise be attributed to combustion. As described above, the H₂:CO factor performs the same service in the other direction for rWGS because rWGS simultaneously increases CO₂ conversion and decreases H₂:CO ratio.

8.2.2: Oxidation Factor range and values

The ideal reaction set for this CO₂ reforming Oxidation Factor would include only CO₂ reforming and combustion and would produce an H₂:CO ratio of one. Pure CO₂ reforming would give a Oxidation Factor of zero because molar CO₂ conversion would equal CH₄ conversion and the H₂:CO ratio would be one, while a 50:50 mix of combustion and CO₂ reforming gives a theoretical Oxidation Factor of one. Pure combustion produces no hydrogen or CO and therefore yields an undefined Oxidation Factor because the denominator is zero and the numerator is undefined, but 99% combustion with no rWGS produces a theoretical Oxidation Factor of 9,801.

This work only involves the low end of the Oxidation Factor scale because all testing was done with relatively small amounts of oxygen and an equimolar CO₂:CH₄ feed. To provide an idea of maximum expected values for the Oxidation Factor, Figure 8.7 provides theoretical values calculated from reaction stoichiometry across the 0 – 40% combustion proportion range. The figure includes a black curve for the binary reaction set of CO₂ reforming and combustion only (i.e., no rWGS and thus an H₂:CO ratio of one) and a pink curve for a reaction set that includes a fixed proportion of rWGS

relative to methane conversion. It also includes an optimized value for the exponent, x , on the $H_2:CO$ ratio in the Oxidation Factor expression (Equation 8.3). Details on the selection of the rWGS proportion and the $H_2:CO$ ratio exponent are provided in Appendix G.

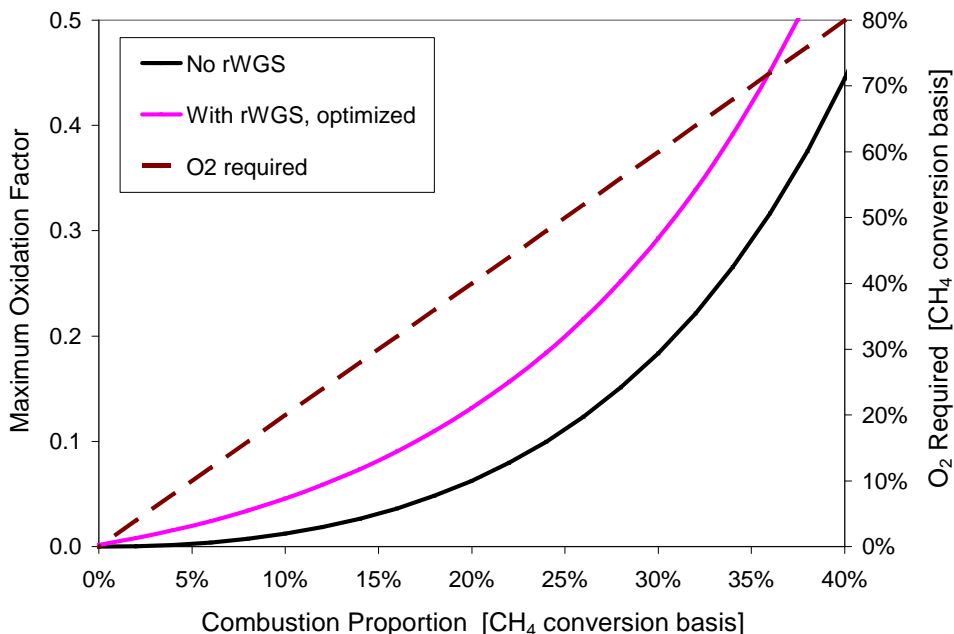


Figure 8.7: Theoretical maximum Oxidation Factor and required O_2 vs. combustion proportion (as % of CH_4 conversion) with and without concurrent rWGS at 65% of CH_4 conversion

The second y-axis in Figure 8.7 (“ O_2 Required”) provides the amount of molecular oxygen needed to produce the amount of combustion indicated on the x-axis. Combustion proportion and required oxygen are both presented as percentages of net methane conversion. For example, a combustion proportion of 40% means 40% of the methane converted was converted by combustion, with the remaining 60% converted by CO_2 reforming. A 40% combustion proportion thus requires a molar amount of oxygen equal to 80% of the net molar methane converted.

8.2.3: Evaluating the Oxidation Factor

Figure 8.8 illustrates the distinguishing capability of the optimized Oxidation Factor, and Figure 8.9 provides the same data but on a finer scale to highlight the differences between the tests with lower Oxidation Factors. The blank tests without catalyst pretreatment align as would be

predicted while the two blank tests with pretreatment (reduced with 0.2% co-fed O₂ and pre-reduced with 1% co-fed O₂) show a clear distinction between their un-pretreated counterparts. The reduced catalyst with 0.2% co-fed O₂ test exhibits the least undesirable oxidation of any co-fed oxygen test, but the pre-reduced catalyst with 1% co-fed O₂ shows significantly more product oxidation than the unreduced catalyst with 1% co-fed O₂. In addition to its dramatically higher methane conversion, the SFC membrane test is distinguished favorably from the blank tests by its consistently low Oxidation Factor.

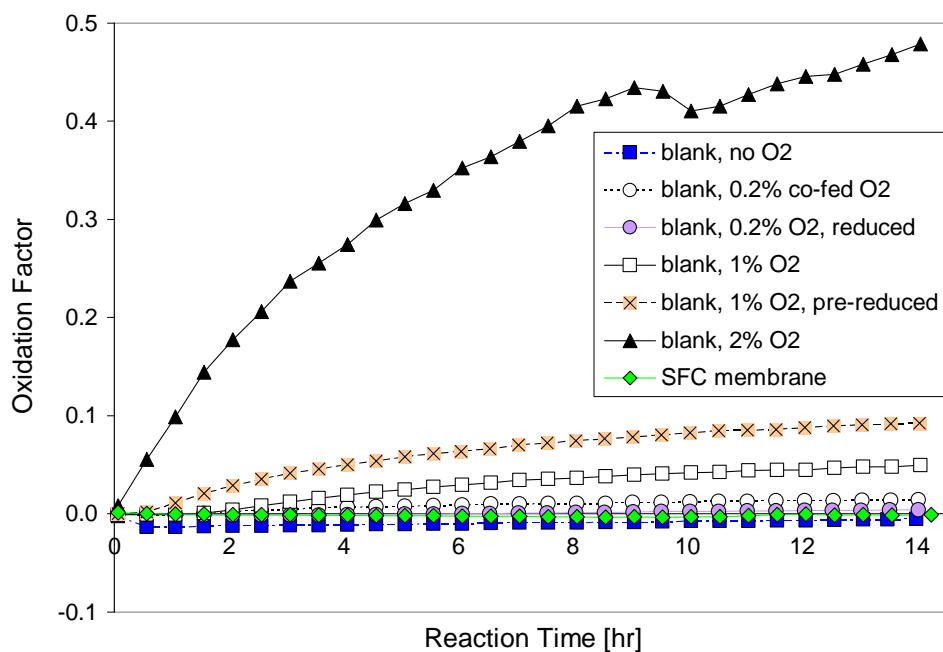


Figure 8.8: Oxidation Factor during CO₂ reforming over a Pt/ZrO₂ catalyst in the improved QTMR. Reaction temperature=800 °C, GHSV=150 L/h/g_{cat}, CH₄:CO₂:Ar/O₂ feed ratio=4:4:2.

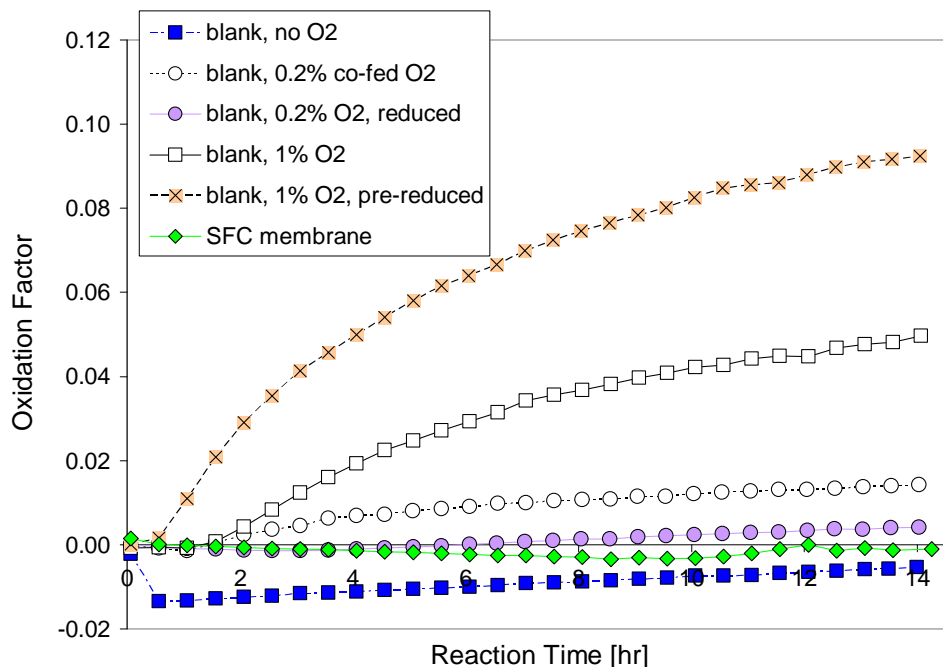


Figure 8.9: Oxidation Factor during CO₂ reforming over a Pt/ZrO₂ catalyst in the improved QTMR. Reaction temperature=800 °C, GHSV=150 L/h/g_{cat}, CH₄:CO₂:Ar/O₂ feed ratio=4:4:2.

As a check on the appropriateness of the proposed Oxidation Factor, values for the 2% co-fed oxygen blank test, which appears to produce the highest amount of undesired product oxidation, are compared to the theoretical maximum Oxidation Factors for a binary reaction from Figure 8.7. As Figure 8.10 illustrates, the actual values are under the theoretical maxima for the optimized Oxidation Factor at all methane conversion values and approach theoretical maxima as methane conversion decreases (i.e., with increasing values on the x-axis).

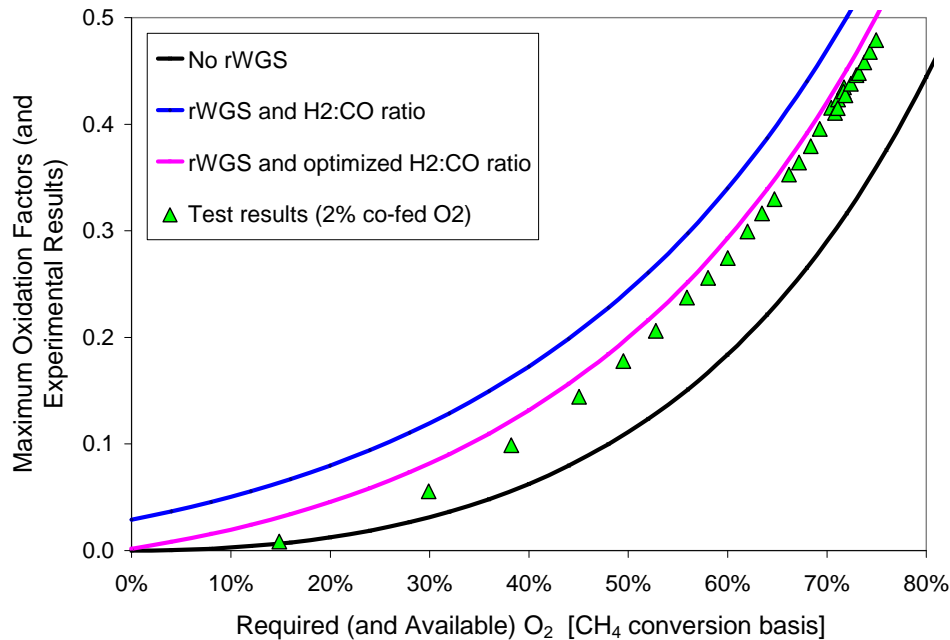


Figure 8.10: Theoretical maximum Oxidation Factor vs. required O_2 with and without concurrent rWGS at 65% of CH_4 conversion; and actual Oxidation Factor for 2% co-fed O_2 test vs. actual available O_2

In contrast to the relationship between the actual test values and the optimized maximum Oxidation Factors, the theoretical maximum values for a Oxidation Factor determined under the assumption of no rWGS are less than the actual values, which validates the inclusion of rWGS as a contributing reaction. However, the point of highest catalyst activity (i.e., the first test point) gives good agreement with the Oxidation Factor calculated under the assumption of no rWGS, which is of interest because this supports the proposal that rWGS can increase as the catalyst deactivates. Similarly, the increasing differences between the actual results and the optimized Oxidation Factor on the left side of the curve correspond to the early portion of the test when it is proposed that the catalyst is most selective for CO_2 reforming. The amount of undesirable oxidation is expected to be significantly less than the theoretical maximum at this point in the test.

Figure 8.11 provides a final means of evaluating the appropriateness of the Oxidation Factor. Using the theoretical numerical contributions of partial oxidation and combustion to the Oxidation Factor and the material balance constraints of actual available oxygen and pre-determined rWGS

activity level, reaction profiles are determined that produce theoretical Oxidation Factors that match the actual Oxidation Factors for the 2% co-fed O₂ test. These results are presented as percent contributions of each of the three methane conversion reactions to the total methane conversion. The greater than eight-fold preponderance of combustion over partial oxidation depicted in Figure 8.11 at the end of the reaction period indicates that 97% of the available oxygen goes to combustion at this point. This conclusion is consistent with the proximity in Figure 8.10 of the experimental Oxidation Factor results to the theoretical maximum values represented by the pink curve.

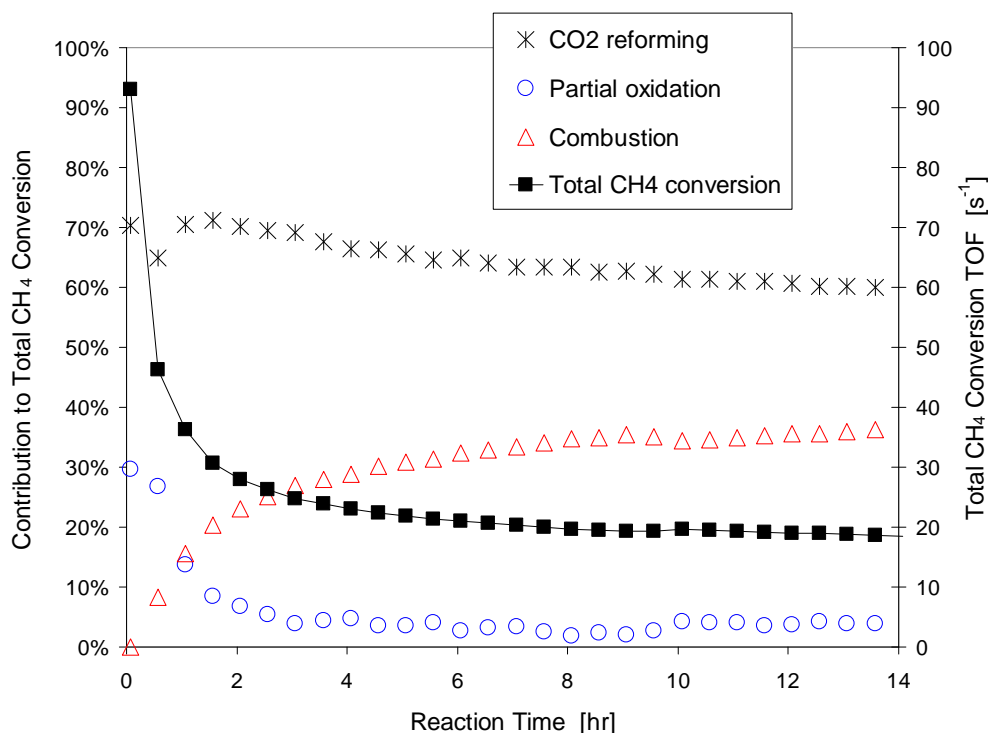


Figure 8.11: CH₄ consuming reaction distribution (as % of total CH₄ conversion) and net CH₄ TOF during CO₂ reforming with 2% co-fed O₂ over a Pt/ZrO₂ catalyst in the original QTMR. Reaction temperature=800 °C, GHSV=150 L/h/g_{cat}, CH₄:CO₂:Ar/O₂ feed ratio=4:4:2.

The methane conversion reaction profiles in Figure 8.11 are not expected to be perfectly representative of the reactions occurring in the blank test with 2% co-fed O₂, but they are stoichiometrically consistent with the actual analytical results and are reasonable (i.e., no contribution percentages below zero or above 100%). This quick analysis thus supports the conclusion that the Oxidation Factor is a meaningful single parameter for distinguishing methane reforming activity from

undesirable oxidation. It has been confirmed to be discriminating for tests with the amount of oxygen in the range of the tests in this work (i.e., less than 5% of the methane feed on a mole basis).

8.3: Pre-Reaction Exposure Testing in a PFR

The relatively high oxygen atmosphere experienced by the catalyst during reactor heat-up because of seal leakage undermines the effectiveness of any low temperature catalyst reduction strategy with the membrane reactor. Additionally, catalyst reduction at or near the reaction temperature may not be an effective alternative on the SFC membrane because the membrane surface itself reduces readily on exposure to hydrogen and evolves oxygen in the absence of hydrogen. Because catalyst pre-treatment options are limited in the membrane reactor, a conventional quartz tube plug-flow reactor (PFR) is used to provide relative catalyst activity data for a selection of catalyst pre-treatment and reactor feed options.

CO₂ reforming tests were performed in the PFR for 12 hours at 800 °C using a catalyst bed that was diluted 40:1 by mass with SiO₂ powder to ensure isothermal operation. The reactor feed and modified space velocity are the same as in the QTMR testing (40% CH₄, 40 CO₂, 20% Ar/O₂ and 150 L/gcat/h, respectively).

8.3.1: Methane conversion in the PFR

As presented in Figure 8.12, the initial CH₄ conversion rate of reduced Pt/ZrO₂ catalyst with no co-fed O₂ is more than twice the initial rate of the unreduced catalyst. However, this activity discrepancy diminishes significantly after 12 hours of CO₂ reforming and the reduced catalyst's deactivation rate is still changing after 12 hours while the unreduced catalyst's deactivation rate stabilizes more quickly, albeit from a lower initial activity level. Nonetheless, reduction prior to reaction clearly has a dramatic effect on the initial activity of the Pt/ZrO₂ catalyst.

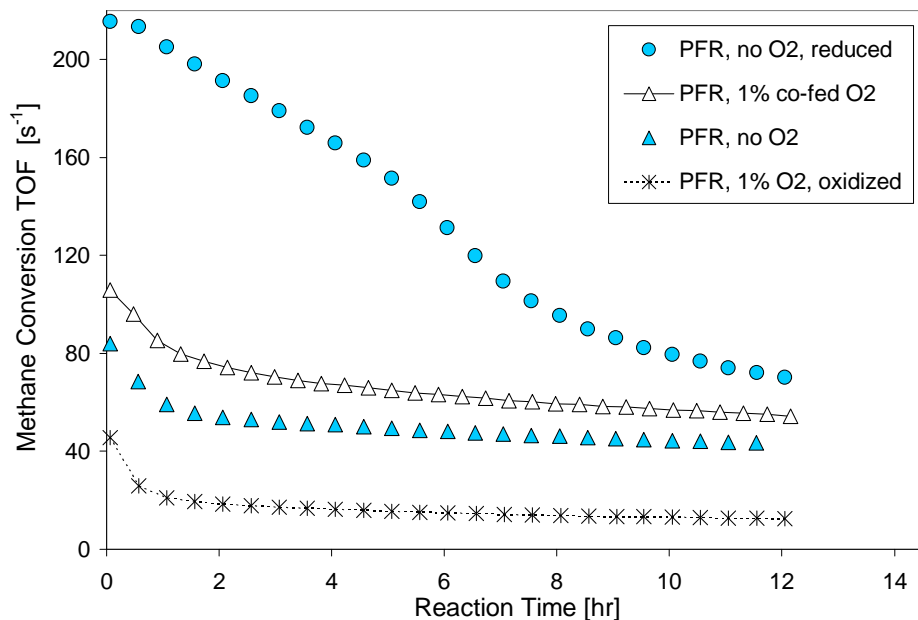


Figure 8.12: CH₄ conversion turnover frequency (TOF) during CO₂ reforming over a Pt/ZrO₂ catalyst in the PFR. Reaction temperature=800 °C, GHSV=150 L/h/g_{cat}, CH₄:CO₂:Ar/O₂ feed ratio=4:4:2.

Figure 8.12 also provides a baseline for the effect of co-fed O₂ on CH₄ conversion. As in the QTMR tests, 1% O₂ is used as an initial representative value for oxygen supplied by an SFC membrane under the applicable reaction conditions. As in the QTMR, CH₄ conversion increases when co-fed oxygen is included in the reactor feed yet the deactivation trends with and without co-fed O₂ are similar. This relationship is also quantitatively consistent with the expected effect of co-fed oxygen: the average difference in TOF is between 12 and 13 sec⁻¹ for the last four hours of each test, which is very close the theoretical amount of methane that could be converted by partial oxidation with 1% O₂ in the reactor feed (i.e., between 13 and 14 sec⁻¹). Finally, as in the initial QTMR test results, unreduced catalyst in the PFR exhibits most of its activity drop over the first two hours of the test.

To evaluate the effect of oxygen exposure during heat-up in the QTMR, 1% O₂ is added to the PFR's pre-reaction argon feed during the pre-heating period prior to CO₂ reforming with 1% co-fed O₂. 1% O₂ in argon was chosen for the heat-up period based on mass spectrometry results that

showed the average air leak during heat-up to be about 5% of the argon feed, which corresponds to about 1% oxygen and 4% nitrogen. The results for this “oxidized catalyst” test confirm that pre-heating in even a small amount of oxygen has a pronounced negative effect on the activity of this catalyst (Figure 8.12), thus predicting generally lower catalyst activity in the QTMR than in the PFR because of the inevitable oxygen exposure on heat-up in the QTMR.

Interestingly, all three unreduced catalyst tests in Figure 8.12 exhibit stable CH₄ conversion after 6-7 hours of reaction time while the lone reduced catalyst test exhibits continually declining catalyst activity throughout its 12-hour test. These trends are consistent with those observed in blank tests in the QTMR. They also indicate that a preliminary catalyst reduction step provides only a temporary benefit with this Pt/ZrO₂ catalyst under CO₂ reforming conditions.

8.3.2: Water production in the PFR

Relative water production results in the PFR testing support the hypothesis that catalyst oxidation increases undesirable oxidation (Figure 8.13). The aged catalyst produced more water per unit methane conversion and the reduced catalyst produced less water. The initial data point for the reduced catalyst in the PFR actually exhibited no water production, which is the expected amount for straight CO₂ reforming with no combustion or rWGS. Interestingly, the two tests without catalyst pretreatment of any kind reached steady state with the same relative water production value, although the 1% O₂ test exhibited higher methane conversion throughout the test period (Figure 8.12). On the other hand, relative water production with the oxidized catalyst increased throughout the test, indicating that the effects of catalyst oxidation are potentially self-propagating just as the effects of catalyst reduction are in the early stages of a test.

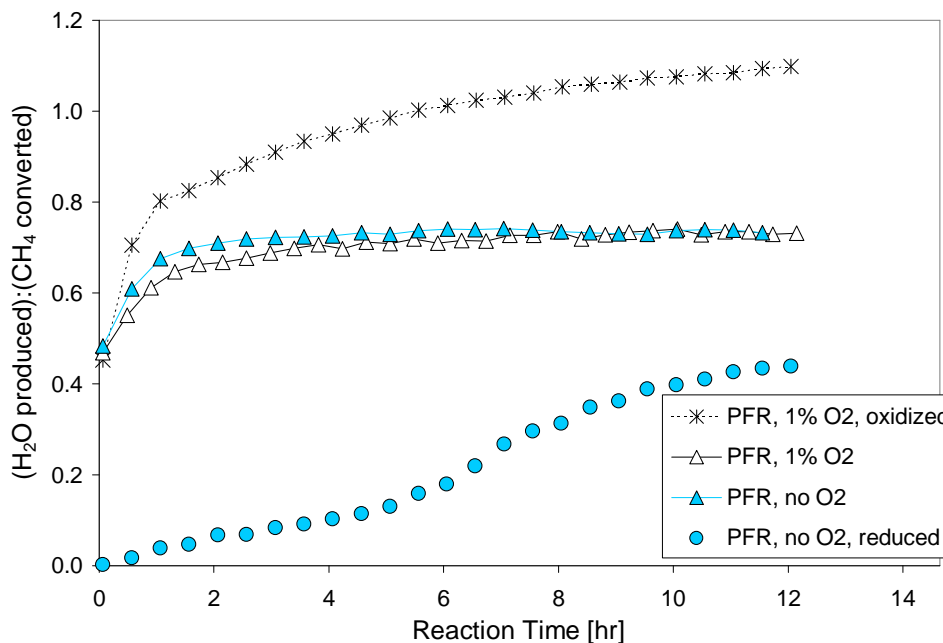


Figure 8.13: Molar ratio of water production-to-CH₄ conversion during CO₂ reforming over a Pt/ZrO₂ catalyst in the PFR. Reaction temperature=800 °C, GHSV=150 L/h/g_{cat}, CH₄:CO₂:Ar/O₂ feed ratio=4:4:2.

8.3.3: CO₂ conversion and H₂:CO ratio in the PFR

Figures 8.14 and 8.15 provide additional supporting trends. The reduced catalyst initially exhibits perfect CO₂ reforming behavior with no rWGS (relative CO₂ conversion and H₂:CO ratio both equal one). However, the rWGS effect appears by the second sample point and increases continuously as indicated by a decreasing H₂:CO ratio in conjunction with increasing relative CO₂ conversion and increasing water production. The reaction profile with the oxidized catalyst and 1% oxygen, on the other hand, does not reach steady state in the 12-hour reaction period. Although methane conversion stabilizes somewhat, H₂:CO ratio, relative water production, and CO₂ conversion values continue to degrade throughout the test. The test exhibits evidence of both increasing combustion over time (i.e., increasing relative water production and decreasing relative CO₂ conversion) and increasing rWGS activity (i.e., declining H₂:CO ratio with relatively stable methane conversion).

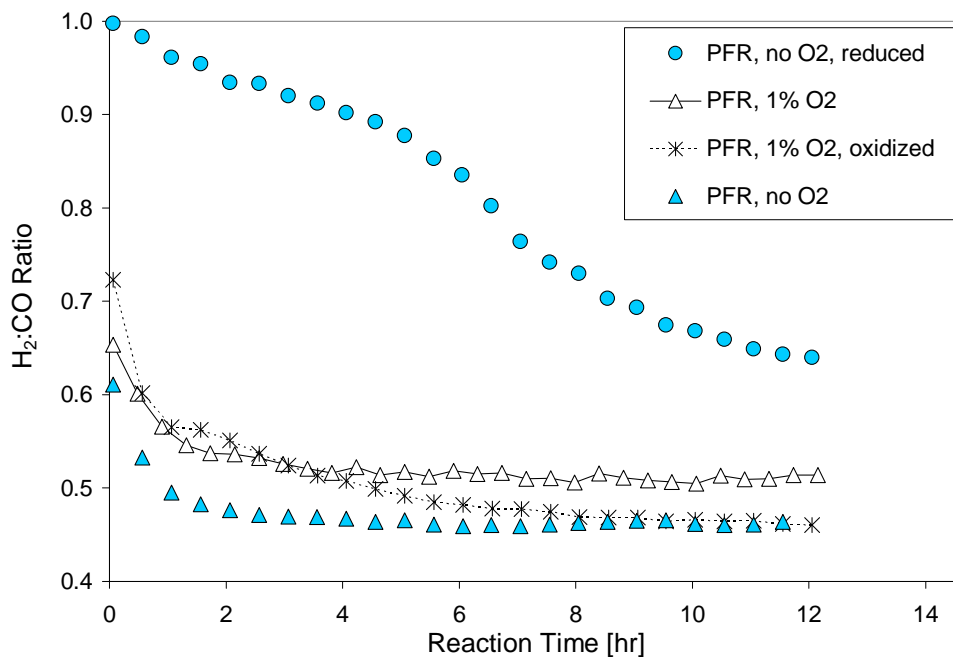


Figure 8.14: H₂:CO ratio during CO₂ reforming over a Pt/ZrO₂ catalyst in the PFR. Reaction temperature=800 °C, GHSV=150 L/h/g_{cat}, CH₄:CO₂:Ar/O₂ feed ratio=4:4:2.

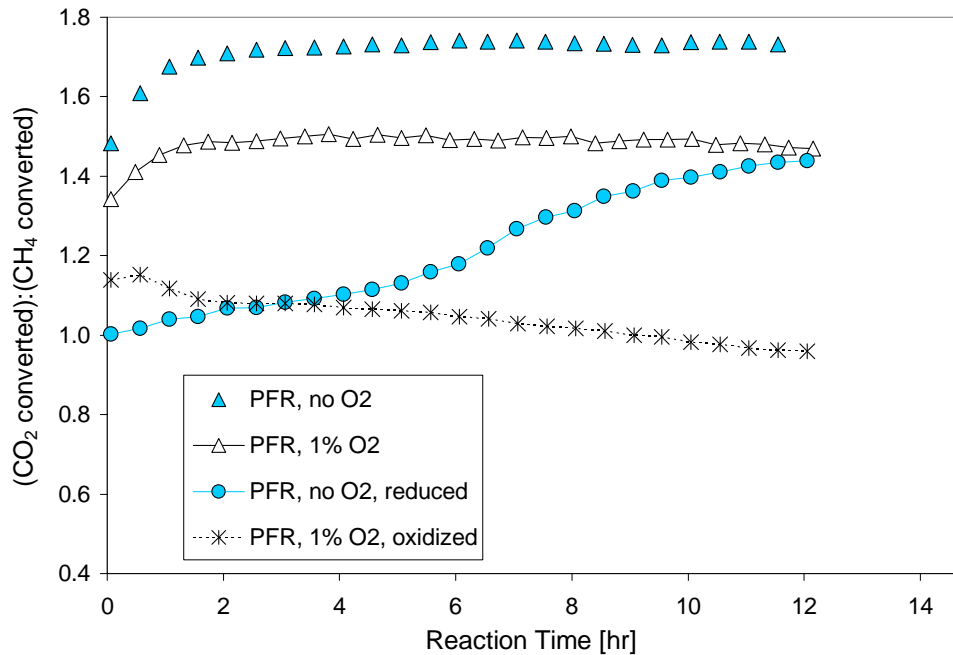


Figure 8.15: Molar CO₂:CH₄ conversion ratio during CO₂ reforming over a Pt/ZrO₂ catalyst in the PFR. Reaction temperature=800 °C, GHSV=150 L/h/g_{cat}, CH₄:CO₂:Ar/O₂ feed ratio=4:4:2.

The lower relative CO₂ conversion values in the standard 1% oxygen test are consistent with expectations. The gap between CO₂ conversion with 1% oxygen and with no oxygen is proportional to the amount of partial oxidation that 1% O₂ could induce. At the end of the test periods, the fractional methane conversion is 9.0% in the 1% co-fed O₂ test and 4.0% in the no O₂ test, giving a methane conversion difference of 5% of the methane fed. The methane mole percentage in the feed is 40%, and 5% of 40% is 2%. This is exactly the stoichiometric amount of methane that 1% co-fed oxygen should convert by partial oxidation.

With all of the co-fed oxygen accounted for and no detectable leak in the PFR, a significant amount of combustion is not possible in this test. As a result, all water produced can be attributed entirely to rWGS, as can the low H₂:CO ratio. The exact overlap at steady state of the relative water production values for the 1% and no co-fed oxygen tests in Figure 8.13 further implies that rWGS is proportional to methane conversion regardless of the presence of co-fed oxygen in the PFR with the Pt/ZrO₂.

8.3.4: Oxidation Factor in the PFR

The newly defined Oxidation Factor provides a final means of assessing the selectivity for reforming reactions over complete oxidation reactions. In Figure 8.16, product oxidation appears to occur to a much greater extent with the oxidized catalyst than with the non-oxidized catalysts, and catalyst reduction diminishes product oxidation even further. Both observations are consistent with the hypotheses proposed in Chapter 6.

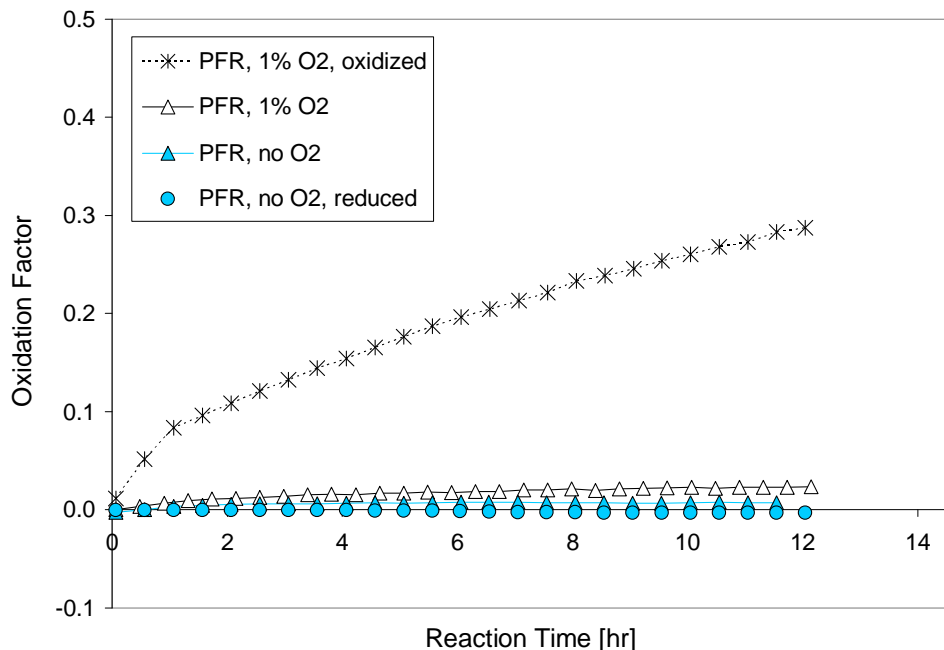


Figure 8.16: Oxidation Factor during CO₂ reforming over a Pt/ZrO₂ catalyst in the PFR. Reaction temperature=800 °C, GHSV=150 L/h/g_{cat}, CH₄:CO₂:Ar/O₂ feed ratio=4:4:2.

8.3.5: Relative rWGS activity in the QTMR and PFR

RWGS extent can be estimated by reaction stoichiometry using product composition and reactant conversions. These estimates should be particularly accurate in tests with no added oxygen because all water production can be attributed to rWGS. Co-fed oxygen tests where the Oxidation Factor is low should also give reliable estimates. Figure 8.17 provides an example of the relative amount of rWGS in the four PFR tests, with the QTMR blank test with no co-fed oxygen and the SFC membrane test included for comparison. *NOTE: the method used to estimate the extent of rWGS is described in Appendix K.*

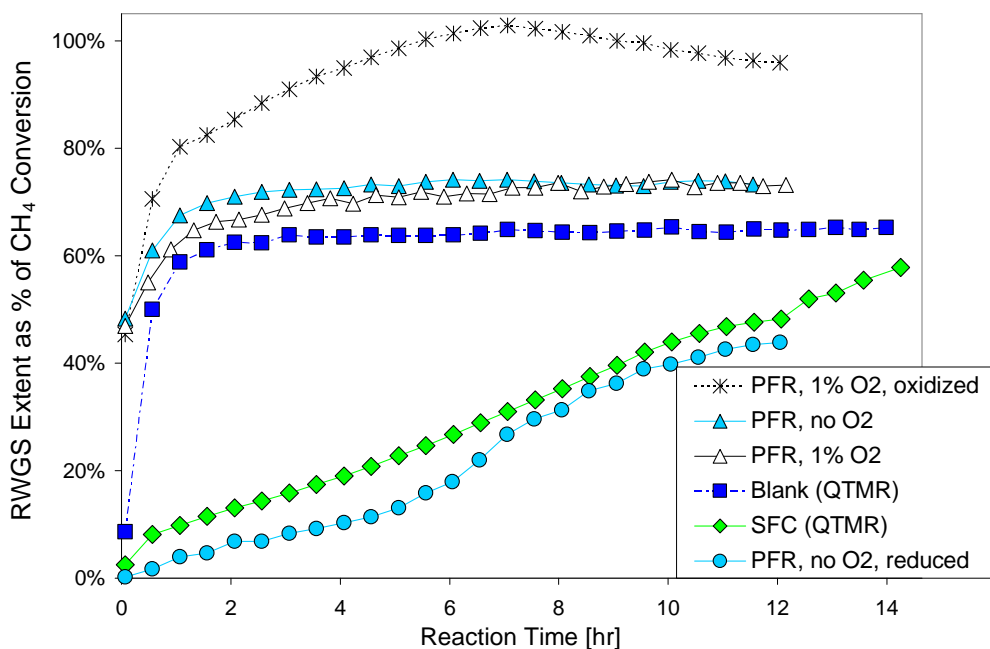


Figure 8.17: RWGS extent during CO₂ reforming over a Pt/ZrO₂ catalyst in both reactor types. Reaction temperature=800 °C, GHSV=150 L/h/g_{cat}, CH₄:CO₂:Ar/O₂ feed ratio=4:4:2.

The tests done in the controlled environment of the PFR demonstrate clearly that the oxidation state of the catalyst has a pronounced effect on the reactor product ratios and thus on the reaction profile. The estimates for the blank QTMR test corroborate the similarity in reaction profiles between the PFR and the QTMR, while the striking similarity between the reduced catalyst PFR test and the SFC membrane test reinforces the *in situ* reduction theory as some portion of the explanation for the effect of the SFC membrane on the Pt/ZrO₂ catalyst.

The relatively small difference in rWGS contribution between the QTMR and PFR tests may be attributed to two of the fundamental differences between the PFR and the QTMR setup. First, the catalyst bed in the PFR is diluted 40:1 with inert quartz powder to guarantee isothermal conditions, which means the catalyst bed volume is greater in the PFR than in the QTMR, and second, there is no bypass in the PFR, which means the entire quantity of gas must pass through the catalyst bed. These two factors create greater average catalyst contact times in the PFR. This additional contact time should allow more secondary reactions such as rWGS, which Figure 8.17 supports.

Figure 8.17 also justifies the use of a proportional amount of rWGS as an approximation in the theoretical maximum Oxidation Factor calculations underlying the curves in Figures 8.7 and 8.10.

8.4: Observations and Conclusions from Chapter 8

- (1) In addition to being an important predictive factor for Pt/ZrO₂ catalyst activity and deactivation rate as predicted in Chapter 7, catalyst oxidation state influences reaction profile.
- (2) SFC membranes do not appear to promote combustion as a substrate for the Pt/ZrO₂ catalyst.
- (3) SFC membranes promote some rWGS (i.e., “membrane-facilitated rWGS”) with the Pt/ZrO₂ catalyst but less than the blank tests as a fraction of methane conversion. The relative amount of rWGS with the membrane increases over time and parallels that which occurs with a reduced Pt/ZrO₂ catalyst and no co-fed oxygen.
- (4) In PFR testing, intentionally oxidizing a catalyst clearly leads to increased combustion activity with 1% co-fed O₂ as well as increasing relative amounts of rWGS over time, both of which confirm the effect of catalyst oxidation on net reaction profile predicted in previous chapters.
- (5) Pre-reaction catalyst reduction in the PFR increases catalyst selectivity to the point where it initially produces straight CO₂ reforming with no rWGS. The amount of rWGS relative to methane conversion increases steadily as the Pt/ZrO₂ catalyst loses activity and changes its net reaction profile, but the temporary existence of straight CO₂ reforming confirms the predicted positive effect of catalyst reduction on net reaction profile.
- (6) The confirmed effects of catalyst oxidation and reduction in the PFR strongly support the hypothesis that *in situ* catalyst oxidation and reduction can be caused by co-fed O₂ and ambient H₂, respectively, and can induce changes in the net reaction profile under appropriate operating conditions.
- (7) The Oxidation Factor defined in this chapter provides a useful single parameter for evaluating the relative contribution of combustion to the total methane conversion in an oxygen-assisted CO₂ reforming reaction test, as well as the existence of the other two undesirable oxidation reactions: hydrogen and CO oxidation. Hydrogen oxidation is the more likely of the two, given the low probability of selective CO oxidation with the high affinity of the SFC membrane for H₂ and with a high concentration of CO₂ in the reactor feed.

Chapter 9: Catalyst Comparison and Membrane Reactor Evaluation

The Pt/ZrO₂ catalyst discussed in Chapters 5 through 8 was chosen because it has relatively low activity and has also been shown to deactivate rapidly. After establishing the effect of the membrane on the Pt/ZrO₂ catalyst, a 17.5% CeO₂ in zirconia support with the same platinum loading was tested (0.42 wt% platinum versus 0.43 wt% for the Pt/ZrO₂ catalyst).

The Pt/ZrCeO₂ catalyst was chosen because zirconia supports promoted with ceria have exhibited higher activity than pure ZrO₂ supports and also reduced deactivation rates [1-4]. The benefit has been attributed to the ability of ceria-promoted zirconia to be reduced and oxidized repeatedly and thereby to act as an “oxygen supply/sink” under reaction conditions. It is important to note that this labile oxygen trait of cerium-zirconium oxides is a milder version of the distinguishing characteristic of O-MIEC ceramics such as SFC. The Pt/CeZrO₂ catalyst was therefore expected to interact more noticeably with oxygen in the reaction chamber than did the Pt/ZrO₂ catalyst.

Baseline catalyst comparisons are established using the PFR prior to testing in the QTMR. QTMR test results with both the blank and SFC are then evaluated to determine the effect of the membrane on the Pt/CeZrO₂ catalyst. In general, the Pt/CeZrO₂ catalyst responds less to the presence of the SFC membrane than does the Pt/ZrO₂ catalyst. However, the responses that do occur to both the SFC membrane and pretreatment conditions provide valuable insight into the mode of activity of the CeZrO₂ support under CO₂ reforming conditions. These insights, in turn, help clarify the potential role of the SFC membrane in enhancing powder catalyst activity.

9.1: Catalyst Comparison in the PFR

9.1.1: Methane and CO₂ conversion

As expected, PFR tests with the Pt/CeZrO₂ catalyst exhibited much higher activity levels and more gradual deactivation rates than their Pt/ZrO₂ counterparts but showed a similar improvement with the addition of 1% co-fed oxygen (Figure 9.1).

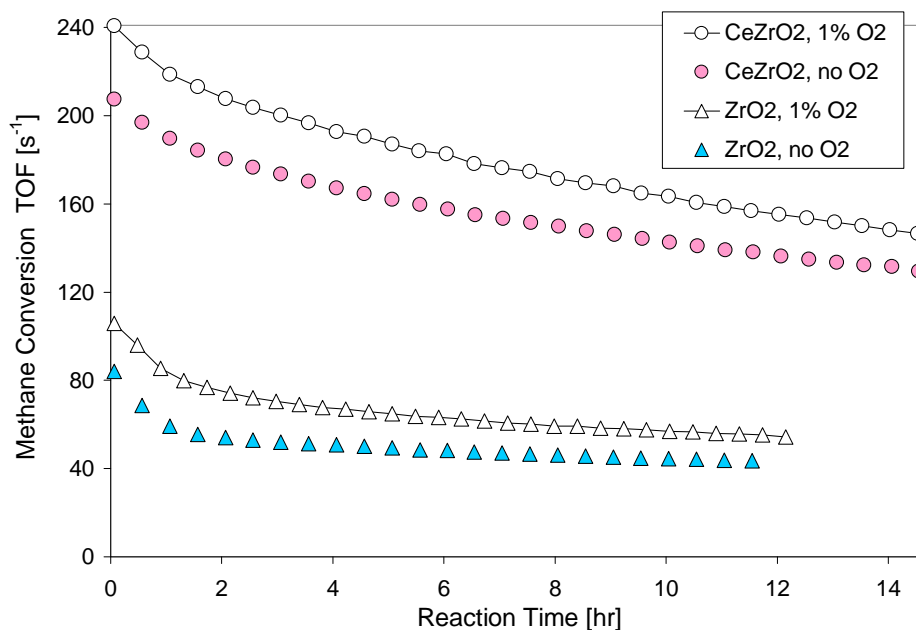


Figure 9.1: CH₄ conversion turnover frequency (TOF) during CO₂ reforming over a Pt/ZrO₂ and a Pt/CeZrO₂ catalyst in the PFR. Reaction temperature=800 °C, GHSV=150 L/h/g_{cat}, CH₄:CO₂:Ar/O₂ feed ratio=4:4:2.

The CeZrO₂-supported catalyst also produced substantially less relative CO₂ conversion as well as a much smaller difference in relative CO₂ conversion between the 1% oxygen and no oxygen tests (Figure 9.2).

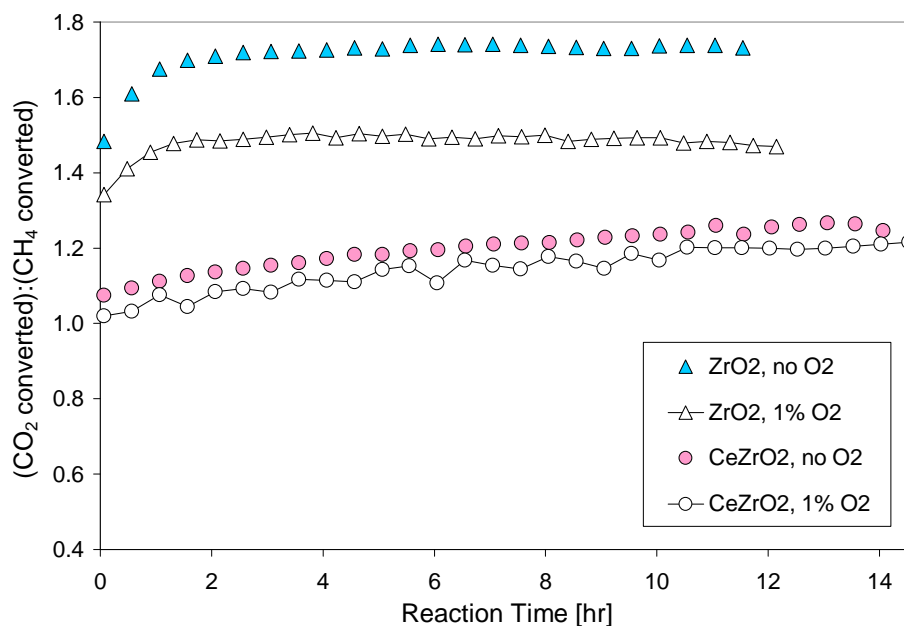


Figure 9.2: Molar CO₂:CH₄ conversion ratio during CO₂ reforming over a Pt/ZrO₂ and a Pt/CeZrO₂ catalyst in the PFR. Reaction temperature=800 °C, GHSV=150 L/h/g_{cat}, CH₄:CO₂:Ar/O₂ feed ratio=4:4:2.

The lower relative CO₂ conversion implies either less reverse water-gas shift reaction per unit methane conversion or more undesirable oxidation. With the CO₂-to-methane conversion ratios all greater than one, a substantial undesirable oxidation contribution to methane conversion is unlikely, meaning the Pt/CeZrO₂ is probably exhibiting less rWGS activity relative to methane conversion than the Pt/ZrO₂ catalyst.

9.1.2: Other ratios

The H₂:CO ratios for the Pt/CeZrO₂ catalyst in Figure 9.3 confirm the suggestion of diminished reverse water-gas shift activity on the Pt/CeZrO₂ catalyst compared to the Pt/ZrO₂ catalyst as they are much higher than those for the Pt/ZrO₂ catalyst. Additionally, the relative water production trends in Figure 9.4 for the Pt/CeZrO₂ catalyst tests in the PFR are quite low—half those of Pt/ZrO₂—which further reinforces the conclusions of less rWGS and minimal combustion with the CeZrO₂ supported catalyst.

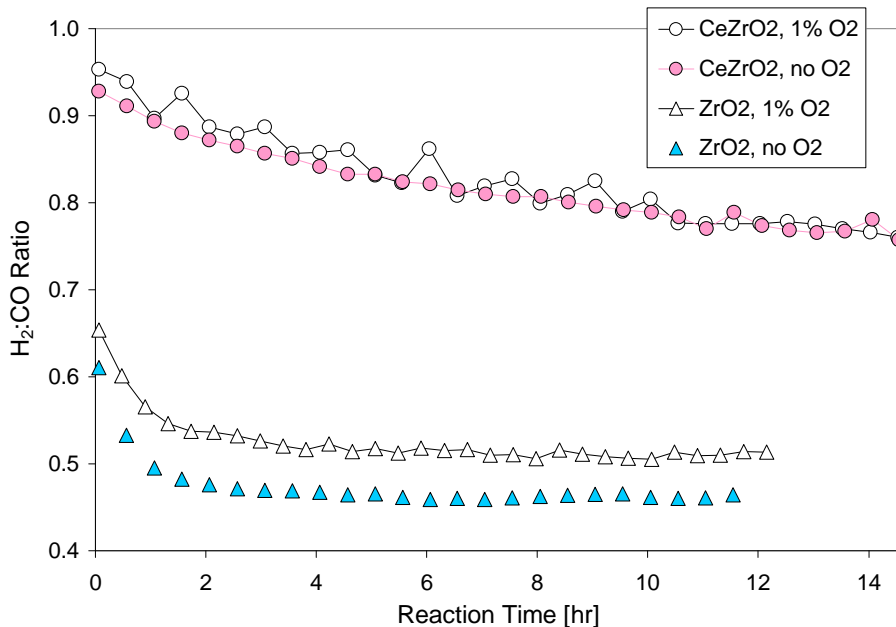


Figure 9.3: H₂:CO ratio during CO₂ reforming over a Pt/ZrO₂ and a Pt/CeZrO₂ catalyst in the PFR. Reaction temperature=800 °C, GHSV=150 L/h/g_{cat}, CH₄:CO₂:Ar/O₂ feed ratio=4:4:2.

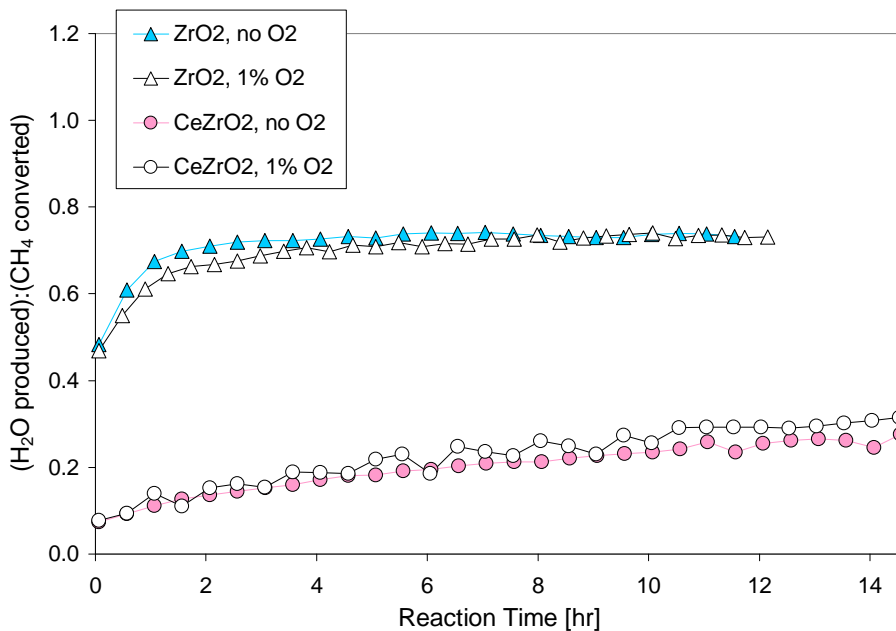


Figure 9.4: Molar ratio of water production-to-CH₄ conversion during CO₂ reforming over a Pt/ZrO₂ and a Pt/CeZrO₂ catalyst in the PFR. Reaction temperature=800 °C, GHSV=150 L/h/g_{cat}, CH₄:CO₂:Ar/O₂ feed ratio=4:4:2.

Unlike with the Pt/ZrO₂ catalyst, adding 1% gas-phase oxygen to the reactor feed with the Pt/CeZrO₂ catalyst does not appear to change the net reaction profile, although it does increase the

overall level of activity. The lack of effect of ambient oxygen on reaction proportions could result from redox interactions between gas-phase oxygen and the CeZrO₂ support that enhance the activity of the catalyst without changing its mode of action. Under this hypothesis, the co-fed oxygen interacts preferentially with the catalyst support to help maintain its oxygen content and the support then provides the oxygen that facilitates the reaction.

9.1.3: Absolute water production

Figure 9.5 demonstrates that the water production increase in terms of absolute water production is the same for both catalysts on the addition of 1% co-fed O₂. The theoretical maximum amount of water that could be produced by this amount of oxygen is approximately 2 mmol/g_{cat}/min for the feed conditions used in these tests, which is very close to the observed increase for both pairs of results in Figure 9.5. In other words, the average increase in net water production from co-fed oxygen is not only the same for the two sets of tests; it also matches the theoretical prediction for a scenario wherein all co-fed oxygen ultimately oxidizes hydrogen to water. If net water production accounts for the majority of the oxygen provided, there can be correspondingly less net CO oxidation, regardless of reaction mechanism. This explains the lower H₂:CO ratios than predicted strictly by reactor feed composition.

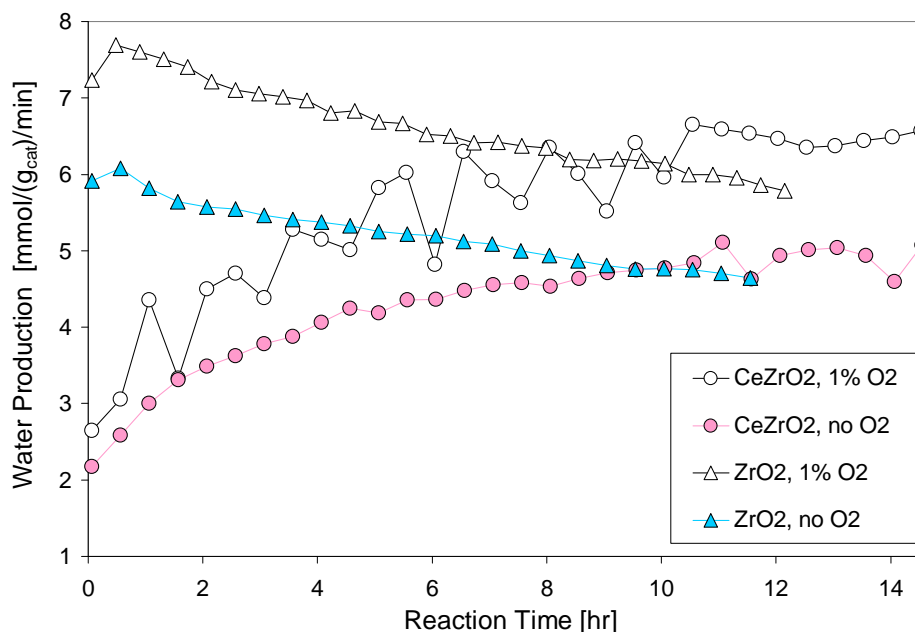


Figure 9.5: Water production during CO₂ reforming over a Pt/ZrO₂ and a Pt/CeZrO₂ catalyst in the PFR. Reaction temperature=800 °C, GHSV=150 L/h/g_{cat}, CH₄:CO₂:Ar/O₂ feed ratio=4:4:2.

9.1.4: Reduction and oxidation of the catalyst supports

The oscillatory water production in the presence of gas-phase oxygen is another intriguing aspect of the Pt/CeZrO₂ results in Figure 9.5. Complementary oscillations are observed in the H₂:CO ratio results (Figure 9.3), indicating that cyclical hydrogen oxidation may be occurring on the support. Additionally, relative CO₂ conversion oscillates in unison with relative water production. Because all of these changes occur with no corresponding oscillations in methane conversion, it is possible that oscillating rWGS activity is responsible for the temporary changes in net reaction profile.

These oscillations appear to be related to the use of co-fed oxygen (although the Pt/CeZrO₂ test with no oxygen exhibits a few small potential oscillations toward the end). With the new perspective offered by the relatively dramatic oscillations with the Pt/CeZrO₂, similar smaller oscillations can be observed with the Pt/ZrO₂ catalyst and co-fed oxygen on a period of approximately one hour. The experimental evidence thus encourages the idea of redox interactions

between gas-phase oxygen and the CeZrO₂ support and possibly even the ZrO₂ support. Given the nature of the ceria-zirconia support, the redox mechanism could be the same as the proposed “membrane facilitated rWGS” mechanism from Chapter 7. In this case, the oscillations are likely occurring because the oxygen-depleted phases in the CeZrO₂ support are less stable than oxygen-depleted phases in SFC.

9.2: Catalyst Comparison in the QTMR

The SFC membrane improves the activity of the Pt/CeZrO₂ catalyst but not as dramatically as it improved the Pt/ZrO₂ catalyst activity. Similar to the response of the net reaction profile (i.e., product distribution) to the addition of co-fed oxygen with the Pt/CeZrO₂ catalyst in the PFR, the membrane has little effect on the net reaction profile with this catalyst in the early part of the test period. The membrane effect appears when the SFC membrane test begins to deviate from the blank test with no co-fed O₂ after approximately eight hours on stream.

9.2.1: Conversion and product ratios

Figure 9.6 presents methane conversion results for the Pt/CeZrO₂ catalyst in the QTMR. The PFR tests are included to help evaluate any differences in the effects of co-fed O₂ and the SFC membrane with this catalyst.

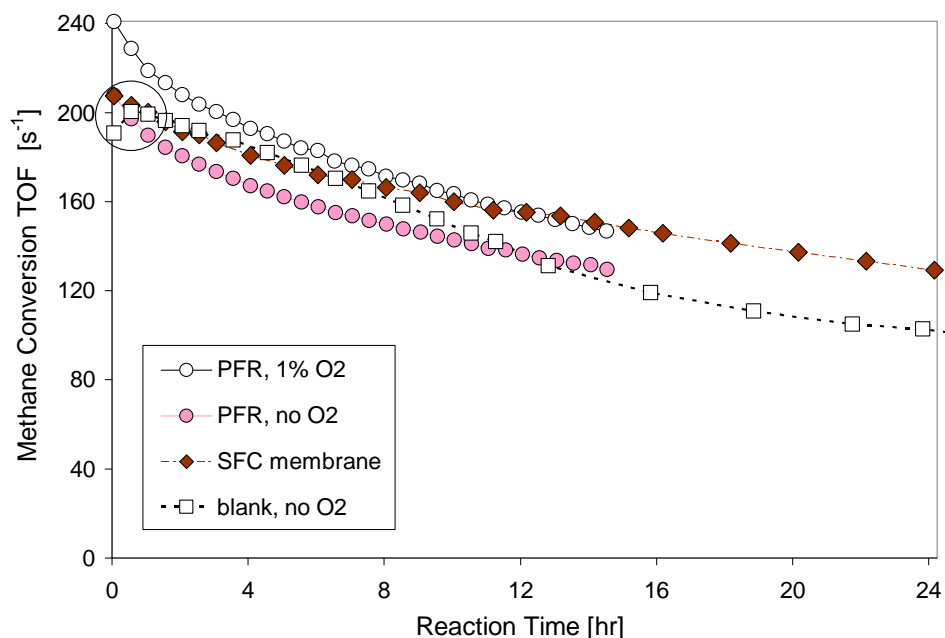


Figure 9.6: CH₄ conversion turnover frequency (TOF) during CO₂ reforming over a Pt/CeZrO₂ catalyst in both reactor types. Reaction temperature=800 °C, GHSV=150 L/h/g_{cat}, CH₄:CO₂:Ar/O₂ feed ratio=4:4:2.

Conversion in the QTMR with the SFC membrane is largely indistinguishable from that with the blank over the first 8 hours of reaction time. After 8 hours, the membrane test begins to exhibit slower deactivation than the blank test. The membrane test also shows a consistently lower deactivation rate than both PFR tests, indicating a detectable benefit even with the higher activity Pt/CeZrO₂ catalyst. The lower initial activity in the membrane reactor tests than in the PFR tests are likely the result of a combination of oxygen exposure during heat-up in the QTMR and the general difference in catalyst contact with the PFR and QTMR. However, the similar activities of the SFC and blank tests early in the test period demonstrate the CeZrO₂ supported catalyst's improved tolerance to pre-reaction oxygen exposure (for comparison, Table 7.1 summarizes the relationship between blank tests and an SFC test with the Pt/ZrO₂ catalyst in the QTMR).

Relative CO₂ conversion, relative water production, and H₂:CO ratio trends are nearly identical for the four tests presented in Figure 9.6, so much so that additional plots would be largely redundant. The Pt/CeZrO₂ results in Figures 9.2, 9.3, and 9.4 can be used to represent the two QTMR

tests (i.e., the SFC membrane test and the blank test with no oxygen) as well as the two PFR tests. Figure 9.7 provides a representative example. The membrane test has a slight advantage in H₂:CO ratio but is otherwise similar. Likewise, the membrane test produced slightly less relative water and converted slightly less relative CO₂ but otherwise tracked with the blank test for those two metrics as well.

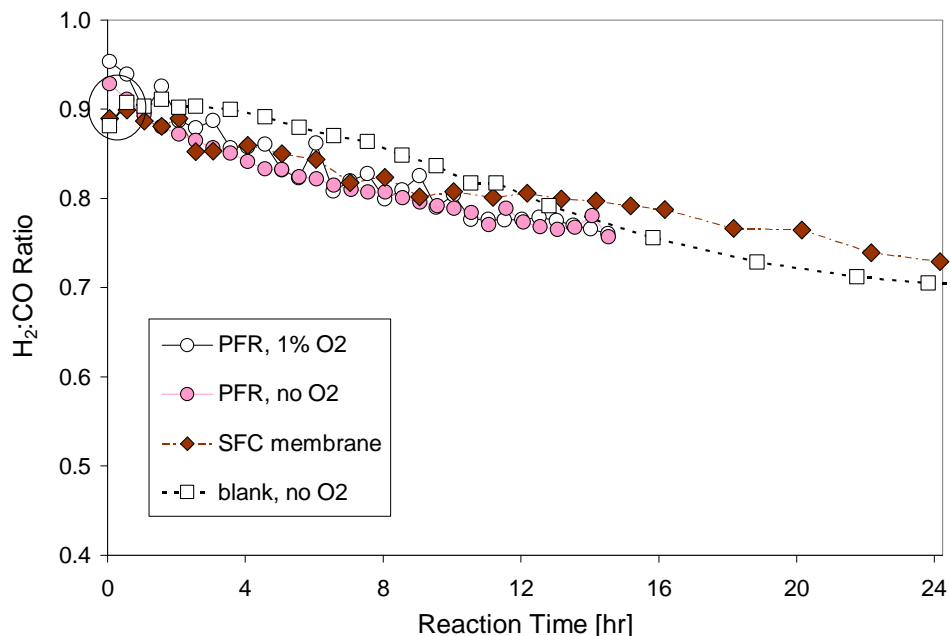


Figure 9.7: H₂:CO ratio during CO₂ reforming over a Pt/CeZrO₂ catalyst in both reactor types. Reaction temperature=800 °C, GHSV=150 L/h/g_{cat}, CH₄:CO₂:Ar/O₂ feed ratio=4:4:2.

9.2.2: Comparison of the evidence for *in situ* reduction

Because of its lower feed flow rate and longer lines, the QTMR system experiences more molecular dispersion than the PFR effluent in the line between the reactor and the analytical instruments. This has the negative consequence of making transitions less distinct, but it has a positive consequence also in that it provides residual evidence of what was leaving the reactor in the time prior to each GC injection (Appendix L provides a discussion of molecular dispersion in the QTMR system). With test points 30 minutes apart, this is not necessarily noticeable when changes in the effluent composition are gradual. However, the first test point occurs three to four minutes after

starting the reaction which is a time with the potential for dramatic change. The composition in the GC for the first test point with the QTMR can therefore

With this in mind, the circled data in Figures 9.6 and 9.7 contain subtle but important evidence of *in situ* reduction. The SFC and blank tests show nearly identical activity for the first eight hours with one exception: conversion on the blank is markedly lower than conversion on the SFC membrane for the first data point. By the third sample point, conversion with the blank is identical to conversion with SFC. Earlier SFC tests with the Pt/ZrO₂ catalyst showed similar lags prior to peak methane conversion (see Figure 6.8), which were ascribed to *in situ* reduction. However, the situation illustrated by Figure 9.6 is unique because the blank test exhibits the lag in peak conversion while the SFC test does not.

9.2.3: Hydrogen concentration in the reactor

The unprecedented lag in peak conversion in the blank test can be interpreted as evidence that the Pt/CeZrO₂ catalyst undergoes *in situ* reduction less readily than the Pt/ZrO₂ catalyst, while the less extensive lag with the SFC membrane indicates that it facilitates *in situ* reduction of the Pt/CeZrO₂ catalyst more rapidly than the blank. Higher early hydrogen levels in the SFC test would support the proposal that it facilitates *in situ* reduction more effectively than the blank, particularly considering that the catalyst in the SFC membrane test is exposed to more oxygen in the pre-reaction period than the catalyst in the blank test because of oxygen flux. Figure 9.8 provides the necessary evidence, with the circled data confirming the higher ambient hydrogen levels in the earliest part of the SFC membrane test.

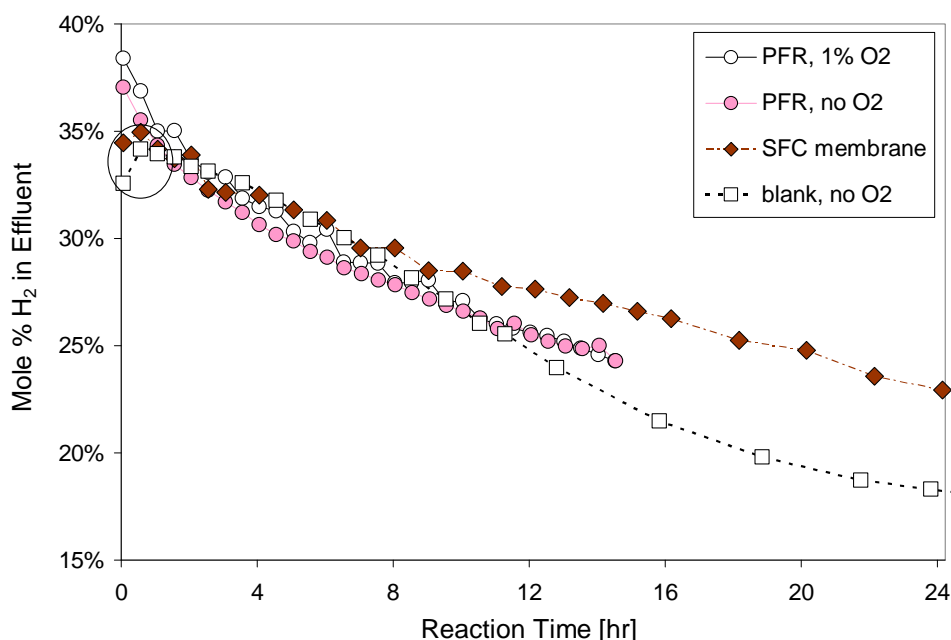


Figure 9.8: Average H₂ concentration in the reactor during CO₂ reforming over a Pt/CeZrO₂ catalyst in both reactor types. Reaction temperature=800 °C, GHSV=150 L/h/g_{cat}, CH₄:CO₂:Ar/O₂ feed ratio=4:4:2.

It seems plausible that at least a portion of the *in situ* reduction phenomenon can be attributed to high ambient hydrogen levels early in the test period.

9.2.4: Delayed membrane effect with the Pt/CeZrO₂ catalyst

The fact that the CeZrO₂ support can be reduced and oxidized leads to a hypothesis that explains both the delayed effect of the SFC membrane on this catalyst as well as the slightly different effect. As mentioned earlier, the redox capability of the CeZrO₂ support parallels the oxygen transport mechanism of the ceramic membranes. The catalyst could therefore be active enough initially to suppress the effect of the low flux SFC membrane. Over time, the CeZrO₂ support could be reduced by ambient hydrogen to the point where its ability to enhance methane conversion diminishes to the point that the SFC membrane begins to have a detectable effect. At this point (about 8 hours of time on stream in the tests in question), methane conversion with the SFC membrane begins to diverge from that with the blank without changing the net reaction profile

significantly. Because no net oxygen is supplied by the SFC membrane over this period (see Figure 9.9) and because the net reaction profile remains nearly the same, the mode of action of the SFC membrane would seem to be either similar to, or supportive of, the mode of action of the CeZrO₂ support in promoting catalytic activity.

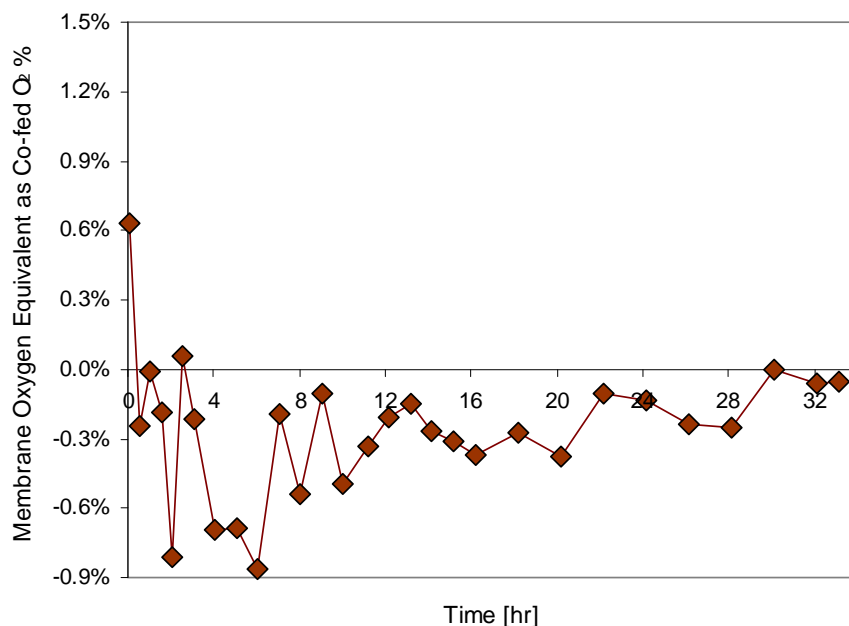


Figure 9.9: Membrane oxygen flux (O₂ equivalent) as mol% of feed during CO₂ reforming over a Pt/CeZrO₂ catalyst in the QTMR with an SFC membrane. Reaction temperature=800 °C, GHSV=150 L/h/g_{cat}, CH₄:CO₂:Ar/O₂ feed ratio=4:4:2.

The calculated net oxygen influx is assigned to the membrane arbitrarily because positive values for oxygen influx are considered to be membrane oxygen flux into the reactor. However, this value is based on an oxygen balance and could therefore come from the powder catalyst as well if it experiences a gain or loss of oxygen over the course of a test. It is possible that the higher affinity for oxygen of the SFC membrane caused the Pt/CeZrO₂ catalyst to become depleted in oxygen during the reaction because of the sustained high ambient hydrogen levels in this test. In any case, it is almost certainly not a coincidence that the largest negative flux estimates coincided with the largest measured quantity of deposited carbon on a catalyst.

This hypothesis that the CeZrO₂ support and the SFC membrane have similar effects on methane conversion and net reaction profile explains why the relative CO₂ conversion, H₂:CO ratio, and relative water production trends remain so similar for the membrane and the blank even as the methane conversion trends in Figure 9.6 diverge. It also provides an explanation for the absence of a membrane oxygen contribution from the SFC membrane in the Pt/CeZrO₂ test: under these circumstances the SFC membrane could serve more as an oxygen exchange medium like the CeZrO₂ support rather than as a net supplier of oxygen.

9.3: Pretreatment Effects on the Pt/CeZrO₂ Catalyst

The final set of PFR reaction tests uses an “aged” portion of the same original batch of Pt/CeZrO₂ catalyst. Prior to testing, the aged catalyst was heated to over 100 °C with an IR lamp for three hours in ambient air and then stored for more than 6 months in uncontrolled conditions. *NOTE: no co-fed O₂ was used in the tests discussed in this section.*

9.3.1: Catalyst oxidation (“aging”) and reduction

Figure 9.10 shows that the aged catalyst exhibits a significantly higher deactivation rate than the fresh catalyst of the earlier tests. Assuming that the low temperature aging process increases platinum particle oxidation, these results confirm the importance of oxidation state on catalyst durability (Figure 9.6).

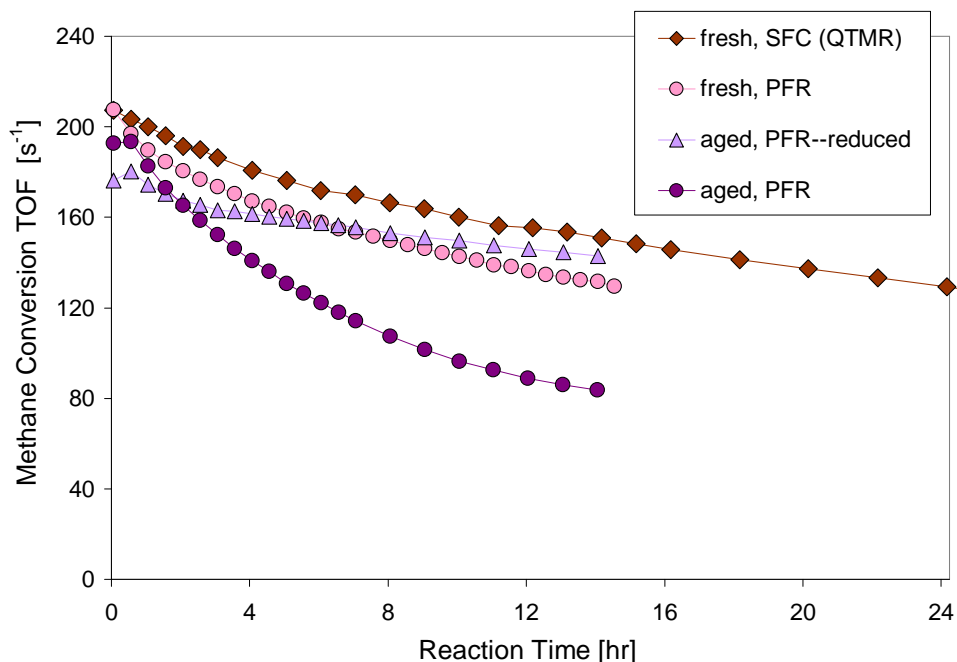


Figure 9.10: CH₄ conversion turnover frequency (TOF) during CO₂ reforming over aged and fresh Pt/CeZrO₂ catalyst in both reactor types with no co-fed O₂. Reaction temperature=800 °C, GHSV=150 L/h/g_{cat}, CH₄:CO₂:Ar/O₂ feed ratio=4:4:2.

A second test with the aged catalyst employs a reduction step, which greatly improves the deactivation rate but, interestingly, also lowers the initial activity. The initial activity effect could be a result of platinum particle sintering or oxygen depletion in the CeZrO₂ support during reduction, either of which would decrease the catalyst's initial ability to facilitate methane conversion. Because methane conversion later exceeds that of the corresponding fresh catalyst test, oxygen depletion in the support is a more compelling theory than particle sintering because deactivation by particle sintering should persist throughout the test.

9.3.2: Additional evidence for *in situ* catalyst reduction

As with the Pt/ZrO₂ catalyst, reduction with hydrogen prior to reaction increases long-term activity and decreases deactivation rate of the Pt/CeZrO₂ catalyst with the stainless steel blank. The effect is similar to the effect of the SFC membrane, which supports the *in situ* reduction hypothesis used to explain the membrane effect. The aged Pt/CeZrO₂ also showed an unprecedented peak

activity lag from the first sample point to the second for PFR testing. This is even more telling than the peak lag discussed above for the QTMR blank tests because no other PFR test of any kind has exhibited this trend. With molecular dispersion thus removed as a potential contributor to the peak lag, Figure 9.10 provides the most compelling evidence yet that catalyst can be reduced *in situ* at the beginning of a reaction period.

9.3.3: Conversion/product ratios

Figures 9.11 and 9.12 show that net reaction profiles with the Pt/CeZrO₂ catalyst change over time on stream in a similar manner to that observed with the Pt/ZrO₂ catalyst: degraded catalyst produces more rWGS than fresh or reduced catalyst. Both CO₂ conversion and water production are higher with the aged catalyst and are highest with the unreduced aged catalyst.

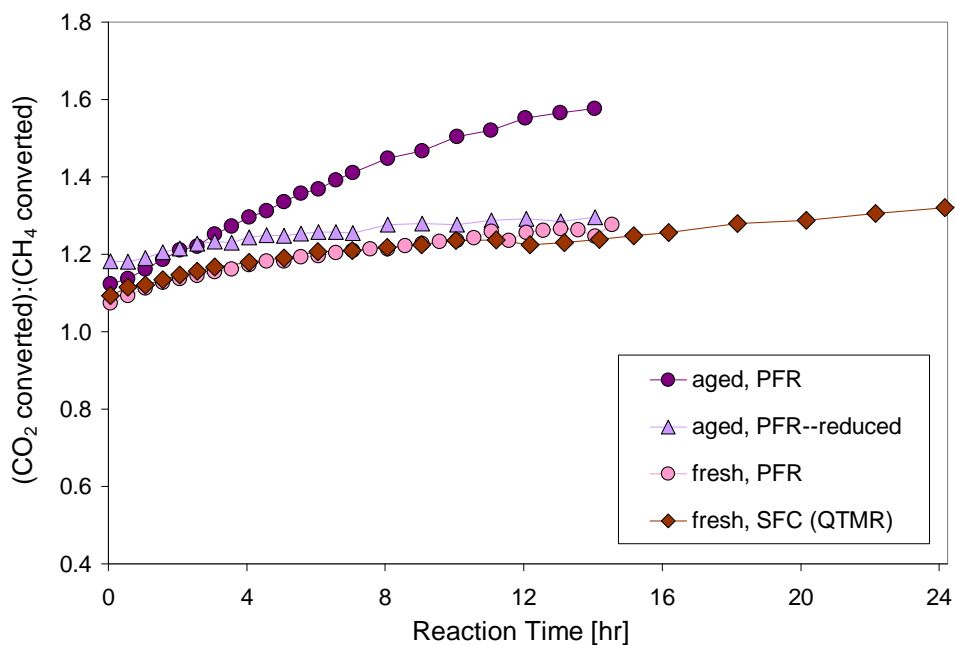


Figure 9.11: Molar CO₂:CH₄ conversion ratio during CO₂ reforming over aged and fresh Pt/CeZrO₂ catalyst in both reactor types with no co-fed O₂. Reaction temperature=800 °C, GHSV=150 L/h/g_{cat}, CH₄:CO₂:Ar/O₂ feed ratio=4:4:2.

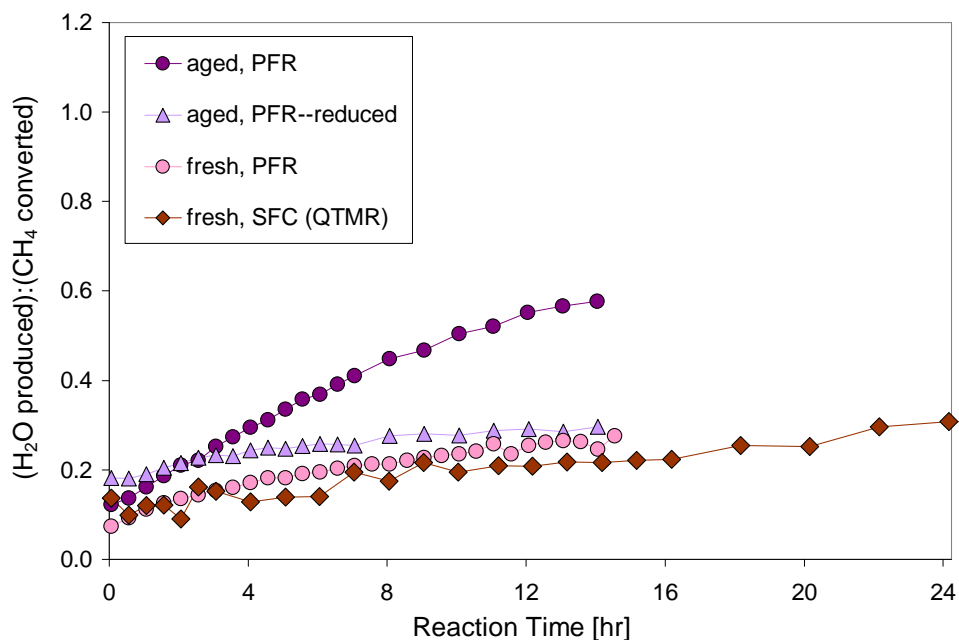


Figure 9.12: Molar ratio of water production-to-CH₄ conversion during CO₂ reforming over aged and fresh Pt/CeZrO₂ catalyst in both reactor types with no co-fed O₂. Reaction temperature=800 °C, GHSV=150 L/h/g_{cat}, CH₄:CO₂:Ar/O₂ feed ratio=4:4:2.

Because water production and CO₂ conversion trend with each other and there is no O₂ available, rWGS rather than combustion must be the source of the increased water output. The H₂:CO ratio data in Figure 9.13 are also consistent with the suggestion of more rWGS with the aged Pt/CeZrO₂ catalyst. As with the water and CO₂ results, reducing the aged catalyst prior to reaction causes the H₂:CO ratio to trend with those of the fresh Pt/CeZrO₂ catalyst, indicating similar net reaction profiles for all three tests.

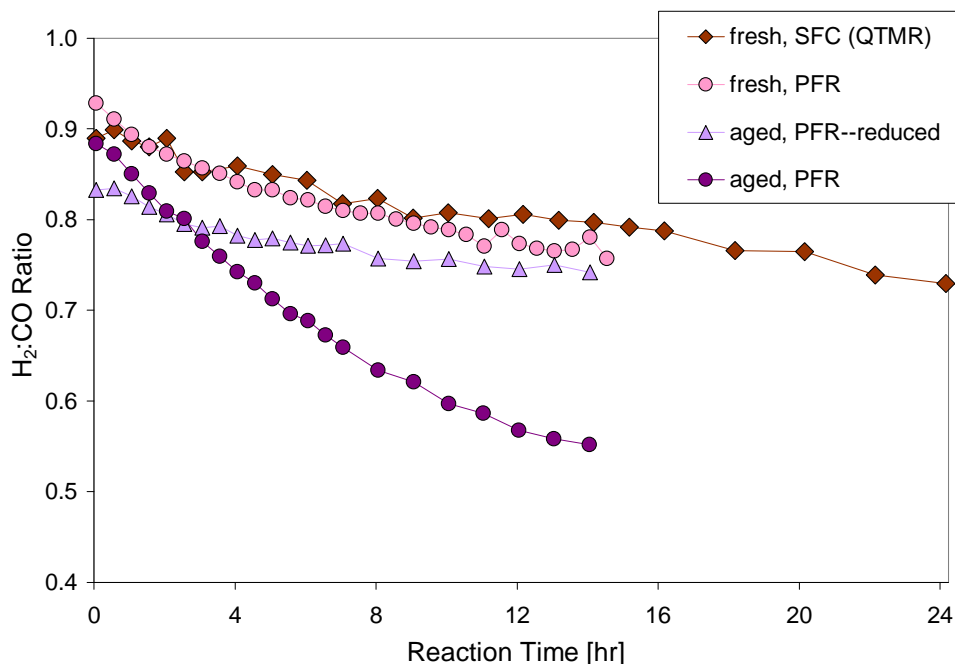


Figure 9.13: H₂:CO ratio during CO₂ reforming over aged and fresh Pt/CeZrO₂ catalyst in both reactor types with no co-fed O₂. Reaction temperature=800 °C, GHSV=150 L/h/g_{cat}, CH₄:CO₂:Ar/O₂ feed ratio=4:4:2.

9.3.4: The impact of the CeZrO₂ support on catalyst activity

Reduction shifted the initial behavior of the aged Pt/CeZrO₂ catalyst in the direction of the Pt/ZrO₂ catalyst behavior for methane conversion, H₂:CO ratio, and water production. Because the ZrO₂ support is believed to be less active than the CeZrO₂ support, these shifts imply that reduction can decrease the initial activity of the CeZrO₂ support. The fact that the catalyst recovers its expected behavior, indicates that the support can recover its activity by exposure to other oxygen sources (e.g., CO₂) over the course of a test. It also confirms the earlier conclusion that the diminished initial activity is caused at least in part by support oxygen depletion.

When applied to the trends for the unreduced, aged Pt/CeZrO₂ catalyst in Figures 9.10 through 9.13, the same line of reasoning illuminates the important contribution of the support. The catalyst has been aged and the metal particles should therefore be more oxidized than those in the fresh catalyst, but the support has not been reduced and should therefore contain more oxygen than

the reduced catalyst. In spite of the oxidation state of its platinum particles, the unreduced catalyst is initially more active than the reduced catalyst and behaves more like the “fresh” catalyst. Because the support is not reduced in this case, its potential to contribute to methane conversion should be comparable to that of the fresh catalyst’s support.

The relatively high initial methane conversion with the unreduced aged catalyst confirms that the support has some ability to compensate for oxidized metal particles. However, the poor extended behavior betrays the degraded state of the catalyst and underlines the importance of metal reduction to extended catalyst activity. The reduced aged catalyst, on the other hand, exhibits the opposite behavior: its activity recovers over time on stream from its low initial level, presumably as the support replenishes its oxygen content in the course of reaction while the reduced platinum particles remain relatively unoxidized. CO₂ acts as the oxygen source for the CeZrO₂ support, putting this mechanism in the same category as that proposed earlier for the SFC membrane.

Oxidation Factors will be presented and discussed in more detail below, but it is important to note here that they are generally very low with the Pt/CeZrO₂ catalyst, even in the aged catalyst test. The Pt/CeZrO₂ catalyst did not appear to promote combustion in this work regardless of reactor configuration, pre-reaction oxidation state, or oxygen source.

9.4: Other Catalyst Performance Comparisons

9.4.1: Oxidation Factor

The Oxidation Factors calculated for the Pt/CeZrO₂ tests are low, but the relationships between Oxidation Factors for different tests are consistent with observations for the Pt/ZrO₂ catalyst. Figure 9.14 compares results for the two catalysts in the PFR. As expected from the preceding conversion/product ratio evaluations, the Oxidation Factors for Pt/ZrO₂ are higher under all reaction scenarios.

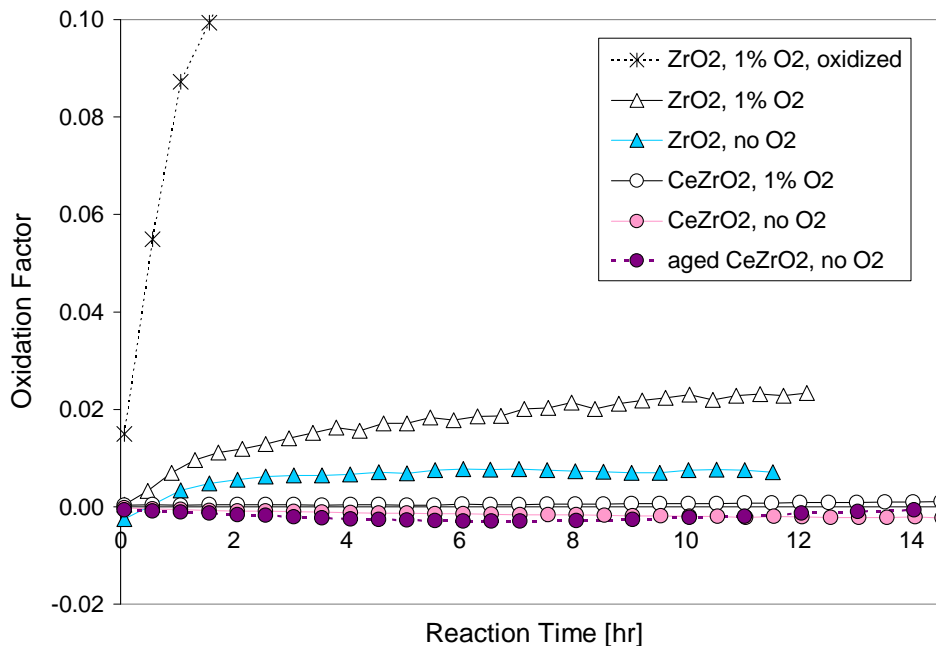


Figure 9.14: Oxidation Factor during CO₂ reforming over a Pt/ZrO₂ and a Pt/CeZrO₂ catalyst in the PFR. Reaction temperature=800 °C, GHSV=150 L/h/g_{cat}, CH₄:CO₂:Ar/O₂ feed ratio=4:4:2.

Figure 9.15 compares QTMR results for both catalyst types. Once again, Pt/CeZrO₂ produces smaller Oxidation Factors for each analogous reaction type, and, once again, the reaction types have the same relationship to each other as do their Pt/ZrO₂ test counterparts. The similar Oxidation Factors for the SFC test and the blank test with no oxygen represent the only significant difference in the Pt/CeZrO₂ data set. With the Pt/ZrO₂ catalyst, the blank test with no oxygen has slightly but consistently higher Oxidation Factors than the SFC test. This further reinforces the conclusion that the effect of the CeZrO₂ support is intrinsically similar to the effect of the SFC membrane under CO₂ reforming conditions.

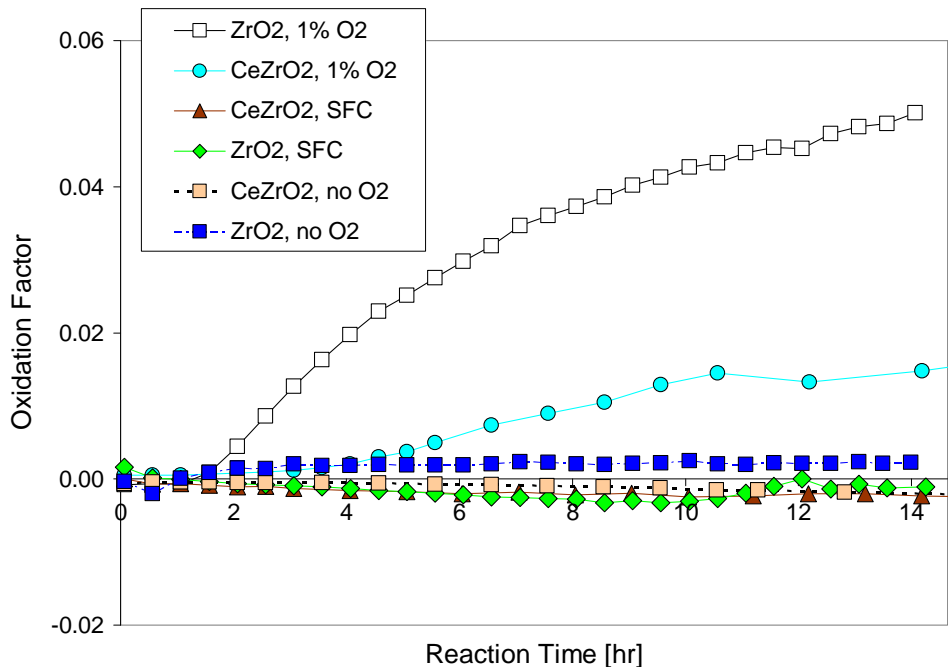


Figure 9.15: Oxidation Factor during CO₂ reforming over a Pt/ZrO₂ and a Pt/CeZrO₂ catalyst in the QTMR. Reaction temperature=800 °C, GHSV=150 L/h/g_{cat}, CH₄:CO₂:Ar/O₂ feed ratio=4:4:2.

Figure 9.16 presents a magnified view of the results for fresh Pt/CeZrO₂ catalyst from both reactor types to demonstrate the small but noticeable difference in Oxidation Factor for the lone Pt/CeZrO₂ test with co-fed oxygen. The numerical differences might be negligible, but the difference in trends is not. The test with co-fed O₂ is clearly increasing in undesirable oxidation, while the tests with no co-fed O₂ are not. A slightly but steadily increasing amount of rWGS could explain the downward trend of the tests without co-fed O₂. *NOTE: the negative values have no conceptual meaning, but they do serve as a reminder of the theoretical nature of the Oxidation Factor. In general, very small positive and negative values are considered the equivalent of zero, but consistent trends are considered significant, regardless of the values involved.*

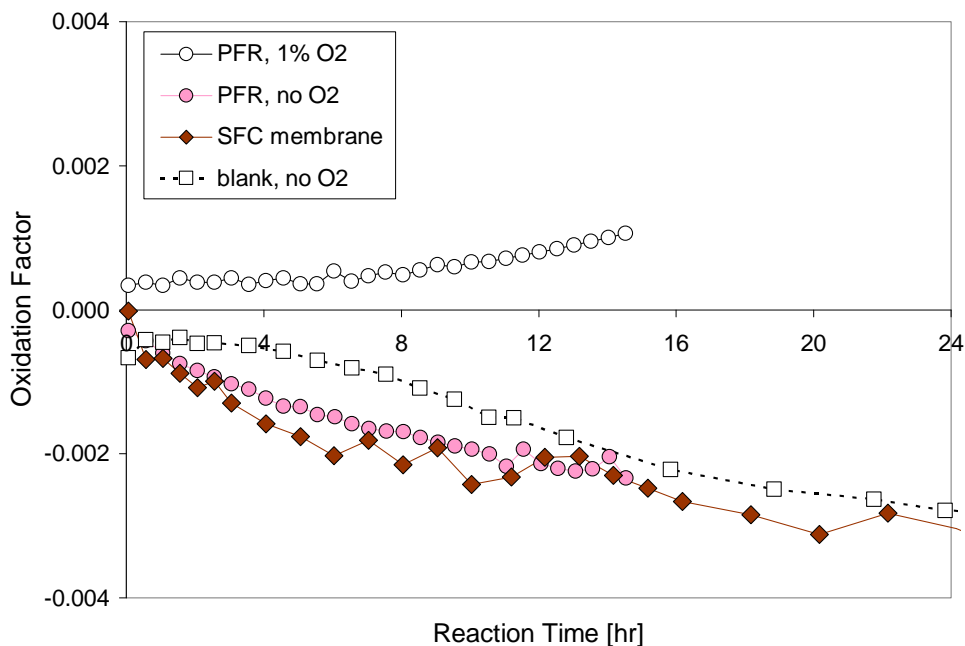


Figure 9.16: Oxidation Factor during CO₂ reforming over a Pt/CeZrO₂ catalyst in both reactors. Reaction temperature=800 °C, GHSV=150 L/h/g_{cat}, CH₄:CO₂:Ar/O₂ feed ratio=4:4:2.

9.4.2: Reverse Water-Gas Shift

As first presented in Chapter 8, the relative extent of the rWGS reaction can be estimated by reaction stoichiometry using reactor effluent composition and reactant conversions. Figure 9.17 provides rWGS extent of reaction results relative to the extent of methane conversion that can be compared with those in Figure 8.17 for the Pt/ZrO₂ catalyst. As with the Pt/ZrO₂ catalyst, co-fed O₂ does not appear to affect the relative amount of rWGS, nor does the presence of the SFC membrane. The lack of a membrane effect on rWGS activity with the Pt/CeZrO₂ catalyst represents significant difference between the two catalysts, as do the generally lower levels of relative rWGS activity, which confirm the superior selectivity of the Pt/CeZrO₂ catalyst.

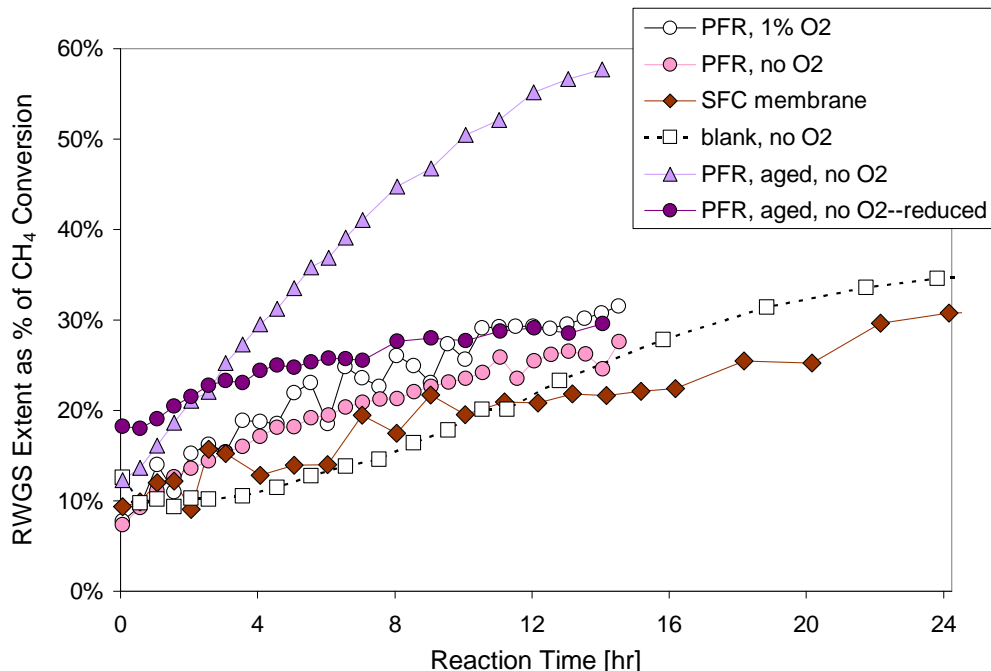


Figure 9.17: RWGS extent during CO₂ reforming over a Pt/CeZrO₂ catalyst in both reactor types. Reaction temperature=800 °C, GHSV=150 L/h/g_{cat}, CH₄:CO₂:Ar/O₂ feed ratio=4:4:2.

The unreduced aged catalyst represents the one exception to the trends with the Pt/CeZrO₂ catalyst. Although unreduced aged catalyst test takes significantly longer to get there than the Pt/ZrO₂ catalyst tests, it approaches the level of relative rWGS activity observed in the Pt/ZrO₂ catalyst tests. In fact, a comparison of the product/conversion ratios of interest shows that it closely approaches the net reaction profile of the PFR test of the Pt/ZrO₂ catalyst with no co-fed O₂. Aging decreases the beneficial effect of the ceria that was added to promote the activity of the zirconia support, producing something with an effect more like pure zirconia.

9.4.3: Carbon deposition

Several additional post-reaction catalyst oxidation tests were performed to estimate the amount of deposited carbon. The procedure described in Section 7.6 is used, and Figure 9.17 provides a summary of the available post-reaction carbon oxidation data.

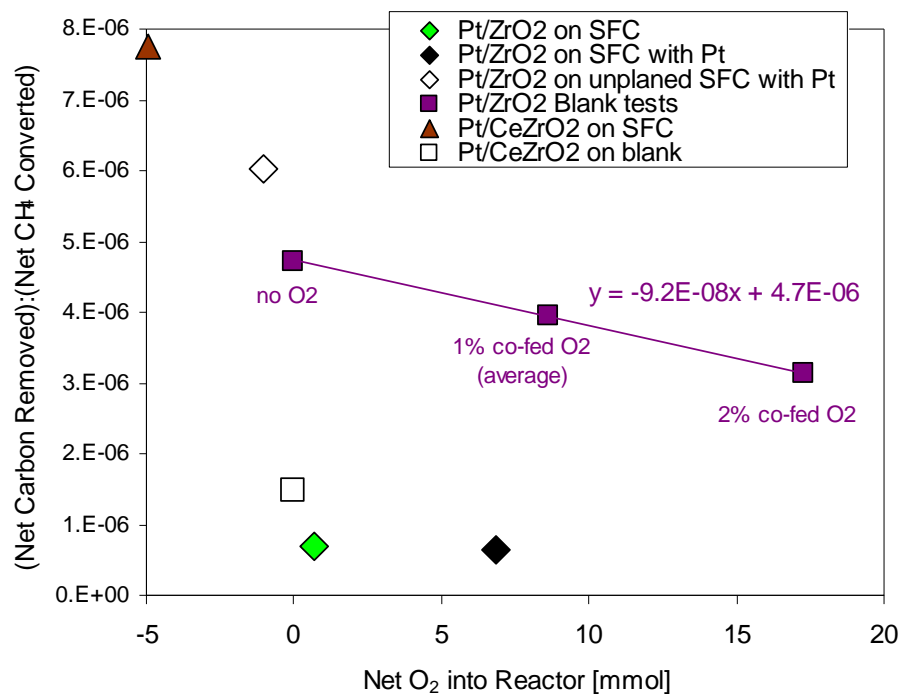


Figure 9.18: Molar ratio of net carbon removed-to-net CH₄ converted from Pt/ZrO₂ and Pt/CeZrO₂ catalysts following CO₂ reforming in the improved QTMR. Obtained by oxidation at 800 °C using 500 μl injections of 10% O₂/Ar into Ar at 20 ccm.

As described in Chapter 7, the carbon accumulation ratio is calculated by dividing the moles of carbon removed by the net moles of methane converted over the duration of the test. This approach is used because test duration is not constant among the tests and conversion activity can vary widely. Net methane converted and net oxygen available are each calculated by summing the estimates from each sample point over the subsequent time interval.

The SFC membrane Pt/CeZrO₂ test that produced the highest relative carbon deposition of any test evaluated for carbon also happened to exhibit a fairly substantial net negative oxygen influx into the reactor over the course of the test, as shown by the membrane flux estimate profile in Figure 9.9. The net negative oxygen for this test coupled with high carbon deposition supports the idea that the catalyst uses CO₂ decomposition to replenish its oxygen content. Conversely, the relatively low carbon deposition in the corresponding blank test with Pt/CeZrO₂ implies that any carbon deposition

that occurs as part of the CO₂ reforming reaction mechanism is reversible under the appropriate operating conditions.

The persistent high activity throughout the Pt/CeZrO₂ test on the SFC membrane in spite of the relatively high carbon deposition gives additional credibility to the suggestion that the support is engaging the CO₂ molecules and thus retaining the deposited carbon. If the carbon were collecting on the metal particles rather than on the CeZrO₂ support, the catalyst activity would be expected to diminish.

9.5: Observations and Conclusions from Chapter 9

- (1) Regardless of reactor system, the Pt/CeZrO₂ catalyst exhibits less rWGS activity than the Pt/ZrO₂ catalyst as well as greater methane conversion.
- (2) The Pt/CeZrO₂ catalyst does not exhibit significant combustion activity in the co-fed O₂ or SFC membrane scenarios tested in this work, nor does time on stream correspond to increasing undesirable oxidation activity to the extent that it does with the Pt/ZrO₂ catalyst.
- (3) With either catalyst, the majority of oxygen added to the reactor ultimately goes to hydrogen oxidation rather than CO oxidation, regardless of the reaction pathway involved or the test scenario.
- (4) The Pt/CeZrO₂ catalyst interacts with gas-phase oxygen in the reactor, likely via redox reactions with the support lattice. The ZrO₂ support exhibits little if any of the same behavior under the CO₂ reforming conditions used in this work.
- (5) The CeZrO₂ support appears to have a similar beneficial effect on catalyst activity as the SFC membrane with the Pt/ZrO₂ catalyst, at least until it becomes too oxygen-depleted to maintain this effect. This could explain the delayed appearance of the membrane effect with the Pt/CeZrO₂ catalyst as well as the similar reactions profiles with the blank and the SFC membrane before and after the membrane effect becomes noticeable.
- (6) Pre-reaction reduction of the Pt/CeZrO₂ catalyst actually decreases initial activity and shifts both methane conversion activity and product ratios toward those observed with the Pt/ZrO₂

catalyst. This emphasizes the importance of support oxygen content to the activity of the Pt/CeZrO₂ catalyst.

- (7) The PFR tests of aged Pt/CeZrO₂ catalyst conclusively confirm the possibility of *in situ* catalyst reduction in a CO₂ reforming reactor.
- (8) Relatively high carbon deposition on Pt/CeZrO₂ in a membrane test with net negative oxygen input supports the idea that the catalyst uses CO₂ decomposition (or adsorption) to replenish its oxygen content. Relatively low carbon deposition in a corresponding blank test implies that such carbon deposition either doesn't occur or is reversible under certain reaction conditions.
- (9) Carbon deposition on the Pt/CeZrO₂ appears to occur primarily on the support rather than on the platinum particles.

References Cited in Chapter 9

1. Stagg-Williams, S.M., F.B. Noronha, G. Fendley and D.E. Resasco, *CO₂ Reforming of CH₄ over Pt/ZrO₂ Catalysts Promoted with La and Ce Oxides*. Jnl of Catal **194**, 2000, p.240-249.
2. Noronha, F.B., A. Shamsi, C. Taylor, G. Fendley, S.M. Stagg-Williams and D.E. Resasco, *Catalytic performance of Pt/ZrO₂ and Pt/Ce-ZrO₂ catalysts on CO₂ reforming of CH₄ coupled with steam reforming or under high pressure*. Catal Lett **90**(1-2), 2003, p.13-21.
3. Mattos, L.V., E. Rodino, D.E. Resasco, F.B. Passos and F.B. Noronha, *Partial oxidation and CO₂ reforming of methane on Pt/Al₂O₃, Pt/ZrO₂, and Pt/Ce-ZrO₂ catalysts*. Fuel Processing Technology **83**, 2003, p.147-161.
4. Wang, W., S.M. Stagg-Williams, F.B. Noronha, L.V. Mattos and F.B. Passos, *Partial oxidation and combined reforming of methane of Ce-promoted catalysts*. Catal Today **98**, 2004, p.553-563.

Chapter 10: Conclusions and Recommendations

In general, the collective reaction tests demonstrate conclusively that the SFC membrane provides a larger increase in CO₂ reforming activity than co-fed molecular oxygen and that the activity benefit occurs only in conjunction with a powder reforming catalyst. The powder catalyst performance enhancement includes somewhat improved reaction selectivity (i.e., more favorable net reaction profiles, as defined in Section 2.7), as well as both greater initial and more persistent catalyst activity. Although apparent oxygen flux with the SFC membranes during CO₂ reforming is lower than was anticipated when this work was first proposed, the benefits of the SFC membrane appear to depend at least as much on the mere presence of the membrane as on membrane oxygen production.

The results of this initial exploratory study are encouraging enough to recommend additional work in the area of membrane oxygen-assisted CO₂ reforming. The hypotheses derived in this work also differ substantially enough from published speculation about the nature of O-MIEC membrane behavior in reforming reactors to merit deeper investigation. Guided by these hypotheses, additional studies of the fundamental phenomena involved should be able to produce a definitive mechanistic theory of the membrane effect in reforming reactors. If the mechanistic evidence ultimately supports the hypotheses from this work, O-MIEC membrane reactor design and reaction application options might need to be substantially altered.

10.1: Overview of Primary Ideas

10.1.1: Net reaction profiles

Net reaction profiles (i.e., estimates of the distribution and extent of molecular-level reactions such as combustion, CO₂ reforming, and rWGS) are a valuable tool for exploring the practical impact of reactor operating conditions, including catalyst choice and the incorporation of a chemically-active membrane. Although they do not individually provide direct insight into the fundamental reactions involved in either the membrane effect or the effect of catalyst oxidation state, collective differences

in net reaction profiles across a range of reactor operating conditions can provide valuable indirect insight into the fundamental reactions.

Rigorous reactor effluent data collection and analysis, which can be challenging and time-consuming, is the key to obtaining meaningful distinctions using this approach. On the positive side, such an approach requires only very careful experimentation as opposed to exotic or elaborate equipment. Given the extreme operating conditions of a methane reforming membrane reactor (i.e., an 800 °C reactor system with which leaks must be avoided as much as possible), real time *in situ* chemical analysis that does not disrupt the reaction system may be prohibitively difficult. The use of reactor feed and effluent compositions to establish net reaction profiles offers a valuable first-pass strategy for determining the primary effects of certain reactor operating conditions or catalyst oxidation state changes. Net reaction profile analysis therefore provides an efficient and economical initial approach to analyzing a complex situation such as the application of an O-MIEC membrane in CO₂ reforming.

A recent publication by Michael et al. reinforces the value of this approach [1]. The reaction apparatus and experimental approach used in the Michael study is substantially different than the membrane reactors used in this work (their reactor is adiabatic, their catalyst loading and oxygen feed levels are much higher, and they studied partial oxidation with added CO₂ and water rather than CO₂ reforming with added oxygen). However, the data analysis approach used is similar in that they analyze the levels of all possible products and draw conclusions about net reaction profiles from the detailed product data. The conclusions of Michael et al. on net reaction priority and probable pathways also mirror (and thus support) those determined in this dissertation.

10.1.2: The influence of reduction on catalyst activity

Because methane decomposition is believed to occur directly on the catalytic metal particles (platinum, in this case), the oxidation state of the metal should be a critical factor for methane

reforming reactions. Proper metal reduction is important for high catalyst activity, but reduction processes are also known to increase particle size and thus reduce total metal surface area and perimeter. In other words, reduction can increase the activity of the available catalytic metal while simultaneously decreasing the amount of perimeter metal. Promoted supports, such as the ceria-promoted zirconia support used in this work, can minimize this effect by minimizing the degree of pre-reaction reduction needed and allowing *in situ* reduction in the early stages of a reaction run. The use of ceramic membranes as a reactor surface appears to have the same potential but with possible advantages even over a catalyst support with high activity.

This work confirms that *in situ* reduction can occur in a CO₂ reforming reaction environment and that an SFC membrane reactor can promote it. Removing or significantly reducing hydrogen requirements in syngas producing reactor systems could have valuable commercial implications, but even more important than that are the persistent benefits and the operational simplicity of a membrane reactor. The membrane appears to provide the equivalent to the catalyst bed of an ongoing low-level reduction process. If this effect is real and can be optimized, it could allow substantial economic savings for syngas production.

10.1.3: *In situ* oxidation and reduction

Tests with two different catalysts, three different reactors, and a variety of pretreatment conditions have shown repeatedly that the membrane effect is similar to but more persistent than the effect of a pre-reaction reduction process. All available evidence correlates the beneficial effect of the SFC membrane with similar effects in tests without a membrane that are caused by factors that influence (or are highly likely to influence) catalyst oxidation state. Across all tests with the SFC membrane, the membrane effect is qualitatively consistent regardless of membrane oxygen flux level and appears to be caused by either *in situ* catalyst reduction or diminished *in situ* oxidation during reaction.

Factors that increase the chance of catalyst oxidation are correlated with increased relative water production as a result of either increased rWGS activity, increased full product oxidation activity, or a combination of the two. Factors that increase the likelihood of catalyst reduction are correlated with lower relative water production and otherwise diminished evidence of rWGS and/or undesirable oxidation reactions. These trends hold for both the Pt/ZrO₂ and the Pt/CeZrO₂ catalysts and for the SSMR, QTMR, and PFR.

10.1.4: Support-SFC analogy

As discussed in Chapter 2, methane decomposition has been proposed in the literature as the rate-limiting step and is believed to occur on the metal particle itself. Because hydrocarbon molecules are believed to interact with the catalytic metal particles, only molecules that adsorb near the perimeter of a platinum particle can also interact with the catalyst support material. Electronic conductivity in a catalyst support material can also enhance metal-support interactions.

The clear and consistent differences in the performances of the Pt/ZrO₂ and Pt/CeZrO₂ catalysts confirm that the mechanisms of the reactions of interest involve the catalyst support. The electronic conductivity and reducibility of the CeZrO₂ support in turn implies that it is capable of interacting electrochemically with the oxygen-supplying molecules (whether O₂ or CO₂, in this work), while the ZrO₂ is largely inert and possesses only limited capability for redox reactions or electron transport. The CeZrO₂ support appears to act as an oxygen exchange intermediate by facilitating the transfer of oxygen from the oxygen-supplying species to the oxygen-receiving species. CeZrO₂ likely promotes methane conversion via CO₂ reforming by providing a surface with labile oxygen species that facilitate oxygen exchange at the metal-support perimeter. The CeZrO₂ surface is thus expected to interact with CO₂, even to the point of potentially replenishing its own oxygen content by reducing CO₂ if the CeZrO₂ lattice becomes sufficiently reduced under reaction conditions.

The SFC membrane material provides a similar function but with a significantly greater capability for electron conduction and lattice oxygen release. The ready availability of oxygen ions and electron holes in the SFC lattice explains why combustion is more prominent than CO₂ reforming when platinum particles are placed directly on the SFC surface—oxygen is so easily extracted from SFC that complete oxidation occurs at the platinum-SFC interface rather than CO₂ reforming. In other words, methane decomposition on a platinum particle in direct contact with SFC yields water rather than hydrogen, and CO₂ is unnecessary as a reactant. Instead, additional CO₂ is produced by carbon oxidation following methane decomposition. The relatively high electronic and ionic conductivity of the SFC substrate also expands the active area around each platinum particle, leading to even more oxidation activity. A combination of hydrogen spillover from the platinum particle and oxygen and electron transport through the SFC lattice could explain the high turnover frequencies and extensive combustion observed with the platinum-patterned membranes.

The CeZrO₂ support, in contrast, appears to require the concurrent (or near concurrent) presence of hydrogen from methane decomposition on a platinum particle and CO₂ as an oxygen source at the platinum-support interfacial perimeter. This mechanism is substantially more restrictive and therefore allows CO₂ reforming, stopping short of combustion. The very small amount of platinum on the 0.43 wt% Pt/CeZrO₂ catalyst and its high dispersion does not provide sufficient contact with the SFC surface to participate in a detectable amount of combustion.

10.1.5: Direct catalyst-membrane interactions

A final significant observation of the behavior of the two catalysts involves their effect on the SFC membrane. Membrane oxygen flux estimates during reaction were lower with the Pt/CeZrO₂ catalyst than with the Pt/ZrO₂ catalyst, with more variability and also more negative flux values. This indicates the possibility of solid state reactions between the catalyst and the membrane. Such interactions are unlikely with the largely inert (i.e., non-conductive) ZrO₂ support, but they are not

surprising with the Pt/CeZrO₂ catalyst given the greater electrochemical activity of the CeZrO₂ support material.

However, because of the very small quantity of platinum on the supported catalysts evaluated in this work (< 0.5 wt%) and the ~1 mm catalyst layer depth, it is believed that direct platinum-membrane interactions are negligible in the membrane reactor tests. It is possible that the support can act as the solid-state chemical intermediate required for the platinum metal and the O-MIEC membrane material to exchange species via solid-state transport mechanisms such as spillover and surface diffusion, but this would require a support with relatively high oxygen activity and electronic conductivity and even then the contribution should be minor compared with gas-phase transport. The results with the Pt/CeZrO₂ catalyst and its known electrochemical activity somewhat encourage this line of reasoning, but the results with and properties of the Pt/ZrO₂ indicate no support-membrane interactions. In any case, the probability of a significant amount of direct platinum-SFC interaction with the powder catalysts in this work is virtually zero.

An electrochemically active support provides the only reasonable possibility for chemical interaction between the membrane and the powder catalyst, but even the Pt/CeZrO₂ catalyst exhibits CO₂ reforming activity rather than combustion activity of the platinum-patterned membranes. The correspondingly high initial activity of the CeZrO₂ supported catalyst on the blank also confirms that any support-SFC interactions with the Pt/CeZrO₂ catalyst occur to a limited extent or at a limited rate relative to its native activity.

If the CeZrO₂ support participates to a limited extent in some form of electrochemical interaction with the SFC membrane and if they also have a similar mode of interaction with the gas-phase species present in these tests, this would explain both the initial similarity and the eventual deviation of the blank test and the SFC membrane test discussed in Chapter 9. The deviation late in the second part of the test period could indicate that interactions with gas-phase species eventually

diminished the activity of the CeZrO₂ support on the blank via lattice oxygen depletion while the SFC membrane was able to delay this effect in the corresponding membrane test. This speculation leaves open the possibility of membrane-catalyst interactions when the catalyst support has high electrochemical activity. However, the evidence against membrane interactions with the low activity ZrO₂ support is conclusive.

10.1.6: Oxygen-assisted CO₂ reforming

Oxygen-assisted CO₂ reforming with co-fed O₂ shows some promise with the Pt/ZrO₂ catalyst but little effect over the short-term with the more active Pt/CeZrO₂ catalyst. Using an O-MIEC as the oxygen source, on the other hand, produces a different and potentially more valuable set of benefits than co-fed O₂. When the costs of obtaining pure O₂ are considered, the benefits of gas-phase O₂ do not appear to be sufficiently valuable to pursue with the Pt/CeZrO₂ catalyst. However, the SFC membrane remains a viable option even with the higher activity catalyst, in part because of the potentially low cost.

In general, the use of O-MIEC membranes as a source of small amounts of oxygen into a CO₂ reforming reactor system appears to be a promising strategy to enhance catalyst activity and longevity. The complete activity mechanism remains to be elucidated, but there is clear potential value to this approach for reactions with high deactivation rates such as CO₂ reforming that could benefit from low levels of highly distributed oxygen. The clear distinction observed between the respective effects of gas-phase O₂ and the SFC membrane emphasizes the importance of using the SFC membrane in close proximity to, if not direct contact with, the powder catalyst.

Design efforts for membrane reactors need to acknowledge the strong evidence that the beneficial reaction mechanisms involve no gas-phase oxygen. Given the relatively high water production and low H₂:CO ratios observed in this work, a multi-stage reactor is likely to be the most effective approach. Rather than presume gas-phase oxygen could be present downstream of the

membrane surface or that combustion will occur in the membrane stage (both of which have been proposed in the literature), it would be best to put the membrane stage first and design the next stage to accommodate high water levels. A membrane reaction stage followed by a steam reforming and/or Water-Gas Shift reaction stage appears to be a promising arrangement.

10.2: Review of the Proposed Hypotheses

Seven hypotheses were proposed in Chapter 6 to be discussed in Chapters 6 through 9. As these hypotheses were determined in the course of this work rather than in advance, it is not surprising that all were found to be justified. They are provided again here as a final reminder of the fundamental concepts that were derived from careful experimental observation and a thorough analysis of the objective test results.

- (1) In the presence of H₂ at high temperature, an SFC membrane does not evolve any gas-phase O₂ but rather oxidizes hydrogen exclusively. SFC does evolve gas-phase O₂ in a non-reducing high temperature environment.
- (2) Only two reactions occur to a significant extent on the SFC surface under CO₂ reforming reaction conditions: H₂ oxidation and CO₂ reduction. The surface must be reduced by H₂ for CO₂ reduction to occur. *NOTE: under the appropriate conditions, CO oxidation should also be possible on an SFC surface, but these tests have too much CO₂ in the feed to observe this.*
- (3) Pt/ZrO₂ catalyst exposed to gas-phase oxygen while at high temperature promotes H₂ oxidation (and possibly complete combustion) more readily than catalyst exposed only to inert or reducing environments which is more likely to promote CO₂ reforming. Platinum oxidation state is therefore affected by gas-phase oxygen even under CO₂ reforming conditions and is a key determining factor for both catalyst activity and reaction selectivity.
- (4) The use of an SFC membrane as a powder catalyst substrate may promote *in situ* catalyst reduction and/or decrease *in situ* oxidation under CO₂ reforming conditions.
- (5) If oxygen is available, combustion is the dominant methane-consuming reaction in the presence of a non-selective catalyst such as oxidized Pt/ZrO₂ or a platinum-patterned SFC membrane.

- (6) A plain SFC surface promotes rWGS in a process referred to as “membrane-facilitated rWGS.” The Pt/ZrO₂ catalyst also promotes rWGS, with the amount of rWGS relative to methane conversion increasing as the catalyst degrades. These related but distinct phenomena are the cause of the low H₂:CO ratios observed in the later stages of all tests with the Pt/ZrO₂ catalyst.
- (7) Steam reforming can occur in a membrane reactor with a CO₂ reforming feed when a powder reforming catalyst layer is added to an SFC membrane. Water produced on the membrane surface by hydrogen oxidation can participate in steam reforming as it passes through the powder catalyst layer after leaving the membrane surface. The combined reaction is stoichiometrically indistinguishable from partial oxidation with membrane oxygen but is substantially more likely.

These hypotheses were derived from the thorough molecular-level examination of a novel CO₂ reforming reactor system created for this dissertation. They can be used to interpret the observations of other researchers in the field of O-MIEC membrane reactors. They also can help narrow the scope of future fundamental investigations in this field. Most important, perhaps, if future fundamental investigations confirm their accuracy, these hypotheses will provide an improved conceptual foundation for establishing priorities in O-MIEC reactor design and performance optimization for any reforming application.

Without a proper understanding of what is actually happening at the membrane surface, neither fundamental research attempts nor reaction engineering attempts are likely to arrive at the best possible results. This work provides a thorough evaluation of the molecular-level effects of O-MIEC membranes, catalyst oxidation state, and reactor feed composition that begins to fill a key gap in the published work of this field. The assumption made by other researchers that membrane oxygen in reforming reactors is utilized as gas-phase O₂ do not appear to be correct. Also, the generally incomplete analysis of reactor effluent data in the O-MIEC reactor literature leaves important questions unanswered. As these previously unanswered questions have critical implications for effective reactor design, the work in this dissertation is a valuable step toward developing our

understanding of the phenomena that underly the intriguing potential of O-MIEC ceramic membrane reactors.

10.3: Recommendations for Future Work

The seven hypotheses provided here contain, intrinsically, the recommended basis for future work. In other words, future work should endeavor to validate or invalidate these seven hypotheses. They were developed and evaluated for this reason and their merit or lack thereof will help establish the priorities for future O-MIEC membrane reactor applications beyond those discussed in this dissertation. Specific to the ongoing work in the Stagg-Williams lab, there are several important and related investigations that would provide valuable insight into the shortcomings and advantages of this experimental approach for testing reforming reactions in an O-MIEC membrane reactor.

10.3.1: Water condensation in the reactor system

Water control and quantification is the most obvious area for improvement in the currently established testing and data analysis methodologies.

To improve resolution in the downstream analytical equipment, many researchers use an inline condenser to remove water from the stream between the reactor and the instruments. This is apparently assumed not to impact the levels of other components in the gas stream analysis, but CO₂ is highly soluble in water. At a minimum, the amount of condensed water should then be determined and an estimate should be made of the amount of dissolved CO₂, but no mention of such efforts is made in the literature. To avoid compromising the material balance with these issues, the lines were heated in an attempt to keep all components in the gas phase throughout the system.

This strategy was effective with the PFR, which has short lines and uses a higher flowrate. It was also effective with low conversion tests in the QTMR. However, the higher conversion tests clearly exhibited significant water condensation in the QTMR system lines. By keeping the lines hot, CO₂, H₂, and CO dissolution in the water should have been minimal, but the water adsorption had to

be accounted for in the effluent data analysis. This was believed to be done accurately using a hydrogen balance, but the potential for bias raises concerns about material balance accuracy.

Because the amounts of water involved are relatively small, adsorption doesn't have a significant impact on methane conversion calculations and doesn't affect H₂:CO ratio (which might explain why these are the two most common metrics in studies of this kind). However, missing water from adsorption (and additional water from desorption) is a critical issue for calculating oxygen flux during reaction and also for calculating the Oxidation Factor proposed in Chapter 8. It is therefore suggested that additional heating and insulation should be added to the lines for tests with effluent water concentrations under ~10 mol%. In this case, efforts should also be made to quantify water content analytically. The gas chromatograph cannot accomplish this as currently used, although the mass spectrometer data can at least indicate trends and thus confirm or contradict hydrogen-balance derived estimates. A two-column approach with the GC should allow water to be measured directly, which would then allow direct calculation of membrane oxygen flux during reaction.

For tests with higher flux O-MIEC membranes that could produce quantities of water greater than 10 mol%, a condenser might be necessary to protect analytical equipment. If so, efforts should be made to quantify the rate of production and CO₂ content of the condensed water. A condenser with a level control mechanism (to allow water production rate to be determined) and a pH probe for the collected condensate (to estimate dissolved CO₂ content) is one example of a system that could accomplish this.

10.3.2: Carbon collection on the SFC membrane

Carbon fate determination is the biggest area of concern for the currently established testing and data analysis methodologies.

Although water condensation is a critical experimental concern, it is believed that the material balance approach used in the data analysis accounts for it successfully. However, this

presumes the carbon balance is managed correctly. The carbon balance is therefore the most fundamental piece of information in the reaction data analysis presented. As a result, adsorption or incorporation of carbon and/or carbonate species on or into the SFC membrane surface is the unexplored topic with the greatest potential impact on the conclusions in this work. The potential importance of carbonate adsorption on O-MIEC membrane surfaces was mentioned on occasion in the literature, most emphatically by Shao et al [2], although their ultimate conclusion was that it was not a significant problem in a hydrogen-containing reaction environment.

In this work, occasional anomalies in CO₂ quantities in the reactor effluent data were suspected in certain PFR and QTMR blank tests, but these are clearly not related to an SFC membrane. Because of the significant amount of water adsorption that is known to occur in the effluent lines, the suspected CO₂ deficits, if they actually exist, were considered water-CO₂ interactions. In addition, the post-reaction catalyst carbon removal tests did not indicate sufficient carbon deposition on the catalyst to impact a material balance perceptibly. However, the SFC membrane surface was not tested post-reaction for carbon or carbonate content.

Determination of the potential of SFC for carbon collection and/or carbonate adsorption is the most important remaining step to validate the overall analytical approach used in this work. A combination of thermogravimetric analysis (TGA) and mass spectrometer-monitored desorption (TPD) and oxidation (TPO) tests on post-reaction SFC membrane pieces would be the simplest approach to this. If conclusive results cannot be obtained with a combination of these three tests, comparisons of fresh and used membrane material via electron-dispersive x-ray analysis (EDX) and powder X-ray diffraction (XRD) for, respectively, element content and crystal structure content and integrity would be the next step.

10.3.3: Isotope tracer studies

Isotope tracer studies offer the easiest and most effective strategy for determining membrane oxygen fate and thus membrane activity mechanism(s).

Isotopically-labeled elements could be tested in a variety of ways. Exposing the oxygen source side of the membrane to labeled oxygen would allow oxygen flux to be evaluated more accurately. It also would allow membrane oxygen “breakthrough” times to be assessed, which would provide true flux rates through the membrane lattice by distinguishing between pre-existing oxygen that is “dumped” after an environment change and newly absorbed oxygen that has diffused from the oxygen source side of the membrane. In reaction tests, isotopically labeled membrane oxygen could be clearly distinguished from both leak oxygen and oxygen from CO₂. Not only would this clarify the reactions behind CO and H₂O production, it could even discriminate between CO₂ that passes through the system unreacted and CO₂ that is produced from CO oxidation on the membrane.

Isotopically-labeled oxygen in the membrane’s oxygen supply gas also enhances the usefulness of an alternative approach to net oxygen flux determination. Pure labeled oxygen could be charged into the “air side” of the reactor system (i.e., the oxygen supply side). This part of the oxygen system would be maintained at a constant pressure through the use of a regulator between the reactor’s air side and an oxygen supply reservoir. This oxygen supply reservoir would be charged initially and would then be allowed to drop in pressure as oxygen is consumed by the membrane.

The oxygen supply reservoir would need to be maintained at a higher pressure than the reactor air side, but this should not be a problem because the reactor air side could be maintained at just above atmospheric pressure (slight positive pressure is needed to minimize air incursions). A low-pressure regulator would allow make-up oxygen to pass as needed from the oxygen supply reservoir into the reactor’s air side. The pressure of the fixed-volume oxygen supply reservoir would be monitored to assess accurately the amount of oxygen that is taken up by the membrane over time. In this test scenario, the exposed perimeter surface of the membrane would need to be sealed to minimize oxygen uptake from the air in the furnace cavity.

The other options for reaction mechanism studies using isotopically-labeled elements involve using CO₂ with either labeled carbon or labeled oxygen or both in the reactor feed. Using labeled

CO₂ in the gas-phase feed would allow isotope tracer tests to be run with both SFC membranes and the stainless steel blank. It thus would allow catalyst-CO₂ interactions to be studied as well as membrane-CO₂ interactions. The utility of labeled oxygen in the CO₂ feed is similar to the use of labeled oxygen on the air side of the membrane. However, testing labeled carbon would also be useful.

If true temperature-programmed oxidation (TPO) testing could be done following a reaction with labeled CO₂ carbon, the mass spectrometer data from the TPO would implicate the original decomposition reaction that was responsible for any carbon deposition that occurred. Additionally, reaction testing (or SFC powder exposure testing) using CO₂ with both the carbon and the oxygen labeled followed by careful TPO would even be able to determine which carbon-containing species, if any, are adsorbed by SFC (e.g., is elemental carbon adsorbed or are carbonates; if carbonates, what are the carbon and oxygen sources?).

10.3.4: Membrane surface reaction thermodynamics

Reaction energetics for the membrane surface reactions need to be determined for SFC in its various states and under various feed conditions.

With the addition of the internal reactor thermocouple, the current QTMR system is capable of detecting changes in reactor effluent gas-stream enthalpy (see Appendix M for examples and an overview of key operating parameters for thermodynamic evaluation with the current system). To obtain membrane surface temperature estimates, the internal reactor thermocouple could also be positioned so that it is in contact with the membrane to determine actual catalyst bed temperatures. If possible, thermodynamic testing should be conducted in conjunction with the isotope tracer tests discussed above. This would help identify rate-limiting steps and could even allow the kinetics of some individual reactions to be estimated.

Thermodynamic testing in the QTMR would answer certain general questions. For examples, which reactions are favored in which conditions, and are the net reactions endo- or exothermic? As part of thermodynamic testing with the QTMR, it will be necessary to determine the actual pressure in the reaction chamber to allow the results to be compared to theoretical equilibrium compositions, which depend on pressure (Appendix N contains equilibrium compositions for atmospheric pressure). In addition to improving the interpretation of effluent composition data, knowledge of the actual reaction chamber pressure is needed to develop an accurate fluid mechanics model of the QTMR.

Another useful tool in the Williams lab for thermodynamic evaluation of surface reactions on SFC is the DSC/TGA (differential scanning calorimeter/thermogravimetric analyzer). High temperature gas exposure studies in the DSC/TGA would confirm the thermodynamics of reactions between SFC and gaseous species via the DSC while the TGA would simultaneously allow accurate mass changes to be determined for SFC surface reactions including oxygen evolution, oxygen uptake, carbon species adsorption, and carbon species oxidation or desorption. These exposure studies must include species-switching tests to evaluate short-lived transient effects. As the reaction tests discussed in this dissertation demonstrated, some of the most informative events occur shortly after exposing the SFC to its new environment and they sometimes only persist for minutes.

The proposed DSC/TGA test results cannot be interpreted with confidence without knowledge of the species involved in the surface reactions. Fortunately, that information can be obtained from the isotope tracer studies in the QTMR discussed in Section 10.3.3.

10.3.5: QTMR modeling and operational configuration

A reasonably accurate model of the QTMR reaction chamber is needed to evaluate gas-phase temperature readings and to properly compare QTMR test results with PFR test results.

A rigorous model for the system in its current state will require simultaneous momentum and energy balances and a numerical solution to predict effluent temperature changes. In addition to the

complex reaction chamber geometry (cylindrical coordinates with irregular boundary conditions and only one negligible dimension), the model must account for heat input from the external furnace and net enthalpy changes for the reactions that occur. It also must include heat capacity and volume changes on reaction for the gas phase and heat capacities and thermal conductivities for multiple solid materials (quartz tubing, SFC membrane, and possibly even the powder catalyst layer). The current QTMR configuration uses the reactor temperature control loop to control the external reactor temperature. This provides a constant temperature boundary condition for the reactor's external surface which translates to a temperature-dependent heat flux across the quartz tube wall. In light of these complexities, among others, it is worth noting that a stand-alone momentum balance would offer valuable insight into the actual amount of catalyst contact time, the fraction of the feed that contacts the catalyst bed (i.e., the complement of a bypass fraction), and the composition of the gas in contact with the membrane surface. As discussed in Appendix N, actual temperature changes in the gas-phase are not believed to be dramatic (e.g., $< 10\text{ }^{\circ}\text{C}$). A quasi-isothermal approach could thus yield a valuable model.

Switching the reactor temperature control signal to the new interior reactor thermocouple would convert the QTMR to a truly isothermal mode of operation. In actual practice, steady isothermal operation is unlikely to occur in the early portion of any reaction test with relatively rapid deactivation, but this approach is nevertheless recommended as a future strategy to minimize temperature variation within and among tests. It was not adopted in this work because the majority of the QTMR tests had already been performed under the reactor exterior control scheme at the time the interior thermocouple was installed, and systematic consistency was considered an important factor. Also, having the reactor feed pass through the outer tube allows better control of the reactor feed temperature and allows the internal thermocouple to more accurately reflect the temperature of the catalyst bed since it is located downstream of the bed rather than upstream.

It is important to note that changing the temperature control loop from the external to the internal thermocouple is a necessary prerequisite for switching the reactor feed from the external (i.e., annular) flow space to the interior tube. If the interior tube were used for the feed without the ability to directly control the reaction chamber temperature, the impact of enthalpy of reaction would be magnified because in this operational scenario the effluent, which now passes through the external annular space, must heat the reactor feed, which now passes through the inner tube. The other shortcoming to this approach is that the thermocouple would be positioned in the inlet stream and might not properly represent the temperature of the gases leaving the catalyst bed.

Both operational approaches have advantages and disadvantages, but acquiring experimental data for both scenarios is the best way to evaluate the robustness of any reactor model.

10.3.6: Membrane-catalyst proximity effect

The effect of the distance between the catalyst bed and the SFC membrane surface on catalyst activity level and effluent composition (i.e., reaction profile) should either confirm or discredit the mechanistic hypotheses in Section 10.2.

If moving the catalyst bed downstream from the membrane surface results in catalyst activity levels and effluent compositions in the direction of those observed in the blank tests with co-fed oxygen, the hypotheses are confirmed. If no changes or different changes are observed, the inconsistent hypotheses must be revisited as appropriate. Beyond some threshold distance at which molecular dispersion of the catalytic reaction products back to the membrane surface becomes negligible, a membrane test should resemble a blank test with a similar amount of co-fed oxygen. Therefore, a set of proximity tests should include a confirmatory blank test at this threshold distance. They also should include more than one reactor feed flowrate to clarify the effect of flowrate on molecular dispersion in the QTMR.

The use of isotopically-labeled oxygen as the membrane oxygen source would be invaluable for a proper interpretation of the results from a series of membrane-catalyst proximity tests. A reactor model would benefit the planning of this set of tests and could, in turn, be improved by the resulting data analysis.

10.3.7: Other membrane materials and catalysts

Expansion of these methodologies to additional membrane and catalyst materials is necessary to establish their general utility.

The testing and data analysis techniques used in this work need to be applied to other membrane materials and catalysts. In particular, higher flux O-MIEC membrane candidate materials (see Table 2.2 for examples) and more affordable nickel-based catalysts should be tested [3-12]. As conventional nickel catalysts such as Ni/ γ -Al₂O₃ are well known to develop filamentous carbon deposits under CO₂ reforming conditions, the effect of an O-MIEC membrane on this behavior should be both interesting and easy to detect.

Adding a breadth of materials to this study would help validate the methodologies and also could illuminate any differences in mode of activity of the different membranes and catalysts. Tests of the impact of pre-reaction catalyst reduction on the membrane effect should be included in this kind of expansion, as this was not investigated in the QTMR. Improving the water handling capability of the system as described in Section 10.3.1 would make such pre-reaction reduction processes more feasible. In this vein, if water management were improved, the existing test foundation could be expanded by testing the Pt/ZrO₂ and Pt/CeZrO₂ catalysts on the SFC membrane with a pre-reaction reduction step. In comparison with the existing results without pre-reaction reduction, this testing should help determine the validity *in situ* reduction proposal.

10.3.8: Long-term testing

Long-term testing (e.g., more than 30 days on stream) is needed to establish the potential practical value of this strategy to improve CO₂ reforming.

The long-term effect of SFC and other O-MIEC membranes on catalyst activity and selectivity should be assessed before conclusions can be drawn about the practical benefit of this approach. More thorough post-reaction catalyst analysis also needs to be performed to determine the actual effect of the SFC membrane on the physical and chemical state of the catalyst. Before beginning any long-term testing with a particular combination of membrane material and catalyst, it is recommended that the general effect of catalyst contact time (i.e., reactor space velocity) on reaction profile and the approximate dependence on membrane oxygen flux of optimal catalyst contact time should be determined to establish baseline operating conditions. A designed multivariate experiment can then be conducted during the long-term testing to assess these effects and their interactions and thereby begin determining a set of guidelines for membrane reactor operation optimization.

References Cited in Chapter 10

1. Michael, B.C., A. Donazzi and L.D. Schmidt, *Effects of H₂O and CO₂ addition in catalytic partial oxidation of methane on Rh*. *Jnl of Catal* **265**, 2009, p.117-129.
2. Shao, Z.P., H. Dong, G.X. Xiong and W.S. Yang, *Syngas Production Using an Oxygen-Permeating Membrane Reactor with Cofeed of Methane and Carbon Dioxide*. *Chinese Chemical Letters* **11**(7), 2000, p.631-634.
3. Wang, H., Y. Cong and W. Yang, *Investigation on the partial oxidation of methane to syngas in a tubular Ba_{0.5}Sr_{0.5}Fe_{0.2}O_{3-δ} membrane reactor*. *Catal Today* **82**, 2003, p.157-166.
4. Feng, S.J., S. Ran, D.C. Zhu, W. Liu and C.S. Chen, *Synthesis gas production from methane with SrFeCo_{0.5}O_y membrane reactor*. *Energy & Fuels* **18**, 2004, p.385-389.
5. Gu, X., L. Yang, L. Tan, W. Jin, L. Zhang and N. Xu, *Modified Operating Mode for Improving the Lifetime of Mixed-Conducting Ceramic Membrane Reactors in the POM Environment*. *Ind Eng Chem Res* **42**, 2003, p.795-801.
6. Choudhary, V.R., K.C. Mondal and T.V. Choudhary, *Partial oxidation of methane to syngas with or without simultaneous steam or CO₂ reforming over a high-temperature stable NiCoMgCeO_x supported on zirconia-hafnia catalyst*. *Appl Cat A* **306**, 2006, p.45-50.

7. Dong, H., Z. Shao, G. Xiong, J. Tong, S. Sheng and W. Yang, *Investigation on POM reaction in a new perovskite membrane reactor*. Catal Today **67**, 2001, p.3-13.
8. Guo, J., Z. Hou, J. Gao and X. Zheng, *Syngas production via combined oxy-CO₂ reforming of methane over Gd₂O₃-modified Ni/SiO₂ catalysts in a fluidized-bed reactor*. Fuel **87**, 2008, p.1348-1354.
9. He, S., Q. Jing, W. Yu, L. Mo, H. Lou and X. Zheng, *Combination of CO₂ reforming and partial oxidation of methane to produce syngas over Ni/SiO₂ prepared with nickel citrate precursor*. Catal Today **148**, 2009, p.130-133.
10. He, S., H. Wu, W. Yu, L. Mo, H. Lou and X. Zheng, *Combination of CO₂ reforming and partial oxidation of methane to produce syngas over Ni/SiO₂ and Ni-Al₂O₃/SiO₂ catalysts with different precursors*. Int J of Hydrogen Energy **34**, 2009, p.839-843.
11. Jing, Q., H. Lou, L. Mo, J. Fei and X. Zheng, *Combination of CO₂ reforming and partial oxidation of methane over Ni/BaO-SiO₂ catalysts to produce low H₂/CO ratio syngas using a fluidized bed reactor*. J of Molecular Catal A: Chemical **212**, 2004, p.211-217.
12. Jing, Q.S. and X.M. Zheng, *Combined catalytic partial oxidation and CO₂ reforming of methane over ZrO₂-modified Ni/SiO₂ catalysts using fluidized-bed reactor*. Energy **31**, 2006, p.2184-2192.

Appendix A
Membrane Transport Fundamentals

A.1: Oxygen transport factors in O-MIECs:

A.1.1: Diffusion vs. surface exchange

In general, transport of oxygen through dense ceramic membranes is limited by two characteristic membrane performance attributes. The surface absorption and desorption of gas-phase oxygen into and out of the membrane's lattice at its surfaces are referred to in the literature as *surface exchange* processes and are modeled using a *surface exchange coefficient*, k_{i0} [cm/s] in conjunction with a chemical potential difference between the gas phase oxygen and the membrane's lattice oxygen ion-electron hole pairs. This rate process is typically represented mathematically by

$$i = k_{i0} \cdot c_i \cdot \left(e^{\mu_g/2RT} - e^{\mu_a/RT} \right) \quad \text{[Equation A.1] [1-3]}$$

where c_i is the ion concentration in the membrane's oxygen exchange surface.

The surface exchange coefficient, k_{i0} , is sometimes treated in modeling work as a mass transfer coefficient that applies to both membrane surfaces. In fact, k_{i0} is an electrochemical reaction rate constant that is specific to the particular surface reaction and therefore should not be used interchangeably for both the anodic and cathodic reactions, as they are opposite reactions. Their rate constants must therefore be evaluated individually and should be treated separately.

The second membrane performance attribute is oxygen ion diffusion down the lattice's oxygen potential gradient. This phenomenon is generally described in the literature using a simple diffusion relationship with an effective diffusivity. A commonly used diffusion equation for a charged species i with effective diffusivity $D_{eff,i}$ [cm²/s] is:

$$J_i = -\frac{c_i \cdot D_{eff,i}}{RT} \cdot \nabla \mu_i \quad \text{(Equation A.2) [1, 3-4]}$$

Appendix A

If desired, an effective diffusivity (D_{eff}) can be calculated from flux results using a simplified flux expression that can be derived from **Equation A.2** by assuming both gas-solid interfaces are in electrochemical equilibrium. This assumption is an extension of the assumption that the membrane is entirely bulk diffusion limited. The oxygen potential gradient can then be integrated using the partial pressure expression for ideal gas-phase oxygen potential for the boundary conditions. The resulting equation is

$$J_i = c_i \cdot D_{eff} \cdot \frac{\ln(p_s/p_p)}{2L} \quad \text{(Equation A.3) [5]}$$

This simplified approach to acquiring an effective diffusivity thus requires a flux value (J_i), an estimate of the oxygen content of the SFC (c_i), the membrane thickness (L), and the gas-phase oxygen partial pressures from the source and permeate sides of the membrane (p_s and p_p , respectively). The factor of two appears in the denominator of **Equation A.3** because each mole of molecular oxygen in the gas phase correlates to two oxygen ions in the membrane material and the surface exchange kinetics are assumed to be fast enough that the two oxygen phases are in equilibrium (i.e., $\mu_{O_2, g} = 2\mu_i$).

When discussing membrane oxygen transport and surface exchange parameters, it must be acknowledged that they can only be determined using a membrane performance model and thus rely entirely on the appropriateness of the model. While the published models are generally useful for oxygen transport into, out of, and within an O-MIEC membrane, their simplifying assumptions are inadequate for the conditions experienced by a methane conversion membrane. The most conspicuous inadequacy is the apparently universal assumption of constant properties across the membrane [1-3, 5-9]. This is reasonable with small oxygen potential gradients such as those found in an air separation system but not for the extreme gradients imposed in a membrane reactor. Also, the aforementioned misapplication of a single surface exchange coefficient to both membrane surfaces is a serious shortcoming to the published models.

Appendix A

A.1.2: Characteristic thickness

Because the relative magnitudes of k_{i0} and D_{eff} represent the relative importance of the two transport modes and their ratio has units of length, the ratio of D_{eff} to k_{i0} has been defined as the *characteristic thickness* of an ion transport material, L_d [10-11]. In theory, this parameter provides an estimate of the point of transition from surface exchange limited to diffusion limited membrane oxygen transport. However, experimentation indicates that diffusion limitations can persist at thicknesses $\ll L_d$ [6], and Steele has proposed that most O-MIEC applications actually occur under a mixed control regime [12]. Subsequent evidence largely supports this claim, although one effect can be more prominent than the other under mixed control [1, 3, 13]. At a minimum, a characteristic thickness value provides a concise indicator of the relative amount of control from each of the two transport mechanisms.

It is important to note that L_d depends on a material's environment and is therefore not a constant or fundamental property of a material. Additionally, both k_{i0} and D_{eff} depend on a material's phase composition and thus will change along with composition in response to persistent changes in temperature and/or partial pressure of oxygen [13].

For perovskite O-MIEC materials, general trends show L_d values increasing with increasing temperature [11, 14], which can be interpreted to mean k_{i0} tends to increase at a slower rate than D_{eff} as a perovskite material's oxygen content decreases. A final complicating factor for L_d determination involves the dependence of oxygen production on variations in membrane surface morphology: surface exchange kinetics have been observed to increase along with microstructural surface roughness [11, 15-16].

A range of typical L_d values for many perovskite oxide materials has been reported to be 50-1000 μm [1], with Bouwmeester et al. presenting values for various La-based perovskites at 800 $^{\circ}\text{C}$ of between 0.01 and 500 μm [11]. Lee et al. used experimental results to discern an L_d for the perovskite $\text{SrCo}_{0.8}\text{Fe}_{0.2}\text{O}_x$ (*SCFO*) of 500 μm but preferred to leave the estimate as 100-1000 μm to

Appendix A

allow for model parameter fitting uncertainties [1]. These wide ranges are understandable considering the requirement of both highly accurate flux data and an accurate model to determine the individual transport parameters in the mixed control regime typical for thick dense membranes.

Regarding SFC in particular, work by Kim et al. on the partial pressure dependence of oxygen transport through SFC provides evidence that it is significantly diffusion limited at ~1 mm thickness under an air:inert oxygen gradient [17]. Thicker membranes would, of course, tend toward diffusion control more than thinner membranes of the same material, but a larger oxygen gradient such as that found across a methane conversion reactor membrane could shift the operating mode toward surface exchange limitations. Based on the literature, the ~2 mm thick SFC membranes used in this work were initially assumed to be diffusion limited.

A.2: Membrane performance enhancement strategies

Improving either of the two transport mechanisms can increase membrane oxygen production. For a given operating temperature, *diffusion limitations* can be reduced in several ways:

- by changing the external environment(s) to increase the oxygen potential gradient across the membrane
- by decreasing membrane thickness to increase the oxygen gradient
- by changing material composition to increase its intrinsic oxygen ion mobility (i.e., increasing oxygen diffusivity).

Modifications to reduce *surface exchange limitations* include:

- increasing the surface area of the membrane face
- coating oxygen exchange surfaces with catalytic or high oxygen exchange capacity materials to facilitate absorption/desorption.

Published attempts to resolve the diffusivity vs. stability dilemma in membranes for methane conversion reactors have largely been limited to explorations of new ceramic compositions and doping strategies. Fortunately, oxygen flux studies, which often focus on membrane material

Appendix A

composition, also document various approaches for improving membrane oxygen flux with a given material. The first two of the three approaches described below are relevant to this work.

A.2.1: Composite ceramic materials

A novel approach to improving membrane performance involves combining two ceramic materials to form a composite material with better properties than either of the individual starting materials. Efforts by Fan et al. to blend the high flux but unstable $\text{SrCo}_{0.8}\text{Fe}_{0.2}\text{O}_x$ (SFCO) perovskite with a Sr-Sn perovskite successfully reduced the activation energy barrier for oxygen transport while concomitantly reducing its thermochemical expansion coefficient [18]. Shaula et al. report that their composite ceramic exhibits oxygen flux intermediate to that of its component materials [19]. As mentioned in **Section 2.3.2**, SFC is a *de facto* composite membrane material of this type. **Appendix B** discusses evidence of desirable characteristics for SFC that are consistent with results reported for intentionally designed composite ceramics.

A.2.2: Composite membrane structures: Membrane surface coatings

This strategy uses surface coating techniques to improve surface exchange kinetics, with the majority of the work involving thin porous layers that can increase a membrane's surface area by orders of magnitude [8]. The potential effectiveness of this approach has also been reported unintentionally in the accounts described in **Section A.1** of the dependence of surface exchange coefficients on surface roughness.

Coating a dense surface with catalytic materials is another technique to facilitate surface exchange processes. For example, early in this work it was found that depositing 5 μm diameter platinum disks (120 nm thick) on the membrane's source side could double the oxygen flux through a 1.5 mm thick SFC membrane [20]. Additional membrane tests with deposited platinum disks were performed, as well as tests of membranes with thin platinum coatings of ~ 6 angstrom thickness.

Appendix A

A.2.3: Composite membrane structures: Supported dense thin film membranes

This approach to increasing membrane oxygen flux was not explored in this work, but it is important enough to justify mentioning. Chen et al. predict that thin ion conducting films should have intrinsically higher ion transport efficiency which would allow comparable performance to a thick membrane under less extreme conditions [21]. Indirectly supporting this prediction, Tunney et al. showed that electronic conductivity increases as O-MIEC film thickness is decreased from 300 nm to 30 nm [22]. A similar effect for ionic conductivity could be confirmed if the effective diffusion coefficients for thin films could be compared with those of thicker membranes of the same material under identical operating conditions. If confirmed, this would provide even more incentive to investigate supported thin O-MIEC films because lower temperature and/or lower oxygen gradient operation would greatly expand membrane reactor feedstock options, membrane support options, and membrane application possibilities.

Another potential benefit unique to thin films can be extracted from a claim by Ritchie et al., who report that their La-Sr-Fe-Ga perovskite material cracked in methane at 780 °C but was stable under an air:methane gradient to much higher temperatures [23]. They hypothesized that the permeated oxygen stabilized the membrane by increasing the oxygen partial pressure on the permeate side and thus limited the difference in oxygen potential across the membrane. A similar idea was mentioned by Akin et al. as they discussed the importance of maintaining permeate side oxygen levels above the so-called “critical partial pressure” for the material [24]. This concept leads to the intriguing proposition that a very thin membrane could stabilize its permeate side surface via its own oxygen production more successfully than a thick membrane with its greater diffusion limitations and lower oxygen production. Testing this hypothesis with a membrane used with an oxygen-consuming reaction would require careful experimentation, because the reaction rate would have to be limited by something other than oxygen availability.

Appendix A

In any case, decreasing dense membrane thickness is the most straightforward conceptual approach to increasing oxygen flux through an O-MIEC membrane with a given ceramic. However, surface treatments are a promising avenue for improvement if thickness decreases alone do not yield sufficient oxygen transport. If membrane stability were assigned its proper priority in membrane reactor design, the need to enhance diffusion in other ways than decreasing dense layer thickness would become critical.

References Cited in Appendix A

1. Lee, T.H., Y.L. Yang, A.J. Jacobson, B. Abeles and M. Zhou, *Oxygen permeation in dense SrCo_{0.8}Fe_{0.2}O_{3-δ} membranes: surface exchange kinetics versus bulk diffusion*. Sol St Ionics **100**, 1997, p.77-85.
2. Zhou, M., H. Deng and B. Abeles, *Transport in mixed ionic electronic conductor solid oxide membranes with porous electrodes: Large pressure gradient*. Sol St Ionics **93**, 1997, p.133-138.
3. Kim, S., Y.L. Yang, A.J. Jacobson and B. Abeles, *Diffusion and surface exchange coefficients in mixed ionic electronic conducting oxides from the pressure dependence of oxygen permeation*. Sol St Ionics **106**, 1998, p.189-195.
4. Heyne, L., *Electrochemistry of mixed ionic-electronic conductors*, in *Solid Electrolytes*, S. Geller, Editor. 1977, Springer: Berlin. p. 169.
5. Maiya, P.S., U. Balachandran, J.T. Dusek, R.L. Mieville, M.S. Kleefisch and C.A. Udovich, *Oxygen transport by oxygen potential gradient in dense ceramic oxide membranes*. Sol St Ionics **99**, 1997, p.1-7.
6. Deng, H., M. Zhou and B. Abeles, *Diffusion-reaction in mixed ionic-electronic solid oxide membranes with porous electrodes*. Sol St Ionics **74**, 1994, p.75-84.
7. Deng, H., M. Zhou and B. Abeles, *Transport in solid oxide porous electrodes: Effect of gas diffusion*. Sol St Ionics **80**, 1995, p.213-222.
8. Lee, T.H., Y.L. Yang, A.J. Jacobson, B. Abeles and S. Milner, *Oxygen permeation in SrCo_{0.8}Fe_{0.2}O_{3-δ} membranes with porous electrodes*. Sol St Ionics **100**, 1997, p.87-94.
9. Kim, S., Y.L. Yang, A.J. Jacobson and B. Abeles, *Oxygen surface exchange in mixed ionic electronic conductor membranes*. Sol St Ionics **121**, 1999, p.31-36.
10. Steele, B.C.H., *Interfacial reactions associated with ceramic ion transport membranes*. Sol St Ionics **75**, 1995, p.157-165.
11. Bouwmeester, H.J.M., H. Kruidhof and A.J. Burggraaf, *Importance of the surface exchange kinetics as rate limiting step in oxygen permeation through mixed-conducting oxides*. Sol St Ionics **72**, 1994, p.185-194.

Appendix A

12. Steele, B.C.H., *Oxygen ion conductors and their technological applications*. Material Science and Engineering **B13**, 1992, p.79-87.
13. Qiu, L., T.H. Lee, L.-M. Liu, Y.L. Yang and A.J. Jacobson, *Oxygen permeation studies of $SrCo_{0.8}Fe_{0.2}O_{3-\delta}$* Sol St Ionics **76**, 1995, p.321-329.
14. Jacobson, A.J., S. Kim, A. Medina, Y.L. Yang and B. Abeles, *Dense oxide membranes for oxygen separation and methane conversion*. Mat Res Soc Symp Proc **497**, 1998, p.29-34.
15. Xu, S.J. and W.J. Thomson, *Stability of $La_{0.6}Sr_{0.4}Co_{0.2}Fe_{0.8}O_{3-\delta}$ perovskite membranes in reducing and nonreducing environments*. Ind Eng Chem Res **37**, 1998, p.1290-1299.
16. Etchegoyen, G., T. Chartier and P. Del-Gallo, *Oxygen permeation in $La_{0.6}Sr_{0.4}Fe_{0.9}Ga_{0.1}O_{3-\delta}$ dense membrane: effects of surface microstructure*. J Solid St Electrochem **10**, 2006, p.597-603.
17. Kim, S., Y.L. Yang, R. Christoffersen and A.J. Jacobson, *Determination of oxygen permeation kinetics in a ceramic membrane based on the composition $SrFeCo_{0.5}O_{3.25-\delta}$* Sol St Ionics **109**, 1998, p.187-196.
18. Fan, C.G., Z.Q. Deng, Y.B. Zuo, W. Liu and C.S. Chen, *Preparation and characterization of $SrCo_{0.8}Fe_{0.2}O_{3-\delta}$ - $SrSnO_3$ oxygen-permeable composite membrane*. Sol St Ionics **166**, 2004, p.339-342.
19. Shaula, A.L., V.V. Kharton and F.M.B. Marques, *Phase interaction and oxygen transport in $La_{0.8}Sr_{0.2}Fe_{0.8}Co_{0.2}O_{3-(La_{0.9}Sr_{0.1})_{0.98}Ga_{0.8}Mg_{0.2}O_3}$ composites*. J of Europ Cer Soc **24**, 2004, p.2631-2639.
20. Murphy, S.M., D.A. Slade, K.A. Nordheden and S.M. Stagg-Williams, xxx??? J of Membr Sci, 2005.
21. Chen, X., N.J. Wu and A. Ignatiev, *Structure and conducting properties of $La_{1-x}Sr_xCoO_{3-\delta}$* J Europ Ceram Soc **19**, 1999, p.819-822.
22. Tunney, J.J., M.L. Post, X. Du and D. Yang, *Temperature dependence and gas-sensing response of conduction for mixed conducting $SrFe_yCo_zO_x$ thin films*. J of ECS **149**(6), 2002, p.H113-H118.
23. Ritchie, J.T., J.T. Richardson and D. Luss, *Ceramic membrane reactor for synthesis gas production*. AIChE Jnl **47**(9), 2001, p.2092-2101.
24. Tsai, C.-Y., A.G. Dixon, Y.H. Ma, W.R. Moser and M.R. Pascucci, *Dense perovskite $La_{1-x}A'_xFe_{1-y}Co_yO_{3-\delta}$ ($A' = Ba, Sr, Ca$) membrane synthesis, applications, and characterization*. J Amer Ceram Soc **81**(6), 1998, p.1437-1444.

Appendix B

SFC Overview

Based on its high stability and conditionally high oxygen transport, SFC was a promising candidate material in some of the earliest literature from this field [1-4]. Its long tenure and somewhat disputed oxygen transport performance has also led to it being a thoroughly characterized ceramic O-MIEC material.

A review of the factors involved in developing a successful membrane reactor leads to the conclusion that membrane material stability must be weighted above all factors, including native oxygen diffusion and surface exchange. The range of published techniques for improving oxygen transport could eventually allow sufficient flux through any material with even moderate native diffusivity and surface exchange rates, but intrinsic material instability cannot be overcome.

Under this rubric, SFC can still be considered a promising candidate material for some applications in spite of its relatively low oxygen conductivity. Although the oxygen diffusivity and phase composition of SFC have been the focus of some debate, the material has repeatedly demonstrated high mechanical stability under the demanding oxygen partial pressure differentials found in partial oxidation of methane (*POM*) membrane reactors. Furthermore, the controversy regarding SFC's intrinsic oxygen transport can be resolved somewhat by conflating the various sample preparation and test conditions used to obtain the conflicting flux results with the published phase composition work.

SFC remains a promising candidate for an O-MIEC membrane reactor for methane conversion not only because of its mechanical stability but also because experimental evidence indicates that it could perform better in the extreme conditions of a commercial POM reactor than it does in less severe laboratory flux testing environments, which distinguishes it from other O-MIEC membrane candidates.

Appendix B

B.1: Phase composition of SFC

SFC has been reported to be quite stable even under the extreme oxygen potential gradients in a POM membrane reactor. The published evidence overwhelmingly supports the conclusion that SFC prefers to exist as an adaptable three-phase solid solution (or “phase assemblage”) with small, highly intermixed phase moieties (see Figure B.1) [2-3, 5-8]. The combination of this evidence with the reports of SFC’s “remarkable structural stability” [1] implies a significant potential for robustness inherent in this intriguing phase arrangement.

The three phase categories reported in SFC are a perovskite phase ($\text{SrFe}_{1-x}\text{Co}_x\text{O}_{3-\delta}$), a spinel phase ($\text{Co}_3-x\text{Fe}_x\text{O}_4$), and the so-called “intergrowth” phase ($\text{SrFe}_{1.5-x}\text{Co}_x\text{O}_{3.25-\delta}$) whose name refers to its structural appearance as interspersed perovskite and brownmillerite units [7].

All three phases are of adjustable stoichiometry, leading to a highly interdependent distribution of cations and the inevitability of phase shifts within phase categories as well

as between phase categories. One additional phase has also been reported to appear, particularly on highly reduced membrane permeate side surfaces: the Co/Fe spinel phase can decompose to a cubic “rocksalt” phase ($\text{Co}_{1-x}\text{Fe}_x\text{O}$) at temperatures greater than 900 °C in air or at lower temperatures in reducing environments [5-6].

All phase transitions have been reported to be stable and reversible at high enough temperature [3, 6], with the only reported instance of material failure occurring when a membrane was cooled in a reducing environment then reheated in an oxidizing environment [3]. Since phase equilibrium kinetics become negligibly slow at low temperatures, the researchers surmised that the membrane material experienced this series of events as an extremely dramatic environment change on its return to a temperature at which significant phase adjustments could occur.

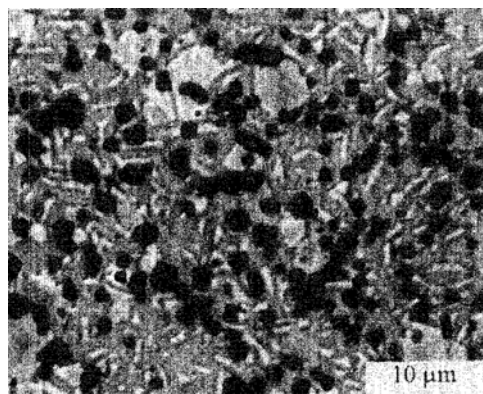


Figure 1: cross-sectional backscattered electron image of SFC’s three-phase assemblage. Perovskite phases are lightest, “intergrowth” phases are medium, and spinel phases are black. From Kim et al. (1998) ²⁴.

Appendix B

All examinations of SFC phases point to the novel idea that the nearly infinite phase combinations in SFC may very well be the source of its reported stability under the severe oxygen potential gradients of a POM membrane reactor. With its continuously and reversibly adjustable phase microstructure, SFC is uniquely suited to accommodate a dramatic phase distribution gradient of the kind mentioned in Section 2.3.2 as long as environmental changes are made at high temperatures. Feng et al. reported recently that the inner and outer wall phase compositions of their used SFC membrane reactor showed respective phase compositions consistent with this phase gradient theory [9].

A final supporting idea proposed by Kim et al. involves the possibility that SFC's stability under environmental changes results from its generally slow phase adjustment kinetics, which they refer to as its "microstructural robustness" [2]. This slow adjustment attribute has caused waiting periods for steady state on the order of weeks in some reactor applications (e.g., Balachandran et al. [1]), but it can also be interpreted as additional evidence of the highly distributed small scale phase changes that we propose to be the source of this material's stability in extreme environments.

B.2: Oxygen Diffusivity in SFC

The wave of scrutiny that followed the initial reports of SFC's high oxygen flux has determined conclusively that an SFC membrane's oxygen flux correlates directly with its perovskite phase content [7-8]. Increased perovskite content was also clearly correlated with high temperature/low pO_2 environments (i.e., low equilibrium oxygen content) [3, 5, 7-8].

Interestingly, single-phase "intergrowth phase" SFC samples prepared by Armstrong et al. showed the lowest oxygen flux of any SFC preparation studied. Armstrong's intergrowth phase oxygen flux was two orders of magnitude lower than that of their example perovskite ($SrFe_{0.75}Co_{0.25}O_{3-\delta}$) and one order of magnitude lower than that of their three-phase SFC "phase assemblage" material [7] (see Table B.1 below). The phase assemblage material included significant proportions of each of the three major phase categories reported in SFC: perovskite phases, spinel

Appendix B

phases, and “intergrown” brownmillerite-perovskite phases. The Armstrong flux results clearly trend with increasing perovskite content. Likewise, Ikeguchi et al reported a 17% decrease in oxygen flux with a decrease in membrane sintering temperature from 1200 °C to 1150 °C [10]. The presumptive cause of the drop in flux is a decrease in perovskite content.

Table B.1: Early values for effective oxygen diffusivity in SFC at 900 °C

| D_{eff} [cm ² /s] | Test Environment | Pre-test Environment(s) | Reference |
|--|---|---|----------------------|
| 8.9×10^{-7} | conductivity relaxation method (tested in air and 0.1% O ₂ /N ₂) | sintered in air at 1200 °C for 5 hrs; cut from a larger slab but not polished | Ma (1996) [11] |
| 5.6×10^{-7} | air:POM gradient | sintered in air at 1200 °C for 5 hrs; no polishing (tubular membranes) | Maiya (1997) [4] |
| 5.8×10^{-8} <i>(estimated from flux)</i> | air:inert gradient | sintered in air at 1200 °C for 5 hrs; no polishing | Ikeguchi (2003) [10] |
| 4.8×10^{-8} <i>(estimated from flux)</i> | | sintered in air at 1150 °C for 5 hrs; no polishing | |
| 1×10^{-8} <i>(estimated from flux)</i> | air:inert gradient --three-phase SFC-- | sintered in air at 1150 °C for 18 hrs; polished on both sides | Armstrong (2000) [7] |
| 1×10^{-9} <i>(estimated from flux)</i> | --single-phase SFC-- | sintered in air at 1150 °C for 10 hrs; annealed at 1000 °C (no details); polished on both sides | |
| 1.1×10^{-7} <i>(estimated from flux)</i> | SrFe_{0.75}Co_{0.25}O_x | | |

The diffusivity estimated by Ma et al. is the highest reported value for SFC in the literature [11], and as such it must be noted that the value was obtained from conductivity relaxation testing rather than from flux experiments. The results in Table B.1 that are parenthetically noted as “estimated from flux” were calculated for this work by applying a simple diffusion-only model (Equation A.3 in Section A.1.1) to the oxygen flux, oxygen partial pressures, and membrane

Appendix B

thicknesses reported in the works in question. This approach was chosen for consistency because it was used by Maiya et al. to generate their diffusivity values [4]. Membrane surface treatment information is included in the table because of its potential effect on oxygen flux through O-MIEC ceramics [12-13]. No published experimental surface exchange coefficient values were found for SFC—all studies concluded that it was bulk diffusion controlled in the thickness range of interest and ignored surface exchange kinetics. However, the fact that the high conductivity relaxation result from Ma et al. is greater than any reported results from flux testing serves as an early indication that this assumption might not be universally correct.

B.3: The Influence of SFC Phase Composition on Oxygen Diffusivity

Effective diffusion coefficients reported for SFC span nearly three orders of magnitude. However, the original reports of high flux were performed under air:POM gradients [3-4] while the lower fluxes used to challenge these results were obtained using much smaller air:inert gradients [2, 7-8]. Furthermore, the test sample preparation methods were not consistent among the investigators, and it has been shown that SFC's initial phase composition can vary substantially with both material preparation and membrane fabrication methods [10]. For example, Xia et al. reported the creation of greater amounts of perovskite phase with annealing temperatures above 1150 °C and also slow conversion back to intergrowth phase at temperatures below 1000 °C (both phenomena were observed under a uniform environment, not an oxygen gradient) [8]. The relatively slow transition to the intergrowth phase at lower temperatures allows “meta-stable” perovskite phases to persist at lower temperatures.

Although 1000 °C is higher than most laboratory membrane reactor tests, both temperature and oxygen partial pressure can determine phase composition (as discussed in Section 2.3.1). For example, a low oxygen environment at 800 °C could potentially produce the same phases in SFC as a uniform environment at 1000 °C. Therefore, lower temperature testing in reduced oxygen environments, such as those produced under reforming reaction conditions, could produce higher

Appendix B

perovskite content and higher oxygen flux over time. Early observations by Maiya and Balachandran support this concept [1, 4].

Rather than undermine the validity of some portion of these results, the wide range of diffusivity estimates for SFC can be interpreted as confirmatory evidence of both the sensitivity of its phase composition to its environment and the importance of the perovskite phases to oxygen diffusion in SFC. In short, different conditions produce different phase distributions which produce different material properties such as oxygen diffusivity. Given the slow phase adjustment kinetics observed for SFC at temperatures under 1000 °C, the discrepancies claimed by Kim et al.[2], Armstrong et al.[7], and Xia et al.[8] may be discounted somewhat as either transient phenomena resulting from SFC powder and membrane preparation technique or true steady state differences resulting from different experimental conditions. The longer duration tests in the original work with SFC by Maiya et al. [4] and Balachandran et al. [1] may or may not have started with a more favorable SFC phase distribution, but they were of sufficient duration to provide some confidence that the final results represent solid state equilibrium under reaction conditions.

Based on this interpretation of the collective evidence, it is reasonable to conclude that SFC under certain circumstances does have the potential for usefully high oxygen transport. Its uniquely adaptable microstructural equilibrium attribute increases its promise further by giving it the potential to withstand extreme conditions without fracturing as a single phase membrane would. The composite phase arrangement and durability of SFC seem analogous to the desirable characteristics of concrete as a building material, and mechanical durability cannot be underestimated as a desirable membrane characteristic.

References Cited in Appendix B

1. Balachandran, U., J.T. Dusek, P.S. Maiya, B. Ma, R.L. Mieville, M.S. Kleefisch and C.A. Udovich, *Ceramic membrane reactor for converting methane to syngas*. Catal Today **36**, 1997, p.265-272.

Appendix B

- Kim, S., Y.L. Yang, R. Christoffersen and A.J. Jacobson, *Determination of oxygen permeation kinetics in a ceramic membrane based on the composition $SrFeCo_{0.5}O_{3.25-\delta}$* . Sol St Ionics **109**, 1998, p.187-196.
- Ma, B. and U. Balachandran, *Phase stability of $SrFeCo_{0.5}O_x$ in reducing environments*. Mat Res Bull **33**(2), 1998, p.223-236.
- Maiya, P.S., U. Balachandran, J.T. Dusek, R.L. Mieville, M.S. Kleefisch and C.A. Udovich, *Oxygen transport by oxygen potential gradient in dense ceramic oxide membranes*. Sol St Ionics **99**, 1997, p.1-7.
- Ma, B., N.I. Victory, U. Balachandran, B.J. Mitchell and J.W. Richardson, *Study of the mixed-conducting $SrFeCo_{0.5}O_y$ system*. J Am Ceram Soc **85**(11), 2002, p.2641-2645.
- Fossdal, A., L.T. Sagdahl, M.-A. Einarsrud, K. Wiik, T. Grande, P.H. Larsen and F.W. Poulsen, *Phase equilibria and microstructure in $Sr_4Fe_{6-x}Co_xO_{13}$ ($0 \leq x \leq 4$) mixed conductors*. Sol St Ionics **143**, 2001, p.367-377.
- Armstrong, T., F. Prado, Y. Xia and A. Manthiram, *Role of perovskite phase on the oxygen permeation properties of the $Sr_4Fe_{6-x}Co_xO_{13+\delta}$ system*. J Electrochem Soc **147**(2), 2000, p.435-438.
- Xia, Y., T. Armstrong, F. Prado and A. Manthiram, *Sol-gel synthesis, phase relationships, and oxygen permeation properties of $Sr_4Fe_{6-x}Co_xO_{13+\delta}$ ($0 \leq x \leq 3$)*. Sol St Ionics **130**, 2000, p.81-90.
- Feng, S.J., S. Ran, D.C. Zhu, W. Liu and C.S. Chen, *Synthesis gas production from methane with $SrFeCo_{0.5}O_y$ membrane reactor*. Energy & Fuels **18**, 2004, p.385-389.
- Ikeguchi, M., K. Yoshino, K. Kanie, M. Nomura, E. Kikuchi and M. Matsukata, *Effects of preparation method on oxygen permeation properties of $SrFeCo_{0.5}$ membrane*. Sep & Pur Tech **32**, 2003, p.313-318.
- Ma, B., U. Balachandran, J.-H. Park and C.U. Segre, *Determination of chemical diffusion coefficient of $SrFeCo_{0.5}O_x$ by the conductivity relaxation method*. Sol St Ionics **83**(1-2), 1996, p.65-71.
- Bouwmeester, H.J.M., H. Kruidhof and A.J. Burggraaf, *Importance of the surface exchange kinetics as rate limiting step in oxygen permeation through mixed-conducting oxides*. Sol St Ionics **72**, 1994, p.185-194.
- Xu, S.J. and W.J. Thomson, *Stability of $La_{0.6}Sr_{0.4}Co_{0.2}Fe_{0.8}O_{3-\delta}$ perovskite membranes in reducing and nonreducing environments*. Ind Eng Chem Res **37**, 1998, p.1290-1299.

Appendix C
Membrane Fabrication

In general, ceramic membranes are produced by pressing metal oxide powders into the desired geometry and then heating the pressed shape in a high-temperature furnace to form a dense membrane. Dense membranes are shaped as needed to produce the desired final dimensions or sanded to remove undesired surface material.

Calcining, sintering, and annealing are three ceramic fabrication processes that all involve holding a material in controlled high temperature environments for predetermined time periods. The distinctions among them are important to a proper understanding the ceramic membrane fabrication process. Calcining produces the target metal oxide particles by removing co-precipitant ions, residual solvents, and any other unwanted residues from freshly prepared ceramic precursor solids. After calcining, the metal oxide powders are pressed into the desired “green membrane” shape and then sintered to fuse the individual grains and create a cohesive solid (this procedure is also referred to as “firing”). Powder structure, pressing procedure, and sintering conditions can be adjusted to control the density or porosity of the sintered product. Converting a sintered membrane to a desired solid phase by holding it in a specific environment is called annealing (or “heat treating”).

In this work, membranes were fabricated from SFC powders obtained originally from Superconductive Components, Inc. and later from Praxair Specialty Ceramics. Midway through the work, a Thermolyne 46100 high-temperature furnace (1700 °C maximum temperature) was obtained and membranes began to be fabricated in-house using the Thermolyne furnace and a 25,000 lb Carver uniaxial press. Prior to this, all membranes were fabricated at Argonne National Laboratory by the staff of Balu Balachandran. The Balachandran fabrication procedure was used at KU after the high-temperature furnace was obtained.

Membranes were characterized using scanning electron microscopy (SEM) imaging, elemental dispersive x-ray analysis (EDX), and powder x-ray diffraction (XRD) to assess the bulk

Appendix C

and surface structures and the element distribution on the surface. The powder diffractometer was a Bruker-AXS D8 with copper K α source and nickel filter for copper K β radiation. *NOTE: the powder diffractometer stopped working properly shortly after XRD testing was initiated and has not been repaired within the time available for this work. Andrew Duncan performed the majority of the work that was completed on membranes fabricated with different sintering temperatures and environments, but the comparisons were inconclusive because of the very low signal-to-noise ratio with the available detector.*

C.1: SFC powders

Both coated and uncoated SFC powders are used for membrane fabrication. Coatings are applied prior to pressing and are intended to improve cohesion of the green membrane and thus improve membrane integrity after sintering. They are therefore sometimes referred to as “binding agents.”

A 1.0 wt% ethylcellulose solution was used as the binding agent. The isopropanol/acetone mixed solvent is allowed to evaporate before pressing, and the residual ethylcellulose burns off between 350 and 450 °C during the sintering process. This burn-off has been confirmed by mass spectrometer and occurs well before the individual ceramic powder grains begin to fuse.

The use of binder does not appear to affect the density of the finished SFC membranes, which was consistently about 94% of the theoretical density for the SFC intergrowth phase regardless of coating status. All powders, whether coated or uncoated, are passed through a 60-mesh sieve prior to pressing to ensure a consistent maximum particle size in the die.

C.2: Green membrane formation

2.75 grams of uncoated SFC powder or 2.78 grams of ethylcellulose-coated SFC powder are added to a 7/8” custom-made die. Before filling, the contact surfaces of the die are coated with a

Appendix C

stearic acid in acetone solution. The acetone evaporates quickly and the remaining stearic acid residue acts as an anti-seize compound to facilitate removal of the green membrane from the die after pressing. The powder in the die is pressed at 5,000 lbs force for 3 minutes in a Carver uniaxial press.

C.3: Sintering

Pressed green membranes are carefully removed from the die and transferred to an alumina tray. The tray is placed in the high-temperature furnace, and the membranes are sintered at 1180 °C for 10 hours in flowing air. Heating and cooling rates range from 1 °C/min to 3 °C/min. Later in the work, thin alumina cover sheets were used to hold the membranes flat during sintering. This produces less curvature of the sintered membranes and thus allows more material to be retained in the planing step. The thickness and diameter of the sintered membranes are approximately 0.077” and 0.758”, respectively.

C.4: Planing and polishing

Sintered membranes are allowed to cool to room temperature before handling. They are then planed to provide flat and parallel contact faces to help avoid membrane fracture on compression in the reactor apparatus. Planing is also necessary to provide an appropriately flat surface for photolithographic deposition of catalyst patterns.

Planing is performed using a lathe and two custom-machined bits. The membrane is adhered to its bit using CrystalBond, a removable adhesive commonly used in the semiconductor industry for its rigid hold and ease of removal. The smaller bit with the membrane is placed in the non-rotating chuck that can be moved along the track of the lathe. The larger bit for the abrasives is inserted into the lathe’s rotating fixed axial position chuck. Adhesive-backed abrasive paper is attached to this bit and replaced as necessary.

Appendix C

The lathe is started with the membrane about one-half inch from the bit holding the abrasive paper. The fine control wheel for the movable chuck is used to bring the membrane carefully into contact with the abrasive. At least two grades of abrasive are used successively, typically 220-grit followed by 400-grit.

The planed surface is then polished successively by hand with 600-grit and 1200-grit sandpapers against a machined metal surface to maximize uniformity. After polishing, the membrane is removed from the bit by heating to melt the CrystalBond. The residual CrystalBond is removed with acetone from the unplaned surface, which is then planed and polished by the same procedure. The finished membrane is significantly thinner than the original membrane, with a final thickness of 0.063" to 0.069", but the two faces are parallel and uniform.

C.5: Surface treatments: patterns and coatings

For some tests, additional catalyst was added to one of the membrane faces either as a very thin film or as a pattern of discrete particles. With both approaches, catalytic metals are added using an electron-beam evaporator (Thermionics three-gun evaporator with 3kW guns). The system is equipped with two sweep controllers, source shutters, a rotating substrate holder, a radiant substrate heater, and an Infinicon XTC/2 deposition controller which allows for the specification of the desired deposition rate and thickness within about two angstroms.

Depositions took place in a pressure range of 1×10^{-6} to 1×10^{-5} torr. Platinum was procured from Kurt J. Lesker (99.99% purity, density 21.4 g/cm^3 , z-ratio 0.245 [acoustic impedance]).

Although thin layers can be deposited on any surface, photolithographic catalyst pattern deposition requires a highly polished surface. Membranes intended for pattern deposition are thus polished further to eliminate surface defects that would prevent reproducible lithography of 1-5 μm features. In this work, a grinding/polishing wheel in the University of Kansas Physics department

Appendix C

(South Bay Technology, Model 900 Grinder/Polisher) is used to polish the membranes with 1 micron abrasives (South Bay Technology, aluminum oxide film, 1 micron 8" discs). The final finish is glass-like, as shown in Figure C.1.



Figure C.1: SFC membrane sintered surface and polished surface

C.5.1: Catalyst pattern deposition

Structured patterns of particles of catalytic materials such as platinum, palladium, and nickel metals and support oxides such as CeO_2 can be successfully and reproducibly deposited onto membrane surfaces using photolithography techniques common for semiconductor processing [1-2]. The membranes patterned with catalyst particles were characterized with SEM imaging (LEO 1550 field effect scanning scope) and EDX (EDAX Phoenix) before and after reaction testing. The Thermionics electron-beam evaporator was also used to deposit thin layers of catalytic metals (platinum and palladium) onto membrane surfaces for this work and to deposit dense SFC thin films onto porous substrates in preliminary work for ongoing studies by the Stagg-Williams lab.

Catalyst pattern deposition requires several steps. First, two layers of photoresist are spun onto the polished membrane. The sample is then exposed to UV light under the desired photomask to

Appendix C

chemically modify the photoresist so it can be removed (or “developed”) by certain solvents. The photomask blocks UV light using the desired pattern for the catalyst particles. The pattern for the eventual catalytic features is developed out of the two layer “resist stack” by washing with solvents that dissolve only the UV-exposed photoresist and not the unexposed photoresist (see Figure C.2).

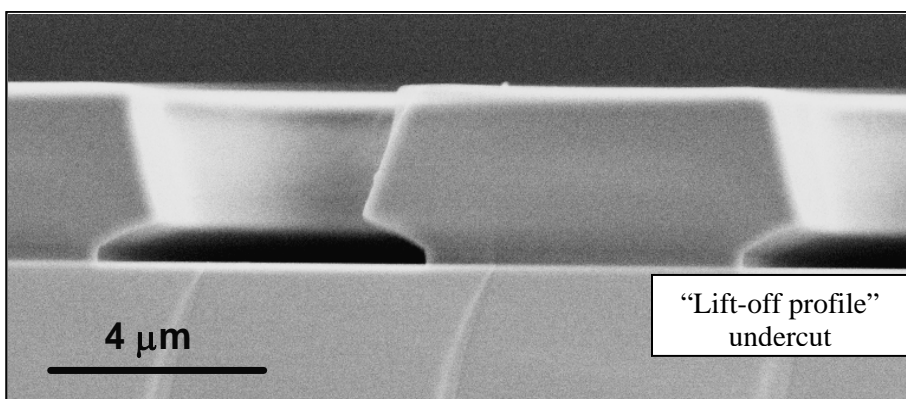


Figure C.2: Photoresist “lift-off profile” with undercut for platinum particle deposition

The exposed and developed surface is placed in the sample chamber of the e-beam evaporator. The chamber is evacuated and the target catalytic material is evaporated into the chamber by a beam of high-energy electrons. The evaporated material settles on all exposed surfaces, including the portions of the SFC membrane that were exposed when the photoresist stack was developed.

The coated membrane is removed from the chamber and a second set of solvents is used to remove the remaining unexposed photoresist. This final solvent wash also removes all catalytic material deposited by the e-beam evaporator onto the photoresist itself, leaving behind only the material deposited on the SFC membrane surface in the pattern provided by the photomask.

One final feature of Figure C.2 worth discussing is the need for two layers of photoresist. Two layers with slightly different solubilities in the developing solvent are required because an undercut in the photoresist known as a “lift-off profile” is necessary to allow for clean stripping after

Appendix C

deposition of the photoresist and any extraneous catalyst. If the masking and development steps are performed carefully, this photolithography technique can produce highly reproducible patterns down to the 1 micron scale.

C.5.2: Thin layer deposition

Electron-beam evaporation is the only step required to deposit thin layers. However, with a target thickness of two atomic monolayers (6 to 7 angstroms for platinum), the deposition procedure requires slow and careful heating of the target material with the electron beam. It is painstaking work to avoid overheating the target and evaporating too much platinum at once, but the results appear to have been successful based on changes in membrane performance reported in this dissertation and by Kirk Gerdes at the University of Houston [3]. Unfortunately, such layers are too thin to be detected by EDX or any other means available to us except two indirect methods. First, transparent tape (“scotch” tape) was used to hold the membranes in place during deposition. Post-deposition, the tape had a faint grey tint that only appeared on exposed tape surfaces (areas of tape underneath an overlap did not turn grey). Second, the similar performance enhancements reported by both groups confirm that something was added to the membranes.

References Cited in Appendix C

1. Murphy, S.M., D.A. Slade, K.J. Nordheden and S.M. Stagg-Williams, *Increasing oxygen flux through a dense oxygen permeable membrane by photolithographic patterning of platinum*. J of Membr Sci **277**(1-2), 2006, p.94-98.
2. Murphy, S., *Fabrication and Catalytic Patterning of Non-porous Ion and Electron Dual-Conducting Membranes Using Electron Beam Evaporation*, in *Department of Chemical and Petroleum Engineering*. 2005, University of Kansas: Lawrence, KS.
3. Gerdes, K. and D. Luss, *Oxygen Flux Increases Through MIEC Membranes by Enhanced Surface Exchange*. AIChE Journal **53**(5), 2007, p.1389-1391.

Appendix D

The Effect of Reaction on Patterned Membranes

D.1: Membrane phase changes under reforming reaction environments

Membranes patterned with Ni, Au/Pd, and Au/CeO₂ were tested for pattern stability in oxidizing and reducing conditions, and Ni-patterned membranes were subjected to both CO₂ reforming and partial oxidation of methane in the SSMR at temperatures up to 700 °C [1]. These studies confirmed the deposited catalyst features did not migrate or degrade but also produced evidence that the membrane surface itself might not be stable under high-temperature reducing environments. The literature reviewed in Appendix B supports these initial observations by demonstrating that the SFC material can undergo a variety of phase transitions depending on its initial stoichiometry and the temperatures and oxygen partial pressures to which it is exposed.

This work confirmed the potential of the SFC material to undergo surface restructuring, which is a shortcoming for applications as a substrate for surface catalyst patterns with high temperature reforming reactions. Fortunately, the catalyst patterning techniques described by Murphy should be easy to transfer to other ceramic substrates should the SFC ultimately prove to be unfit for membrane reactor work [2]. The surface restructuring was observed on the reaction side only, so catalyst patterning of the oxygen supply side of SFC membranes could be an option.

Figure D.1 shows an SEM image of the surface of a polished membrane patterned with 5 μm platinum circles (120 nm thick) after significant use, including an oxygen flux study and reduction at 750°C in hydrogen followed by CO₂ reforming of CH₄ at 750°C for 11 hours. Although the outline of the platinum pattern is still visible, significant restructuring of the membrane surface is obvious compared to the untested membrane surface in Figure D.2. Surface characterization by electron-dispersive x-ray analysis (EDX) revealed the outgrowths to be rich in iron and cobalt, suggesting a segregation of iron and cobalt from the bulk SrFeCo_{0.5}O_x material under these conditions [1]. As shown in Figure D.1, EDX analysis also confirmed the presence of the platinum in its original pattern.

Appendix D

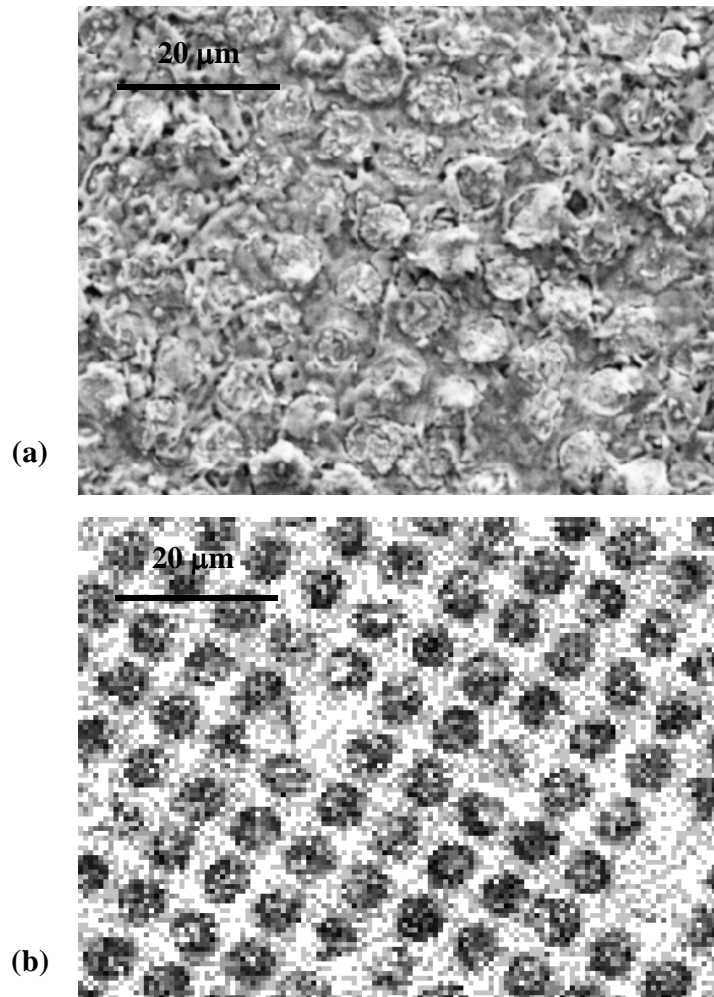


Figure D.1: (a) Polished membrane surface with 5 micron Pt features after reduction and CO₂ reforming of CH₄ at 750 °C and (b) corresponding EDX platinum map, from Murphy [1]

Similar work using membranes with 3 μm platinum disks was performed. These deposits were only 20 nm thick, and, as portrayed in Figure D.3, the thinner platinum features were not discernible after exposure to CO₂ reforming conditions for 13 hours following reduction in diluted hydrogen at 750 °C. Again, the outgrowths on the surface were shown to contain mostly iron and cobalt oxides, but this time no evidence of the original platinum particles was found using EDX. The disappearance of the platinum features is believed to result from their thinner depth and the possibility

Appendix D

of complete coverage by the membrane outgrowths. Based on the studies with the 5 μm platinum features, platinum lability is not suspected.

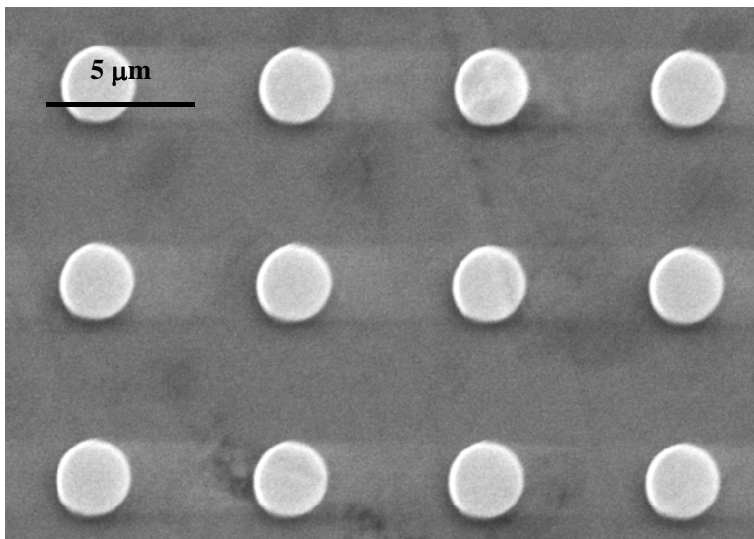


Figure D.2: SEM image of an SFC membrane patterned with 60 μm thick 3 mm diameter Pt particles, from Murphy [1]

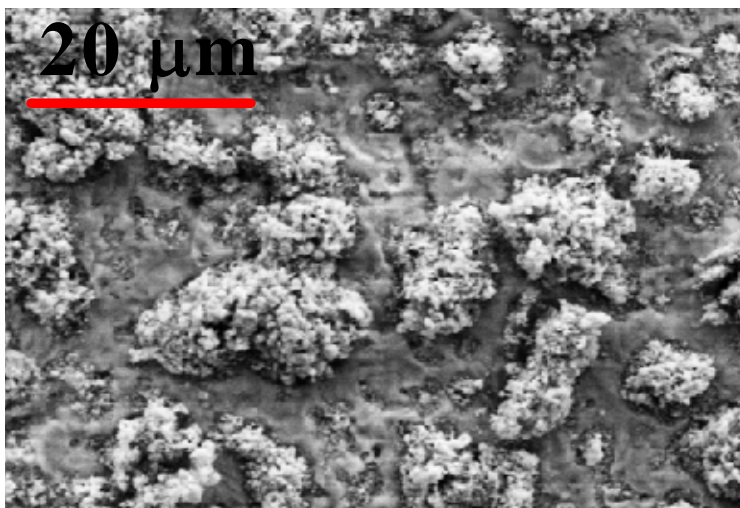


Figure D.3: Polished membrane surface with 3 micron Pt features after CO_2 reforming of CH_4 at 750°C for 13 hours (with pre-reaction reduction), from Murphy [1]

Appendix D

In discussions, Dr. Utham Balachandran at Argonne National Laboratory indicated that their previous studies had shown cobalt could segregate from the membrane in the presence of moisture and high temperatures. In order to determine if the membranes' surface reconstruction was caused by water created during the reduction step at 750 °C, similar experiments were performed without reduction on a 3 μm platinum patterned membrane. Figure D.4 shows the surface of a patterned membrane after 6 hours of CO₂ reforming at 750 °C with no pre-reaction reduction step.

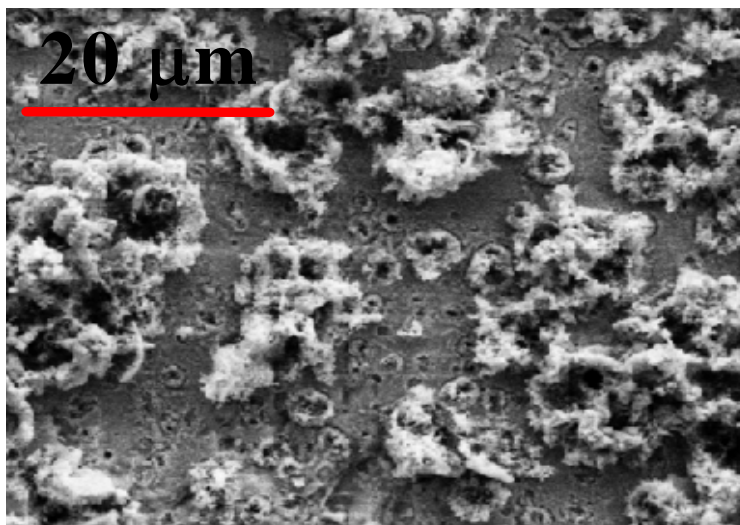


Figure D.4: Polished membrane surface with 3 μm Pt features after CO₂ reforming of CH₄ at 750 °C for 6 hours (no pre-reaction reduction), from Murphy [1]

It is clear from this SEM image that the reduction step is not solely responsible for the reconstruction as the outgrowths are still observed. Balachandran's theory that water formed at 750 °C causes the restructuring does not properly explain these phase outgrowths. It seems more likely that the surface restructuring results from a continuous reduction of the mixed oxide SFC material on the membrane's reaction side surface by hydrogen oxidation, whether during a preliminary catalyst reduction step or the test reaction period. Other investigations of SFC have used XRD to confirm the formation of surface areas of significant phase changes to reduced phases, particularly Co-Fe spinel

Appendix D

and cubic (or “rocksalt”) phases [3-7]. Water is thus merely evidence of the reduction process that produces the phase restructuring; it is not the cause of the restructuring.

Ma et al and Feng et al observed that SFC can decompose under reforming conditions to increase its bulk perovskite content, which is a more strontium-rich phase than the starting material (strontium is the “A” cation in the ABO_3 perovskite phase), and form the aforementioned spinel and cubic phases, which are depleted in strontium, on the surface [3, 7]. Because the metal ions do not vaporize significantly under our test conditions, this proposed phase transition requires the concentration of iron and cobalt on the surface. Murphy observed just such behavior on our the reaction-side surface of the SFC membranes discussed in this dissertation using EDX for elemental analysis before and after reaction [1]. The outgrowths in the SEM images in this Appendix were shown to be enriched in cobalt and iron relative to the bulk starting material.

Early, shorter tests of patterned membranes in lower temperature oxidizing and reducing environments did not result in this phase restructuring behavior. Since all patterned membranes tested were prepared at Argonne National Laboratory, it is possible the batch of membranes used for the reaction studies received different pretreatment at ANL and thus behaved differently than those used for the lower temperature oxidation and reduction studies. However, it is also possible (and much more likely) that the generally milder conditions (i.e., lower temperature and less reducing environments) were the cause of the difference, as lower temperature means lower oxygen lability and thus less extensive membrane material restructuring.

The hypotheses put forth in this work lead to the conclusion that moisture is a co-symptom of the membrane restructuring rather than the cause. The membrane is highly reducible and will therefore react readily with hydrogen. If it provides oxygen to oxidize hydrogen faster than it can be replenished by solid state diffusion, the top surface of the membrane will become depleted in oxygen and will begin to undergo the phase transitions described above and in Appendix B.

Appendix D

The final possible cause of surface reconstruction considered was the platinum pattern itself. To evaluate this possibility, we examined a polished but un-patterned membrane that had been exposed to 750 °C reduction and reforming reaction environments. Although this reaction test was stopped after only 4 hours because of low activity, the membrane surface still showed some segregation of iron and cobalt oxides (Figure D.5). The phase outgrowth was not as dramatic, but this plain membrane also did not produce significant methane conversion during its brief reaction period, which means the amount of hydrogen it was exposed to was minimal compared to the patterned membranes.

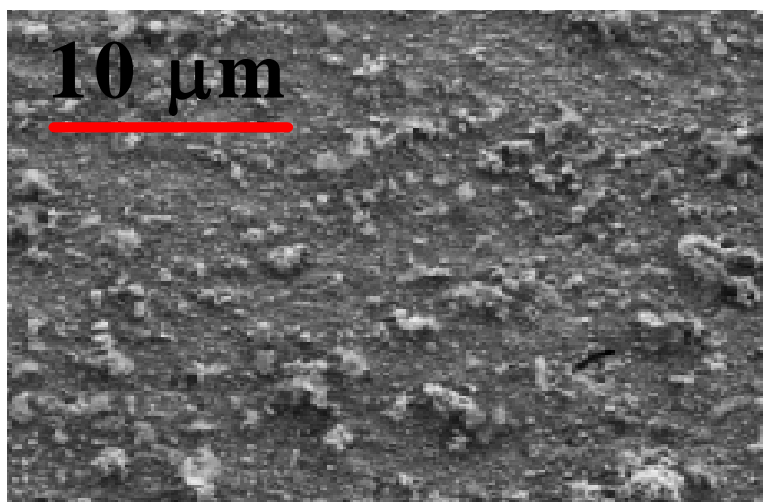


Figure D.5: Polished membrane surface after reduction and CO₂ reforming of CH₄ at 750°C for 4 hours (no deposited features).

All experimental evidence indicates the reaction environment itself is the likely cause of the observed surface reconstruction, with higher methane conversion leading to greater degrees of reconstruction. More methane conversion produces more hydrogen and therefore a more reducing environment. This work proposes that the previously described phase reconstruction occurs because the SFC is reduced by hydrogen and that water is merely a byproduct of the reduction process rather than the cause of the solid-state phase changes.

Appendix D

D.2: Catalyst dispersion calculations for patterned membranes discussed in Chapter 5

Methane conversion turnover frequency results were presented for the patterned membranes in Chapter 5 for both exposed and total platinum. These estimates for the 3-micron patterned membranes were calculated on the following basis:

- 1) Platinum unit cell dimension = 5.842 angstroms, back-calculated using:
 - Atomic packing factor for platinum of 0.79 [(atoms/unit cell)·(atom vol./unit cell vol.)]
 - Face-centered cubic (FCC) unit cell structure with 14 atoms per unit cell
 - Atomic radius of 1.39 angstroms
- 2) Platinum atom surface exposure = 1.465×10^{15} atoms/cm², calculated using:
 - Unit cell dimension of 5.84 angstroms (above)
 - 5 exposed platinum atoms per unit cell face (FCC geometry)
- 3) Platinum area fraction in pattern = 0.11045, calculated using:
 - 3 micron diameter platinum particles (photomask dimension)
 - 5 micron edge-to-edge spacing (photomask dimension)
- 4) Total patterned area per membrane = 1.533 cm², calculated using:
 - 0.55 inch diameter patterned area (photomask dimension)
- 5) Exposed surface area per platinum particle = 7.257 μm², calculated using:
 - Cylindrical particle geometry (photomask)
 - 20 nm particle side height (deposition thickness)

With 6.023×10^{23} atoms per mole, the above parameters give **4.23×10^{-10} moles of exposed platinum** per patterned membrane.

The total overall platinum per patterned membrane can be calculated with the following additional parameters.

- 6) Particle volume per membrane = 3.386×10^5 μm³, calculated using:
 - 1.533 cm² total pattern area (above)
 - 0.11045 platinum area fraction in pattern (above)
 - 20 nm particle side height (deposition thickness)
- 7) Platinum atom density = 7.022×10^{10} atoms/μm³, calculated using:

Appendix D

- Unit cell dimension of 5.84 angstroms (above)
- 14 platinum atoms per unit cell (FCC geometry)

This gives **3.95×10^{-8} moles of total platinum** per patterned membrane.

A dispersion values was never calculated for these membranes because exposed platinum was actually estimated before total platinum was, but, for the record, these values give a **platinum dispersion of 1.07%**.

References Cited in Appendix D

1. Murphy, S., *Fabrication and Catalytic Patterning of Non-porous Ion and Electron Dual-Conducting Membranes Using Electron Beam Evaporation*, in *Department of Chemical and Petroleum Engineering*. 2005, University of Kansas: Lawrence, KS.
2. Murphy, S.M., D.A. Slade, K.J. Nordheden and S.M. Stagg-Williams, *Increasing oxygen flux through a dense oxygen permeable membrane by photolithographic patterning of platinum*. *J of Membr Sci* **277**(1-2), 2006, p.94-98.
3. Feng, S.J., S. Ran, D.C. Zhu, W. Liu and C.S. Chen, *Synthesis gas production from methane with SrFeCo_{0.5}O_y membrane reactor*. *Energy & Fuels* **18**, 2004, p.385-389.
4. Fossdal, A., L.T. Sagdahl, M.-A. Einarsrud, K. Wiik, T. Grande, P.H. Larsen and F.W. Poulsen, *Phase equilibria and microstructure in Sr₄Fe_{6-x}Co_xO₁₃ (0 ≤ x ≤ 4) mixed conductors*. *Sol St Ionics* **143**, 2001, p.367-377.
5. Kim, S., Y.L. Yang, R. Christoffersen and A.J. Jacobson, *Determination of oxygen permeation kinetics in a ceramic membrane based on the composition SrFeCo_{0.5}O_{3.25-δ}*. *Sol St Ionics* **109**, 1998, p.187-196.
6. Armstrong, T., F. Prado, Y. Xia and A. Manthiram, *Role of perovskite phase on the oxygen permeation properties of the Sr₄Fe_{6-x}Co_xO_{13+δ} system*. *J Electrochem Soc* **147**(2), 2000, p.435-438.
7. Ma, B., N.I. Victory, U. Balachandran, B.J. Mitchell and J.W. Richardson, *Study of the mixed-conducting SrFeCo_{0.5}O_y system*. *J Am Ceram Soc* **85**(11), 2002, p.2641-2645.

Appendix E
Flux Test Methodology and Data Analysis

E.1: QTMR Set-Up Procedures for Membrane Flux Testing

- 1) a) Confirm that the surfaces of the large quartz tubes that will contact the membrane are free of defects (to ensure a good seal). If they are not in usable condition, then re-finish the tube faces as needed or take them to the glassblower in the Chemistry department for re-finishing.
b) If using a new ceramic membrane, plane both sides and then sand to the desired smoothness
c) Glue a gold gasket to the top side of the prepared membrane. Use a few small drops of glue and compress the first gasket against the membrane immediately; then allow the glue to dry for at least 60 minutes. Repeat on the other side of the membrane for the bottom gasket, if desired.
- 2) a) Revise the Camile program as needed before anything else is started. (The Camile program must be running for gases to flow, and a program can't be changed while it is running.) After revising the program, make sure the "max_start_temp" variable is set to zero and then start the Camile program.
b) Begin flushing the shorted reactor line and mass spectrometer (MS) with Ar at a moderate flowrate the night before a test is to begin. If possible, also flush the bypass/GC line overnight with air (or start the air flow as soon as possible the next day).
c) The next day, turn on the MS before Step 3 to monitor the flushing process. Allow the MS filament and the detector signals to stabilize.
- 3) a) Increase the Ar flowrate through the bypass/MS to the maximum value (if not already there) to get an MS signal for 100% Ar and minimum signals for everything else.
b) After the MS signals have stabilized and before doing anything else, start saving MS data to record the maximum/minimum signal data. Continue to save MS data during the subsequent calibration steps.
c) Determine Ar flowrate setpoints for ALL Ar flowrates that will be required for MS calibration (see Step 4b below). If possible, proceed from the highest to the lowest flowrate and wait as long as necessary for each flowrate to stabilize completely.
d) Begin assembling the two reactor parts if they are not already assembled.
e) At some point during this step, connect an air cylinder to the input line for CO₂ (but don't start flowing air until the next step).
- 4) a) After all Ar setpoints have been determined, ensure that the bypass line is not flowing to the MS and flush the bypass with air at the maximum flowrate for at least 20 minutes. Then establish a very low flow rate for air (5-10 ccm). Wait at least 15 minutes to confirm that the flowrate is stable before proceeding.
b) To calibrate the MS for flux and leak quantification, flow two different mole fractions of air in Ar through the reactor bypass line. For best results, use a constant air flowrate (the low flowrate from Step 4a) mixed with two different high Ar flowrates (from Step 3c). The chosen oxygen mole fractions should bracket the maximum mole fraction expected during the study.

Appendix E

- c) If GC air calibration data are desired, GC injections can be done for each of the air mole fractions in Step 4b (NOTE: this will increase the time for this step).
- d) *During this MS calibration work, the Oxygen Analyzer can be calibrated in Camile, if desired.*
- 5) a) After air calibration work is complete, switch the Ar flow to the reactor inlet/outlet “short circuit” line to finish flushing the reactor lines. Flush is complete when the MS signals have stabilized.
- b) Install the reactor after the reactor “short circuit” line is fully flushed.
- 6) a) After the installed reactor is fully flushed, set the Ar flowrate to the desired sweep gas rate (established in Step 3c).
- b) Create Camile data logging files and start logging data. Record reactor temperature, furnace temperature, furnace output, and oxygen analyzer data.
- c) If desired, start saving flowmeter data for the reactor outlet flowrate.
- d) Once MS signals have stabilized, start the flux test program in Camile: confirm that the “program_selector” variable is set to 2 and increase the “max_start_temp” variable value above the current reactor temperature.
- 7) After the reactor reaches its maximum temperature, the gold ring gaskets have sealed, and the membrane has equilibrated, do a helium (He) permeation test to check for membrane cracks:
- a) Ensure that the He cylinder delivery pressure zero, then open the main cylinder valve.
- b) Turn off the air supply and switch the air side inlet line to the He cylinder. Increase the cylinder pressure until the gas flow is just audible with the air side outlet next to your ear (turn off the hood for this step so the gas flow can be heard). This corresponds to a flowrate of more than 1000 ccm (too high to measure with the flowmeter).
- c) Leave the He flowing for about 5 minutes, then reduce the He cylinder delivery pressure to zero and wait for the line pressure to drop.
- d) Switch the air side inlet line back to the air compressor and observe the He signal in the MS for about 5 more minutes. The magnitude of the increase in the He signal indicates the relative magnitudes of the leaks through the gold ring seal and the membrane itself.
- 8) Ensure MS is operating properly and is collecting data at the desired rate, then start the Camile program.

Table E.1: Approximate time required for QTMR set-up procedures

| Step # | 2 | 3 | 4 | 5 | 6 | 7 | Total |
|------------------------|-------|-------|--------|-------|----|--------|---------------------------|
| Approximate time [min] | 10-60 | 60-90 | 90-120 | 15-30 | 15 | 75-120 | 265-435 (4 – 7.25 hrs) |

Appendix E

E.2: Flux Data Analysis Overview

After testing is complete the MS data can be imported into the Excel spreadsheet “Flux worksheet” to calculate flux estimates over the period of interest. “MS flux worksheet (DAS) 03-2010” uses the two calibration data points to estimate mole fractions of oxygen, nitrogen, and argon from individual MS data points over any period of interest. It compares the signal ratio of oxygen and nitrogen to that determined for air in the calibration data and then calculates the oxygen excess or deficiency from the calibration ratios.

Signal ratios must be used instead of individual signal because substantial signal drift is observed with this particular mass spectrometer, in spite of the manufacturer’s denials that this is possible. Signals consistently drop in reducing environments (e.g., with some fraction of hydrogen in the feed) and rise in oxidizing environments (e.g., during air/argon calibration flow periods). The practice of using ratios to calculate fluxes was adopted and has worked very well.

“MS flux worksheet (DAS) 03-2010” has the option of using an exponential curve fit to the calibration data, but good results have been obtained with a simple linear fit as well. The linear fit is recommended for simplicity but the exponential functionality was left in the spreadsheet in case it is needed. Calibration curve fits must be done manually at this point.

E.3: Additional Details for Flux Testing Set-Up

These notes are provided in terms of the step they correspond to in the start-up procedures in Section E.1. This is why the numbering is unusual.

- 1) b) Anything painted with the BN_3 paint (e.g., the stainless steel blank) must be baked at ~ 450 °C for ~ 2 hours (or more) to remove solvents and carbon-containing compounds from the paint. BN_3 paint will interfere with the seal between the gold gasket and the blank membrane, so use a “mask” when painting the blank to keep the gasket seat areas free of paint.
- c) A painted stainless steel blank must be baked BEFORE attaching the gold gaskets. Otherwise, the glue will degrade in the baking process.
- 2) a) The “max_start_temp” variable is used to allow the program to be started so gas flows can begin but to prevent the actual steps of the program from beginning. If the value of “max_start_temp” is greater than the temperature reported by the Reactor Furnace thermocouple, then the program steps will be initiated. If this happens, the only way to stop the progress of the program is to stop the program itself. However, you can also immediately increase the value of the “pre_rxn_hold” parameter to delay the start of the heating ramp.
- b) The gold gaskets will not seal until the reactor is heated, so the final system flush is not possible until the gaskets soften and seal at 800 °C. However, beginning to flush the system as early as possible greatly accelerates the steps that follow.

Appendix E

- c) The mass spectrometer should be baked for at least 12 hours prior to a new test to remove residual water from the sample chamber. The valve must be open during baking and Ar should be flowing past the inlet at > 40 ccm during the baking process. After baking, the MS must be allowed to cool for several hours. It is best to increase the Ar flowrate prior to stopping the baking process to maintain a dry and inert environment during cooling.

NOTE: to confirm that a line is fully flushed with Ar, change the Ar flowrate and observe the MS signal change. If the signals stabilize quickly after both an increase and a decrease in Ar flowrate, then the lines are flushed.

- 3) a) While the Ar flow is at its maximum, set the zero point of the Oxygen Analyzer calibration, if it is being used.
- 4) a-d) The maximum O₂ mole fraction observed with the SFC membrane has been ~ 0.015 for *flux studies* at 800 °C with 20 ccm sweep gas, which corresponds to an air mole fraction of 0.08, so I have typically used approximately 5 and 10% air in Ar to calibrate for flux studies. The 10% air/Ar flow should also be used as the maximum value for the Oxygen Analyzer calibration after its signal stabilizes. The quickest way to get two relatively accurate air/Ar compositions is to set the air to a low flowrate (I use 5-10 ccm) after the line has been flushed with air for a while. Then DON'T TOUCH that setpoint until you turn off the air (lower flowrates are less stable and less accurate (relatively) than high flowrates, and even small changes in flowrate can have a large effect on your calibration. Because drifts occur after set point changes, set point changes should be minimized). Use two different high flowrates of Ar with this steady air flowrate (high flowrates are more reliable than low ones, and this approach compensates somewhat for the greater relative error in the air flowrate). The two Ar flowrates I use are ~ 90 ccm and ~ 190 ccm. Setting the lower flowrate first will minimize flowrate stabilization times.

NOTE 1: the actual flowrates for this calibration don't matter as long as they are measured and recorded accurately, so it is better not to spend time trying to get a specific flowrate because each adjustment to the flow controller takes time to stabilize. Once you are close to the desired flowrate just allow the flow to stabilize and record the result.

NOTE 2: the two Ar flowrates discussed above should have been determined in Step 3c. It is too late to determine them accurately once the air flow has been started (unless the air flow is stopped, which is bad, and the lines are thoroughly flushed with Ar again, which will take at least 30 more minutes).

- 6) a) Standard sweep gas flowrate: 20 ccm (Ar)

At room temperature there will be a substantial leak in the reactor, so the actual reactor effluent flowrate will be much less than the sweep gas feed flowrate. This means that it can take a long time for the MS signals to stabilize after you switch to the final sweep gas flowrate. If the measured outlet flowrate is less than 10 ccm, I will turn up the feed flowrate until the outlet flowrate is ~ 10 ccm. After the seal improves enough that the outlet flowrate increases to greater than 50% of the current inlet Ar flowrate (whatever it is), I return the Ar setpoint to the 20 ccm value.

- b) Standard data logging interval for Camile: 1 minute
c) Standard data save interval for the Flowmeter: 20 seconds

Appendix E

7) The standard equilibration time has been between 2.25 and 2.5 hours at 800 °C. This should also be done with the stainless steel blank to maintain consistent catalyst pre-treatment.

- c) The He exposure should not be too long or it will affect the oxygen content of the membrane. If it is not long enough, then any He permeation can be difficult to assess. Four to five minutes is a good time.

Appendix F
Flux Study Overview

F.1: Flux Test Set Summaries

Two different batches of membranes were tested for the effect of surface treatments including platinum particle deposition and multicomponent particle deposition (See Section F.2 for multicomponent particle information). The first set presents results for “first generation” membranes made at Argonne National Laboratory from SFC powder procured from Superconductive Components, Inc. and tested in the SSMR. The second set contains results for so-called “large batch” membranes also from ANL and from Superconductive Components SFC. The same SFC powder was used for the “large batch” but it had been stored in uncontrolled conditions in our lab for a year. This batch of membranes was significantly larger than the previous batch, even though ANL reported that they used exactly the same preparation method and amount of powder. It is possible that the aged powder had changed and did not sinter with the same crystal structure as the earlier batch. Flux testing allows a comparison of the two batches.

F.1.1: First generation membrane flux test results

The platinum patterned membrane had 5-micron diameter platinum particles spaced 3 microns edge-to-edge in a rectangular grid. The pattern was positioned on the air side of the reactor (bottom side). These results were published by Murphy et al. in 2007 [1].

In general, temperatures were tested sequentially from coolest to hottest in the early flux tests. However, the 650 °C point that is off of the curve for the plain membrane was obtained on cool-down from the maximum temperature of 800 °C and was therefore out of sequence, with a notable hysteresis effect. This was the result of an incorrect Camile programming step and was not intentional. Because the 650 °C point was collected out of sequence and appeared to be biased by that fact, it was not included in the published data.

Appendix F

The hysteresis effect is not surprising, as multiple researchers reported sustained increasing flux with SFC membranes and higher temperature exposure [2-4]. The increased flux is attributed to an increase in perovskite content at the higher temperature that then persists as the membrane is cooled because of slow solid state phase change kinetics at the lower temperatures.

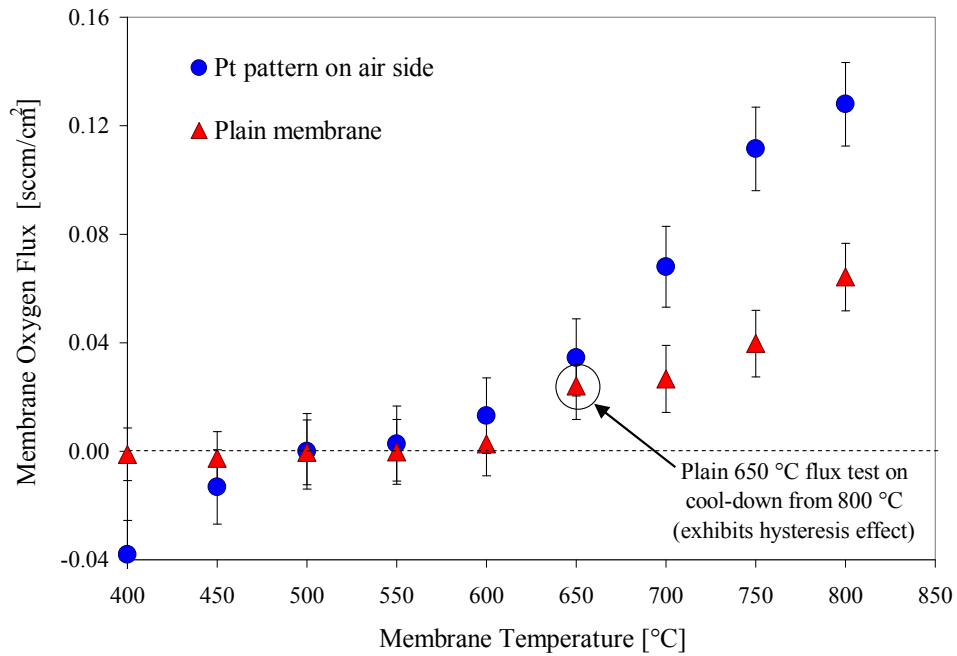


Figure F.1: First generation SFC membrane oxygen flux test results under an air:argon gradient as sccm/cm² O₂ in the reactor effluent

Figure F.2 provides an Arrhenius plot for these flux results that are greater than zero. The data are not linear, but they are close enough that reasonable lines can be fit through them to allow a comparison. The slopes (i.e., exponential factors) are similar for the two types of membrane.

Appendix F

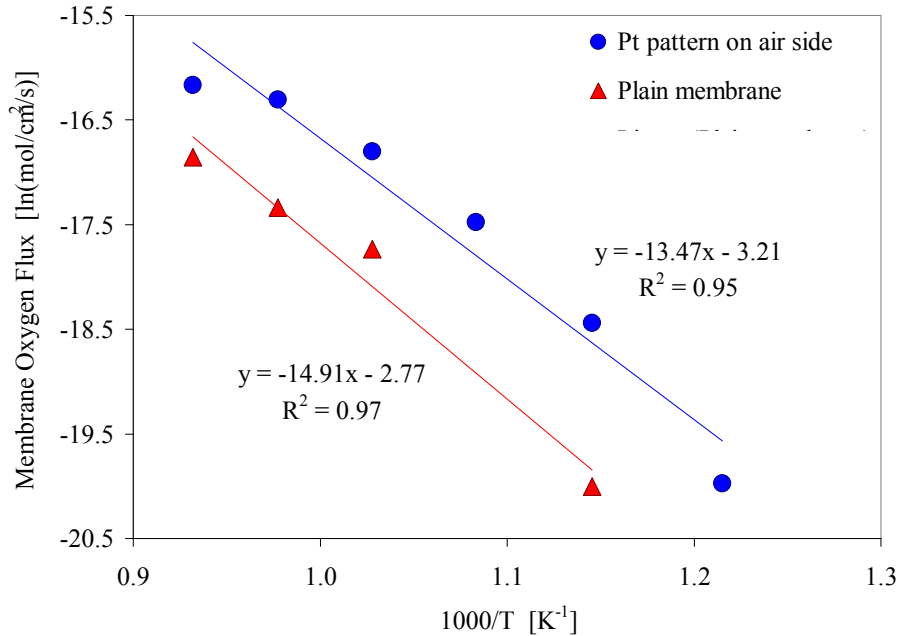


Figure F.2: First generation SFC membrane oxygen flux test results under an air:argon gradient presented as an Arrhenius plot with lines fit by Excel

F.1.2: “Large batch” membrane flux test results

The platinum patterned membranes in these tests had 3-micron diameter particles on 5 micron edge-to-edge spacing rather than 5 micron particles as in Section F.1.1. There was therefore less total platinum on these membranes. Also, the platinum pattern was placed on the oxygen collection (or top) surface in the reactor because reaction tests were conducted after the flux testing. In spite of these differences (i.e., larger membranes, smaller particles, platinum on top instead of bottom), the flux of the patterned membranes was similar to the patterned membrane flux in Figure F.1. However, the plain membrane flux is significantly higher in Figure F.3, indicating that the SFC powder storage period and potentially different sintering process did not have a negative effect on these membranes.

Appendix F

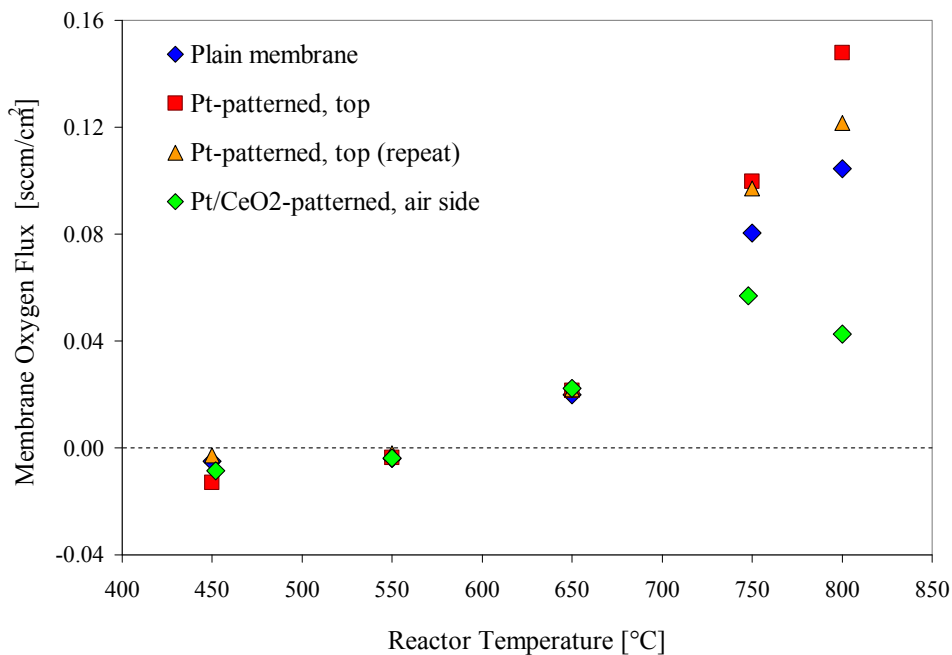


Figure F.4: “Large batch” SFC membrane oxygen flux test results under an air:argon gradient as sccm/cm² O₂ in the reactor effluent

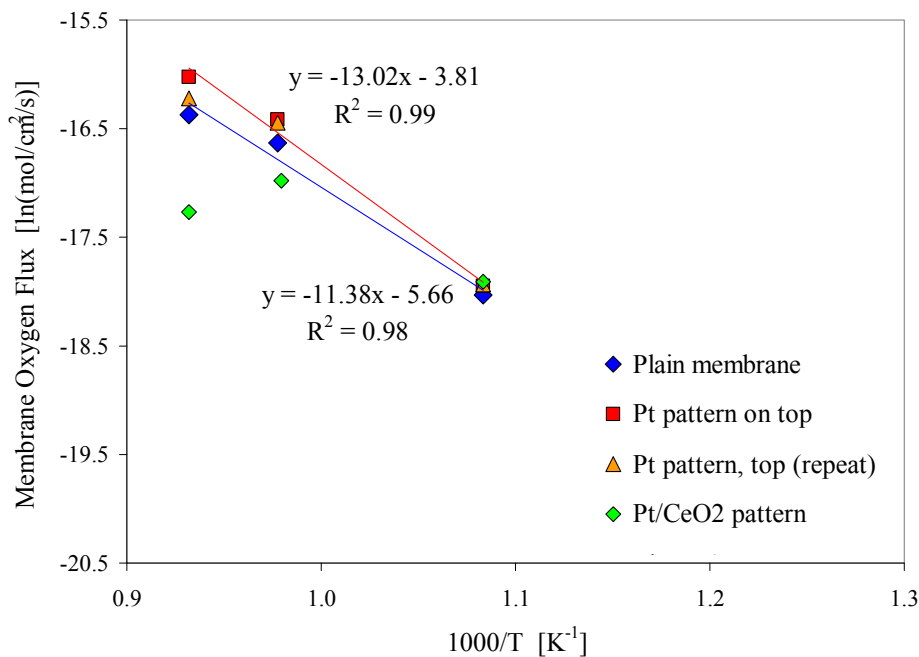


Figure F.4: “Large batch” SFC membrane oxygen flux test results under an air:argon gradient presented as an Arrhenius plot with lines fit by Excel

Appendix F

The Arrhenius plots in Figure F.4 show a similar shape to those in Figure F.2 as well as somewhat similar values. The trend of decreasing flux temperature dependence with increasing temperature appears to be a characteristic of these SFC membranes.

The “large batch” of membranes also included the multicomponent patterned membrane described in Section F.2. Because substantial SFC surface restructuring on the oxidizing side (or anodic) side of the membrane had been observed at this point, the Pt/CeO₂ composite particle surface was tested on the oxygen supply (or cathodic) side of the reactor. It is very interesting to note that the composite particle membrane shows good agreement with the other membranes until the reactor temperature gets above 650 °C, at which point it deviates fairly sharply. This observation is consistent with later observations in the CO₂ reforming tests with the powder Pt/CeZrO₂ catalyst that the ceria-doped zirconia support appears to interact with oxygen in the reaction chamber. Flux estimates during reaction with the SFC membrane were largely negative, indicating that something in the reactor was incorporating oxygen (from CO₂, in that case). In this flux test with Pt/CeO₂ particles, it appears that the Pt/CeO₂ particles might be extracting oxygen from the membrane above a certain temperature, or otherwise be preventing the oxygen from the air supply to be incorporated into the SFC membrane.

F.2: Multi-Component Patterning

Multi-component catalyst features have also been fabricated on polished membrane surfaces using a serial photolithography process with an electron-beam evaporation step after each photolithography step. Figure F.a shows an SEM image of 2 μm Pt clusters deposited on top of 5 μm ceria clusters. The square in the image indicates the area of the surface at which an EDX spot scan was performed. The results of the spot scan are shown as Figure F.6 and confirm the presence of Pt, Ce, and the membrane components (Sr, Fe, Co, O). Figures F.5 through F.7 and an explanation of the fabrication process were originally published by Murphy [5].

Appendix F

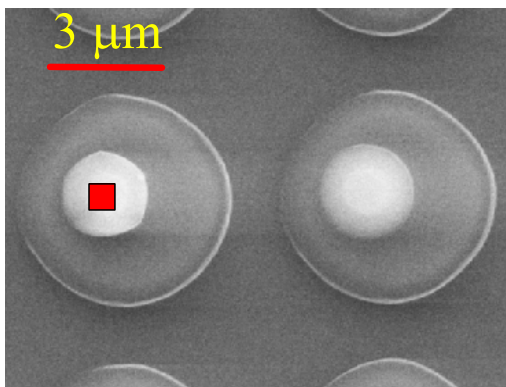


Figure F.5: Polished membrane surface with 2 μm Pt features deposited on 5 μm CeO₂ features.

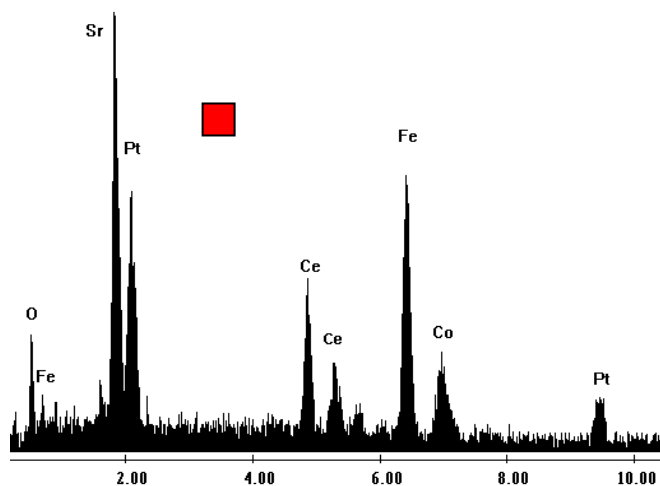


Figure F.6: EDX spot scan results at the location of the red square in Figure F.5

One goal for the developed membrane patterning process was to deposit large arrays of identical supported catalyst particles on membrane surfaces. Not only would such arrays reduce the catalyst variability inherent in traditional methods of supported catalyst synthesis, but they would also produce supported catalyst particles in direct contact with the membrane surface. By removing mass transfer steps and allowing the utilization of different oxygen species that might be present on the membrane surface, such patterning could eventually lead to an increase in membrane oxygen utilization over that by a traditional powder catalyst. Such a mono-disperse supported catalyst array could also greatly improve studies of particle size effects and particle/support interactions. Figure F.7 shows a larger region of the same membrane as Figure F.a in which each small dot represents one of the multi-component catalyst features shown in Figure F.a.

Appendix F

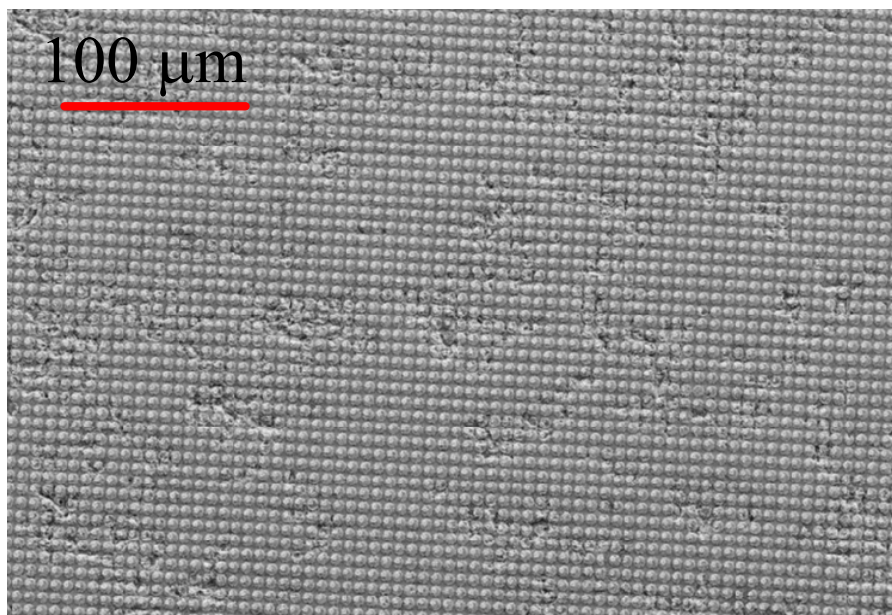


Figure F.7: Expanded view of membrane in Figure F.5

References Cited in Appendix F

1. Murphy, S.M., D.A. Slade, K.J. Nordheden and S.M. Stagg-Williams, *Increasing oxygen flux through a dense oxygen permeable membrane by photolithographic patterning of platinum*. J of Membr Sci **277**(1-2), 2006, p.94-98.
2. Fossdal, A., L.T. Sagdahl, M.-A. Einarsrud, K. Wiik, T. Grande, P.H. Larsen and F.W. Poulsen, *Phase equilibria and microstructure in $Sr_4Fe_{6-x}Co_xO_{13}$ ($0 \leq x \leq 4$) mixed conductors*. Sol St Ionics **143**, 2001, p.367-377.
3. Ikeguchi, M., K. Yoshino, K. Kanie, M. Nomura, E. Kikuchi and M. Matsukata, *Effects of preparation method on oxygen permeation properties of $SrFeCo_{0.5}$ membrane*. Sep & Pur Tech **32**, 2003, p.313-318.
4. Ma, B., N.I. Victory, U. Balachandran, B.J. Mitchell and J.W. Richardson, *Study of the mixed-conducting $SrFeCo_{0.5}O_y$ system*. J Am Ceram Soc **85**(11), 2002, p.2641-2645.
5. Murphy, S., *Fabrication and Catalytic Patterning of Non-porous Ion and Electron Dual-Conducting Membranes Using Electron Beam Evaporation*, in *Department of Chemical and Petroleum Engineering*. 2005, University of Kansas: Lawrence, KS.

Appendix G

Reaction Test Methodology and Data Analysis

G.1: Improvements to the QTMR after the Initial Set of Tests

The following improvements were made to the QTMR system after the first round of testing was completed and evaluated.

- 1) To reduce water condensation in the effluent line, line heating was enhanced and additional insulation was added to the top portion of the reactor where the effluent line is located.
- 2) A short piece of Teflon tubing was added to the top of the reactor to minimize the lateral forces that had been applied to the top by the stainless steel tubing that was in place. This diminished the ability to heat the line, but the compromise appears to be worthwhile because the seal improved and, most important, reactor assembly became much easier. Also, the Teflon tube piece is translucent, so condensed water can be observed directly if the insulation is moved aside.
- 3) The pneumatic press was improved with custom-made Viton gaskets and the use of a silicone lubricant. This also made reactor assembly easier and more predictably (a membrane had been broken on assembly in an earlier test when the press caught during pressurization and then suddenly and violently came free under pressure).
- 4) A custom mixed cylinder of calibration gas containing precisely known amounts of methane, CO₂, carbon monoxide, and hydrogen was obtained from Praxair. These four components are present in the custom calibration gas in roughly equal proportions. This composition was selected based on observations of previous tests as representative of the reactor effluent during periods of moderate to high methane conversion for our reaction conditions. The calibration gas cylinder allows a rigorous “before and after” calibration protocol to be implemented. Prior to this, calibrations were performed by mixing individual gases, which placed the entire burden of accuracy on the Mass Flow Controllers that controlled the component gas flows. This approach had been implicated in certain systematic inaccuracies. However, these inaccuracies were minor compared to problems caused by detector drift and response decay in the GC. By bracketing each reaction test with calibration gas injections, any drift in the GC signals can be observed directly. The reactor feed is tested before and after the reaction as well, so any drift or changes in the reactor feed composition over time can be observed directly. The calibration gas removed two significant sources of experimental error and can be considered a major success. It is safe to say that membrane oxygen flux estimates during reaction depend on it. The GC calibration procedure using the calibration gas is detailed in Section G.2.
- 5) The soap-film flowmeter was replaced with a digital flowmeter that allowed reactor effluent flowrate to be measured both continuously and more accurately during flux and reaction testing. Like the calibration gas cylinder, this acquisition also had a major impact on the quality of the analytical results. The only shortcoming to the flowmeter is its sensitivity to water. Streams with more than about 1% water cause its quartz crystal mechanism to stop working. It therefore can only be used intermittently during reaction testing. However, this actually has little impact on the utility of the flowmeter, because flow readings are taken at the same time as the GC injections, which allows a flowrate to be known for each effluent composition.

Appendix G

G.2: Summary of Reaction Test Procedures (General)

- 1) a) Load catalyst into reactor, install reactor, and then flush reactor with Ar for as long as possible prior to starting the test (e.g., overnight).
b) If using the PFR, flush the system's reactor bypass/GC line with the Calibration Mixture gas [25% each CH₄, CO₂, CO, and H₂] at a high flowrate (~100 ccm) for at least one hour prior to starting calibration injections. NOTE: the reactor outlet should be flowing past the MS inlet at this time.

- 2) a) Start saving MS data for the reactor outlet stream, then set the Ar flowrate to the desired value for reactor heat-up. Wait at least 15 minutes to confirm flowrate stability.
b) After completing the temperature profile for the test (either in Camile or with the Omega temperature controller), start the reactor heating ramp. NOTE: with the Omega controller, enter a longer reaction hold time than you think you will need, as this time can't be increased after the program is initiated but the program can be stopped manually at any time.
c) Start a pre-reaction GC calibration injection series with the Calibration Mix gas as soon as possible (but after at least one hour of flow). NOTE: be sure to open the air cylinder for the GC's FID unit and ignite the FID before starting the GC injections.

- 3) a) Stop the Calibration Mix gas flow after the third or fourth GC injection and begin establishing the reactant gas flow setpoints through the reactor's bypass line. Each gas's flowrate must be set individually.
b) For each gas, flush the bypass line for at least 15 minutes with a very high flowrate (>100 ccm) before setting the target flowrate. Wait at least 15 minutes to confirm flowrate stability before proceeding to the next gas. NOTE: CO₂ takes the longest to stabilize, so be particularly patient with it.
c) Leave the last reactant gas flowing once its flowrate is steady and start the other gases one at a time with a small pause (~1 minute) between each gas (add CO₂ last, if possible).

- 4) a) Allow the reactant gas mixture to flow for at least 1 hour before starting a pre-reaction reactor feed "blank" injection series with the GC. Then do as many blank injections as possible with the final one starting not less than 25 minutes before the desired reaction start time.
b) At some point prior to starting the reaction, the GC outlet (with the reactant gas mixture) should be switched to the MS. To observe the MS signals for the reactant mix this should be done at least 15 minutes before the reaction. It can also be done immediately prior to starting the reaction.

- 5) a) To start the reaction, stop the Ar flow to the reactor and switch all of the reactant gases to the reactor simultaneously. Record the time that this is done and set up the reaction GC injection series in the GC software (PeakSimple). NOTE: enter a larger number of injections than you think you will need, as this number can't be changed after the series is initiated.
b) After the MS signals have stabilized somewhat, begin the reaction GC injection series. NOTE: This should not be done less than 4 minutes after starting the reaction.

Appendix G

- 6) a) When the reaction test is complete, stop it after the final reaction GC injection by switching all of the reactant gases to the bypass/GC line simultaneously and re-starting the Ar flow through the reactor.
- b) Depending on the goals of the test, monitor either the reactant mixture or the reactor outlet with the MS at this time.
- c) Do a series of post-reaction “blank” GC injections with the reactant gas mixture through the bypass.
- 7) a) After the final “blank” injection, stop the reactant mixture gases and start the Calibration Mix gas at a high flowrate (>100 ccm) through the bypass/GC (and the MS also, if the reactor outlet is no longer being monitored).
- b) Do a series of post-reaction GC calibration injections with the Calibration Mix gas.
- 8) a) After the final calibration injection event, stop the flow of the Calibration Mix gas. NOTE: be sure to close the FID’s air supply cylinder after the GC’s temperature profile is complete.
- b) Close all gas cylinders and “bleed” all MFC (Mass Flow Controller) feed lines.
- c) When no more MS data needs to be collected, stop the MS “measure” program and turn off the MS filaments. NOTE: ensure that the MS inlet line is fully flushed with Ar before doing this. Keep the MS valves open and Ar flowing past the inlet when the instrument is not in use.

Table G.1: Approximate time required for reactor set-up and shutdown procedures

| Step # | 2 | 3 | 4 | 5 | 6 | 7 | 8 | Total [min] |
|----------------------|-----|-----|-----|----|-----|-----|----|--|
| Estimated time [min] | 150 | 150 | 150 | 15 | 100 | 100 | 30 | 465 / 230 (<i>setup / shutdown</i>) |

NOTE 1: the setup time in Table G.1 does not include any time for Step 1. To avoid unexpected delays or incomplete reactor flushing, it is best to do this step the evening before the reaction test is to be started.

NOTE 2: The following procedures are specific to the QTMR

G.3: Reaction Test Set-Up Procedure for the QTMR

- 1) a) Confirm that the surfaces of the large quartz tubes that will contact the membrane are free of defects (to ensure a good seal). If they are not in usable condition, then re-finish the tube faces as needed or take them to the glassblower in the Chemistry department for re-finishing.
- b) If using a new ceramic membrane, plane both sides and then sand to the desired smoothness

Appendix G

If using the stainless steel blank, paint both surfaces with a thin coat of BN_3 paint then bake the painted blank at $450\text{ }^\circ\text{C}$ for at least 2 hours. Cover the perimeter of each face with a “mask” before painting and then remove any paint around the perimeters.

- c) Glue a gold gasket to each side of the prepared membrane (ceramic or blank). Use a few small drops of glue and compress the gasket against the membrane immediately; then allow the glue to dry for at least 60 minutes. Repeat on the other side of the membrane.
- 2) a) Revise the Camile program as needed before anything else is started. (The Camile program must be running for gases to flow, and a program can't be changed while it is running.) After revising the program, make sure the “max_start_temp” variable is set to zero and then start the Camile program.
b) Begin flushing the “shorted” reactor line and mass spectrometer (MS) with Ar at a moderate flowrate (~50 ccm) the night before a test is to begin. If possible, also flush the bypass/GC line overnight with air through the CO_2 gas channel (or start the air flow as soon as possible the next day).
c) Turn on the MS before the next step (Step 3) to monitor the flushing process. Allow the MS filament and the detector signals to stabilize.
 - 3) a) Increase the Ar flowrate through the bypass/MS to the maximum value (if not already there) to get an MS signal for 100% Ar and minimum signals for everything else.
b) After the MS signals have stabilized and before doing anything else, start saving MS data to record the maximum/minimum signal data. Continue to save MS data during the subsequent calibration steps.
c) Determine Ar flowrate setpoints for ALL Ar flowrates that will be required for MS calibration (see Step 4b below). If possible, proceed from the highest to the lowest flowrate and wait as long as necessary for each flowrate to stabilize completely.
d) Begin assembling the two reactor parts if they are not already assembled
 - 4) a) Ensure that the bypass line is not flowing to the MS and flush the bypass with air at the maximum flowrate for at least 20 minutes (this can be done before during Step 3; the actual time depends inversely on how long air has previously been flowing). Then establish a very low flow rate for air (5-10 ccm). Wait at least 15 minutes to confirm that the flowrate is stable before proceeding.
b) To calibrate the MS for flux and leak quantification, flow two different mole fractions of air in Ar through the reactor bypass line. For best results, use a constant air flowrate (the low flowrate from Step 4a) mixed with two different high Ar flowrates (from Step 3c). The chosen oxygen mole fractions should bracket the maximum mole fraction expected during the study.
c) If GC air calibration data are desired, GC injections can be done for each of the air mole fractions in Step 4b (NOTE: this will increase the time for this step).
d) *During this MS calibration work, the Oxygen Analyzer can be calibrated in Camile, if desired.*
 - 5) a) After air calibration work is complete, switch the Ar flow back to the reactor inlet/outlet “shorted” line to finish flushing the reactor lines. Flush is complete when the MS signals have

Appendix G

stabilized. NOTE: The reactor outlet should be flowing through the “MS” line and into the MS itself so reactant flowrates can be established through the bypass line.

- b) Disconnect the air cylinder from the CO₂ line and re-connect the CO₂ cylinder.
 - c) From the PFR reactor system, begin flowing the Calibration Mix gas (~25% each CH₄, CO₂, CO, and H₂) at a high flowrate (~100 ccm) through the GC and to the vent but NOT to the MS, which should still be receiving Ar from the QTM reactor’s outlet. Wait at least 30 minutes, then start GC injections of the Calibration Mix gas.
 - d) Install the reactor after the reactor “short” is fully flushed. NOTE: the maximum recommended flowrate with loose catalyst on a membrane surface is ~80 ccm.
- 6) a) After the installed reactor is fully flushed, set the Ar flowrate to the desired sweep gas rate (established in Step 3c).
- b) Create Camile data logging files and start logging data. For flux & reaction studies, record reactor temperature, furnace temperature, furnace output, and oxygen analyzer data; for reaction-only studies, only furnace and reactor temperatures need to be recorded.
 - c) If desired, start saving flowmeter data for the reactor outlet flowrate. NOTE: water vapor exposure can damage the solenoid valve in the flowmeter. Because reactions can produce water, the flowmeter should be used intermittently and only for short time periods during the reaction itself.
 - d) Once MS signals have stabilized, start the reaction test program in Camile: confirm that the “program_selector” variable is set to 1 and increase the “max_start_temp” variable value above the current reactor temperature.
- 7) a) Monitor the initial heating ramp and pre-reaction hold with the MS (and save the data!).
- b) If not started already, start GC calibration injections with the Calibration Mix gas from the PFR system as soon as possible.
 - c) After the final Calibration Mix gas calibration injection, stop the Calibration Mix gas flow and establish individual reactant gas flowrates through the QTM reactor system’s bypass line. Enter each setpoint into the Camile program as it is determined.
 - e) Do pre-run blank injections with the entire reactor feed mixture. DO NOT stop or adjust the flow of the reactant gases once the entire mixture is started (i.e., allow them to flow continuously until the reaction is complete and the post-reaction blank injections are done).
- 8) After the reactor reaches its maximum temperature, the gold ring gaskets have sealed, and the membrane has equilibrated, do a helium (He) permeation test to check for membrane cracks [NOTE: this is not necessary with the SS blank]:
- a) Ensure that the He cylinder delivery pressure zero, then open the main cylinder valve.
 - b) Turn off the air supply and switch the air side inlet line to the He cylinder. Increase the cylinder pressure until the gas flow is just audible with the air side outlet next to your ear (turn off the hood for this step so the gas flow can be heard). This corresponds to a flowrate of more than 1000 ccm (too high to measure with the flowmeter).

Appendix G

c) Leave the He flowing for about 5 minutes, then reduce the He cylinder delivery pressure to zero and wait for the line pressure to drop.

d) Switch the air side inlet line back to the air compressor and observe the He signal in the MS for about 5 more minutes. The magnitude of the increase in the He signal indicates the relative magnitudes of the leaks through the gold ring seal and the membrane itself.

9) a) When starting a reaction, the reactor outlet must be switched to the GC inlet line (i.e., the heated metal line) and the MS inlet valve must be switched to the GC outlet line. Stop the Ar sweep gas before adjusting these valves. After adjusting the valves, the reactant mixture should flow into the reactor (this was previously flowing through the bypass to the GC) and the reactor effluent should flow to the GC and MS (previously to the MS directly).

b) Wait for the MS signals to reflect all of the changes (and stabilize somewhat), then begin the reaction GC injections.

Table G.1: Approximate time required for QTMR set-up procedures

| Step # | 2 | 3 | 4 | 5 | 6 | 7 | 8 & 9 | Total |
|------------------------|-------|-------|--------|-------|----|---------|--------|---------------------------|
| Approximate time [min] | 10-60 | 60-90 | 90-210 | 15-75 | 15 | 150-300 | 75-120 | 415-870 (7 – 14.5 hrs) |

G.4: Additional details for the Reaction Test Procedures

These notes are provided in terms of the step they correspond to in the Start-up procedures for reaction testing in Sections G.2 and G.3. This is why the numbering is unusual.

1) b) Anything painted with the BN₃ paint (e.g., the stainless steel blank) must be baked at ~450 °C for ~2 hours (or more) to remove solvents and carbon-containing compounds from the paint. BN₃ paint will interfere with the seal between the gold gasket and the blank membrane, so use a “mask” when painting the blank to keep the gasket seat areas free of paint.

c) A painted stainless steel blank must be baked BEFORE attaching the gold gaskets. Otherwise, the glue will degrade in the baking process.

2) a) The “max_start_temp” variable is used to allow the program to be started so gas flows can begin but to prevent the actual steps of the program from beginning. If the value of “max_start_temp” is greater than the temperature reported by the Reactor Furnace thermocouple, then the program steps will be initiated. If this happens, the only way to stop the progress of the program is to stop the program itself. However, you can also immediately increase the value of the “pre_rxn_hold” parameter to delay the start of the heating ramp.

b) The gold gaskets will not seal until the reactor is heated, so the final system flush is not possible until the gaskets soften and seal at 800 °C. However, beginning to flush the system as early as possible greatly accelerates the steps that follow.

Appendix G

- c) The mass spectrometer should be baked for at least 12 hours prior to a new test to remove residual water from the sample chamber. The valve must be open during baking and Ar should be flowing past the inlet at > 40 ccm during the baking process. After baking, the MS must be allowed to cool for several hours. It is best to increase the Ar flowrate prior to stopping the baking process to maintain a dry and inert environment during cooling.

NOTE: to confirm that a line is fully flushed with Ar, change the Ar flowrate and observe the MS signal change. If the signals stabilize quickly after both an increase and a decrease in Ar flowrate, then the lines are flushed.

- 3) a) While the Ar flow is at its maximum, set the zero point of the Oxygen Analyzer calibration, if it is being used.
- 4) a-d) The maximum O₂ mole fraction observed with the SFC membrane has been ~0.015 for *flux studies* at 800 °C with 20 ccm sweep gas, which corresponds to an air mole fraction of 0.08, so I have typically used approximately 5 and 10% air in Ar to calibrate for flux studies. The 10% air/Ar flow should also be used as the maximum value for the Oxygen Analyzer calibration after its signal stabilizes. The quickest way to get two relatively accurate air/Ar compositions is to set the air to a low flowrate (I use 5-10 ccm) after the line has been flushed with air for a while. Then DON'T TOUCH that setpoint until you turn off the air (lower flowrates are less stable and less accurate (relatively) than high flowrates, and even small changes in flowrate can have a large effect on your calibration. Because drifts occur after set point changes, set point changes should be minimized). Use two different high flowrates of Ar with this steady air flowrate (high flowrates are more reliable than low ones, and this approach compensates somewhat for the greater relative error in the air flowrate). The two Ar flowrates I use are ~90 ccm and ~190 ccm. Setting the lower flowrate first will minimize flowrate stabilization times.

NOTE 1: the actual flowrates for this calibration don't matter as long as they are measured and recorded accurately, so it is better not to spend time trying to get a specific flowrate because each adjustment to the flow controller takes time to stabilize. Once you are close to the desired flowrate just allow the flow to stabilize and record the result.

NOTE 2: the two Ar flowrates discussed above should have been determined in Step 3c. It is too late to determine them accurately once the air flow has been started (unless the air flow is stopped, which is bad, and the lines are thoroughly flushed with Ar again, which will take at least 30 more minutes).

- 6) a) Standard sweep gas flowrate: 20 ccm (Ar)

At room temperature there will be a substantial leak in the reactor, so the actual reactor effluent flowrate will be much less than the sweep gas feed flowrate. This means that it can take a long time for the MS signals to stabilize after you switch to the final sweep gas flowrate. If the measured outlet flowrate is less than 10 ccm, I will turn up the feed flowrate until the outlet flowrate is ~10 ccm. After the seal improves enough that the outlet flowrate increases to greater than 50% of the current inlet Ar flowrate (whatever it is), I return the Ar setpoint to the 20 ccm value.

- b) Standard data logging interval for Camile: 1 minute
c) Standard data save interval for the Flowmeter: 20 seconds

Appendix G

7) Immediately after the reaction is complete, do this same process in reverse. Without stopping the reactant gases, switch them to the reactor bypass line and do post-reaction blank injections. Then stop these gases and start the Calibration Mix gas again to do a final set of GC calibration injections. This strategy allows you to determine the actual composition of your reactor feed immediately before and immediately after the reaction. Also, these post-reaction flows can be monitored in the MS to obtain calibration data for it as well (not needed at this time, but they could be useful).

- c) flush the line with the highest flowrate of each gas for at least 15 minutes before setting the flowrate. Then be patient when setting the flowrate to allow it to stabilize completely. This can take up to 30 minutes for CO₂ (CH₄ is the fastest to stabilize, then H₂, then Ar or Ar/O₂, then CO₂).
- d) after all setpoints are determined, start each gas one by one in this order: Ar (or Ar/O₂), CH₄, and CO₂. Wait at least 1 minute before starting the next gas, then wait at least 15 minutes for all of the flowrates to become fully established before starting the GC injections (a longer wait is even better).

8) The standard equilibration time has been between 2.25 and 2.5 hours at 800 °C. This should also be done with the stainless steel blank to maintain consistent catalyst pre-treatment.

- c) The He exposure should not be too long or it will affect the oxygen content of the membrane. If it is not long enough, then any He permeation can be difficult to assess. Four to five minutes is a good time.
- 9) b) Try to be consistent with the timing at the beginning of the run. I start the GC injections 4 or 5 minutes after the reaction products first appear in the MS. Later than this would be ok, but not earlier. Somewhere between 4 and 10 minutes is probably best.

Appendix H

Summary of Membrane Reactor Test Results

H.1: Additional Reaction Data Comparisons

The evidence for the proposed SFC activity hypothesis can be summarized by comparing results from reaction tests on the SFC membrane and on the stainless steel blank. Not only do the membrane tests show higher CH₄ conversion but they ultimately exhibit both higher H₂ levels and higher water levels than the blank tests (Figures H.1 and H.2). Hydrogen levels are expected to be higher over the membrane because of higher CH₄ conversion, but concomitantly higher water content is consistent with the hypothesis that the membrane is acting primarily to oxidize hydrogen and not as a source of gas-phase oxygen under reaction conditions.

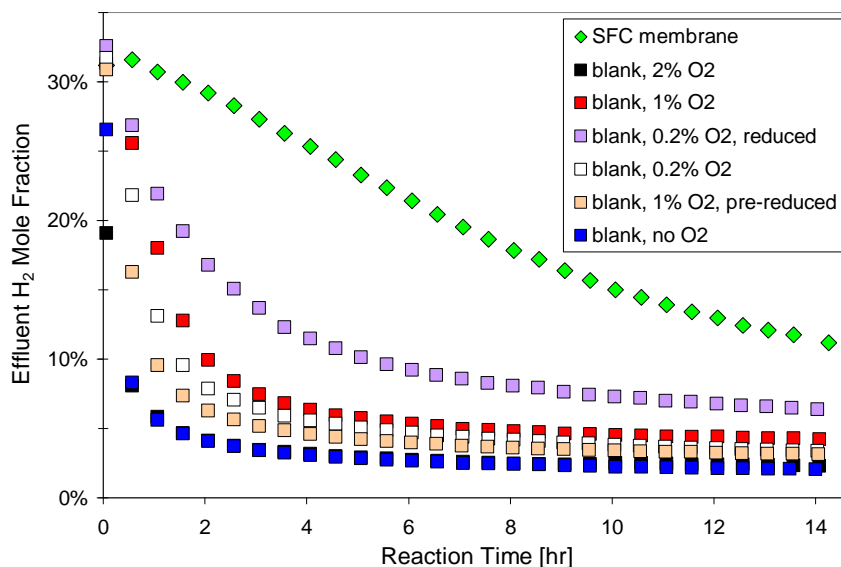


Figure H.1: Effluent hydrogen concentration in the QTMR with the Pt/ZrO₂ catalyst.

Appendix H

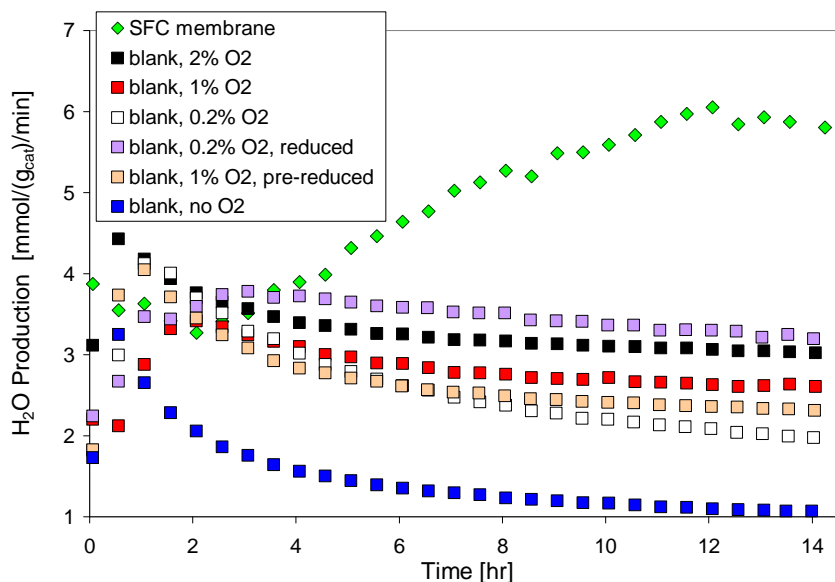


Figure H.2: Water production in the QTMR with the Pt/ZrO₂ catalyst.

The combination of increasing water levels, increasing CO₂ conversion, and generally higher methane conversion with the SFC membrane implicates steam reforming as a more likely candidate for higher methane conversion than combustion. The water for this steam reforming is presumed to be produced on the membrane at the base of the catalyst bed. The distinction between the blank and membrane tests can be enhanced by taking this analysis one step further. The water-to-hydrogen ratios in the products over the SFC membrane (Figure H.3) do not implicate combustion as the expected source of higher conversion over the SFC membrane. Figure H.3 does strongly imply that 2% co-fed oxygen causes some combustion to occur, however.

Appendix H

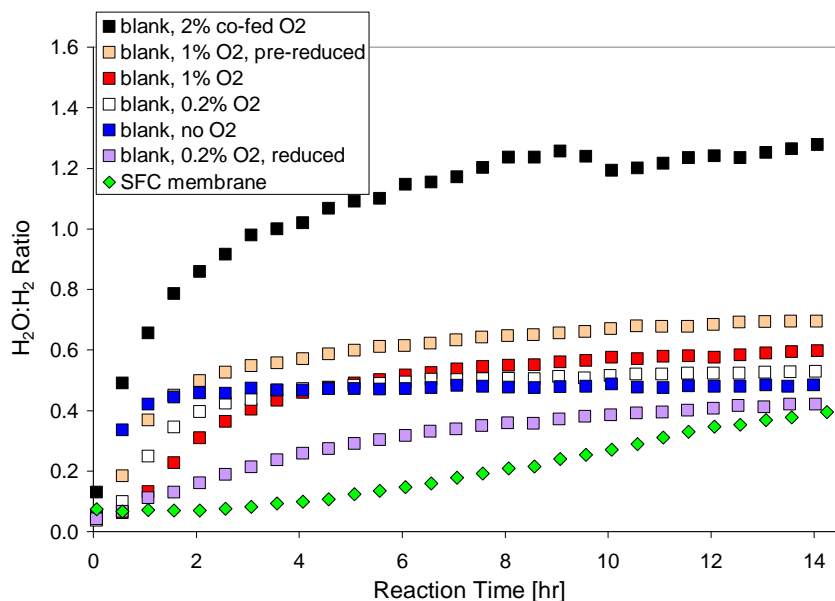


Figure H.3: Water-to-hydrogen production ratio in the QTMR with the Pt/ZrO₂ catalyst.

As depicted in Figure H.4, relative water production levels in tests with unreduced catalyst vary directly with the amount of co-fed oxygen. This is predictable, but the reduced catalyst test does not fit this trend. Although Figure H.2 shows that the reduced catalyst produces a slightly larger quantity of water than the other blank tests, Figures H.3 and H.4 show that it exhibits less water production per unit methane conversion than any of the unreduced catalyst tests. The reduced catalyst on the blank therefore behaves more like catalyst on the SFC membrane, once again. The available evidence fully supports the proposal that the SFC membrane enhances and preserves the catalyst's activity by creating a more reducing or less oxidizing environment than co-fed oxygen.

Appendix H

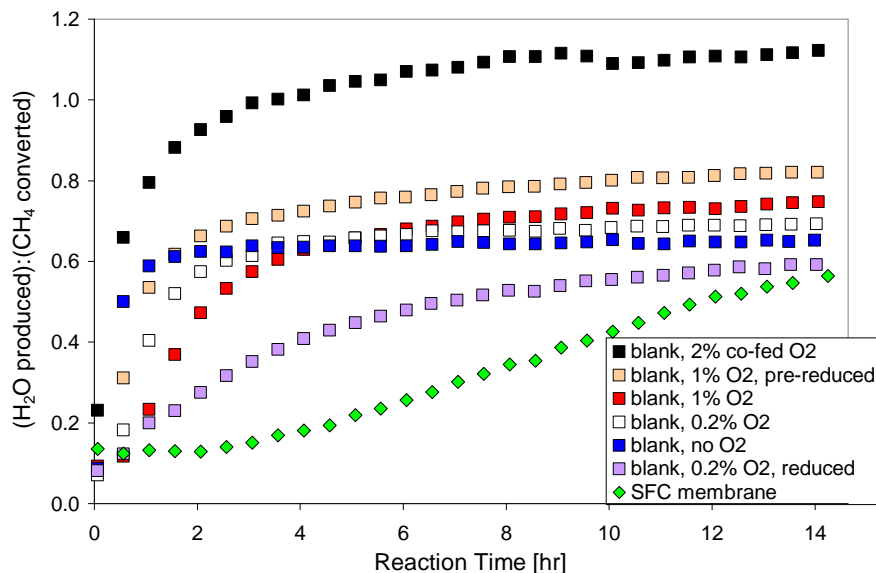


Figure H.4: Water production-to-CH₄ conversion ratio in the QTMR with the Pt/ZrO₂ catalyst.

From a molecular perspective, catalyst on an SFC membrane is exposed to higher ambient hydrogen levels and almost no ambient oxygen—conditions that could contribute to either more *in situ* reduction or less *in situ* oxidation when compared to the blank tests. Figure H.4 suggests that, with Pt/ZrO₂, catalyst oxidation state rather than ambient oxygen level is the determining factor for reaction selectivity (e.g., water production relative to catalyst activity). This is a compelling argument for the use of an O-MIEC membrane instead of co-feeding oxygen to obtain the benefits of oxygen-assisted CO₂ reforming.

H.1: Final Evidence for the SFC Activity Hypotheses

Hydrogen content in the reactor effluent should trend directly with methane conversion, as shown in Figure H.5 below. As a result, it is difficult to distinguish the effect of hydrogen on membrane activity. However, the converse relationship of the one we have been pursuing could provide insight into the SFC membrane effect. In other words, instead of looking at the effect of the membrane-catalyst combination on hydrogen production, how can we look at the effect of hydrogen levels on the membrane-catalyst system?

Appendix H

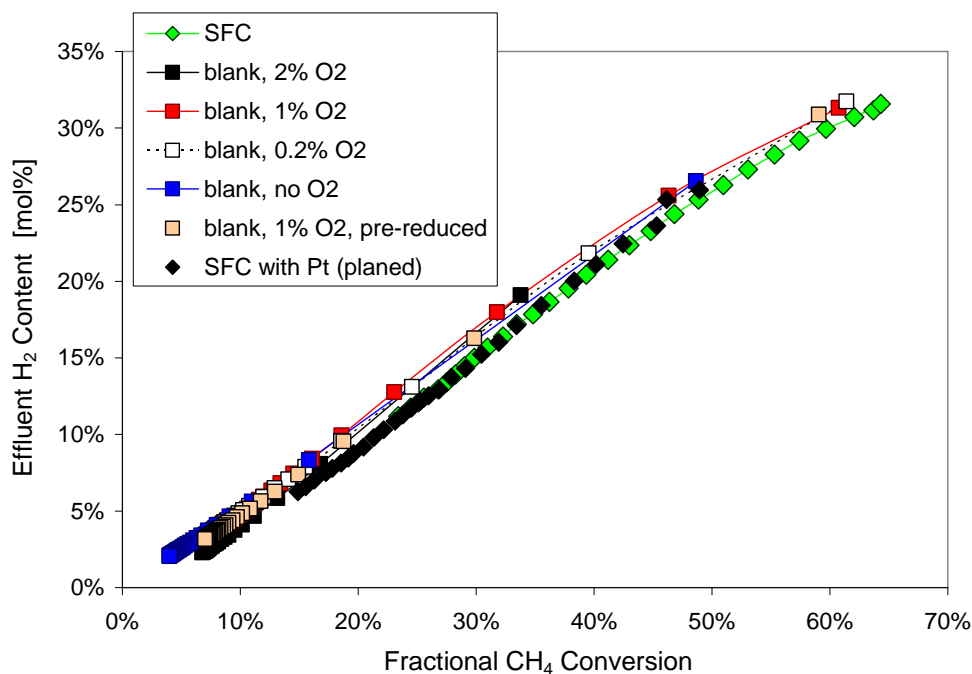


Figure H.5: Effluent hydrogen concentration as a function of methane conversion in the QTMR with the Pt/ZrO₂ catalyst.

Figure H.6 presents methane conversion as a function of reactor hydrogen content with a 30 minute delay (this is the time between subsequent GC injections for these tests). In other words, the methane conversion data are offset from the hydrogen content data in an attempt to look for a causal relationship. Interestingly, this creates a small gap between the trends for the membrane tests and those of the blank tests.

Appendix H

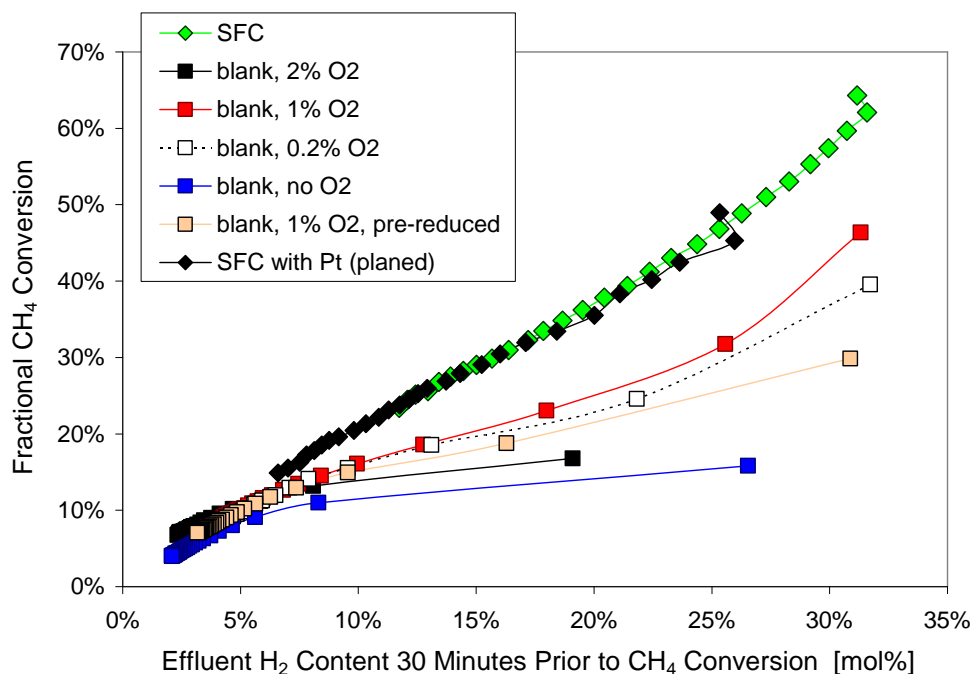


Figure H.6: Effluent hydrogen concentration as a function of methane conversion in the QTMR with the Pt/ZrO₂ catalyst with a 30 minute delay on methane conversion.

The blank test with 0.2% oxygen plus reduction is not included in Figure H.6, but, as might be expected, it falls in the space between the two sets of data and its trend more closely follows the two membrane tests than the blank tests. It appears possible, therefore, that maintenance of a more favorable catalyst oxidation state due to higher ambient hydrogen levels and the absence of gas-phase oxygen might be a significant part of the explanation for the membrane effect.

Figure H.7 shows one more interesting trend that distinguishes the SFC membrane from the blank tests. Effluent water content is consistently higher relative to methane conversion for the SFC membrane, which has been discussed before but not illustrated as clearly as in Figure H.7

Appendix H

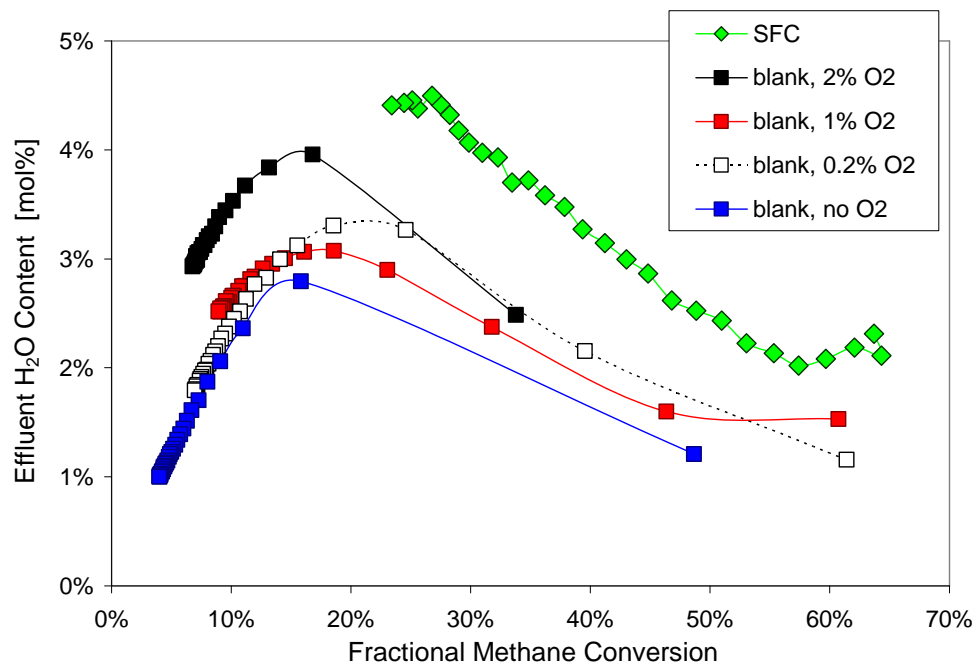


Figure H.7: Effluent water concentration as a function of methane conversion in the QTMR with the Pt/ZrO₂ catalyst

Appendix I
Calculating Membrane Oxygen Flux During Reaction

I.1: Estimating Membrane Oxygen Flux:

The “conversion data (v2)” worksheet in the Excel file “GC reaction data spreadsheet (DAS) 03-2010” can be used to calculate implicit oxygen flux estimates during membrane reaction tests using an iterative process. The process must be iterative because water cannot be measured directly, but an iterative approach allows the hydrogen and oxygen atom balances to be closed simultaneously. The decision to use this approach was based on repeated observations that water was being adsorbed in the system and therefore real time water concentrations could not be derived from the measured values for the remaining components.

As described in Appendix G, the gas chromatograph (GC) data analysis approach to reaction test results has been improved to the point that we can have a much higher confidence in the measured mole fractions of H₂, CO, CH₄, and CO₂ in the reactor effluent than in any other pieces of information available (within 0.5% relative error for peak area determination). The weakest link in the approach used in this work is the assumption that carbon losses in the system have a negligible effect on the carbon atom balance. This is believed to be true based on post-reaction carbon oxidation tests and other observations, but it has not been confirmed conclusively. Nevertheless, until it is proven otherwise, this approach is recommended.

I.1.1: Oxygen flux estimation using the “conversion data (v2)” worksheet

The worksheet is set up to calculate effluent mole fractions according to the calibration procedure outlined in Appendix G.

- 1) Copy the GC peak area data into the proper areas of the “GC reaction data spreadsheet (DAS) 03-2010” Excel spreadsheet as follows:
 - i. Assign the calibration gas peak areas correctly in the calibration section of the “raw data” worksheet and the “Feed composition decay factors” section of the “conversion data (v1)” worksheet
 - ii. Assign the reactor feed peak areas correctly in the “Feed composition decay factors” section of the “conversion data (v1)” worksheet

Appendix I

- iii. Copy the reaction test peak areas into the “GC injection data” section of the “conversion data (v1)” worksheet
 - iv. Ensure that all additional information is added to the “conversion data (v1)” worksheet (e.g., run name, brief description, GC control file name, flowmeter temperature, pre-reaction leak estimate, etc.)
- 2) Perform the iterative process to simultaneously converge the hydrogen and oxygen atom balances
- i. Select the yellow highlighted cell H45 for “Excess H₂O” and type CTRL-O. This uses a macro to iterate the values in the “Adsorbed H₂O” column to push the corresponding “Excess H₂O” values to zero. It also affects the oxygen balance, so...
 - ii. Next, select the yellow highlighted cell L45 for “O₂ deficit” and type CTRL-O again. This uses the same macro to iterate the “O₂ Flux estimate” values to push the corresponding “O₂ deficit” values to zero. It also affects the hydrogen balance, so...
 - iii. Repeat the previous two steps until the values in both columns stop changing when CTRL-O is selected.

NOTE: the macro is set up for 30 rows of data. If there are fewer than 30 rows, it will stop itself when it reaches the first empty column. If there are more than 30 rows, you can simply select CTRL-O again and it will continue down the column, then stop itself when it reaches the first empty row. This gives an error message, but it does no harm. This is the fastest way to deal with data sets of different sizes, but the macro can be modified as you wish.

Appendix J

Oxidation Factor Sensitivity Assessment and Optimization

J.1: Optimizing the Oxidation Factor

To confirm that the proposed Oxidation Factor is an appropriate parameter to distinguish desirable catalyst activity from undesirable oxidation reactions, the effect of partial oxidation, steam reforming, and reverse Water-Gas Shift on the Oxidation Factor were assessed. The Oxidation Factor is intended only to respond significantly to undesirable oxidation reactions (i.e., H₂ to water and CO to CO₂, whether in combination as combustion or individually as in hydrogen oxidation, for example). As such it is desired that it be as insensitive as possible to other potential net reactions, namely rWGS, steam reforming, and partial oxidation. These three reactions will all bias the Oxidation Factor in either direction depending on the level of contribution.

J.1.1: Sensitivity of the Oxidation Factor to other reactions

For the discussion that follows, all theoretical values are based strictly on reaction stoichiometry and Equation 8.3 (provided again below) for the theoretical reaction sets (i.e., steam reforming and CO₂ reforming, partial oxidation and CO₂ reforming, and rWGS and CO₂ reforming only). The bias caused by the second reaction is evaluated relative to a baseline of zero, because straight CO₂ reforming should produce an Oxidation Factor of zero. Reaction percentages represent the molar extent of the second reaction relative to the total methane conversion.

$$OF = \left[1 - (\text{relativeCO}_2\text{conversion}) \cdot \left(\frac{H_2}{CO} \right)^x \right] \cdot \left[\frac{(\text{relativeH}_2O)}{(\text{relativeCO}) \cdot (\text{relativeH}_2)} \right] \quad \text{Equation 8.3}$$

Figure J.1 provides a full-range assessment of binary combinations of CO₂ reforming with partial oxidation, steam reforming, and rWGS, respectively, using Equation 8.3 without the H₂:CO ratio included in Equation 8.3. Because both partial oxidation and steam reforming require an oxygen source (even if only to produce water in the case of steam reforming), the figure includes an indication of the amount of oxygen required for those side reactions to occur in the reaction set. Note

Appendix J

that partial oxidation and steam reforming both overlap on the zero line (which is desirable, since neither should contribute to the Oxidation Factor), but that rWGS exhibits a dramatic deviation

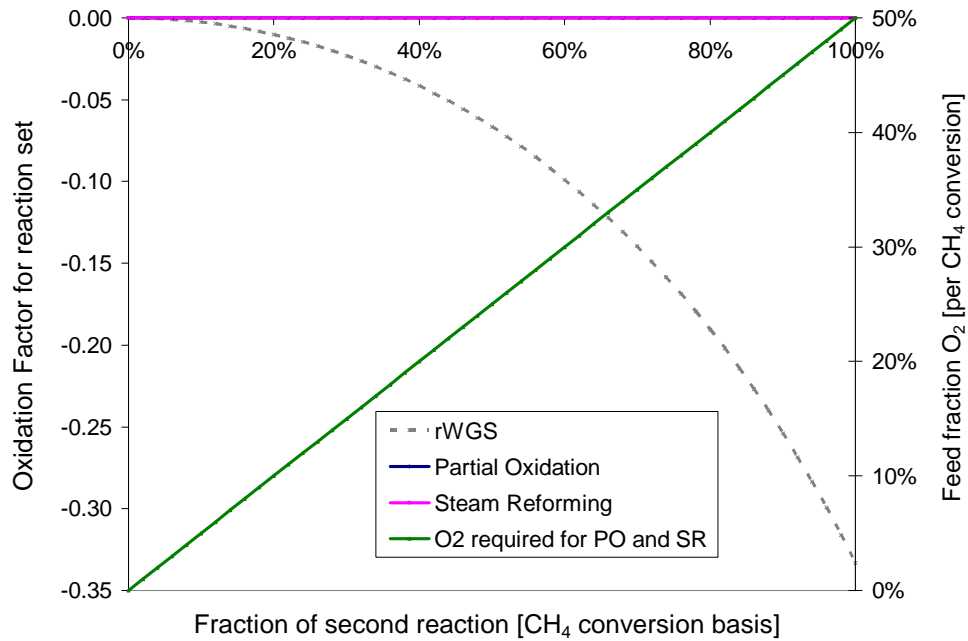


Figure J.1: Theoretical Oxidation Factors for binary reaction sets of CO₂ reforming plus the indicated second reaction. H₂:CO ratio not included in Equation 8.3.

Figure J.2 demonstrates the effect of including the H₂:CO factor in Equation 8.3 with an exponent of $x = 1$. The selectivity expression is otherwise the same, but the beneficial effect of even the unoptimized H₂:CO factor is obvious for the rWGS reaction. There is a detrimental effect for steam reforming, but it is not significant until the contribution of steam reforming to total methane conversion exceeds 50%, which would require a minimum oxygen supply of 25 mol% of the total methane conversion. Since rWGS is believed to occur far more extensively than steam reforming and because oxygen is a limiting reactant in this work, it was decided to optimize the Oxidation Factor expression based on rWGS.

Appendix J

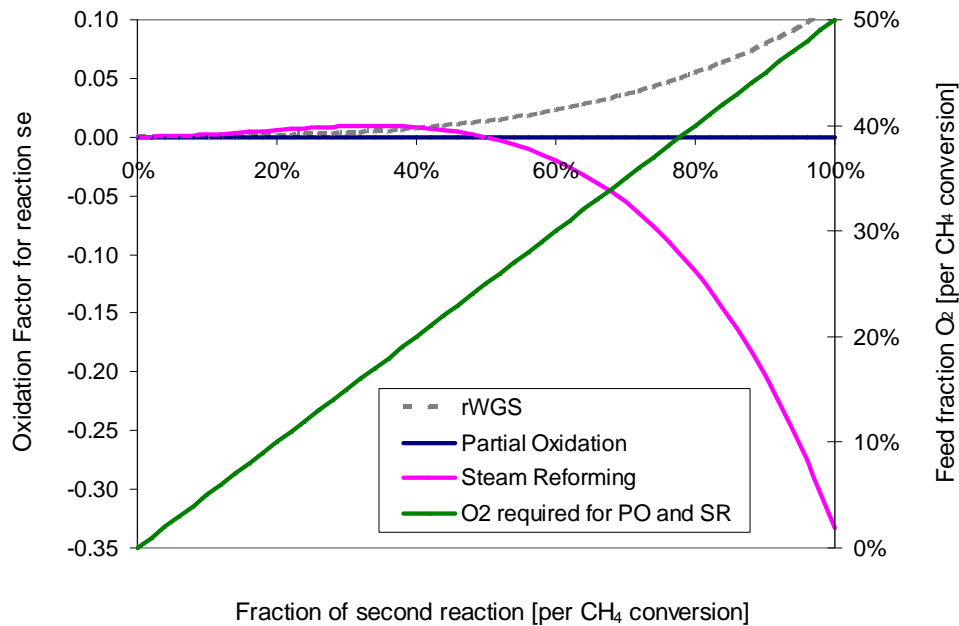


Figure J.2: Theoretical Oxidation Factors for binary reaction sets of CO₂ reforming plus the indicated second reaction. H₂:CO ratio included in Equation 8.3 with an exponent of $x = 1$.

NOTE: partial oxidation does not add anything to the Oxidation Factor as part of a binary reaction set with CO₂ reforming because it does not product any water and therefore has a numerator of zero in Equation 8.3. It does contribute when rWGS is added to the reaction set as a proportion of total methane conversion, as discussed in Chapter 8.

J.1.2: Optimizing the selectivity expression

Because rWGS is the dominant secondary reaction, the selectivity expression was optimized based on the binary rWGS-CO₂ reforming reaction set. The rWGS range used for optimization was zero to 80% rWGS, which was chosen based on the observation that it covered a substantial majority of the experimental results. The optimization criterion was the sum of the squared deviations from a value of zero for the theoretical Oxidation Factor and the independent variable was the exponent x on the H₂:CO ratio factor. The value of 0.756 for the exponent x produced the minimum value of the least-squares optimization criterion.

Appendix J

Figure J.3 provides the optimized Oxidation Factors for the same binary sets. Although the change does not appear large based on the scale of the y-axis, if it recalled that distinctions smaller than 0.01 were obvious in the data presented in Chapters 8 and 9 the improvement becomes more apparent.

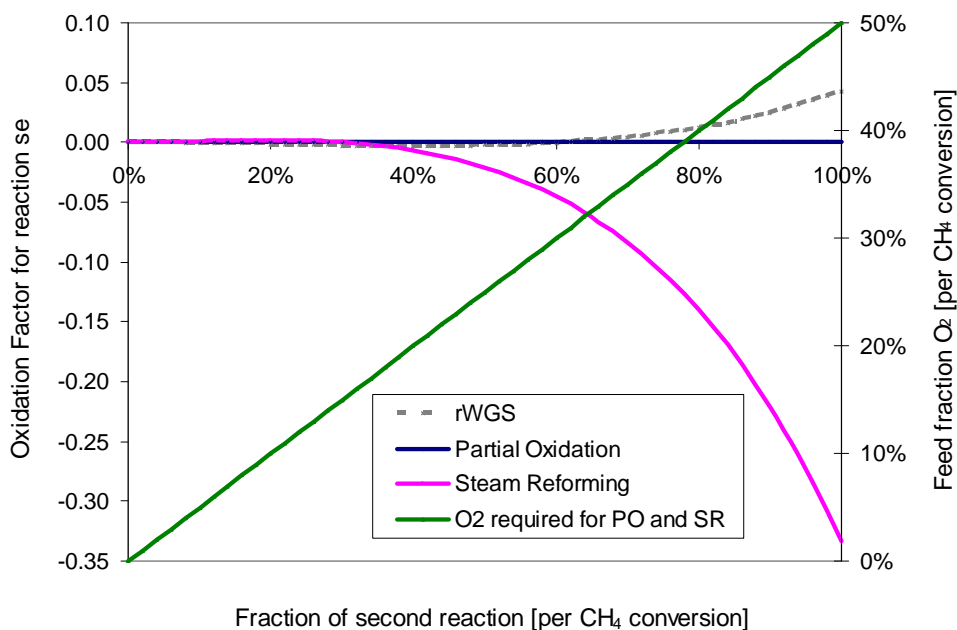


Figure J.3: Theoretical Oxidation Factors for binary reaction sets of CO₂ reforming plus the indicated second reaction. H₂:CO ratio included in Equation 8.3 with an optimized exponent of $x = 0.756$.

Finally, Figure J.4 provides values for a more typical tertiary mixture of reactions including rWGS with either partial oxidation or steam reforming and assuming a 65% rWGS contribution. The 65% rWGS is included for theoretical interest only and is not part of the Oxidation Factor calculations for experimental data. It was chosen as a representative value based on the extent of reaction estimates for all of the Pt/ZrO₂ tests with no co-fed or membrane oxygen. Good agreement between theoretical and actual Oxidation Factors would indicate that the chosen percent contribution for rWGS is representative.

Appendix J

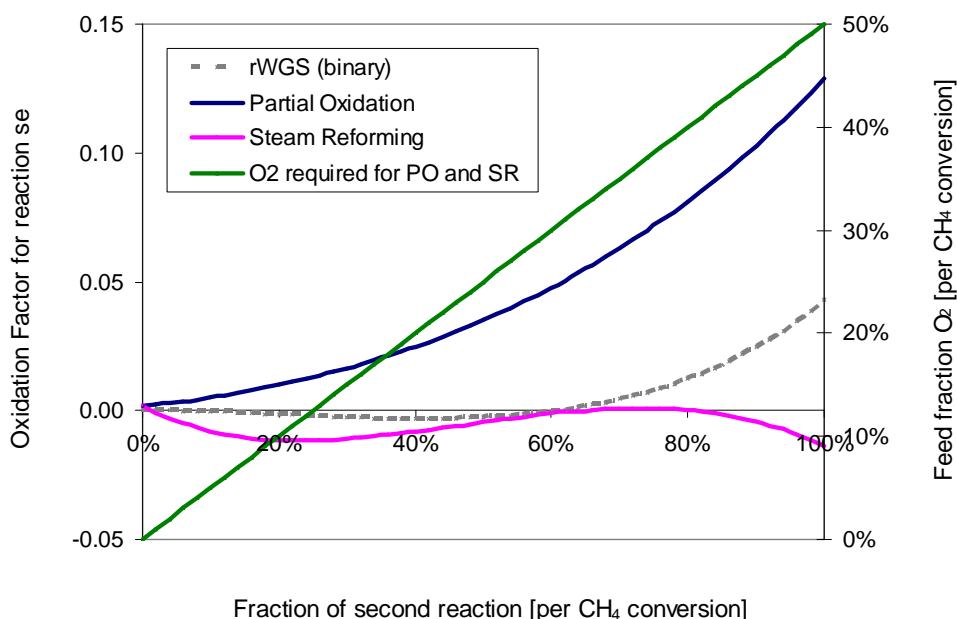


Figure J.4: Theoretical Oxidation Factors for CO₂ reforming plus the indicated second reaction and a 65% rWGS extent of reaction (CH₄ conversion basis); optimized exponent of $x = 0.756$.

J.1.3: Assessing the Oxidation Factor

In the analysis behind these figures, the four factors in the selectivity expression (i.e., the production amounts of the four species of interest: CO₂, H₂O, H₂, and CO) are scaled by the methane conversion amount. Partial oxidation and steam reforming supplant CO₂ reforming to the indicated extent, while rWGS occurs in addition to CO₂ reforming and does not decrease it (i.e., CO₂ reforming accounts for 100% of methane conversion in the rWGS curve). A baseline value of the Oxidation Factor for CO₂ reforming was calculated to be 0.0016 using a rWGS contribution of 65% relative to methane conversion. This value for rWGS contribution was taken from the water production data for the blank test with no oxygen discussed for the first time in Chapter 6 by assuming that rWGS was the only source of water in an oxygen-free test. The actual experimental value for the Oxidation Factor as calculated from the steady state data for the blank test with no oxygen is also 0.0017 (Figure 8.9).

Appendix J

In other words, the experimentally determined Oxidation Factor for the no oxygen blank test matches the theoretical result for pure CO₂ reforming assuming a 65% rWGS contribution. The conclusion for this test would therefore be that no undesirable oxidation occurred at steady state and an Oxidation Factor less than 0.002 is negligible because the theoretical value includes no oxygen consuming reactions. Also, the estimate of 65% rWGS contribution is justified and Figure J.4 can be used as a meaningful reference for expected minimum Oxidation Factors for combined and oxygen-assisted CO₂ reforming.

In another interesting coincidence, the experimental Oxidation Factor for the 0.2% oxygen test with reduced catalyst increased from 0.000 to 0.004 over the course of the test and its theoretical predicted value with only partial oxidation, CO₂ reforming, and 65% relative rWGS is 0.002. This theoretical value assumes all of the oxygen supplied produces partial oxidation and the remainder of the methane conversion occurs by CO₂ conversion. The experimental and theoretical Oxidation Factor appears to coincide well even for very small values. Chapter 8 demonstrated the same coincidence with a relatively large amount of oxygen (2% co-fed).

It is worth noting that the 0.2% oxygen test with unreduced catalyst does not match the theoretical value with only partial oxidation and CO₂ reforming. The experimental Oxidation Factor at the end of the unreduced catalyst test with 0.2% oxygen was 0.014. A value larger than the theoretical value indicates that some undesirable oxidation may be occurring at this point in the test. Given the relatively large water production-to-methane conversion ratio, it appears that the additional oxidation is entirely hydrogen oxidation. This is what is reflected in the larger Oxidation Factor.

J.2: Extending the Optimization Factor to Other Reforming Reactions

For partial oxidation or steam reforming tests in which no CO₂ is included in the feed, the first factor in the numerator of the selectivity expression should be replaced with CO₂ production, which can be determined directly when there is no CO₂ in the feed. Reverse Water-Gas Shift will be

Appendix J

less significant in a partial oxidation scenario because CO₂ will only be present at low levels (unless significant combustion occurs). The exponent for the H₂:CO ratio factor would need to be re-evaluated using a theoretical binary mixture of partial oxidation and rWGS.

For steam reforming, the water production factor must be modified in the same way that the CO₂ production factor was modified in this work for CO₂ reforming (see Chapter 8). H₂:CO ratio can be used as a multiplier for the water conversion term as it was here for the CO₂ conversion term. As with partial oxidation, the exponent on the H₂:CO factor would need to be optimized using binary reaction combinations of steam reforming and WGS rather than the binary combinations of CO₂ reforming and rWGS that were used in this work.

Appendix K
Extent of Reaction Calculations

K.1: Estimating Extents of Reaction:

Extents of reaction for the net reactions of interest can be estimated from the analytical results using reaction stoichiometry and a reaction assignment rubric. In reforming reaction discussions, multiple reaction pathways can lead to the same product compositions because the net reactions that are commonly discussed are combinations of fundamental reactions and are not independent. The reaction profiles that result from the approach described in this appendix therefore do not provide any guarantees about the actual reaction pathways involved, but a comparison of profiles among tests with different operating conditions can provide valuable insight into differences between tests.

The validity of the reaction assignment methodology described below has recently been supported by an outside source. Experimental work by Michael et al. on methane partial oxidation with CO₂ and/or water in the feed concluded that mixed reforming product compositions are largely determined at steady state by WGS and rWGS activity [1]. This upholds the decision herein to assign discrepancies between CH₄ and CO₂ conversions that can't be attributed to partial oxidation to the rWGS reaction.

Additional supporting evidence was observed during the preparation of Appendix N for this dissertation. The methodology from this appendix was applied to equilibrium composition results calculated by Thermosolver [2] for the range of feed conditions tested in this work. As these were theoretical data, a fundamental flaw in the reaction assignment methodology should have been exposed. However, the assigned reactions were reasonable and fit the theoretical equilibrium results without a discrepancy.

K.1.1: Possible net reactions

Appendix K

The “Extents of rxn” worksheet in the Excel file “GC reaction data spreadsheet (DAS) 03-2010” calculates implicit extent of reaction estimates for the presumed set of possible net reactions in Table K.1.

Table K.1: Possible net reactions for extents of reaction estimates

| Net Reaction | Chemical Equation |
|-----------------------------------|---|
| Partial oxidation | $CH_4 + \frac{1}{2}O_2 \rightarrow CO + 2H_2$ |
| CO ₂ reforming | $CH_4 + CO_2 \rightarrow 2CO + 2H_2$ |
| Reverse Water-Gas Shift | $H_2 + CO_2 \Leftrightarrow H_2O + CO$ |
| Steam reforming | $CH_4 + H_2O \rightarrow CO + 3H_2$ |
| Net CO ₂ decomposition | $CO_2 \rightarrow CO + \frac{1}{2}O_2$ |
| Net hydrogen oxidation | $H_2 + \frac{1}{2}O_2 \rightarrow H_2O$ |
| Combustion | $CH_4 + 2O_2 \rightarrow CO_2 + 2H_2O$ |

K.1.2: Fundamental reactions

The fundamental reaction set, for which extents can be calculated explicitly from the GC composition data and known reactor feed and effluent flowrates, includes four reactions.

Table K.2: Fundamental reactions considered in extent of reaction calculations

| Fundamental Reaction | Chemical Equation |
|--------------------------------------|---|
| Rxn 1: Methane Decomposition | $CH_4 \rightarrow C(s) + 2H_2$ |
| Rxn 2: Carbon Oxidation | $C(s) + \frac{1}{2}O_2 \rightarrow CO$ |
| Rxn 3: CO ₂ Decomposition | $CO_2 \rightarrow CO + \frac{1}{2}O_2$ |
| Rxn 4: Hydrogen Oxidation | $H_2 + \frac{1}{2}O_2 \rightarrow H_2O$ |

Appendix K

Once these four extents are known, extents for the set of reactions of commercial interest in Table K.1 can be calculated implicitly using the set of assumptions discussed in Section K.1.3.

NOTE: as of this time, carbon deposition on the membrane has not been accounted for in the mass balance (see Chapter 10). Therefore, CH₄ decomposition and carbon oxidation are always assumed to occur together. If future investigators determine a way to estimate carbon deposition from methane decomposition in real time, the reaction category is available and built into the worksheet. If, on the other hand, carbon or carbonate deposition from CO₂ is determined to have a significant impact on the material balance, a fifth fundamental reaction will have to be added and estimated, possibly from evidence other than GC results.

K.1.3: Fundamental reaction assignment rules used in the “Extents of rxn” worksheet

- 1) All methane conversion is assigned to Fundamental Reaction 1
- 2) Any discrepancy in carbon between the reactor feed and the reactor effluent is assigned to Fundamental Reaction 2 (none at this time, as discussed in the NOTE above).
- 3) All CO₂ conversion is assigned to Fundamental Reaction 3
- 4) All net water production is assigned to Fundamental Reaction 4

NOTE: All reaction extents are calculated on a molar rate basis for the primary reactant (i.e., the first reactant listed in Tables K.1 and K.2).

K.1.4: Net reaction assignment rules used in the “Extents of rxn” worksheet

- 1) Partial oxidation (*PO*):
 - i. If *Rxn 3* is negative or zero, *PO* is assumed to be zero
 - ii. If *Rxn 3* is positive and *Rxn 1* is greater than the stoichiometric amount of partial oxidation corresponding to the non-membrane oxygen into the reactor (i.e., leak and co-fed O₂), *PO* is assumed to correspond to the amount of non-membrane oxygen into the reactor minus the amount of oxygen consumed by any *Combustion* (see below for *Combustion* rule)
 - iii. If *Rxn 3* is positive and *Rxn 1* is less than the stoichiometric amount of partial oxidation corresponding to the non-membrane oxygen into the reactor, *PO* is assumed to correspond to the difference between *Rxn 1* and any *Combustion* (see below for *Combustion* rule)
- 2) CO₂ reforming (*CO2 Ref*):
 - i. If *Rxn 3* is negative or zero, *CO2 Ref* is assumed to be zero

Appendix K

- ii. If *Rxn 3* is positive and greater than the difference between *Rxn 1* and *PO*, *CO2 Ref* is assumed to correspond to the difference between *Rxn 1* and *PO*
 - iii. If *Rxn 3* is positive and less than the difference between *Rxn 1* and *PO*, *CO2 Ref* is assumed to correspond to *Rxn 3*
- 3) Reverse Water-Gas Shift (*rWGS*)
- i. If *Rxn 3* is positive, *rWGS* is assumed to equal *Rxn 3 – CO2 Ref – Net CO2 Decomp*
 - ii. If *Rxn 3* is negative or zero, *rWGS* is assumed to equal the difference between the amount of *Combustion* and the absolute value of *Rxn 3*
- 4) Steam reforming (*H2O Ref*)
- i. If *Rxn 1 – PO – CO2 Ref – Combustion* is negative, *H2O Ref* is assumed to be zero
 - ii. If *Rxn 1 – PO – CO2 Ref – Combustion* is non-negative, *H2O Ref* is assumed to be equal that amount
- 5) Net CO₂ decomposition (*Net CO2 Decomp*)
- i. If membrane oxygen flux is negative, *Net CO2 Decomp* is assumed to correspond to the molar equivalent of the oxygen uptake by the membrane
 - ii. If membrane oxygen flux is non-negative, *Net CO2 Decomp* is assumed to be zero
- 6) Net hydrogen oxidation (*Net H2 Oxid*)
- i. If membrane oxygen flux is positive, *Net H2 Oxid* is assumed to correspond to the difference between the molar amount of total oxygen and the stoichiometric oxygen consumption from the sum of *PO* and *Combustion*.
 - ii. If membrane oxygen flux is negative or zero, *Net H2 Oxid* is assumed to correspond to the difference between the molar amount of non-membrane oxygen and the stoichiometric oxygen consumption from the sum of *PO* and *Combustion*.
- 7) Combustion (*Combustion*)
- i. If *Rxn 3* is positive, *Combustion* is assumed to be zero
 - ii. If *Rxn 3* is negative and the absolute value of *Rxn 3* is more than half the molar amount of total oxygen available, *Combustion* is assumed to correspond to half the molar amount of total oxygen available.
 - iii. If *Rxn 3* is negative and the abs value of *Rxn 3* is less than half the molar amount of total oxygen available, *Combustion* is assumed to correspond to the absolute value of *Rxn 3*

NOTE: all italicized words, acronyms, and terms in Section K.1.4 correspond to the respective column headings for those values in the “Extents of rxn” worksheet. All values in this section of the worksheet are on a molar rate basis [mmol/min].

References Cited in Appendix K

1. Michael, B.C., A. Donazzi, and L.D. Schmidt, *Effects of H₂O and CO₂ addition in catalytic partial oxidation of methane on Rh*. *Jnl of Catal*, 2009. **265**: p. 117-129.

Appendix K

2. Barnes, C. and M. Koretsky, *Thermosolver*. 2003, John Wiley & Sons, Inc.: Oregon State University.

Appendix L

Molecular dispersion and Adsorption in the QTMR System:

The rapid decrease in the Pt/ZrO₂ catalyst activity masked somewhat the evidence of molecular dispersion in the QTMR system. However, the protracted deactivation in the Pt/CeZrO₂ tests allows differences between the QTMR and PFR systems to be observed more clearly. Figure L.1 offers a more focused view of the data originally presented in Figure 8.6 to better highlight this effect.

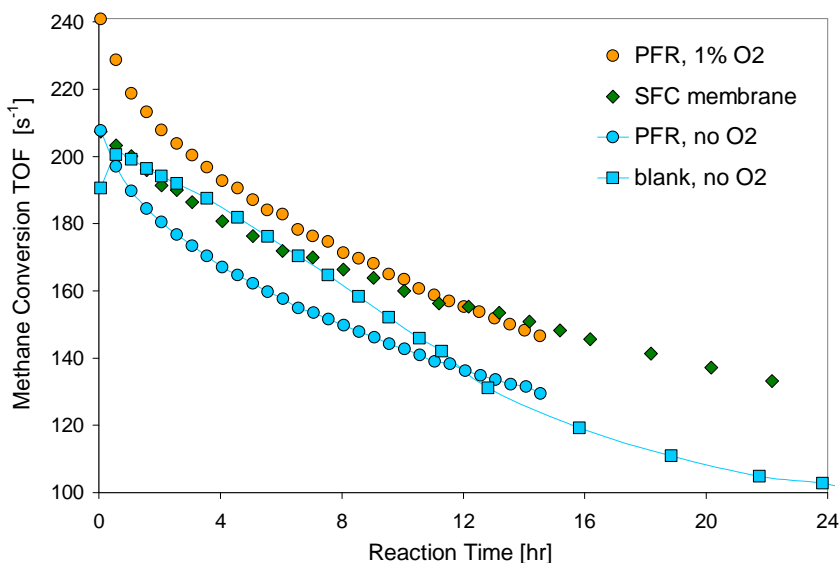


Figure L.1: Methane conversion TOF results for Pt/CeZrO₂ catalyst tests in the PFR and QTMR

The blank test with no oxygen begins and ends with lower activity than the PFR test with no oxygen, yet it exhibits the aforementioned initial increase in activity along with a markedly slower deactivation rate. The blend of current and previous reactor effluent that molecular dispersion creates at the point of analysis offers the best explanation for this difference in apparent deactivation rate.

For the two no oxygen tests in Figure L.1, the lower initial and ultimate activity in the QTMR are consistent with the expectation that the QTMR should exhibit somewhat lower conversion than the PFR because of the opportunity for catalyst bed bypass in the QTMR. The higher apparent

Appendix L

methane conversion in the intermediate period then requires an explanation, and molecular dispersion is the most reasonable explanation for the apparently protracted deactivation process.

Molecular dispersion can also explain the previously unremarked upon differences in apparent deactivation rate with the Pt/ZrO₂ catalyst. Figure L.2 compares PFR and QTMR blank data for the Pt/ZrO₂ catalyst, and the two sets of tests show clearly similar trends with the QTMR tests taking longer to reach “steady state” and ending at a lower activity level in general.

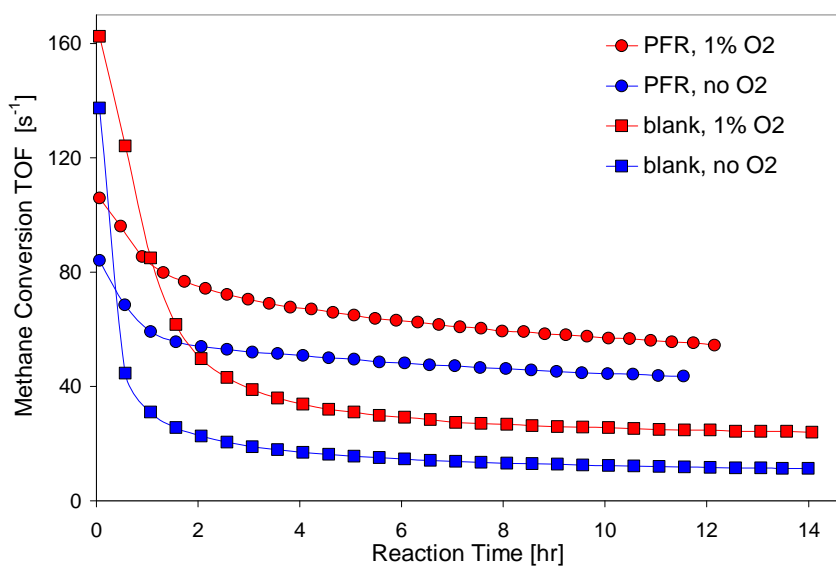


Figure L.2

Figure L.2: Methane conversion TOF results for Pt/ZrO₂ catalyst tests in the PFR and QTMR

The QTMR data appear to be a delayed version of the PFR data with a lower endpoint. For easy comparison, the QTMR data were re-plotted with a time shift. Figure L.3 confirms the similarity of the trends, but obtaining the alignment depicted required the use of different shift times for the two QTMR tests: a 75 minute shift for the 1% oxygen QTMR data but only a 30 minute shift for the no oxygen QTMR data. The adjustments provide a compelling comparison but the difference in delay time creates yet another question.

Appendix L

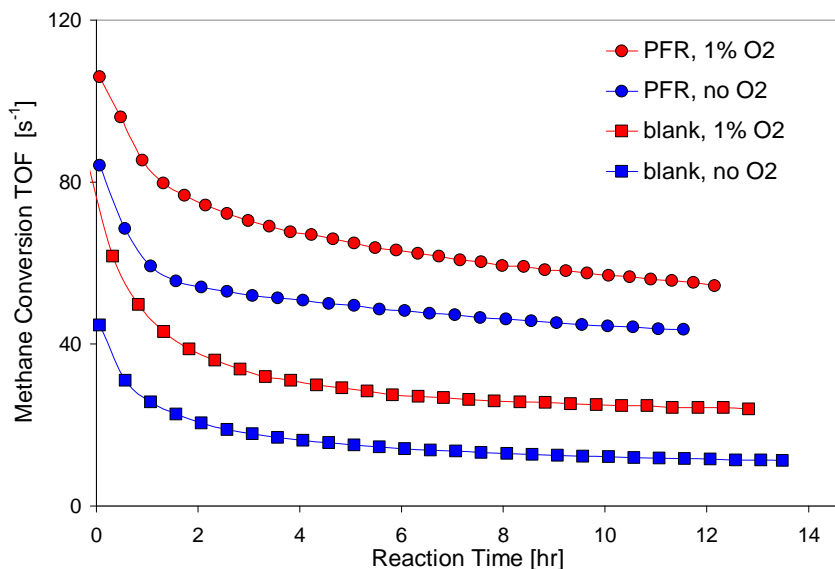


Figure L.3

Figure L.3: Methane conversion TOF results for Pt/ZrO₂ catalyst tests in the PFR and QTMR with an artificial time shift applied to the QTMR blank results: a 30 minute shift for the “blank, no O₂” results and a 75 minute shift for the “blank, 1% O₂” results.

One distinction that could explain the difference in shift time between the 1% oxygen and no oxygen QTMR tests is the quantity of water produced in the two tests. Hydrogen balances, visual observations, and post-reaction mass spectrometer monitoring have all confirmed that water adsorbs in the lines between the reactor and the analytical instruments. When the other components in the reactor effluent interact with the water coating the lines, the lines become, in effect, a coated chromatography column that can slow the progress of each species through the system. The column's diameter is much larger than a typical capillary column (1/8" compared to 30 microns), so only a fraction of the amount of the various species would be delayed by the water coating the surface of the lines. Water would, of course, be delayed the most significantly, with CO₂, hydrogen, CO, and methane delayed in that order based on solubility assumptions.

NOTE: the identical differences in steady state methane conversion between the co-fed O₂ and no O₂ cases in both the PFR and the QTMR imply that all of the oxygen reacts regardless of the reactor.

Appendix L

All system conditions being equal, the quantity of adsorbed water by a given system will depend on the mole fraction of water in the reactor effluent (Figure L.4). If the delay in the progress of other species through the lines does indeed depend on interactions with the condensed water, adsorption delays should be proportional to the relative amount of water leaving the reactor. Figure L.4 not only confirms the implied prediction, but it also provides two additional insights.

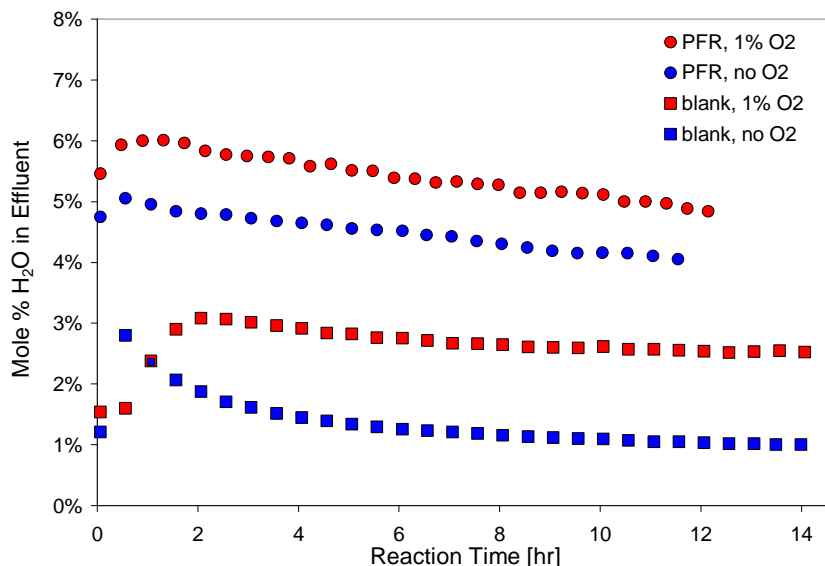


Figure L.4: Effluent water concentration for Pt/ZrO₂ catalyst tests in the PFR and QTMR

First, the PFR data indicate that the PFR system is less susceptible to water adsorption (shorter, larger diameter lines and higher flowrates), although the early increase in apparent water production could easily be the result of adsorption rather than a difference in reaction profiles as speculated earlier. Second, the QTMR data show an early cross-over that could be interpreted as indicating less water initially with co-fed oxygen but is perhaps better explained as the result of higher water production leading to more water adsorption (i.e., water will absorb more water). This explanation assumes that the amount of water needed to saturate the lines is not a fixed constant but rather depends on the ambient mole fraction of water in more of an equilibrium relationship. In other words, the low water “no oxygen” test saturates first because of the lower fraction of water in the

Appendix L

effluent while the higher water 1% oxygen test takes longer to saturate the line because the adsorbed water layer can grow if the ambient conditions contain a large enough mole fraction of water.

As Figure L.5 demonstrates, estimates of water adsorption (from hydrogen balance) are consistent with the proposal that adsorption increases with increasing water production and also with the suggestion that the delay in appearance of water is related to water production level.

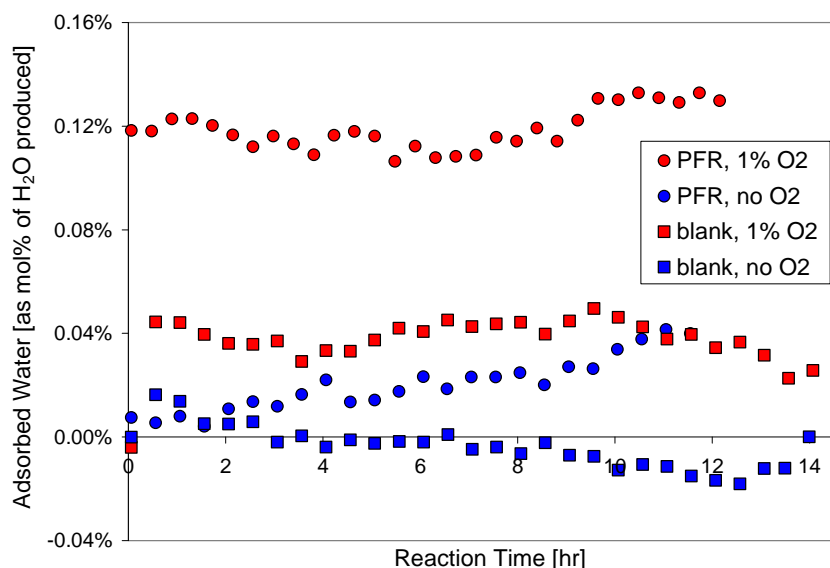


Figure L.5: Fraction of water produced that is adsorbed from the reactor effluent for Pt/ZrO₂ catalyst tests in the PFR and QTMR as estimated by hydrogen atom balance

The fact that the PFR could actually adsorb more water is not as inconsistent as it might first seem. The apparatus has larger diameter tubing (1/4" instead of 1/8") with less surface area per unit volume, has shorter tubing spans, and uses higher volumetric flowrates. Larger diameter tubing means less gas interaction with the adsorbed water layer on the tubing walls and slightly lower linear flowrates. During reaction, there could thus be more adsorption relative to the QTMR system because of the lesser velocity gradient, but as soon as the water stops coming out of the reactor it leaves the tubing inner surface and is less likely to re-adsorb as it moves downstream (i.e., no chromatography effect in the tubing).

Appendix L

One final example of the difference between the adsorption behaviors of the two systems is the amount of time it takes for the water signal in the mass spectrometer to drop to its baseline values during an argon sweep following a reaction test. Water clears from the PFR system within 30 minutes of ending a test, while the QTMR system can take more than two hours to clear the last of its adsorbed water. The long narrow lines with their high surface area-to-volume ratio exhibit slow chromatography column-like transport which delays the disappearance of the last of the adsorbed and condensed water, even though the relative amount of water delayed is less than in the PFR tests.

Appendix M

Thermochemical Interactions between SFC and Individual Gaseous Species

Following a multi-temperature flux test in the QTMR as described in Appendix E, the system was allowed to re-equilibrate at 800 °C with an argon sweep gas (20 mL/min) across the top side. Individual species were then added to the argon sweep gas (methane, H₂, and CO, in that order). The system was allowed to re-equilibrate under the argon sweep gas between each species. Mass spectrometer and internal and external reactor thermocouple data were recorded throughout the test.

M.1: Background on QTMR Temperature Data

The QTMR system originally included only one thermocouple (the external one, referred to as the “Furnace T” thermocouple. See Figure 4.3 for its typical location). Because it was the only thermocouple available for the majority of the QTMR testing, the Furnace T thermocouple provides the feedback signal to the furnace’s control loop and is maintained at a constant temperature during reaction testing. The internal reactor temperature is thus allowed to vary according to reaction thermodynamics and heat transfer to the gases from the reactor walls and the membrane.

For consistency among tests, this temperature control approach was continued even after the addition of the internal thermocouple (the “Reactor T” thermocouple). Fortunately, the gas flowrates and catalyst amounts used are small enough and the thermal mass of the reactor and membrane are large enough that gas-phase temperature changes under reaction conditions are relatively small (i.e., changes of less than 10 °C from the pre- and post-reaction temperatures). Changes in the “Reactor T” thermocouple reading that occur in conjunction with “Furnace T” changes are attributed to heat transfer from the reactor exterior, particularly if they follow changes in the furnace output level (or “Furnace OP” value). Such fluctuations are a result of the activity of the PID control loop for the exterior surface temperature of the reactor. *NOTE: the control loop should be tuned if fluctuations persist or exceed acceptable tolerances.*

Appendix M

The installation of the internal thermocouple in late August, 2006 allows changes in the effluent gas temperature to be quantified and recorded and thus allows the thermal effect of reactions to be assessed. Unfortunately, a loose signal connection prevented reliable data from being collected consistently until the problem was corrected in January, 2007, but the thermocouple was in good working order when the individual species testing described below was undertaken in June, 2007.

M.1.1: Factors that affect internal reactor temperature readings

The following operational parameters can affect the “Reactor T” thermocouple reading.

Direct effects:

- Reactor feed flowrate to the QTMR top section and gas heat capacity
- Reactor effluent flowrate and heat capacity (if different from those of the feed flowrate because of chemical reaction)
- Reaction type and extent of reaction (how exo- or endothermic is the reaction set?)
- SFC membrane or stainless steel blank (the blank should have higher thermal conductivity)
- Reactor thermocouple position (how close is the interior thermocouple to the membrane surface?). *NOTE: this factor and membrane type are likely to have the largest impact.*
- Membrane cracks or other leaks

Indirect effects:

- Air feed flowrate to the QTMR bottom section
- Furnace thermocouple position (where is the external thermocouple positioned?)
- Furnace position and insulation (how big is the pre-heat zone on the top part of the reactor and how well insulated is the system for a particular test?)

M.2: Individual Species Test Results

The individual species test results are reported below as three graphs of mass spectrometer and QTMR system data. Mass spectrometer signal ratios were used instead of individual signals because of the signal drift problem discussed in Appendix E. Argon is used as the comparison signal, so the individual argon signal is also reported (after being multiplied by 2×10^8 to match the scale of

Appendix M

the signal ratios) Information on some of the operational parameters listed in Section M.1.1 is provided as notes on the graphs below. All tests were performed with a controlled external reactor temperature of $800\text{ }^{\circ}\text{C} \pm 1\text{ }^{\circ}\text{C}$.

Because an air compressor is used for the air supply to the bottom side of the QTMR and occasional fluctuations in air flowrate can occur as the compressor recharges its reservoir, air flow across the reactor bottom was turned off prior to species testing for CH_4 and H_2 to remove the possibility of an impact from compressor activity. The consequence of this decision was the possibility for a drop over time in the gas-phase oxygen content on the oxygen supply side of the membrane. However, the 6" long outlet line on the air side was left open, and molecular diffusion was assumed to be sufficient to maintain the oxygen partial pressure, particularly given the extremely low flux of this particular membrane ($\sim 0.0006\text{ sccm/cm}^2$ at $800\text{ }^{\circ}\text{C}$ prior to individual species testing).

M.2.1: Methane testing

Figure M.1 presents the mass spectrometer and temperature change results for methane testing on the SFC membrane. A 33% CH_4 in argon feed was sent to the reactor for approximately 30 minutes, after which the same feed was sent directly to the mass spectrometer via a bypass line.

Appendix M

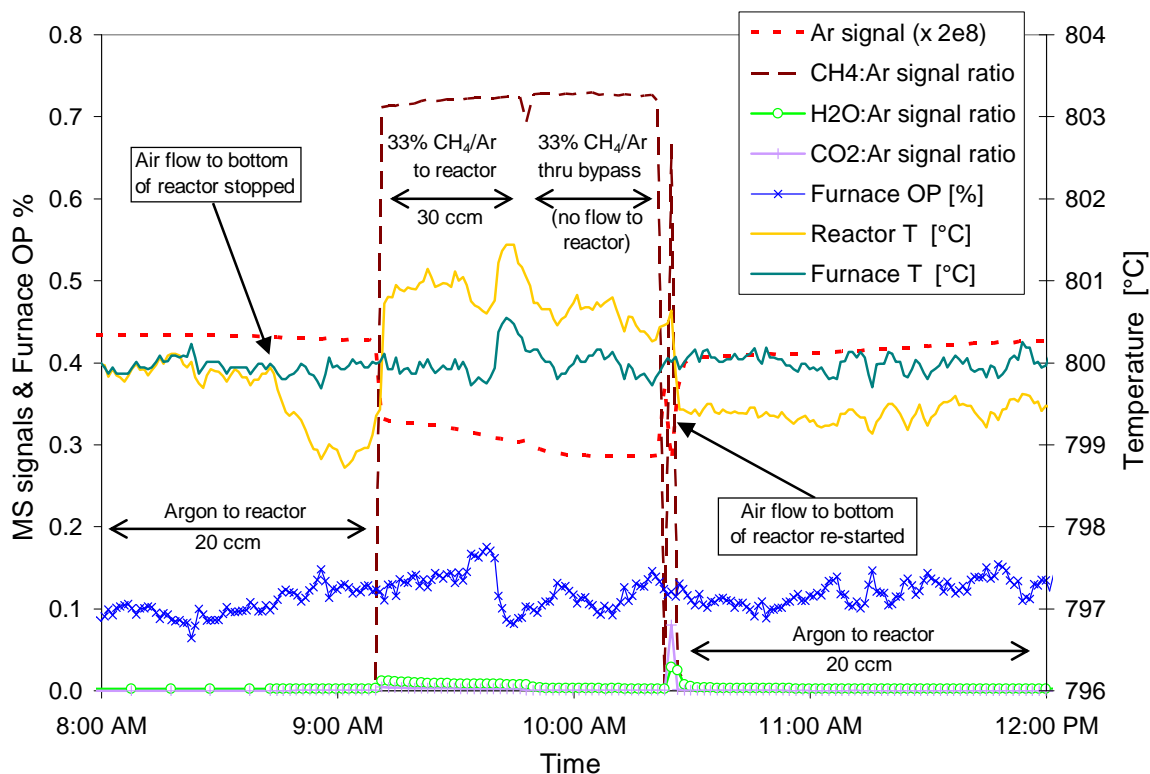


Figure M.1: Membrane CH₄ exposure at 800 °C following flux testing (no catalyst)

Although changing the feed from straight argon to 33% methane (and increasing the feed rate from 20 mL/min to 30 mL/min) results in a reactor temperature increase of 1 – 2 °C, there is little evidence of chemical reaction on the membrane surface. The parity between the CH₄ signals for the reactor effluent and the subsequent signals for the bypass stream indicates that the amount of methane conversion is very small. This conclusion is supported by the very small increase in water and the even smaller increase (if any) in CO₂ during methane exposure. The H₂ and CO signals throughout the period depicted in Figure M.1 are not included on the graph because they are essentially zero, so no measurable amount of H₂ or CO is produced either. A fractional methane conversion of ~0.6% is estimated from the mass spectrometer signals, which is consistent with the results observed in the CO₂ reforming tests with no catalyst (see Section 6.4 for a summary of the reaction tests with no catalyst).

Appendix M

The small temperature change therefore appears to be largely unrelated to methane conversion on the membrane. One possible alternative explanation is the much larger heat capacity of methane (Table M.1 provides heat capacity data). The QTMR was designed with feed gas pre-heating as a priority, so the top portion of the reactor occupies more than 50% of the furnace area. Also, the hottest air inside the furnace cavity should accumulate by convection around the upper part of the reactor because the extensive insulation should allow minimal air flow out of the furnace cavity. It is even possible that the pre-heated feed gas helps to heat the reaction chamber where the “Reactor T” thermocouple is located. If so, the higher heat capacity of the methane/argon mixture would allow more heat transfer to the reaction chamber and the tip of the Reactor T thermocouple than the pure argon sweep gas. This could explain some of the observed temperature increase.

Table M.1: Heat capacities for gaseous components at 800 °C (data from the online CRC Handbook, KU Libraries)

| Species | CH ₄ | CO ₂ | CO | H ₂ O | H ₂ | Ar | O ₂ |
|------------------------------------|-----------------|-----------------|------|------------------|----------------|------|----------------|
| C _p at 800 °C [J/mol/K] | 76.8 | 55.2 | 33.6 | 42.3 | 30.5 | 20.8 | 35.2 |

Two final notes on the methane test results in Figure M.1: first, when the feed gas is diverted to the bypass, leaving the reactor with no forced flow on either side, the reaction chamber temperature changed only slightly. Second, there is one significant increase in temperature for both the Reactor T and the Furnace T thermocouple, near the end of the methane exposure test. However, the furnace output level (Furnace OP) clearly increases just before these temperature increases are observed, and the temperature both drop following the subsequent decrease in furnace output %. It appears that the temporary temperature increase could be the result of the temporary furnace output increase. In other words, it is caused by a temperature control excursion.

M.2.2: Hydrogen testing

Figure M.2 presents the hydrogen exposure test results. In this test, baseline signals for the 33% H₂ in argon feed gas were obtained through the bypass line prior to sending the feed to the

Appendix M

reactor. After the methane exposure test, the membrane was allowed to re-equilibrate for approximately 2.5 hours after before sending the H₂/Ar mixture to the reactor at a flowrate of 30 mL/min.

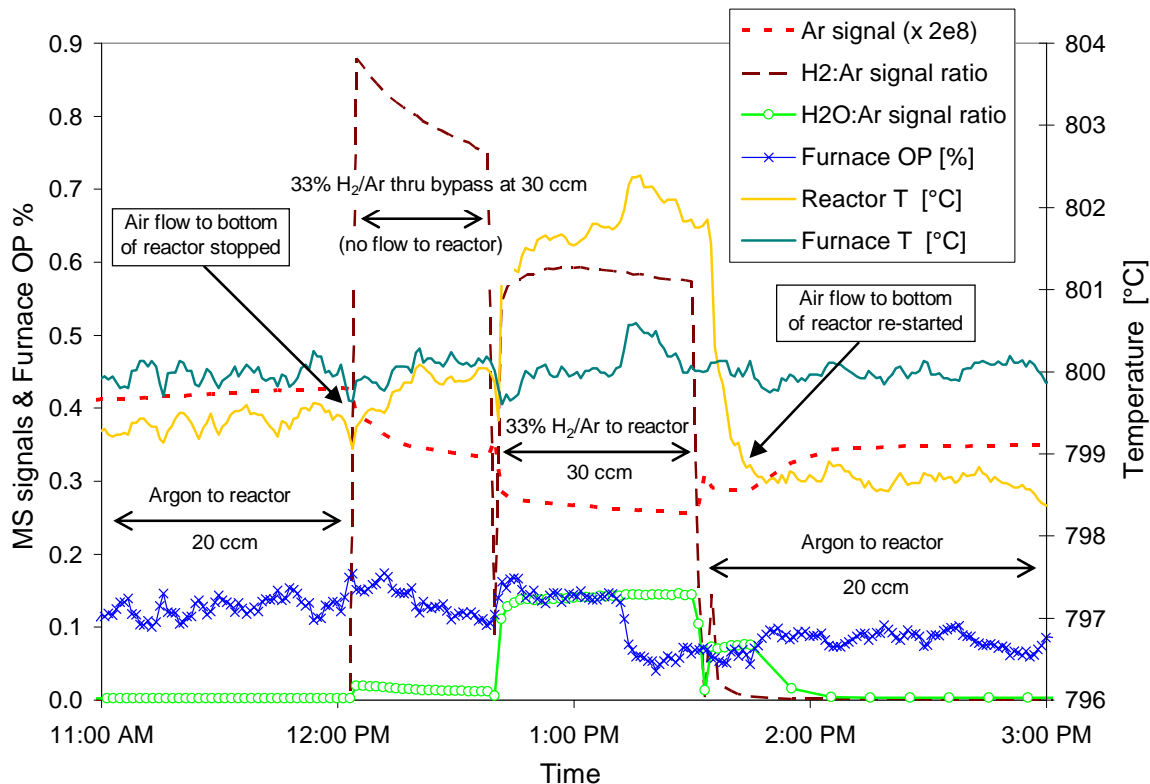


Figure M.2: Membrane H₂ exposure at 800 °C following CH₄ exposure (no catalyst)

The drop in the H₂:Ar signal ratio and corresponding increase in the water:argon signal ratio demonstrate that hydrogen is oxidized steadily, even with no air flow on the oxygen source side of the reactor. This indicates that the driving force for hydrogen oxidation is strong because the overall oxygen content of the membrane is likely diminishing throughout the one hour test yet water production and hydrogen consumption are maintained. They even appear to increase slightly over time. CO₂, CH₄, and CO signal ratios are not included because they were essentially zero throughout this test period.

A fractional hydrogen conversion of ~20% is estimated from the mass spectrometer signals. This corresponds to an effluent water content of just under 7%, which is consistent with the H₂O:Ar

Appendix M

signal ratio of 0.14 observed during this period. It also corresponds to membrane oxygen production of ~ 0.5 sccm/cm², which is three orders of magnitude greater than the pre-test estimate of 0.0006.

The thermal effects of hydrogen exposure at first appear similar to the effect of the methane exposure, with an immediate increase of about 2 °C. The similarity is surprising, since there is clear evidence of hydrogen oxidation on the membrane and a larger temperature increase would therefore be expected. However, given that the oxidation reaction is believed to occur on the membrane surface, the membrane could be absorbing the majority of the heat of reaction. The gradual increase in the internal reactor temperature over the first 30 minutes of exposure time could reflect this, particularly since the external “Furnace T” temperature does not also follow this trend.

The sudden increase in both internal and external temperatures that occurs after 30 minutes appears similar to the event in the methane exposure test. However, in this case the temperature increase coincides with a decrease in furnace output %, indicating that the control loop is turning down the furnace in an attempt to reverse an ongoing temperature excursion. The internal and external temperatures slowly follow the furnace output %, but, unlike in the methane exposure test, the furnace output % remains significantly lower after the event than it was before. This is consistent with the hypothesis of the membrane itself absorbing the majority of the heat of reaction and acting as a detectable heat source once it is hot enough to transfer a measurable amount of additional heat to the gas phase. The control thermocouple is adjacent to the membrane’s outer edge, which should be the last part of the membrane to increase in temperature and which also should exhibit the smallest temperature change given its exposure to the constant temperature furnace cavity. The relationship between the Furnace T and Reactor T data in Figure M.2 are consistent with the hypothesis that the heat of reaction is largely absorbed by the center top surface of the membrane.

The thermodynamics of SFC reduction offer a final possible contributing explanation for the lower than expected heating of the reactor effluent gases during hydrogen oxidation. If SFC reduction is endothermic, as expected, then the removal of oxygen from the SFC lattice would

Appendix M

counteract to an unknown extent the exothermic hydrogen oxidation reaction. It is also reasonable to expect that the amount of energy required to remove oxygen from the SFC lattice will change as the phase composition of the SFC changes, becoming more difficult (and thus probably more endothermic) as oxygen depletion progresses.

M.2.3: CO testing

The CO exposure test was performed using a 30% CO in argon pre-mixed gas cylinder that was available in the lab. The flowrate was set at 20 ccm to match the argon sweep gas flowrate rather than at 30 ccm. Because the hydrogen test was believed to have significantly depleted the oxygen content of the SFC membrane, a longer re-equilibration period of just over 7 hours was allowed. The oxygen-nitrogen signal ratio was monitored prior to the CO exposure test to determine when the membrane had re-attained steady state with respect to oxygen.

Figure M.3 presents the results for this test, in which the CO/Ar mixture is first sent to the reactor and then sent through the bypass to establish baseline signals. It should be noted that a mistake was made on the initial attempt to establish the mass spectrometer signal baseline values (a supply valve was left closed, resulting in decreasing flow through the bypass line over time), so the CO/Ar gas was tested again after 11:00 p.m. Following the CO/Ar baseline signals, a CO₂ reference signal was established using an available pre-mix cylinder of CO₂/He, although these signals are not used in the calculations that follow.

Appendix M

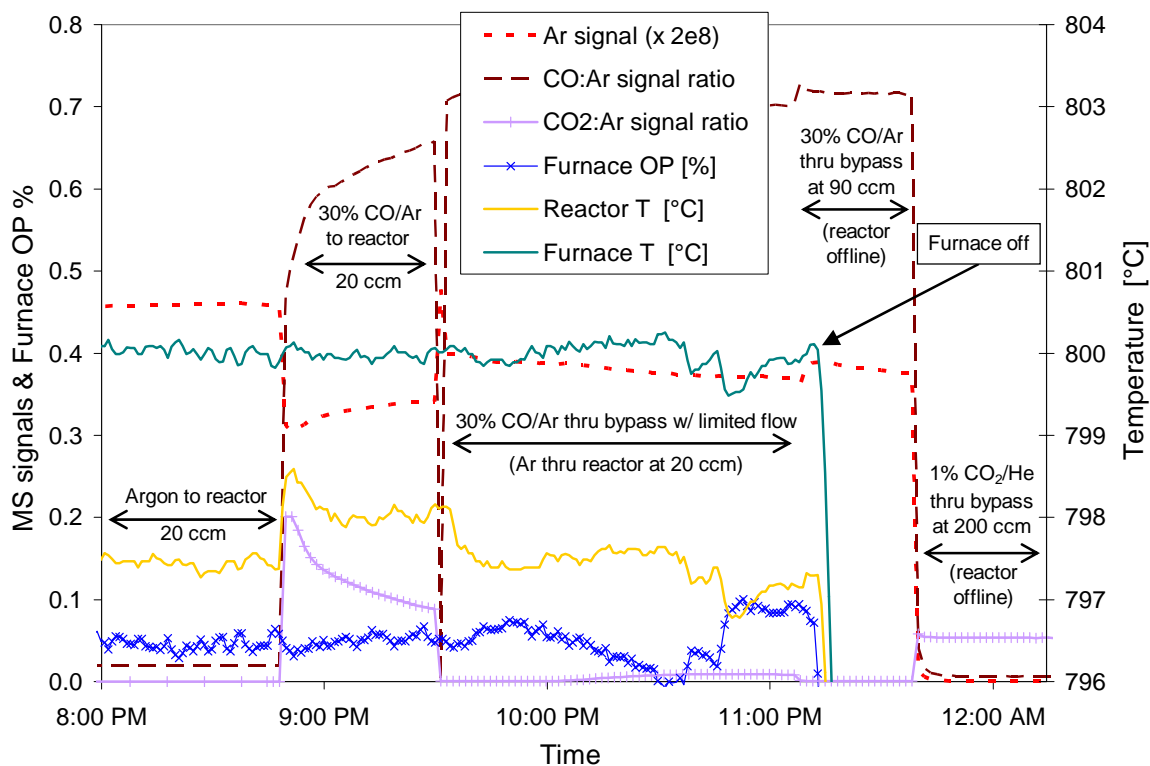


Figure M.3: Membrane CO exposure at 800 °C following H₂ exposure (no catalyst)

With the SFC membrane in a fully replenished state (as demonstrated in Section M.2.4), there is initially a significant amount of CO conversion, but the conversion begins to decline fairly quickly, indicating that CO oxidation via SFC is not as thermodynamically favored as H₂ oxidation which persisted throughout its ~1 hour test period. Because the flowrate and initial reactant concentration are different in the CO exposure test, fractional conversion results cannot be compared directly with those of the other two tests. They must first be converted to molar conversion rates. The initial and final fractional conversions of 28.9% and 8.9% from the data for Figure M.3 correspond to molar CO conversion rates of 0.07 and 0.02 mmol/min, respectively, while the molar H₂ conversion rate is consistently about 0.09 mmol/min. Table M.2 below provides a summary of the conversions observed for all three component tests.

Appendix M

Table M.2: Conversion on SFC for individual species at 800 °C (balance of feed is Ar)

| Species tested | CH ₄ | H ₂ | CO, initial | CO, final |
|-------------------------------------|-----------------|----------------|-------------|-----------|
| Feed concentration | 33% | 33% | 30% | 30% |
| Fractional conversion | 0.6% | 22.4% | 28.9% | 8.9% |
| Molar conversion rate [mmol/min] | 0.002 | 0.090 | 0.070 | 0.021 |

CO oxidation is not as intense or as persistent as H₂ oxidation on the SFC membrane and it appears to be declining steadily towards zero over time, but it nevertheless occurs to a significant extent when the membrane is not depleted in oxygen. The decline in conversion as oxygen is removed from the SFC indicates that it might not occur to a significant extent under reforming conditions, particularly CO₂ reforming because of the likelihood of surface oxygen depletion from hydrogen exposure and the high concentrations of CO₂, which is the product of CO oxidation.

Among the individual species exposure tests, the thermal evidence in Figure M.3 is most consistent with thermodynamic expectations: the initial temperature increase is higher than the final temperature increase and temperature decreases along with the observed decrease in CO oxidation. The decreased conversion is evident in the signals for both CO and CO₂. Also, the reactor temperature returns to its pre-test temperature after the test, and the external Furnace T temperature does not change significantly at any point in the test.

M.2.4: Membrane re-equilibration

One last observation can be made from the mass spectrometer and thermocouple signals obtained during the 7.5 hour interlude between the H₂ exposure test and the CO exposure test (Figure M.4). The O₂:N₂ signal ratio is added to this graph to demonstrate again the interactions of an oxygen-depleted membrane with air from the leaks into the system, which—although small in this case—are inevitable. Although not shown on the graph, the nitrogen signal itself is steady throughout the period depicted in Figure M.4, but no oxygen signal is present for the first two hours following

Appendix M

the H₂ exposure test. This indicates substantial oxygen depletion in the SFC. After two hours the oxygen signal slowly increases, eventually rising over the next four hours to the expected level for air (plus a small amount of oxygen from the flux through the membrane). *NOTE: the temporary jump in internal reactor temperature during the helium leak test was observed in every helium leak test that was performed.*

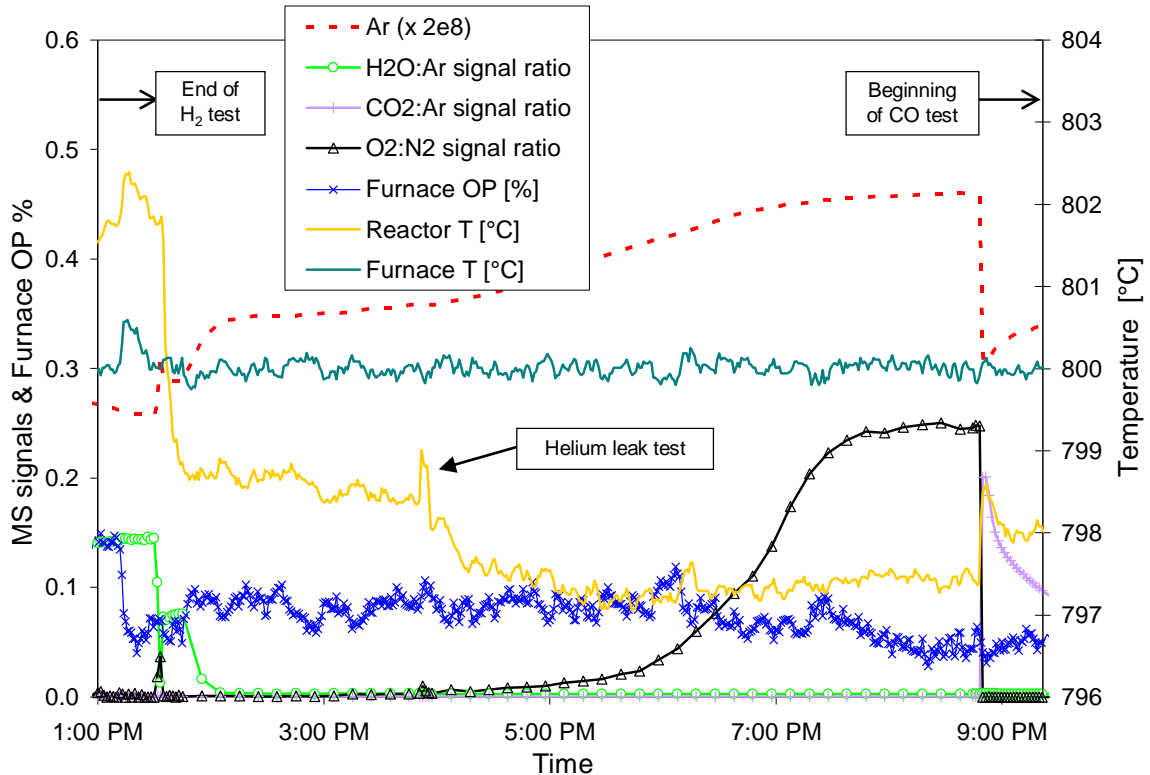


Figure M.4: Membrane argon exposure at 800 °C following H₂ exposure. No catalyst.

The relationship between internal reactor temperature (“Reactor T”) and oxygen uptake offers a valuable insight into the thermodynamics of the reversible interactions of SFC and oxygen. Since the oxygen signal is zero for the first two hours of the interlude in Figure M.4, it is not possible to directly determine the potential maximum oxygen uptake rate of the SFC membrane in its most depleted state. However, it seems safe to assume that the driving force (i.e., the change in molar Gibb’s free energy) for oxygen incorporation into oxygen-depleted SFC in the presence of excess oxygen should be highest initially and should then decrease as the material approaches equilibrium.

Appendix M

If the internal reactor temperature profile is viewed under this assumption, the steady decrease in temperature can be interpreted as evidence that the oxygen incorporation process is exothermic. This is consistent with electrochemical expectations, as oxygen incorporation is an oxidation process and the individual oxidation processes for strontium, iron, and cobalt (SFC) are exothermic.

The important conclusion from this observation is its mandatory opposite. Namely, if oxygen incorporation is exothermic, then oxygen evolution must be endothermic, as postulated in Section M.2.2. This conclusion is consistent with all observations to date, including the lower than expected temperature changes during the oxidation reactions presented in this Appendix.

Appendix N

Reaction Equilibrium Values and QTMR Thermal Effects

N.1: Reaction Equilibrium Constants

As discussed in Chapter 7, equilibrium product compositions for the various reactor feed compositions used in the QTMR were determined using the Thermosolver software program [1]. In addition to equilibrium compositions, equilibrium constants for the reactions discussed in this work were also obtained from Thermosolver over the temperature range of 550 to 850 °C. Figures N.1 and N.2 provide these results as a reference for earlier comparisons of reaction data from tests at different temperatures, particularly in Chapter 5.

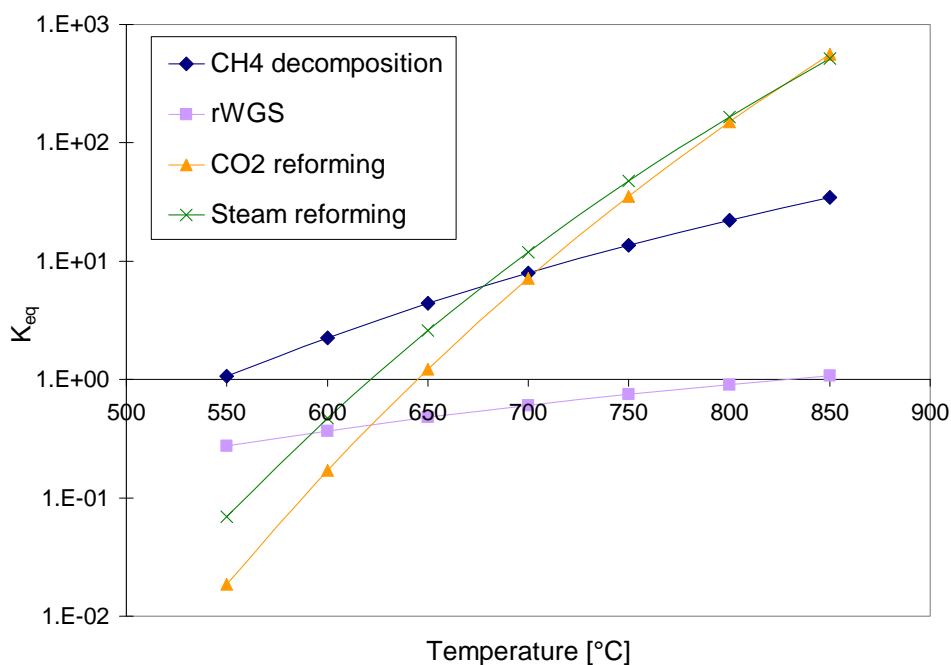


Figure N.1: Equilibrium constants for reactions relevant to syngas production for which K_{eq} increases with increasing temperature

Appendix N

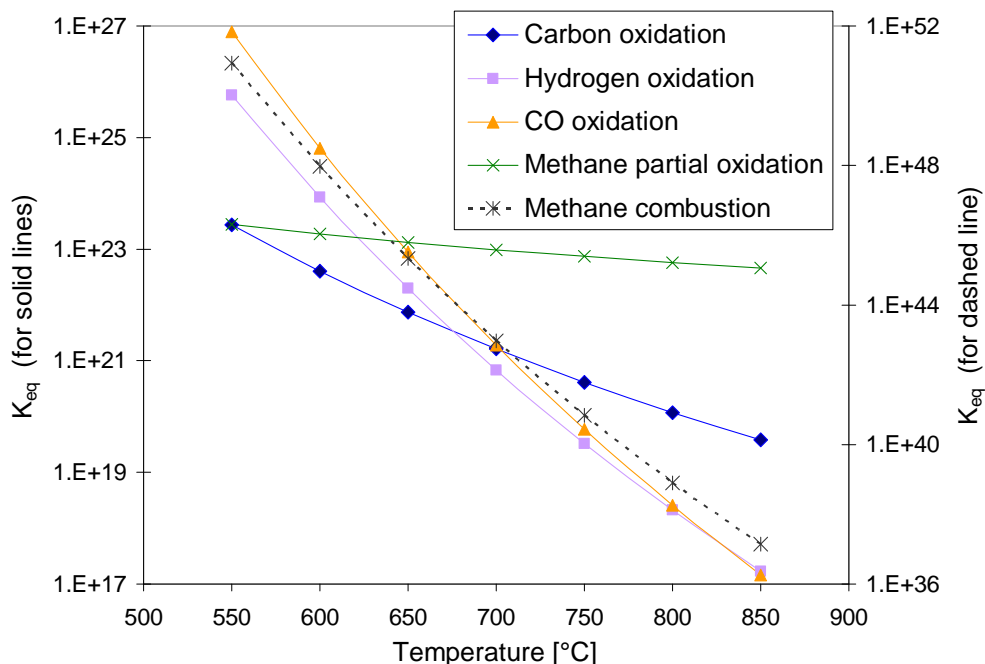


Figure N.2: Equilibrium constants for reactions relevant to syngas production for which K_{eq} decreases with increasing temperature

N.2: Equilibrium Product Compositions by Reactor Feed Composition

Table 7.2 contains the overview of the aforementioned equilibrium compositions. As an added reference for future work, Table N.1 provides an expanded version of Table 7.2 that includes overall reaction enthalpies corresponding to the equilibrium product compositions and the theoretical extent of reaction for rWGS relative to total CH_4 conversion. The experimental data for one of the most successful QTMR tests, the Pt/CeZrO₂ catalyst test on an SFC membrane, are also included in Table N.1. The initial values for the Pt/CeZrO₂ test on SFC are somewhat similar to the equilibrium values, but the long-term experimental results from the final sample time of 33 hour on stream reflect the tendencies for decreasing methane conversion and increasing rWGS that have been a focus of this dissertation.

Appendix N

Table N.1: Equilibrium data for isothermal CO₂ reforming with a feed of 40% CH₄, 40% CO₂, O₂ as indicated, and balance Ar. Temperature = 800 °C; pressure = 1 atm.

| Oxygen in Reactor Feed | No O ₂ | 0.2% O ₂ | 1% O ₂ | 2% O ₂ | SFC w/ Pt/CeZrO ₂ | |
|--|-------------------|---------------------|-------------------|-------------------|------------------------------|--------|
| | | | | | Initial | 33 hrs |
| CH ₄ conversion | 91.3% | 91.7% | 93.3% | 94.7% | 73.8% | 40.4% |
| H ₂ :CO ratio | 0.958 | 0.961 | 0.968 | 0.977 | 0.890 | 0.679 |
| CO ₂ :CH ₄ conversion ratio | 1.045 | 1.036 | 1.005 | 0.970 | 1.093 | 1.385 |
| Relative H ₂ O production | 0.044 | 0.047 | 0.059 | 0.075 | 0.137 | 0.381 |
| ΔH_{rxn} [kJ/total moles in feed] | 91.0 | 90.3 | 87.4 | 83.4 | 69.5 | 42.5 |
| ΔH_{rxn} [kJ/mol CH ₄ converted] | 249 | 246 | 234 | 220 | 238 | 264 |
| Ratio of rWGS-to-CH ₄ conv. | 4.5% | 4.7% | 5.9% | 7.6% | 9.4% | 38% |
| Equilibrium values from Thermosolver [1] | | | | | <i>Experimental values</i> | |

The reaction enthalpies in Table N.1 were calculated using the equilibrium quantities of the products and reactants and their standard enthalpies of formation at 25 °C. The molar extents of the rWGS reaction at equilibrium were determined according to the guidelines described in Appendix K, along with reaction extents for partial oxidation and CO₂ reforming. The calculated reaction extents closed the material balance by design, so to confirm that there were no computational errors, an independent enthalpy balance using the extents of reaction and their standard enthalpies of reaction was performed. The extent of reaction enthalpy balance matched the net reaction enthalpy balance that had been performed using the feed and equilibrium product compositions.

N.3: Equilibrium Product Compositions by Reaction Temperature

Chapter 5 compares SSMR results for tests at two different temperatures (700 and 750 °C). It includes a brief discussion of the effect of temperature on reforming reaction kinetics, but the effect of temperature on chemical equilibrium was deferred to this appendix. Table N.2 provides the chemical equilibrium data for the reaction conditions corresponding to the work discussed in Chapter 5, as well as other data of interest. The 790 °C results are included to represent the observed temperature decreases during CO₂ reforming on the SFC membrane when temperature is controlled

Appendix N

by the external thermocouple rather than the newly installed internal thermocouple (see Appendix M for additional discussion of this topic).

Table N.2: Equilibrium data for isothermal CO₂ reforming. Reaction temperatures as indicated; pressure = 1 atm; CH₄:CO₂ feed ratio = 1:1 with no Ar/O₂ dilution (unless noted)

| Reaction Temperature | 700 °C | 750 °C | 800 °C | 800 °C w/ 20% Ar | 790 °C w/ 20% Ar |
|--|----------------------|--------|--------|---------------------------|---------------------|
| CH ₄ conversion | 72.2% | 83.3% | 90.3% | 91.3% | 90.3% |
| H ₂ :CO ratio | 0.875 | 0.923 | 0.953 | 0.958 | 0.951 |
| CO ₂ :CH ₄ conversion ratio | 1.134 | 1.082 | 1.050 | 1.045 | 1.049 |
| Relative H ₂ O production | 0.134 | 0.082 | 0.050 | 0.044 | 0.049 |
| ΔH _{rxn} [kJ/total moles in feed] | 91.2 | 104 | 112 | 91.0 | 89.8 |
| ΔH _{rxn} [kJ/mol CH ₄ converted] | 253 | 250 | 249 | 249 | 249 |
| Ratio of rWGS-to-CH ₄ converted | 13.4% | 8.2% | 5.0% | 4.5% | 4.9% |
| | Chapter 5 conditions | | | Chapters 6 – 9 conditions | |

In addition to improving methane conversion, increasing reaction temperature also improves product selectivity and decreases energy input requirements (on a methane conversion basis) by reducing the relative extent of rWGS. It is interesting to note that diluting the reactor feed by 20% with an inert gas (argon, in this case) leads to very similar equilibrium composition and energetics as for an undiluted reactor feed composition at 800 °C.

N.4: Thermal Effects in the QTMR during CO₂ Reforming

Given the strongly endothermic reaction set involved in the tests for this work (CO₂ reforming, steam reforming, and rWGS, with only a small amount of partial oxidation or combustion possible because of the limited oxygen supply), there is no chance of hot spots or runaway reactions. There is also little chance that the catalyst bed cooled significantly more than indicated by the effluent gas temperature, as explained by the following operational conditions and their consequences.

Appendix N

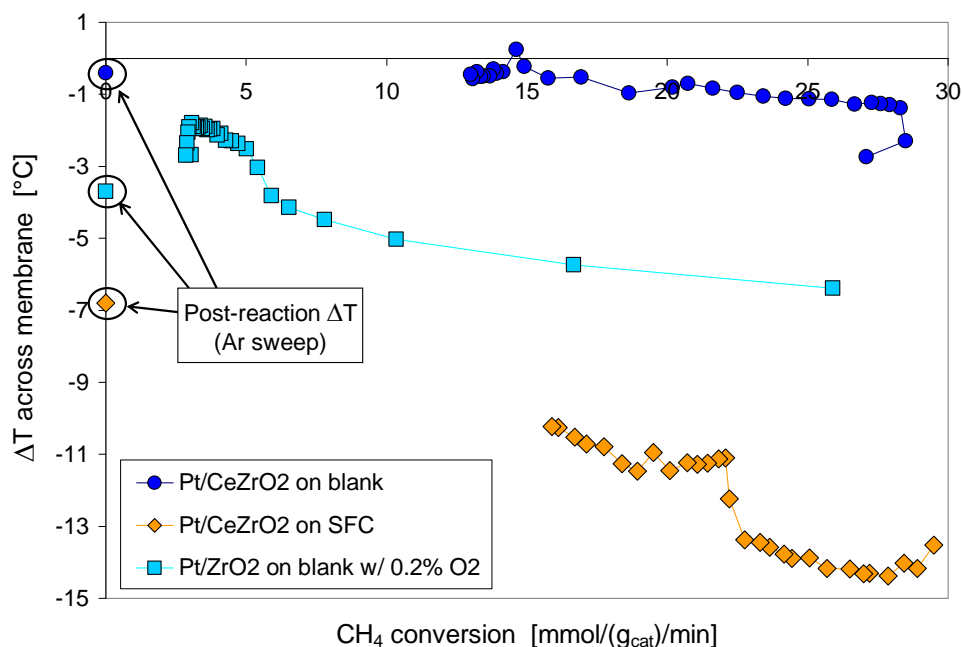
- 1) The very thin catalyst bed is positioned on a relatively large SFC membrane (10 mg vs. 2.8 g) and inside a relatively massive system of quartz tubes. Both conductive and radiant heat transfer from the available thermal mass should be significant.
- 2) The rate of conductive and radiant heat transfer to the catalyst bed will increase instantaneously with any drop in temperature.
- 3) The 6-inch long cylindrical furnace provides a substantial amount of heat (> 500 W) to the mid-section of the QTMR. The maximum incremental heat required for isothermal operation that was estimated from reaction enthalpy, heat capacity, and volumetric flowrate changes in the reaction chamber is 1.3 W.
- 4) Although the internal thermocouple was not physically touching the catalyst bed, it was positioned as close as possible without touching it and there was little opportunity for additional heating for the center-line gas streamlines between the catalyst bed and the thermocouple tip.
- 5) As Figures N.1 and N.2 and the work in Chapters 5 and 6 show, lowering the reaction temperature produces different reaction profiles and product distributions, including higher relative CO_2 conversion and lower H_2 :CO ratio. The inclusion of the SFC membrane led to both higher methane conversion and greater temperature drops in the reactor effluent, which is consistent with expectations for endothermic reactions. However, it did not produce lower H_2 :CO ratios and higher relative CO_2 conversions.
- 6) Endothermic reactions are self-limiting. If the catalyst bed were significantly cooler than the reactor effluent indicates, methane conversion should have been lower rather than higher with the SFC membrane. At this point, there is little reason to suspect that the measured temperature change was not at least somewhat representative of the actual temperature change in the catalyst bed.

Appendix N

NOTE: Other published work shows large catalyst bed temperature changes, particularly the work by Michael et al. [2] However, most published work, including the Michael study, uses significantly larger catalyst beds, which are inherently more prone to internal temperature changes. Also, the Michael study was performed in Lanny Schmidt's lab at the University of Minnesota using an adiabatic reactor that is clearly more susceptible to catalyst bed temperature changes than the reactor set-up used in this work.

N.5: Trans-reactor Temperature Differential Data

Because of intermittent problems with the internal thermocouple, complete reaction temperature information was obtained for only three tests, all of which are depicted in Figure N.3. Results are discussed as temperature differentials between the internal and external thermocouples in the QTMR system, with the post-reaction temperature differential serving as the reference point for each test (negative values indicate a lower temperature in the reaction chamber than the outside surface of the reactor). Section M.1.1. in Appendix M provides a list of the factors that can affect both the reference value for the temperature differential and the values during operation.



Appendix N

Figure N.3: Equilibrium constants for reactions relevant to syngas production for which K_{eq} increases with increasing temperature

With the stainless steel blank, the temperature in the reaction chamber drops only slightly (1 – 2 °C) during reaction compared to the post-reaction temperature differential. As expected for the net endothermic reaction sets involved in this work, temperature differential magnitude tends to decrease with decreasing methane conversion. Also, the temperature differentials observed with the blank align on average with the post-reaction temperature differential. The temperature differential magnitudes from the SFC membrane test are greater than those observed with the stainless steel blank, as is the post-reaction differential, which accounts for some of the difference. However, the differential with the SFC membrane increases by as much as 7 °C during reaction and is always greater in magnitude than either the pre- or post-reaction differential.

Even though the product distributions represent net endothermic reaction sets at all times for all tests, individual data points in the blank tests can exhibit smaller temperature differentials than their respective post-reaction values, as demonstrated in Figure N.4. This might be a result of the specific heat capacity effect discussed in Appendix M, or it might be a consequence of other systematic uncertainties.

Appendix N

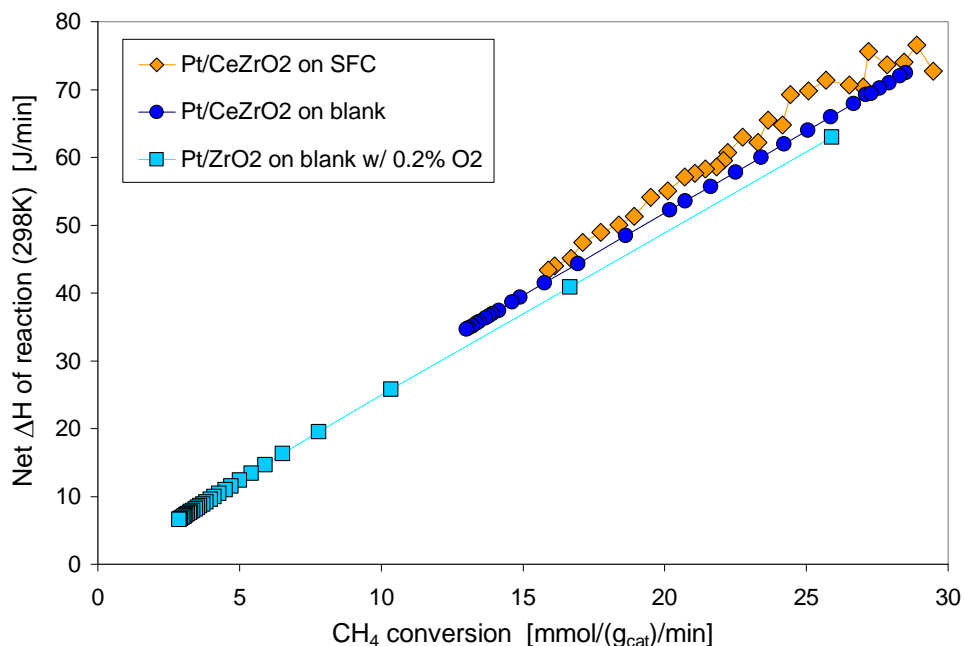


Figure N.4: Net enthalpy change between products and reactants for all tests with reaction chamber temperature data. Reaction temperature = 800 °C, GHSV = 150 L/h/g_{cat}, CH₄:CO₂:Ar/O₂ feed ratio = 4:4:2; oxygen feed and catalyst as indicated.

As observed in Appendix M, the temperature differential between the internal and external thermocouple readings does not appear to remain constant throughout a test. Likewise, the three tests in Figure N.3 all exhibit different temperature differentials before and after reaction testing. Because the internal temperature data are the newest addition to the set of QTMR test results, this temperature differential “drift” phenomenon has not been investigated. Changes in SFC phase composition might account for some of the unidirectional change in temperature differential observed over time in the mass spectrometer data in Appendix M. However, the potential to exhibit a temperature differential that is smaller than the pre- and post-reaction temperature differential has only been observed with the stainless steel blank. The consistently greater temperature differential with the SFC membrane thus supports one important conclusion from Appendix M: the removal of oxygen from the SFC membrane appears to be an endothermic process.

Appendix N

In addition to an endothermic contribution from SFC reduction, the stainless steel blank should be a better thermal conductor than the ceramic SFC membrane. Heat conduction from the external furnace to the reaction chamber via the stainless steel blank could therefore be a contributing factor to the observed difference in reaction chamber temperatures between the blank tests and the SFC membrane tests.

References Cited in Appendix N

1. Barnes, C. and M. Koretsky, *Thermosolver*, 1.0 (2003), John Wiley & Sons, Inc.
2. Michael, B.C., A. Donazzi and L.D. Schmidt, *Effects of H₂O and CO₂ addition in catalytic partial oxidation of methane on Rh*. *Jnl of Catal* **265**, 2009, p.117-129.

Appendix O

QTMR Dimensions and Parts Identification

The QTMR is constructed from the stainless steel Swagelok™ parts listed in Table O.1 and the two sizes of quartz tubing listed in Table O.2. Teflon ferrules provide an effective seal between the Swagelok™ fittings and the quartz tubing without damaging the tubing. They can be re-used many times as long as they are not overtightened. It can be difficult to judge when a Teflon ferrule is being overtightened because once they are fully compressed they offer little resistance to further tightening. Instead of resisting additional compression, the soft Teflon ferrules begin to extrude down the tubing into the fitting with no perceptible change in resistance. This has no effect on the seal quality but does deform the ferrule past the point of additional use.

Table O.1: Swagelok™ parts for the QTMR

| Item | Swagelok Part # | Description | Material of Construction | Quantity |
|-------------|------------------------|---|---------------------------------|-----------------|
| 1 | SS-12M0-R-12-BT | 12mm x 3/4" Reducer (12mm bore) | Stainless steel | 2 |
| 2 | SS-1210-3-12-6 | Reducing Union Tee, 3/4" (3/8" side port) | SS | 2 |
| 3 | SS-400-R-6 | 1/4" x 3/8" Reducer | SS | 1 |
| 4 | SS-4-UT-A-6 | 1/4" x 3/8" Ultra-Torr Adaptor | SS | 1 |
| 5 | SS-400-6-2 | 1/4" x 1/8" Reducing Union | SS | 2 |
| 6 | T-12M3-1 | 12mm front ferrule | Teflon | 2 |
| 7 | T-12M4-1 | 12mm back ferrule | Teflon | 2 |
| 8 | T-1213-1 | 3/4" front ferrule | Teflon | 2 |
| 9 | T-1214-1 | 3/4" back ferrule | Teflon | 2 |
| 10 | B-400-6-2 | 1/4" x 1/8" Reducing Union | Brass | 2 |

The only significant shortcoming of Teflon ferrules is that they will sublime if heated above 260 °C. Care must therefore be taken when applying insulation to the QTMR. The approach used successfully in this work was to cover the reactor parts below the fitting with the Teflon ferrules

Appendix O

completely to maintain the large tubing at the target temperature but to leave the inter-tube steel fitting itself (Item #1 in Table O.1) uncovered. The small tubing portion that extends above the inter-tube fitting is also insulated thoroughly to minimize additional cooling downstream of the fitting (this is done to minimize water condensation in the line).

The inter-tube fitting is a “bored-through” part that allows the inner tube to extend beyond the outer tube. The bore diameter is precisely machined to fit 12 mm tubing, so the smaller diameter quartz tubing (i.e., the inner tube) must be purchased to a tighter size tolerance than the standard range for commercial tubing suppliers. In particular, it must not exceed the actual bore diameter of the Swagelok fitting. This requirement must be explained to the quartz tubing supplier when ordering the 12 mm tubing. In the past, the supplier was willing to hand select individual tubes for our order.

Table O.2 provides the dimensions and approximate lengths of the tubing pieces for the upper portion of the reactor. The lower portion has more flexibility in tubing lengths because it is only supplying air to the membrane. For example, the inner tube does not need to extend to the membrane surface, so tubing remnants that are too short for the upper portion may be used in the lower portion. The actual length required depends on variables such as the current position of the bottom support in the reactor frame and will therefore need to be determined any time changes are made.

Table O.2: Quartz tube dimensions for the QTMR

| Parameter | Inner tube | Outer tube |
|---|-------------------|-------------------|
| Outside diameter [mm] | 12 | 19 |
| Inside diameter [mm] | 6 | 13.5 |
| Flow area [mm ²] | 28.3 | 30.0 |
| Typical length, top portion of reactor [cm] | 22.5 | 11.7 |